The Use of Heterocomplementary Hydrogen Bonding Motifs for Supramolecular Materials Chemistry

Kelly Ann Houton

Submitted in accordance with the requirements for the degree of
Doctor of Philosophy

The University of Leeds

School of Chemistry

March 2015

Intellectual Property and Publication Statements

The candidate confirms that the work submitted is her own, except where work, which has formed part of jointly-authored publications, has been included. The contribution of the candidate and the other authors to this work has been explicitly indicated below. The candidate confirms that appropriate credit has been given within the thesis where reference has been made to the work of others.

Chapter 1- Introduction; adapted from a review article 'Hydrogen-bonded polyurethanes', Houton, K.A and Wilson, A. J. Polymer International, **2015**; 64, 165-173. The contributions of the authors are as follows: KAH (the candidate) wrote the corresponding sections of the review and produced related figures, whilst AJW edited the manuscript into its present form.

Chapter 2- Light-triggered supramolecular self-sorting cascades; the work reported in this chapter formed part of a research paper 'Sequential and Photo triggered Supramolecular Self-Sorting Cascades Using Hydrogen-Bonded Motifs', Chemical Science, **2013**, 4, 1825-1829. The contributions of the authors are as follows: AJW, MLP and KAH (the candidate) designed the research, KAH (the candidate) performed the research and characterisation of AIC motifs appended with a light-cleavable motif, and drafted the corresponding section of the manuscript. MLP performed the non-triggered self-sorting experiments and AJW edited the manuscript into its present form.

Chapter 3- Mechanical properties of supramolecular polymers; the work reported in this chapter formed part of a research paper 'Tuneable Self-Assembled Elastomers Using Triply Hydrogen-Bonded Arrays', Macromolecules, **2012,** 45, 4723-4729. The contributions of the authors are as follows: AJW, AG, CIL, AS, CN and KAH (the candidate) designed the research, KAH (the candidate) performed the research and characterisation of control compounds bearing mismatching hydrogen bonding

motifs and their assembly behaviour, and drafted the corresponding section of the manuscript. AG synthesised and characterised all supramolecular polymers assembled using the DAC motif with the UIM macromonomer. CN aided characterisation and performed compression moulding. CIL, AS and AJW edited the manuscript into its present form.

Chapter 4- Reducing the environmental impact of polyurethane synthesis; the work reported in this chapter formed part of a research paper: 'Development of Solvent-Free Synthesis of Hydrogen-Bonded Supramolecular Polyurethanes', Houton, K.A, Burslem, G.M and Wilson, A. J. Chemical Science, **2015**, 6, 2382. The contributions of the authors are as follows: KAH (the candidate) and AJW designed the research, KAH (the candidate) performed the research on 1-propanol and PEG based reactions and produced related figures, GMB performed research on the ether diol and produced related figures, whilst AJW edited the manuscript into its present form.

Acknowledgments

Thank you primarily to Professor A.J. Wilson, for the support and guidance throughout the whole of this project. The dynamic of the Wilson Group can only be attributed to your exceptional judgement of character. I'll never forget the many Christmas dinners, summer trips, barbeques, group welcome drinks and of course interesting discussions with Huntsman.

Tremendous thanks to all Wilson members past and present.

Especially my original next-hood-neighbour Maria, my H-bond sister! To Kérya, Tasha and Panchami for welcoming me into the office and the lab. I will always listen to Taylor Swift and the eHarmony 'I love cats' song with fond memories.

To George P, for always making coffee and playing Smashing Pumpkins in the lab. Dave, Valeria, Phil and Giorgia for our long days building a pretty awesome imaginary company- and all the laughs/trials we had along the way. Sarah, for addressing the vegetarian *vs.* meat-eaters balance within the group. The 'foreign office' members: Irène, for just being you- letting us draw on your house, always getting too drunk and always speaking the truth. Jayapal- purely for your amazing giggle. Even when you're stressed you still look happy. Sìlvìa for always looking out for my best interests, I knew we'd always be friends from the first day you came into the lab and I cleared that desk for you.

To our lab parents, Ludwig and Anna, for showing us the light at the end of the tunnel and that it was possible to achieve a PhD.

George Burslem, my brother from another mother (told you I'd write it!). Thank you for all the pints, pep talks, uncomfortable (for you) hugs, cups of tea, cake, encouragement and inventive obscenities. I definitely wouldn't have got this far alone.

To Steven Kane, we'll never remember how we became friends, but I'm glad we did. Thank you also for all the pints and half pints, advice and agony-aunting, cups of coffee, nights out, memes and lab visitations. I'm sorry I broke your ankle, but it cemented our friendship for sure.

To the best MChem ever, Aisling, who became a true friend. To Dr. “Sri” Sridharan, for always telling me I was Andy’s favourite and I worked too hard.

With the greatest thanks to my family; my mum who always called this thesis “homework” and my sister Corrie who always knew someone who ‘might do something like you talked about once’.

The inspiring teachers who led me to a Chemistry degree in the beginning… Dr. Hanmer, Mrs. Hennah and Mrs. Harris.

The Core- de Bray and Tayler- we went our separate ways after Southfields and scattered ourselves across the country in the process, but we’ve never lost our closeness. Thank you for all the Skypes, escapes to different cities and most of all for always lending an ear.

Last but not least, thank you to my future husband, Matthew Squires, to whom this thesis is dedicated. As my best friend and non-scientist, I appreciate the patience you’ve had with the long hours I’ve worked the past 3 years. You have supported me through the highs and lows of this PhD, and I’m not sure I could have completed it without you. We took a few big steps together during my time at Leeds and I can’t wait for our next one.

Abstract

Hydrogen bonding is one of the most useful of the non-covalent interactions. Highly directional and easily tuneable, the strength of hydrogen bonded arrays enable controlled assembly of macromolecular structures. Because association can be designed to be selective, self-assembly involving low-molecular-weight amides and ureas has been expanded to higher order polymeric structures, so called 'supramolecular polymers'. Chapter 1 introduces and develops upon the current themes of research in small-molecule hydrogen bonding, and the subsequent application towards the assembly of supramolecular polymers, in particular polyurethanes.

The Wilson group is focused on the development of orthogonal recognition pathways, and their future application in the controlled assembly of polymers. The work presented in this thesis, therefore focuses on the development of self-sorting cascades- where molecules capable of hydrogen bonding have defined partners at specific stages of the cascade. Selecting two heterocomplementary hydrogen bonding arrays, and using them to form supramolecular polymers then advance this.

Chapter 2 introduces the design and investigation of these self-sorting pathways involving hydrogen bonding arrays reported both in the literature and from within the Wilson group. The application of two of these hydrogen bonding motifs to assemble supramolecular polyurethanes is described in Chapter 3. The effect of the thermal history of supramolecular polyurethanes is then investigated, highlighting the change in response to thermal stimuli dependent on previous processing and treatment. The latter part of Chapter 3 introduces a 'toolbox' for supramolecular chemists, whereby components of the supramolecular polymer are changed systematically to gauge effect on subsequent mechanical properties.

The synthetic route to supramolecular polymers is then discussed in Chapter 4, and the evolution of a solvent-free route to this particular class of polyurethanes is realised.

Table Of Contents

List of Tables

List of Figures

List of Schemes

List of Equations

List of Abbreviations

$\lambda_{(max)}$-	Wavelength of maximum absorption
2D-	Two dimensional
2(θ)-	Bragg reflection
3D-	Three dimensional
A-	Hydrogen bond acceptor
AFM-	Atom force microscopy
AIC-	Amido*iso*cytosine
AIC*-	Amido*iso*cytosine with light cleavable appendage
AThy-	Alkyl thymine
ATRP-	Atom transfer radical polymerisation
A.U.-	Arbitrary units
BAP-	*Bis*-amidopyridine
BHC-	Bromohydroxycoumarin
BINA-	*N*,*N*-*bis*-(2-hydroxyethyl) *iso*nicotinamide
CD_2Cl_2-	Deuterated dichloromethane
$CDCl_3$-	Deuterated chloroform
D-	Hydrogen bond donor
DABCO-	1,4-diazabicyclo[2.2.2]octane
DAC-	Diamido*iso*cytosine
DAN-	Diamidonaphthryidine
DAP-	Diamidopyridine
DMAc-	*N*,*N*-Dimethylacetamide
DMSO-d_6-	Deuterated dimethylsulfoxide
DMTA-	Dynamic mechanical thermal analysis
DNA-	Deoxyribonucleic acid
DSC-	Differential scanning calorimetry
E'-	Storage modulus
E''-	Loss modulus
ESI-HRMS-	Electrospray ionisation high resolution mass spectroscopy
Et_3N-	Triethylamine
FTIR-	Fourier transform infra-red spectroscopy
GPC-	Gel permeation chromatography
HDI-	Hexamethylene diisocyanate

HMBC- Heteronuclear multiple bond correlation

HMDI- Hydrogenated methylene diphenyl diisocyanate

HMQC- Heteronuclear multiple-quantum correlation

IPDI- Isophorone diisocyanate

IR- Infra-red

K_a- Association constant

K_{dim}- Association constant for dimerisation

LAG- Liquid assisted grinding

LCMS- Liquid chromatography mass spectroscopy

M_n- Number average molecular weight

MPa- Mega Pascal

M_w- Weight average molecular weight

MDI- Methylene diphenyl diisocyanate

N_0- Initial monomer concentration

N- Monomer concentration after time X

NapyO- Naphthrydinone

NMR- Nuclear resonance spectroscopy

NOESY- Nuclear Overhauser Effect spectroscopy

P- Extent of reaction

PBMA- Poly(butyl methacrylate)

PCL- Poly(caprolactone)

PDI- Polydispersity index

PEB- Poly(ethylene-*co*-butylene)

PEG- Poly(ethylene glycol)

PEG-PPG-PEG- Poly(ethylene glycol)-Poly(propylene glycol)-Poly(ethylene glycol)

PEK- Poly(ether ketone)

PIB- Poly(*iso*butylene)

Ppm- Parts per million

PS- Poly(styrene)

P(THF)- Poly(tetrahydrofuran)

PU- Poly(urethane)

ROMP- Ring opening metathesis polymerisation

SAXS- Small-angle X-ray spectroscopy

SMP- Supramolecular polymer(isation)s

SPU- Supramolecular poly(urethane)

STPU- Supramolecular thermoplastic poly(urethane)

TBD- 1,5,7-Triazabicyclo[4.4.0]dec-5-ene

T_c- Crystallisation temperature

TDI- Toluene diisocyanate

T_g- Glass transition temperature

TLC- Thin layer chromatography

T_m- Melting temperature

TPU- Thermoplastic poly(urethane)

UCyt- Ureidocytosine

UG- Ureidoguanosine

UIM- Ureidoimidazole

UPy- 2-ureido-4-pyrimidone

UTIZ- Ureidothiazole

UV- Ultra-violet

WAXS- Wide-angle X-ray spectroscopy

X_n- Degree of polymerisation

Chapter 1

Introduction

1 Introduction

1.1 Covalent Polymers

Polymers possess unique properties such as solvent, chemical and electrical resistance. This allows them to be used for myriad applications as a variety of mechanical strengths can be achieved through judicious choice of functional monomers. The molecular weight of the polymer often determines its properties. Generally, tensile and impact strength increases with molecular weight, **Figure 1.1**, so high-molecular-weight polymers are commonly desired. Tensile strength confers the ability to withstand large stresses whilst the material undergoes deformation.

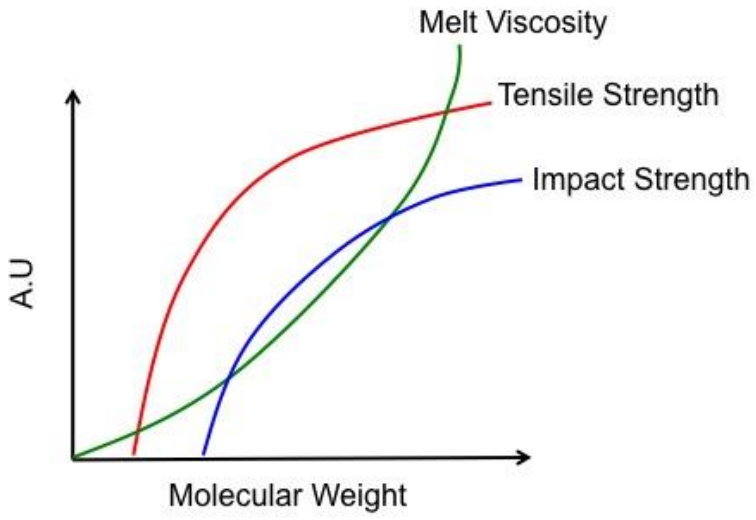

Figure 1.1 Variation in melt viscosity (green), tensile strength (red) and impact strength (blue) with molecular weight. A.U abbreviates arbitrary units

An increase in melt viscosity with molecular weight reduces the appeal of ultra-high-molecular-weight polymers. Entanglements of long polymer chains rigidify the material, and hence high temperatures are needed to process them in the melt state. A compromise is therefore often sought between materials properties and ease of processability.[1] The generation of high-molecular-weight polymers generally relies

on two common polymerisation synthetic routes; step- and chain- growth polymerisation.

1.1.1 Step-Growth and Chain- Growth Polymerisation

Step-growth polymerisation, such as the production of Nylon **3**, **Scheme 1.1**, utilising two different bifunctional monomers **1** and **2**, enables a slow increase of molecular weight. The monomers add indiscriminately, either to other monomers, or to an already growing polymer chain so that an ensemble of different length oligomers is present in solution at any one time. A high level of conversion is therefore required to obtain a high-molecular-weight polymer, **Figure 1.2**.

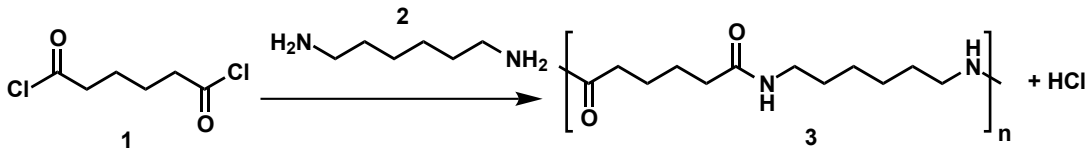

Scheme 1.1 Synthesis of polyamide Nylon-6,6 3 from hexamethylenediamine 1 and adipic acid 2

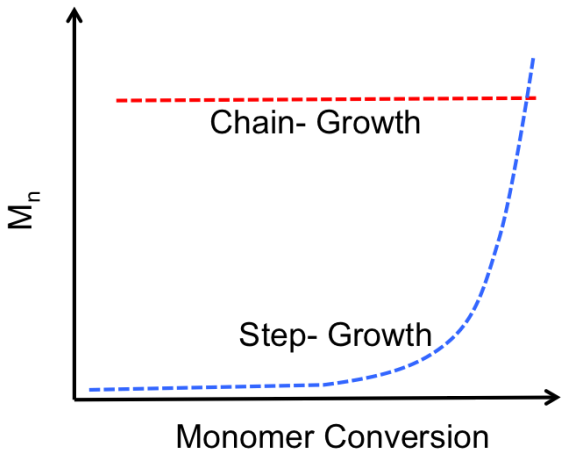

Figure 1.2 Difference in molecular weight growth based on two different polymerisation mechanisms, step-growth (blue) and chain-growth (red). M_n represents number average molecular weight

The degree of polymerisation, X_n, during a step-growth condensation can be calculated for a given monomer conversion, *p*, *via* the Carothers's equation, **Equation 1.1**.

$$\overline{X}_{n=} \frac{1}{1-p} \qquad \text{where } p = \frac{N_0 - N}{N_0}$$

Equation 1.1 Carothers's Equation for degree of polymerisation (Xn) of a linear polymer formed from monomers in equimolar quantities. Extent of reaction (p) is defined by monomer present (N0) minus monomer remaining (N) divided by N0

Chain-growth polymerisation differs from step-growth in that it consists of three distinct reaction steps, often involving intermediate radicals. These are initiation; where the reaction is started; chain propagation, where the polymer chain is extended and chain termination; where polymerisation is ceased. A high-molecular-weight polymer by this mechanism is formed more effectively, because the monomer adds only to growing chains of oligomers, **Figure 1.2**. Due to the significant advances that have been seen in chain-growth polymerisation, such as atom transfer radical polymerisation (ATRP),[2] ring opening metathesis polymerisation (ROMP)[3] and living anionic/cationic polymerisation,[4] chain-growth polymerisation is synthetically favoured due to high reliability and control of polydispersity index (PDI), **Equation 1.2**. If PDI tends towards 1, a more homogenous, monodisperse size of polymer is obtained.

$$PDI = \frac{M_w}{M_n} \qquad \text{Where } M_w = \frac{\sum_i N_i M_i^2}{\sum_i N_i M_i} \text{ and } M_n = \frac{\sum_i N_i M_i}{\sum_i N_i}$$

Equation 1.2 PDI is defined by weight average molecular weight (M_w) divided by number average molecular weight (M_n). N_i and M_i represent number of polymer chains at a given molecular weight and that molecular weight respectively

M_w takes into consideration that larger polymers contain more of the molecular weight than smaller oligomers. M_n is a simple arithmetic mean of the polymer sample as a whole.

1.1.2 Condensation Polymerisation

Whilst significant advances in chain-growth polymerisation have been seen, some monomer systems in addition to the synthesis of Nylon **3** are amenable to (step growth) condensation polymerisation; where functionalised monomers react, losing a small molecule as a by-product, such as water. Polyesters **6** and polyamides **3** are an example of this class of polymer, **Scheme 1.2**. Polyurethanes (PUs) are normally categorised under this broad term, as they are generated by a step-growth mechanism, but are technically formed *via* addition polymerisation, as no small molecules are lost during synthesis.[5]

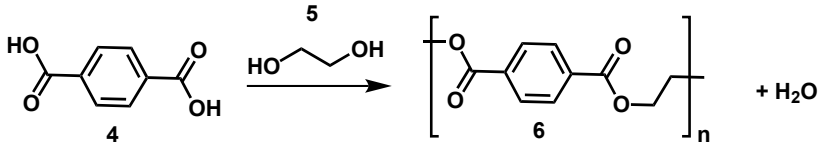

Scheme 1.2 Reaction of a diol 5 with a dicarboxylic acid 4, producing the corresponding ester 6, releasing water as a by-product

1.1.3 Polyurethanes

PUs which are formed from the addition of diols and diisocyanates, are a common component of thermoplastic, thermosetting and elastomeric materials.[6] Their properties, like other classes of polymers, are diverse and easily controlled based on the reaction components. Commonly employed is the prepolymer, or 'one pot' synthetic method, which Bayer reported for the first time in 1947.[7, 8] A telechelic diol is reacted with a difunctional isocyanate which is in excess, before the remaining free isocyanate groups are covalently chain extended by reaction with low-molecular-weight diols or diamines, **Scheme 1.3**. Telechelic polymers are defined as a macromolecule that possesses two reactive end groups capable of further reaction.[9] Industrially, aromatic diisocyanates such as methylene diphenyl diisocyanate (MDI) **7** and toluene diisocyanate (TDI) **8** are used for synthesis, along with their aliphatic counterparts isophorone diisocyanate (IPDI) **9** and hydrogenated MDI (HMDI) **10 Figure 1.3**.[10] Typical telechelic diols in this field of research

include poly(tetrahydrofuran) **11**,[11] poly(isobutylene),[12] **12** poly(caprolactone)[13] **13** and variants of poly(ethylene) glycols.[14] **14** 1,4-Butane diol and diamines **15** are commonly used as low-molecular-weight covalent chain extenders, introducing rigidity and high abrasion resistance.[10]

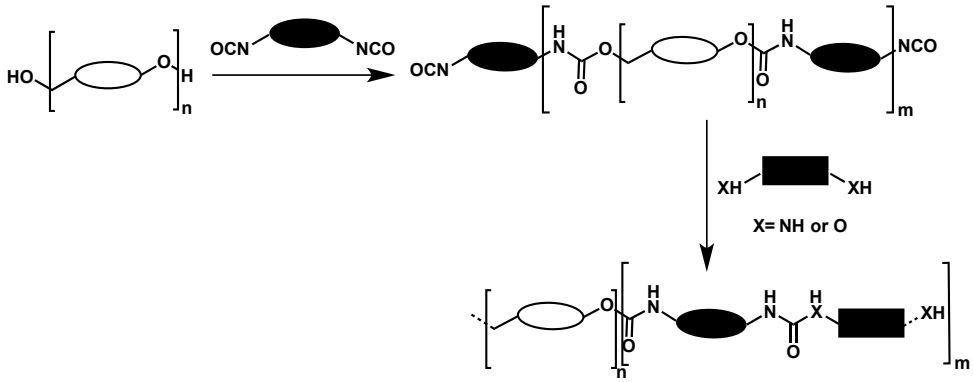

Scheme 1.3 Cartoon of poly(urethane) synthesis, using a generic diisocyanate (black oval) and a polymeric diol (white oval). Chain extension with an amine or alcohol (rectangle) generates the corresponding urea or carbamate linkage

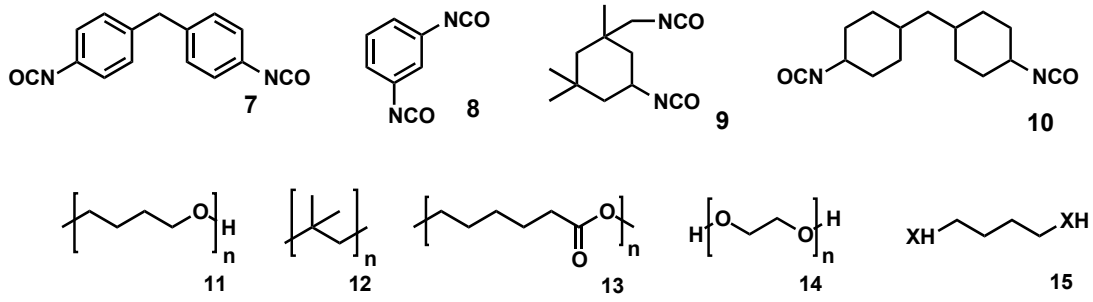

Figure 1.3 Top row- common diisocyanates used for poly(urethane) synthesis, 7-10. Bottom row- five well-utilised components for the synthesis of poly(urethanes), 11-15

This process results in phase separated materials, **Figure 1.4**. Phase separation is a consequence of the affinity between crystalline domains (represented by black ovals in **Scheme 1.3** and **Figure 1.4**), driven by the presence of hydrogen bonds and polar moieties which create physical crosslinks between polymer chains.[15] Aromatic isocyanate moieties and low-molecular-weight aliphatic chains contained in the chain extension units contribute to the crystalline domain.[16] The high crystallinity,

and hence 'hard' character bestows the PU with mechanical strength. The hard domains, which are dispersed in a soft and flexible matrix originating from amorphous polyol segments (represented by white ovals in **Scheme 1.3** and **Figure 1.4**), allow for mechanical deformation, and subsequently, retention of original shape. The ratio between soft and hard domains, and their miscibility, can regulate properties of the PU, such as stiffness and malleability.[6]

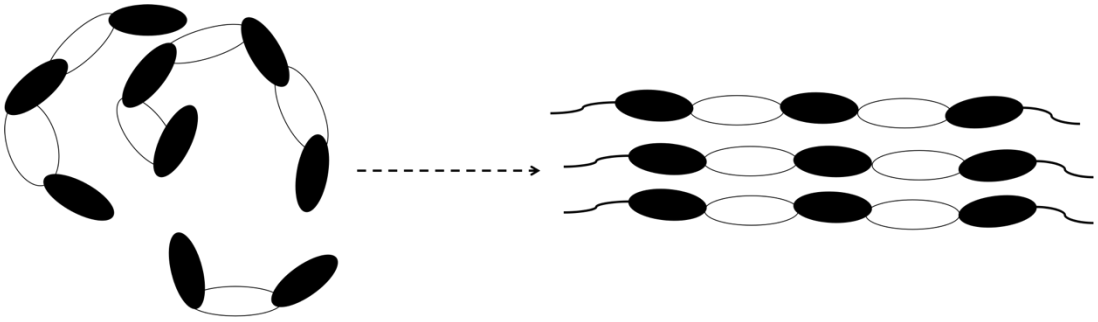

Figure 1.4 Cartoon representing the self-assembly of poly(urethanes), forming phase separated networks encouraged by lateral hydrogen bonding between hard (black) segments

The focus of this thesis is on PUs. They are industrially relevant, contributing to a diverse range of everyday items, such as corrosion protection on cars, adhesives and pleather (plastic leather) for vegan shoes and clothing. PUs are employed due to high impact resistance, particularly at low temperatures.[6] The demand on the performance of PUs is therefore very high because of the diverse applications in which they are used.

1.2 Supramolecular Polymers

A polymerisation is classified as supramolecular when moderately strong and highly directional but reversible non-covalent interactions between appropriately substituted monomers afford high-molecular-weight polymers under dilute conditions.[17]

The development and advancement of supramolecular polymers (SMPs) has permitted the construction of responsive materials[18] *via* the prepolymer method

introduced in Chapter 1.1.3. The application of non-covalent interactions as a means of assembling high-molecular-weight polymers[18-23] can result in mechanical properties comparable to those of covalent polymers in the bulk state,[24] whilst the non-covalent links between building blocks permit reversible and stimuli-responsiveness.

There are many approaches for SMP formation, such as the use of metal complexation, hydrogen bonding and π-π stacking. The formation of supramolecular structures using metal ion binding has been investigated by Rowan and colleagues[25] amongst others.[26] *Bis*-benzimidazole pyridine moieties **16** have been shown to chelate zinc **17** or lanthanum ions, **Scheme 1.4**, resulting in SMPs, **18**, which form thin films once processed, possessing appreciable mechanical properties produced by phase-separation within the macrostructure.

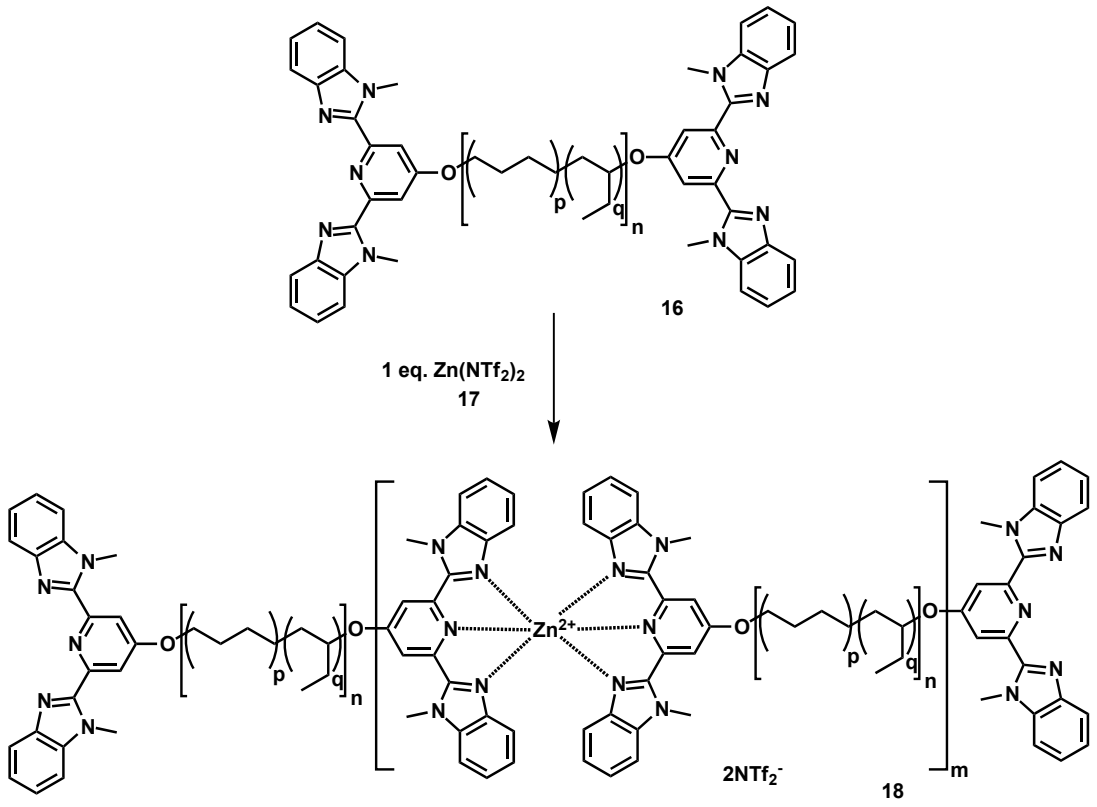

Scheme 1.4 Chelation of Zn^{2+} ions 17 to form the metallo-supramolecular polymer 18

Hydrogen bonding as a non-covalent force is particularly useful for supramolecular materials assembly due to the high directionality, dynamic behaviour and combined strength, which results when several hydrogen bonds are used in tandem.[27]

Inspired by the canonical Watson-Crick base pairings of adenine with thymine (A:T) **21:22** and cytosine with guanine (C:G) **19:20**, Figure 1.5, which control the double helix structure of deoxyribonucleic acid (DNA),[28] significant attention has been devoted to the design and synthesis of high affinity hydrogen bonded arrays for use as supramolecular synthons.[27, 29-32]

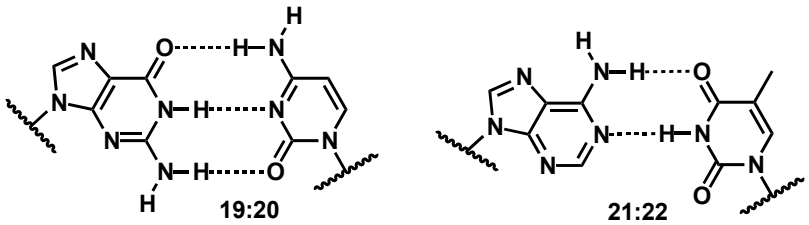

Figure 1.5 Canonical Watson-Crick C:G 19:20 and A:T 21:22 DNA base pairings

SMPs were first reported by Lehn and colleagues, using difunctional, also referred to as ditopic, linear arrays of hydrogen bonds, forming liquid crystals from tartaric acid functionalised with thymine **22** and ditopic diamidopyridine (DAP), **23:24** **Figure 1.6**.[33] Although these assemblies were not sufficiently stable to be classed as true SMPs, the synthesis of these compounds demonstrated the foundation of basic design rules for the self-organisation of molecules into materials. Lehn and colleagues stated that for self-recognition events to take place, the information for such assembly must be stored within the components.[34]

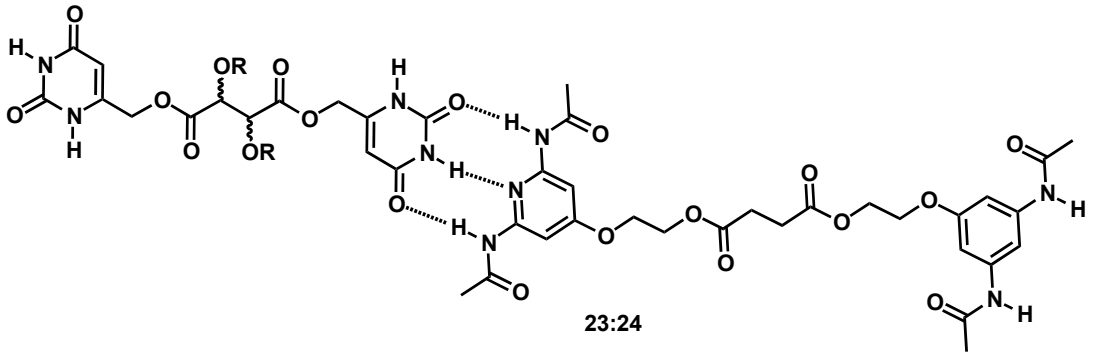

Figure 1.6 Thymine and diaminopyridine functionalised acids used by Lehn and colleagues to form supramolecular liquid crystals 23:24

1.2.1 Controlling hydrogen bond strength

In contrast to covalent polymers, an increase in temperature results in dissociation of hydrogen bonds and hence disassembly; subsequently reducing viscosity and mechanical strength. Such dynamic behaviour permits processing at reduced temperatures and allows self-healing[16, 35] and shape memory. [36, 37] In combination with typical polymer-like behaviour, SMPs possessing some or all of these characteristics may represent superior responsive materials. Such properties depend critically on hydrogen bond strength.

The association constant (K_a), dimerisation constant (K_{dim}), and hence the stability of hydrogen bonded complexes, is the sum of several factors. Whilst number of hydrogen bonds is a good indicator of the relative strength of arrays, intramolecular hydrogen bonding, pre-organisation, secondary interactions, tautomerisation and electronic substituent effects all play an important role; and directly influence the fidelity[38] and affinity of hydrogen bonded complexes.[27, 29]

Secondary interactions arise when hydrogen donor (D) and hydrogen acceptor (A) groups on the same molecule are adjacent in space.[39] Substantial electrostatic interaction exists when repulsive or attractive secondary interactions are present, and destabilisation or stabilisation of the complex affords lower binding constants respectively, **Figure 1.7**.

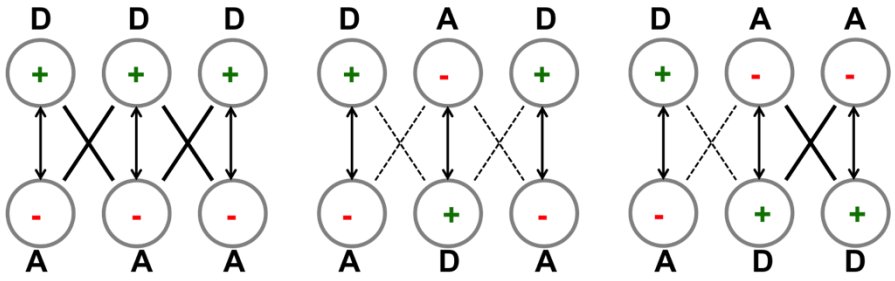

Figure 1.7 Effect of secondary interactions on the stability of a hydrogen bonded complex. Solid black lines denote reinforcing interactions, dashed black lines denote destabilising interactions. Green crosses denote hydrogen bond donating groups (D) and red dashes denote hydrogen bond accepting groups (A)

Blight and colleagues reported an example of the influence of electrostatic interactions in 2009.[40] Assembly of a heterocomplementary hydrogen bonded array

consisting of AAA and DDD **25:26**, occurs with an association constant of 3×10^{10} M^{-1} in CD_2Cl_2, **Figure 1.8**. The poor binding constant of 90 M^{-1} in $CDCl_3$ described by Pranata and colleagues of **27:28** which has an alternating DAD triple hydrogen bonded array, **Figure 1.8** is also consistent with this theory.

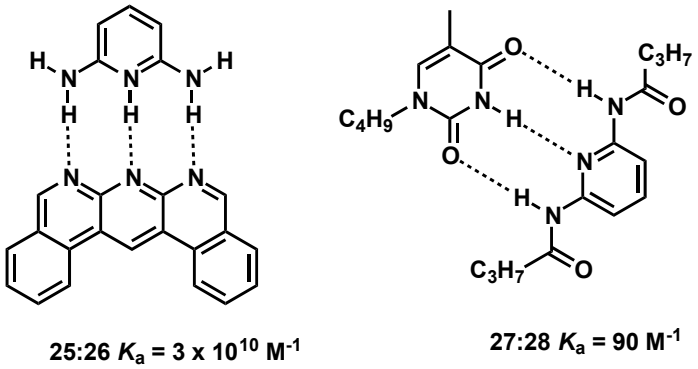

Figure 1.8 Left- strongly associating AAA:DDD hydrogen bonded complex 25:26 reported by Blight and colleagues. Right- weakly associating ADA:DAD complex 27:28 reported by Pranata

Etter's rules state that intramolecular hydrogen bonding to form six-membered rings will occur in favour to intermolecular hydrogen-bonding[41] between complementary units. Supramolecular synthons use pre-organisation to ensure the desired hydrogen bonding motif is presented. Compound **29a**, **Figure 1.9**, is an example when Etter's rules act to give an undesired hydrogen bond array **29b**, resulting in a low binding affinity toward complementary partner **31**, K_a = 84 M^{-1}.[42] When the complementary partner presented the desired hydrogen bonding array, **30**, as a result of pre-organisation, the binding affinity increased from K_a = 84 M^{-1} to 33400 M^{-1}.[38] Pre-organisation is therefore attractive due to the absence of conformational changes upon binding, reducing the entropic cost of binding, which in turn impacts positively on association constant.[43]

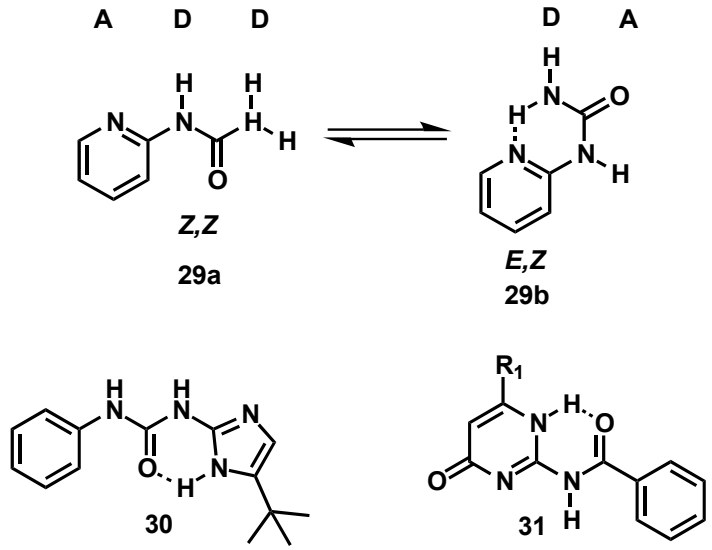

Figure 1.9 29a- desired triple hydrogen bonding array, which participates in intra- instead of inter- molecular hydrogen bonding to complementary partner 31. Pre-organised 30 binds to 31 with a larger K_a than 29a/b. R_1 is Me

The build up of molecular weight of SMPs in dilute solution depends upon the strength of the hydrogen bonding interaction, which in turn controls the degree of polymerisation.[19] The degree of polymerisation can then be related back to conversion of monomer to SMP (extent of reaction) *via* the Carothers's Equation. Supramolecular polymer linear chain growth, described by de Greef and co-workers as similar to step-growth condensation polymerisation,[17] can be subjected to Flory's principle of reactivity, in that each functional group reacts independently of molecular weight or neighbouring group effects.[44] In terms of SMPs, this means that each hydrogen bonding end group retains the same affinity for its intended partner which is further unaffected by molecular weight.

Whilst the relationship between degree of polymerisation, association constant and properties of supramolecular polymers in dilute solution is understood, this does not translate to predictable bulk properties of the materials as polymer morphology and crystallinity also influence materials properties. The systematic study of hydrogen bonding motifs for supramolecular polymer assembly has hence been an active area since Lehn's report in 1990.

1.2.2 Homocomplementary hydrogen bonding motifs for supramolecular polymers

The exploration of SMP materials grew rapidly after the introduction of the homocomplementary 2-ureido-4-pyrimidone (UPy) motif by Meijer and co-workers. 2-Butylureido-4-pyrimidinone, **32 Figure 1.10**, was found to self-associate in $CDCl_3$ with an association constant of 6×10^7 M^{-1}.[45]

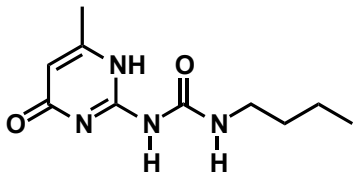

32

Figure 1.10 Homocomplementary UPy AADD quadruple hydrogen bonding 32 motif with a $K_{dim} = 6 \times 10^7$ M^{-1}

Alkyl chains functionalised at each termini with UPy monomers **33** were shown to assemble into linear chains in dilute solution **33:33**. The unidirectional association through the self-complementary hydrogen bonding motifs meant that assembly was controlled, gelation was avoided and a strong and reversible polymer was formed, **Figure 1.11**.[46] The UPy motif has since been used to investigate the assembly of many different supramolecular polymers,[47] and found commercial use.[21]

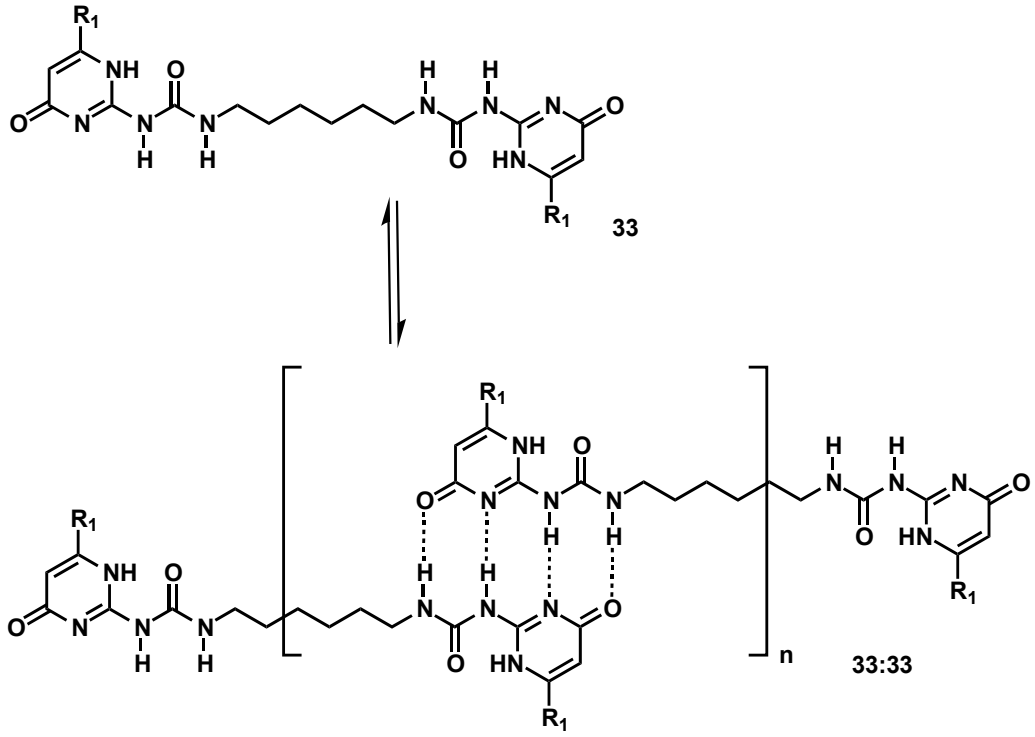

Figure 1.11 Equilibrium between monomer 33 and supramolecular polymer 33:33 UPy chains. R_1 denotes Me

Meijer showed that the bifunctional UPy motif **33** exhibited viscosity changes that were dependent on both concentration and temperature. Addition of monofunctional UPy unit **32** resulted in a viscosity reduction of the solution, which was indicative of a decrease in degree of polymerisation, similar to the way in which Carothers describes the inhibition of condensation polymerisation by addition of monomeric reactants. These findings provided a step forward in the synthesis of SMPs as the product had a sufficient degree of polymerisation to impart real materials properties and included reversible interactions; leading to extensive oligomerisation in dilute solution.

Hailes and colleagues described the application of ureido functionalised cytosine (UCyt) **34**, **Figure 1.12**, as an alternative homocomplementary DDAA quadruple hydrogen bonding array to UPy **32**.[48] Without the intramolecular N-H-----O lock of UPy **32**, UCyt **34** retains conformational flexibility and exists in both folded **34b** and unfolded **34a** states.[49] In apolar solvents, UCyt **34** existed exclusively in the unfolded **34a** state and exhibited a dimerization constant of more than 2.5×10^5 M^{-1} in $CDCl_3$.

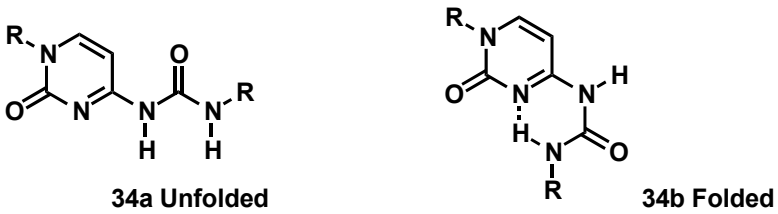

Figure 1.12 UCyt presenting both unfolded 34a and folded 34b forms due to conformational flexibility. R denotes generic alkyl chain

Whilst UPy **32** displays a higher K_{dim} than UCyt **34a** (6×10^7 M^{-1} *vs*. 2.5×10^5 M^{-1} in $CDCl_3$), and hence could produce a higher molecular weight polymer due to the strength of the non-covalent interactions, the supramolecular polymer becomes less dynamic due to a slower rate of association and disassociation.[27] Nevertheless, several groups have reported an improvement in mechanical properties of polymers, which feature the UPy motif. Telechelic polyethers, polyesters, and polycarbonates have all been studied, which are furnished with UPy units.[50]

Anthammaten and colleagues used rheological methods to investigate acrylate elastomers crosslinked non-covalently with UPy.[51] At low temperatures, hydrogen bonds were able to contribute to the storage modulus, but at high temperatures, the hydrogen bond lifetime was too short to contribute, with elasticity arising only because of covalent bonds present in the soft block. The resultant materials exhibited properties consistent with those of conventional high-molecular-weight polymers, but showed beneficial processability arising from the strong temperature dependence of the melt viscosity, which in turn correlates to the strength of main chain hydrogen bonding.

Liu and colleagues reported a PU based on poly(propylene oxide), MDI and 1,4-butanediol.[52] Upon functionalisation of the polyol with the UPy cross-linking motifs, **Figure 1.13**, the glass transition temperature (T_g) of the core polymer rose from 28.3 °C to 73.3 °C, as evidenced by thermal analysis. It was proposed that this change in T_g originated from the increase in order and rigidity of polymer chains provided by directional assembly through the UPy motifs. The strength of the hydrogen bonds contributed to the ordered, crystalline domain, increasing phase separation and hence temperature of the glass transition.

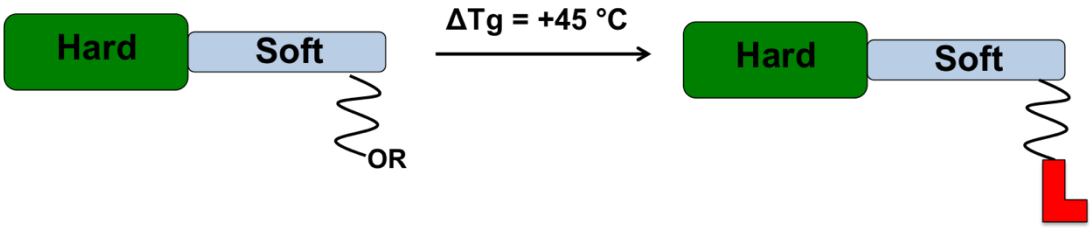

Figure 1.13 Cartoon to show the increase in T_g of the soft block achieved by Liu and co-workers by adding a pendant UPy hydrogen bonding unit (red) to cross-link polymer chains

1.2.3 Heterocomplementary hydrogen bonding motifs for supramolecular polymers

Heterocomplementary assemblies are gaining more interest as hydrogen bonding motifs due to their ability to form more complex structures through the availability of a larger range of constituent monomers.[27] An emerging theme in supramolecular chemistry is to mimic the ability of nature to assemble intricate and adaptive networks. This requires complexity and control; multiple assembled units are needed at defined locations and at specific times. The development of dynamic supramolecular architectures that can respond to chemical or physical stimuli by the changing structure is the subject of focused, ongoing research.

Macromolecular assemblies capable of changing structure, or reorganising constituent units can be referred to as self-sorting assemblies. During the self-sorting process, multiple molecular recognition events happen either simultaneously, requiring orthogonal assembly of one or more components, or sequentially, where building blocks are required to be promiscuous in their recognition behaviour. If affinity for dissimilar molecules is shown, then this is called social self-sorting,[53] and affinity for similar molecules is called narcissistic self-sorting.[54] Social self-sorting can then be further sub-divided as non-integrative or integrative; yielding more than one complex, or the integration of all components into one complex, respectively, **Figure 1.14**.[55]

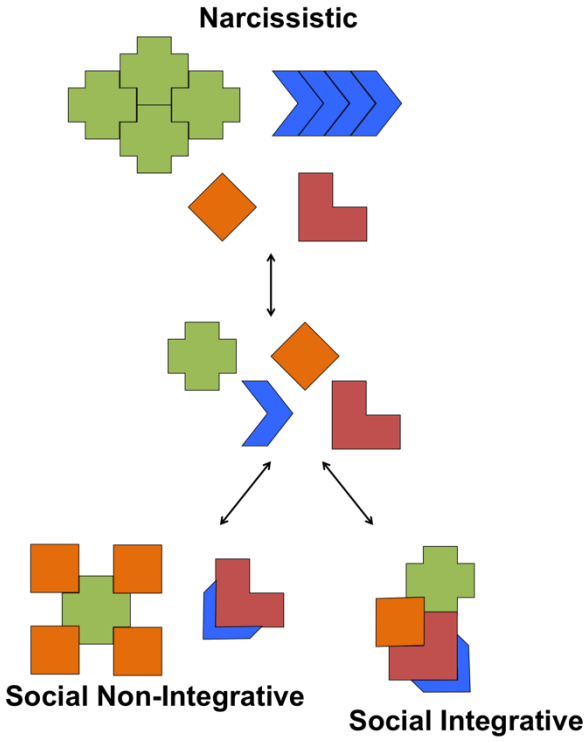

Figure 1.14 Cartoon of the various types of self-sorting available for promiscuous (bottom) hydrogen bonding units and those of a narcissistic nature (top)

1.2.4 Designing orthogonal supramolecular polymers from simple hydrogen bond scaffolds

Heterodimers are often used in supramolecular chemistry to assemble pseudo block copolymers. Pseudo block copolymers are so named for their ability to mimic the way in which traditional covalent block copolymers are formed through the linkage of two or more macromonomers.[56] Supramolecular block copolymers must maintain high affinity for association between different macromonomers, but a low affinity for homoassociation for formation to be successful.[57] Supramolecular block copolymers demonstrate an alternative approach to high-molecular-weight copolymers without complicated and prolonged synthesis.[47]

Zimmerman and co-workers have identified some motifs capable of selective homodimerisation. A series of studies focused on the development of linear arrays capable of high-fidelity molecular recognition.[58-60] Notably, the ureidoguanosine: diamidonaphthyridine (UG:DAN) **37:38** complex, which forms with a high affinity, but exhibits minimal interference from competitor motifs. The co-workers reported a

polymer blend based on the DAN:UG motifs, which functionalised polybutyl methacrylate (PBMA) **35** and polystyrene (PS) **36** respectively, **Figure 1.15**.[57]

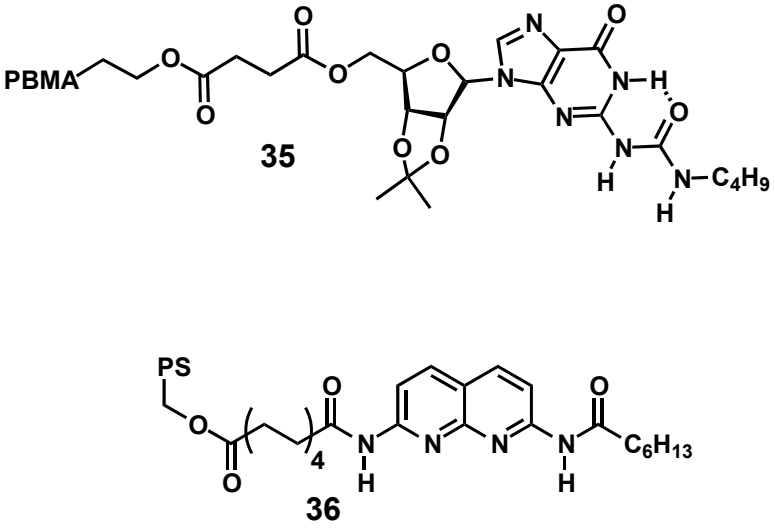

Figure 1.15 Polybutyl methacrylate 35 and polystyrene 36 functionalised with UG 38 and DAN 37 hydrogen bonding motifs

Blends of the normally immiscible PS/PBMA polymer pair, functionalised with heterocomplementary recognition motifs, formed colourless and transparent films with no evidence of microphase separation. Differential scanning calorimetry (DSC) studies further demonstrated only one T_g, indicative of the formation of a homogeneous blend. Zimmerman and colleagues attributed the remarkable behavior of UG **38** and DAN **37** to the high stability and fidelity of the heterocomplex.

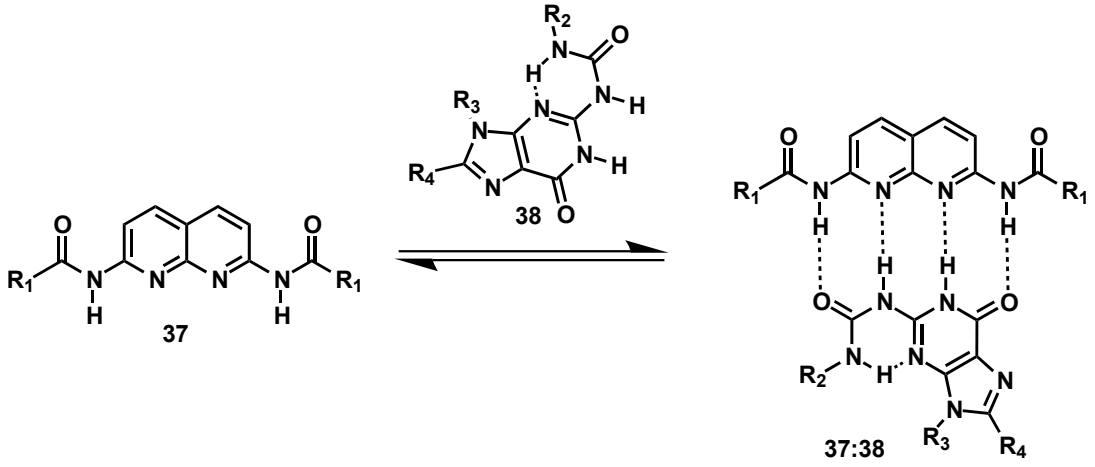

Figure 1.16 DAN:UG heterocomplex 37:38 designed and utilised by Zimmerman and colleagues. R_1 denotes C_4H_9, R_2 denotes C_4H_9, R_3 denotes H and R_4 denotes C_4H_9

In contrast to DAN:UG **37:38**, the UPy motif **32** has poor fidelity and displays promiscuous molecular recognition because it forms such strong homodimers primarily, but also strong heterodimers with DAN **37** motifs, **Scheme 1.5**.

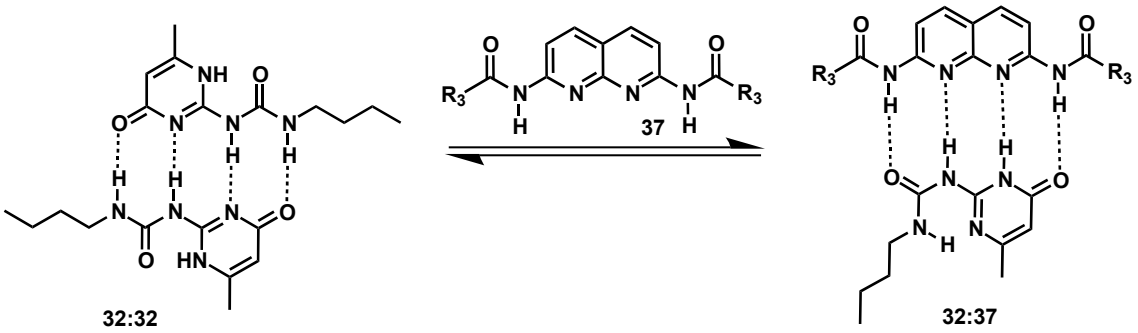

Scheme 1.5 Dynamic equilibrium between UPy homodimers 32:32, and UPy:DAN 32:37 heterodimers when DAN 37 is added in equimolar amounts in a non-polar solvent. R_3 denotes C_4H_9

Supramolecular block copolymers have been achieved by functionalising telechelic polymer chains with these hydrogen bonding motifs. Lighart *et al.* showed that the switchable complexation behaviour of UPy **33** results in concentration-dependent selectivity, favouring UPy:DAN **33:37** heterocomplexation over UPy homodimerisation **33:33** above a concentration of 0.1 M.[61] Because of this concentration-dependent selectivity, supramolecular block copolymers with high degrees of polymerisation have been possible.[59, 62, 63]

The Wilson group has also been able to identify several hydrogen bonding motifs, which are capable of orthogonal recognition.[64] An amidoisocytosine (AIC) **31** and an ureidoimidazole (UIM) **30**, designed within the group, were shown to assemble in the presence of UPy **39** and DAN **37**, as two sets of heterodimers, **30:31** and **32:39**. Tested over a range of concentrations, the nuclear magnetic resonance (NMR) spectrum of the system did not change significantly, suggesting a high fidelity between these partners, **Figure 1.17**. The well-documented promiscuity of UPy **39** was exploited by the addition of several different hydrogen bonding units, enabling the UPy unit **39** to switch between homo- and heterodimeric states. Preparation of self-sorting arrays from these hydrogen bonding motifs is further discussed in Chapter 2.

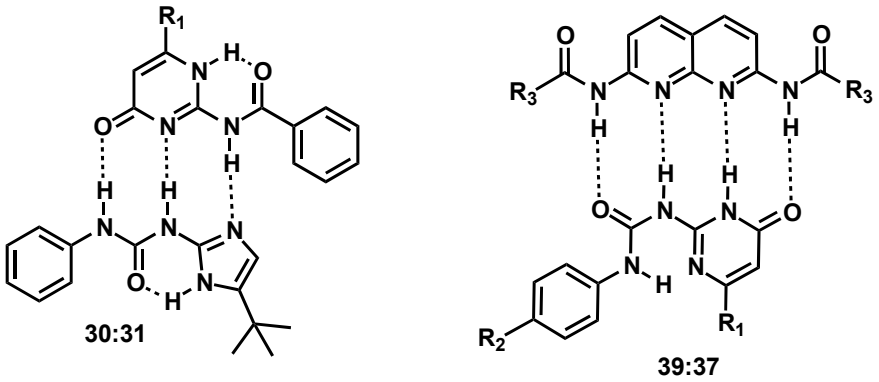

Figure 1.17 Structures of the two sets of hydrogen bonded partners investigated by Wilson and colleagues, which shows preferred complex formation. R_1 denotes Me, R_2 denotes *para*-benzyl ethyl ester and R_3 denotes C_4H_9

Binder *et al.* reported a pseudo block copolymer, in which the polyol components were immiscible with each other, but formed a macroscopically homogenous polymer when functionalised with hydrogen bonding units.[65] Interaction between weakly associating (~800 M^{-1}) poly(*iso*butylene) (PIB) end-capped with thymine **41** and poly(ether ketone) (PEK) end-capped with heterocomplementary triazine **40** moieties showed macrophase separation when the SMP **40:41** was heated up to the T_g of the PEK component, 150 °C. Replacement of these weakly associating hydrogen bonding units with strongly associating (about $10^4 – 10^6$ M^{-1}) Hamilton Wedge **43** and heterocomplementary barbiturate **42** resulted in microphase separation of the SMP **42:43** past the T_g of the PEK component **42**, 230 °C, **Figure 1.18**.

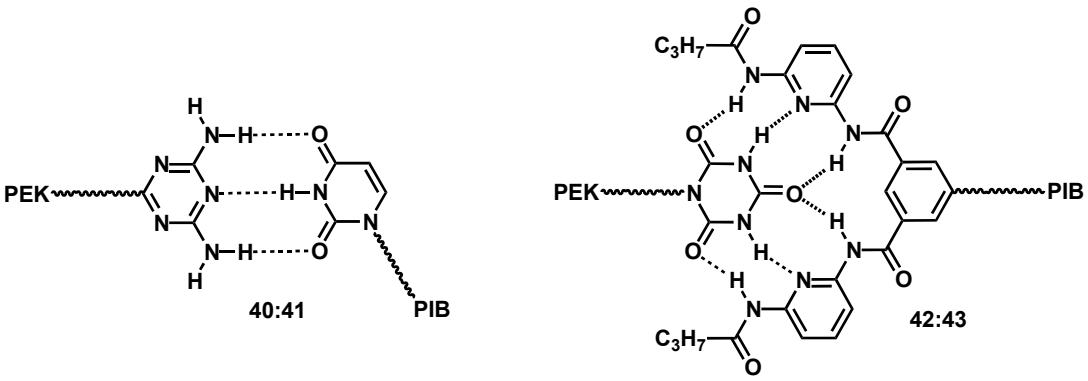

Figure 1.18 PEK and PIB functionalised with different hydrogen bonding units, forming supramolecular block co-polymers of different strengths. 40:41 and 42:43

The work by Binder above highlights a particularly attractive feature of SMPs in that they can facilitate the formation of miscible polymer blends from immiscible polymers, whilst maintaining reversibility.[66] Miscibility and therefore structural uniformity can provide novel materials that display improved mechanical behaviour and elasticity through incorporation of all the physical properties of the polymers present, with a single T_g.[67]

The regulation of supramolecular copolymer sequences hence allows a higher level of control over physico-chemical properties of the copolymers. By combining more than one non-covalent force, which can be controlled orthogonally, this control is more accessible. Weck and colleagues exquisitely describe directional and orthogonal assembly by incorporating both hydrogen bonding units and metal coordination centres along a polymer backbone.[68] Selective uncross-linking *via* either of the non-covalent moieties allows control over final materials properties. By utilising cyanuric acid **44** as the hydrogen bonding 'arm' and SCD palladacycles **47** as the transition metal containing 'arm', the linear polymer can be cross-linked selectively, using either a diaminotriazine **45**, or a bis-pyridyl alkane **48**, respectively.

The hydrogen bonded network alone formed a stable gel, which saw a sharp decrease in viscosity with an increase in temperature. In contrast, the metal coordination based cross-linked materials were thermally stable, and showed retention of viscoelasticity at elevated temperatures. Selective disruption of the hydrogen bonded network **44:45:44**, **Scheme 1.6**, was achieved by the addition of a monofunctionalised Hamilton Wedge **46**, which showed a greater K_a for cyanuric acid:Hamilton Wedge **44:46** than that of cyanuric acid:diaminotriazine **44:45:44**.

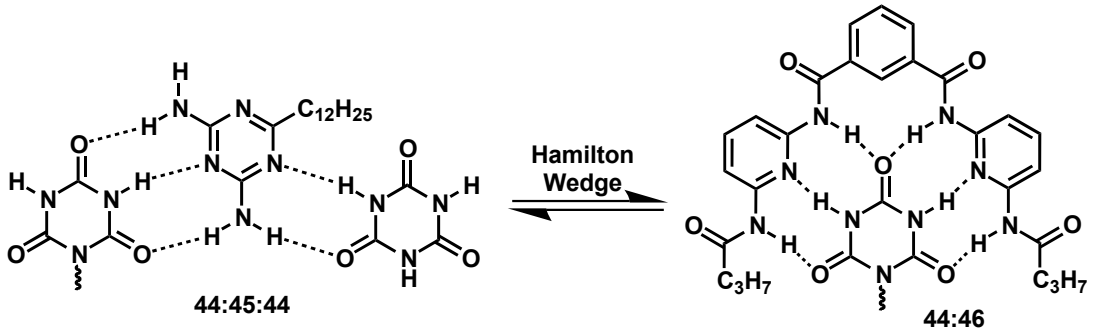

Scheme 1.6 Equilibrium between weakly associating diaminotriazine:cyanuric acid 44:45:44 and strongly associating cyanuric acid:Hamilton Wedge 44:46

Disruption of the metal coordinated network was effected by addition of triphenylphosphine **49** to promote ligand displacement, **Scheme 1.7**. This resulted in the selective de-crosslinking of Pd-pyridine **47:48** in favour of the formation of stronger Pd-triphenylphosphine **47:49** complexes.

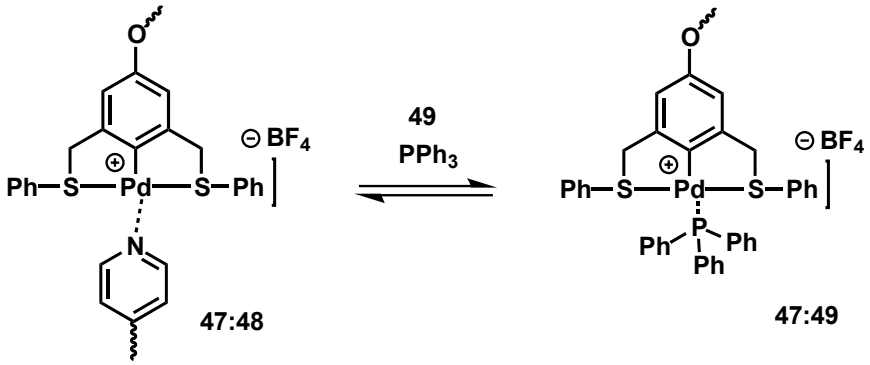

Scheme 1.7 Displacement of pyridine 48 with triphenylphosphine 49 as a 'depolymerising' agent

1.2.5 Design of Supramolecular Polyurethanes and Application

Synthetically, it is desirable to look for cheaper and more efficient ways of producing novel PUs with unique properties.[69] It is important to develop alternative synthetic methods, which can utilise both easier processing and recycling conditions, or exploit renewable source materials. Whilst the synthesis of covalent PUs has been studied in depth, the application of non-covalently assembled polymeric materials in the last few decades has increased.[18-23] These materials can display mechanical properties comparable to those of covalent polymers in the bulk state, whilst benefitting from the reversible and stimuli-responsiveness imparted by non-covalent links between building blocks.

1.2.6 Supramolecular Thermoplastic Elastomers

Because thermal responsiveness is a particularly useful attribute of SMPs, it predisposes them to application as thermoplastic elastomers.[24, 70] Thermoplastic

elastomers exhibit the ability to melt upon heating and return to a glassy state upon cooling, but also to possess elasticity at an ambient temperature.[47]

Supramolecular thermoplastic elastomers are non-covalent analogues of block copolymers,[71] shown in Chapters 1.1.3 and 1.2.3, that incorporate high-molecular-weight low-polarity segments, alternated with low-molecular-weight, high polarity segments.[72] Crystalline areas are created by the strong attraction between separate hard segments, which results in phase separation (1.1.3) in the same way as covalent PUs, which affords supramolecular polyurethanes (SPUs) with their thermoplastic properties.

The response of SPUs to temperature and external forces can be controlled by fine tuning both the soft and hard block through appropriate functionalisation. Desired properties can then be either introduced or optimised.[72]

It is well known that urea containing hard blocks can give high strength[72] due to the strong hydrogen bonding ability[73] they possess, and are a favoured motif due to the various synthetic routes which are available for synthesis.[74] Urea motifs can also promote interactions between chains of polymers *i.e. via* lateral interactions.[72, 75] Ureas terminating, or being located throughout a macromonomer unit can promote lateral assembly as shown by Taha and colleagues. The role of lateral hydrogen bonding between polyurethane-ureas was studied. Low temperatures resulted in folding of tetra-urea chains **50b** and disabled the formation of a supramolecular polymer.[70] When the temperature was increased above 105 °C, an unfolded conformation was preferred **50a** and cross-linked polymers formed, **Figure 1.19**.

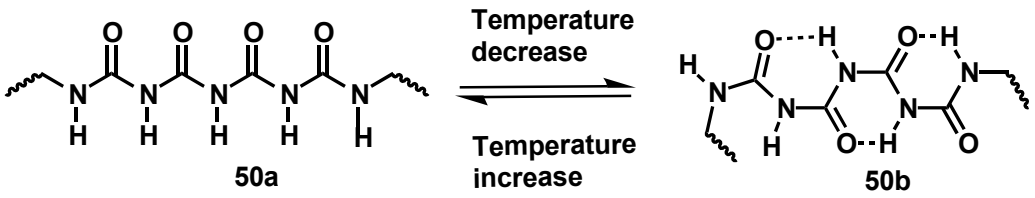

Figure 1.19 Tetra urea chains and their response to temperature. Temperature increase encourages unfolding of the chain 50a and cross-linking of polymers

Understanding the role of lateral hydrogen bonding in higher molecular weight species was explored in a key series of experiments performed by Hayes and co-

workers. Building on studies that investigated the assembly of PUs end- capped with a variety of groups able to hydrogen bond,[76] Hayes and co-workers developed urea and carbamate terminated poly(ethylene-*co*-butylene) (PEB) PUs, **51 a-c** which were shown to self-assemble into thermally responsive elastomeric materials, **Figure 1.20**.[76]

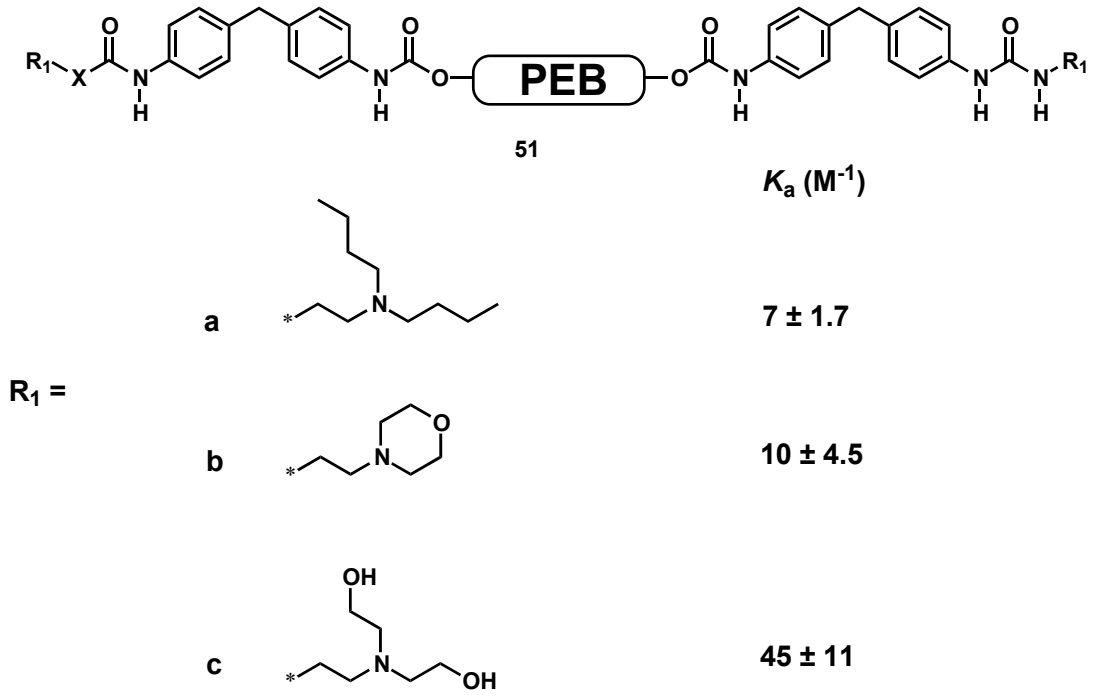

Figure 1.20 Structure of *bis*-urethane PEB 51 used by Hayes and colleagues for research on the effect of lateral hydrogen bonding. The end units for Hayes' PEB *bis*-urethane 51a-c displayed a range of hydrogen bonding strengths

The extent of hydrogen bond assisted assembly was observed with rheological techniques. The solid-like properties of the PUs were seen to change based on the end-group; the PEB diol showed one transition in storage modulus, whereas the PU end-capped with moieties able to participate in hydrogen bonding, **Figure 1.20 51 a-c**, showed two distinctive transitions in storage modulus, indicative of phase separation between soft and crystalline phases. The transition observed at higher temperatures depended on the hydrogen bonding ability of the end-group and hence the functional group appendage. Subsequent studies highlighted the rheological data was consistent with a phase separated morphology and showed that storage modulus of the plateau region as well as the two transitions were strongly dependent on

hydrogen bonding strength.[77] PUs end-capped with morpholine (**Figure 1.20 51b**) which had a K_a of approximately 10 M^{-1} lost five orders of magnitude in storage modulus from 1 MPa between 50 and 100°C, resulting in a free flowing liquid. This compares against PUs end-capped with *N,N* diethanol termini, **Figure 1.20 51c**, which had a K_a of approximately 45 M^{-1} and lost only 1 order of magnitude in storage modulus over the same temperature range.

Phase separation in these systems was also quantified by small-angle X-ray scattering (SAXS), showing an increase in domain spacing (and hence phase separation) with temperature for polymers end-capped with the most polar moieties.[78] Polar moieties result in increased electron density in the hard block, directly enhancing the ability to form distinct, crystalline phases.

Meijer also described the enhancement of the mechanical properties of PEB based SPUs by incorporating side-chain functionalities into the ditopic supramolecular chain extenders **52 - 56**, *e.g.* hydrogen bonding arrays or sterically demanding substituents to give additional stability and rigidity to the main polymer chain.[72] Strong inter-chain interactions were achieved by integration of the UPy motif **56** as a strong end-to-end associator in combination with ureas **54** or urea-urethanes **52** as lateral reinforcers, **Figure 1.21**.

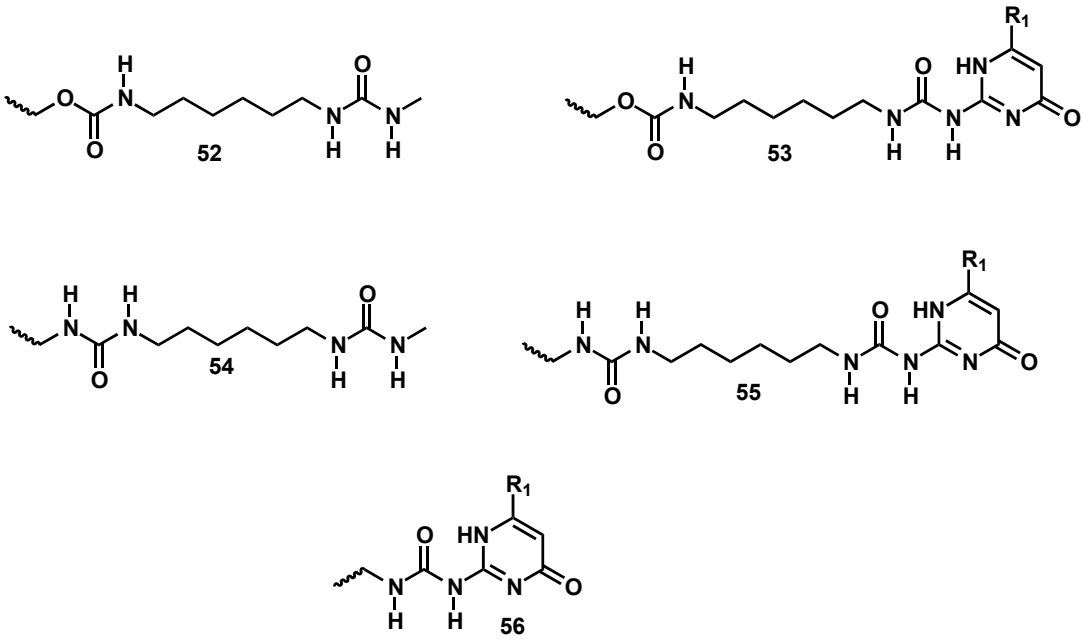

Figure 1.21 Range of both end- 56 and chain- 52, 54 functionalised ditopic units, used by Meijer and colleagues to investigate the effect of lateral hydrogen bonding on the morphology of supramolecular structures. R_1 denotes $C_{13}H_{27}$

The room temperature morphology of these materials was investigated with tapping mode atomic force microscopy (AFM). Whilst films of only end-to-end (**56**, **Figure 1.21**) interacting SPUs lacked any distinct morphological features, films produced from SPUs with two means of functionalisation (**53** and **55**, **Figure 1.21**) had distinct fibril-like morphologies. This important paper highlighted the cooperative behaviour between end-to-end and lateral non-covalent interactions, which has influenced the work in this thesis reported in Chapter 3.

The Wilson group has developed heterocomplementary triple hydrogen bonding motifs; the heterocomplementary AIC **31** and conformer independent UIM **30** motifs have a K_a in excess of 10^4 M^{-1} in $CDCl_3$.[38, 42, 79] A self-assembled material using this pairing was obtained by reacting a 2 kg mol^{-1} poly(ethylene glycol)-poly(propylene glycol)- poly(ethylene glycol) diol (PEG-PPG-PEG diol) **57** with bifunctional isocyanate MDI **58**.[80] Remaining free isocyanate functionality **59** was then reacted on with an aromatic amine **60**, which introduces the ureidoimidazole **61**. The heterocomplementary diamidoisocytosine (DAC) **62** is then added to form the SPU, **Scheme 1.8**.

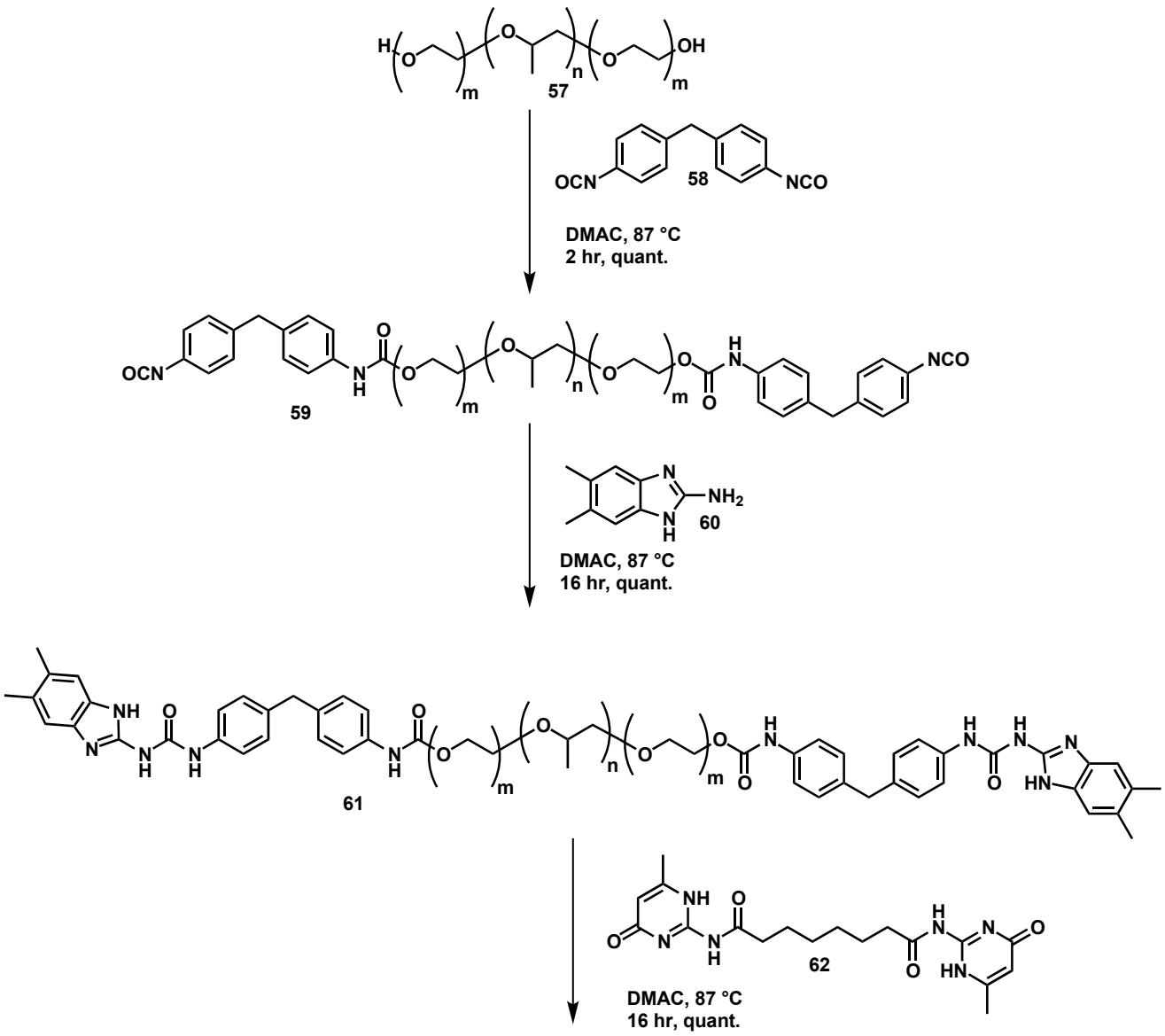

Supramolecular Polymerisation

Scheme 1.8 Formation of heterocomplementary supramolecular polymers investigated by Wilson and colleagues. Reaction of a PEG diol 57 with a diisocyanate 58 and subsequently a mono-functionalised amine 60 results in a poly- urethane-urea 61. Addition of heterocomplementary chain extender DAC 62, results in supramolecular polymerisation

The macromonomer **61** core contains the soft block, comprising the PEG diol **57**. The aromatic, hydrogen bonding unit that terminates the macromonomer **61** contributes to the crystalline phase of the polymer, in combination with the heterocomplementary supramolecular chain extender **62**. This design differentiates these elastomeric materials from others previously reported, as the elastomeric morphology and properties of the material are observed only when both the

macromonomer **61** and supramolecular chain extender **62** are present, demonstrating a requirement for selective and orthogonal recognition to occur in the presence of other competing non-covalent forces.

Thermal analysis showed two distinct transitions of the SPU, one attributed to the T_g of the PEG diol **57** and the second, to the melt and/or the disruption of the hydrogen bonded network. The presence of a phase separated morphology was further confirmed by SAXS, where a single Bragg peak was observed suggesting a microphase separated morphology.

1.2.7 Self- Healing

Traditional building materials such as concrete, tarmac and cement suffer from the inability to self-heal and hence become damaged with age. Upon fracture, non-covalent interactions and some thermally reversible covalent reactions, may readily undergo molecular reorganisation, so the system has the ability to heal through formation of new links.

Zhang and colleagues identified covalently thermally reversible self-healing linear PUs using a furfurylamine **63** and maleimide **64** capable of performing Diels Alder reactions, **Scheme 1.9**.[81] Initial heating to 120 °C for 5 minutes followed by maintenance at 60 °C resulted in recovery of 66% of the original strain-at-break after introducing a cut into the material.

Zhang also obtained self-healing PUs using a coumarin moiety **66** as a group capable of 2+2 photodimerisation, **67 Scheme 1.10**.[82]

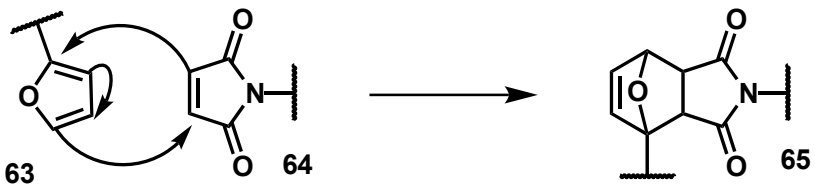

Scheme 1.9 Diels-Alder reaction between furfurylamine derivatives 63 and maleimide 64 furnished PUs to form bicyclic product 65

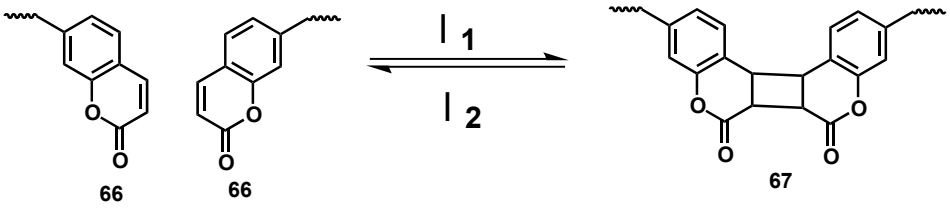

Scheme 1.10 Photo-initiated 2+2 dimerisation of coumarin 66 moieties

A healable rubber, reported by Leibler and co-workers, used small molecules possessing amide and urea groups capable of hydrogen bonding, **68**-**70 Figure 1.22**.[83]

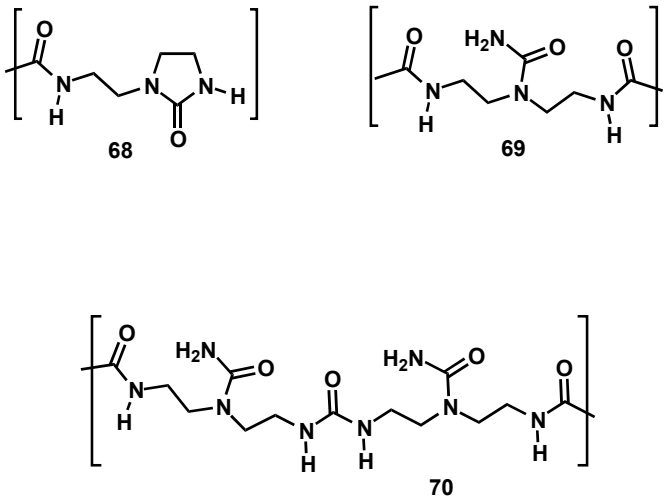

Figure 1.22 Moieties investigated by Leibler and co-workers for effect on ability of rubbers to self-heal

1.2.8 Shape Memory

Shape memory PUs have previously been identified that do not deform upon heating, which occurs to traditional plastics.[84] This desirable property is also plausible for SPUs, as Chan and co-workers have shown the development and evolution of SPUs that have shape memory. Novel *N*,*N*-bis-(2-hydroxylethyl) isonicotinamide (BINA) **71** based PUs, exhibited phase separation behaviour demonstrated by a similar supramolecular material, to those reported by Hayes.[24, 77, 78, 85] BINA **71** was reacted through the diol functionality with hexamethylene diisocyanate (HDI) to form *bis*-urethane linkages.

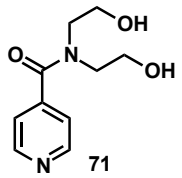

Figure 1.23 The terminal diol functionalities of the BINA 71 molecules were reacted with an isocyanate to from a shape memory PU

T_g was shown to be controlled by BINA **71** content, with the pyridine moiety acting as a molecular switch, turning hydrogen bonding on and off in response to a change in temperature. It was also found that these SPUs were moisture sensitive, and as a result, humidity was used as an alternative to temperature to stimulate shape memory. By exposing deformed samples of the SPU to a range of temperatures and humidity, it was found that approximately 90% strain recovery was exhibited at 34 °C and 85% relative humidity, after only 100 minutes. Calorimetric analysis showed that shape memory increased upon a decrease in BINA **71** content.[85] Further Fourier transform infra-red spectroscopy (FT-IR) experiments illustrated hydrogen bond dissociation in the pyridine ring at the point at which strain was seen to recover, indicating a role for the BINA unit **71** as a molecular switch.[86]

1.2.9 Biomedical Devices

Supramolecular materials are promising candidates for medical devices or delivery systems due to their responsive mechanical properties and potential biodegradability. Meijer and co-workers have demonstrated that PEG and poly(caprolactone) (PCL) end-capped with UPy can function as biocompatible thermoplastic elastomers.[87-89] Initial studies involving these materials as scaffolds for cell-interacting peptide sequences could be non-covalently integrated *in vivo*, allowing supported cell growth.[87] This series of supramolecular polymers has also been shown to form transient networks in water, allowing them to be loaded with a bioactive protein which can be delivered by injection.[88]

1.3 Project Aims

The desire for more complex and adaptive networks using non-covalent forces has fuelled the investigation of hydrogen bonding arrays for supramolecular applications. A wider variety of heterocomplementary arrays in particular, that can show selective recognition are continuously required.

To this end, this thesis describes the development of small molecule hydrogen bonding motifs, which are able to show fidelity based on the presence or absence of particular binding partners. Two of these heterocomplementary arrays are then taken forward to investigate materials properties of supramolecular polymers, and their potential application in dynamic polymer systems.

Chapter 2

Self- sorting cascades using non-covalent interactions

2 Chapter Two

2.1 Sequential supramolecular self-sorting cascades using non-covalent interactions

Cell signalling processes depend on the ability for simultaneous and sequential recognition events to occur between many different biomacromolecules. Simultaneous events require entities which are able to self-sort,[90, 91] *i.e.* to perform orthogonal molecular recognition.[92-94] Sequential recognition requires entities to exhibit both high-fidelity and promiscuous behaviour towards specific partners (**Figure 2.1**). Promiscuous partners allow 'intermediate' complexes, which are rapidly disassembled to form those with a higher K_a and hence fidelity. By carefully considering the order of addition of each molecule to the self-sorting system, promiscuity can be exploited in an artificial system.[92, 95, 96]

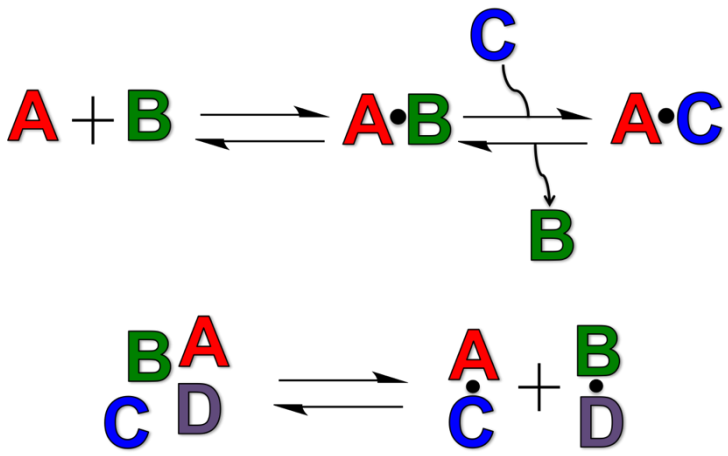

Figure 2.1 Sequential (top) vs. simultaneous (bottom) self-assembly. Sequential assembly requires promiscuous units, which are capable of forming more than one complex. Simultaneous assembly requires high-affinity units capable of orthogonal recognition

DNA polymerases are capable of organising the manufacture of complementary DNA strands, which relies on the correct association of the linear hydrogen bonded

canonical base-pairs.[97] Artificial chemical systems aim to mimic such highly accurate and efficient processes, but are beyond the scope of this thesis.

Several groups have reported on the spontaneous assembly and discrimination of self from non-self, and numerous articles have been published on this topic.[54, 55, 90-96, 98-102] This behaviour has principally been described in terms of 2- and 3-dimensional metallostructures.[94] Nitschke described the ability of Co-(II) complexes to coordinate five perchlorate anions, **Figure 2.2**, which resulted in a structural change of the complex, presenting a pocket with high affinity for a chloride anion.[103] This is comparable to how biological systems are able to process external inputs (*i.e*. the addition of perchlorate), which triggers a response or function (*i.e*. binding of chloride).

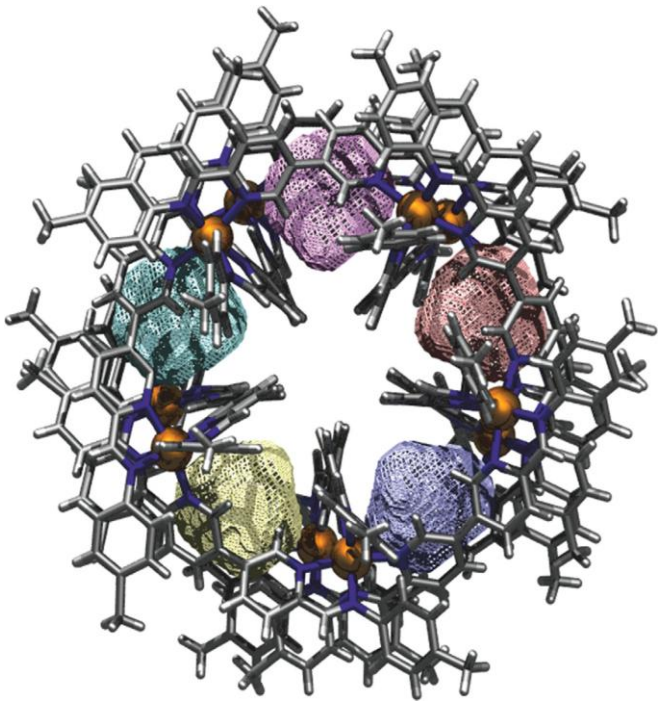

Figure 2.2 View down the centre of the assembly, revealing the empty central channel, which has high affinity for chloride ions. The five perchlorate ions are shaded in different colours. Adapted with permission from Macmillan Publishers Ltd: Nature Chemistry 4, 751–756, copyright 2012

Whilst metal complexation as a means of self-sorting is relatively well documented, the ability of small organic molecules to exhibit orthogonal recognition is known to be challenging.[64] Reliant on linear hydrogen bonded arrays, the ability to find partners with high-fidelity and a high combined strength is a difficulty. The

metallostructures reported by Nitschke and others benefit from shape complementarity and additional non-covalent stabilisations, for example π-π stacking. Zhao and co-workers have previously proposed orthogonal assembly from hydrazide **72-73**, urea **39** and amide **37** moieties *via* linear hydrogen bonds only.[104] Two complexes were desired (**Figure 2.3**) from the four units, **39:37** and **72:73**. It could be seen, however that the UPy unit **39** was present in both homo- and heterodimer forms. It was therefore concluded that the system had low fidelity because of the inability for UPy to differentiate self from non-self.

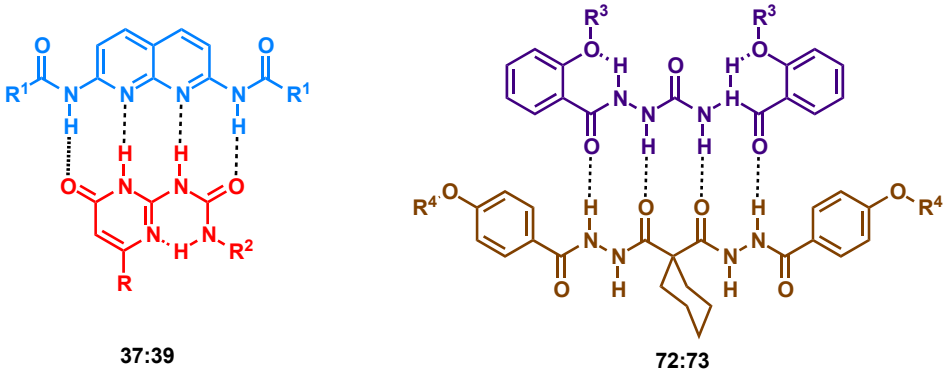

Figure 2.3 The self-sorting system designed by Zhao *et al.* based on hydrogen bonding arrays. R donates Me, R_1 denotes C_4H_9 R_2 denotes C_4H_9 R_2, R_3 denotes C_8H_{17} and R_4 denotes $C_{12}H_{25}$

2.2 Design of a sequential photo-triggered supramolecular self-sorting cascade using hydrogen bonded arrays

The objective of our study was to be able to identify a series of molecules possessing linear arrays of hydrogen bonds, which are capable of orthogonal recognition. This was then further expanded on by utilising a photolabile group, which could mask the triple hydrogen bonding array of one of the molecules, introducing stimuli-responsive behaviour.

Our group previously reported a heterocomplementary dimer which, forms a well-defined complex **30:31** in $CDCl_3$ (**Figure 2.4**).[42] The conformationally independent DDA array, UIM **30**, was complemented by the AAD array, AIC **31**.

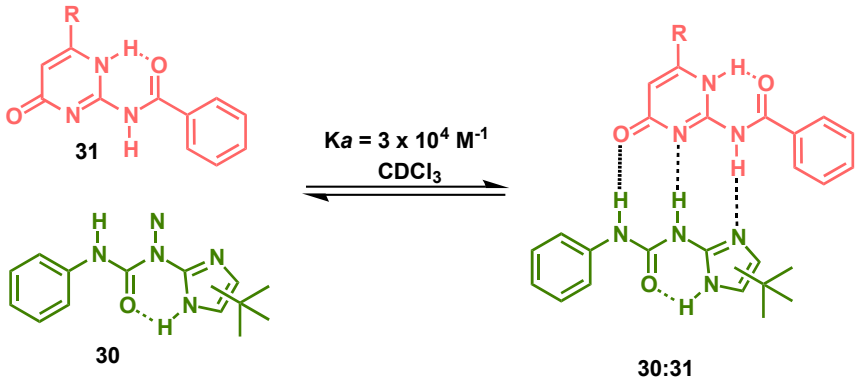

Figure 2.4 The association of AAD-DDA array UIM:AIC 30:31 in $CDCl_3$. R denotes Me

This heterocomplementary dimer, in combination with the promiscuous nature of the UPy motif **39** as documented by Zhao and colleagues, was appealing for construction of a new sequential self-sorting cascade. The self-complementary AADD homodimer of UPy **39** is known to be disrupted by addition of DAN **37**,[105] which is complementary to one of UPy's tautomeric forms, and could be used to our advantage (**Figure 2.5**).

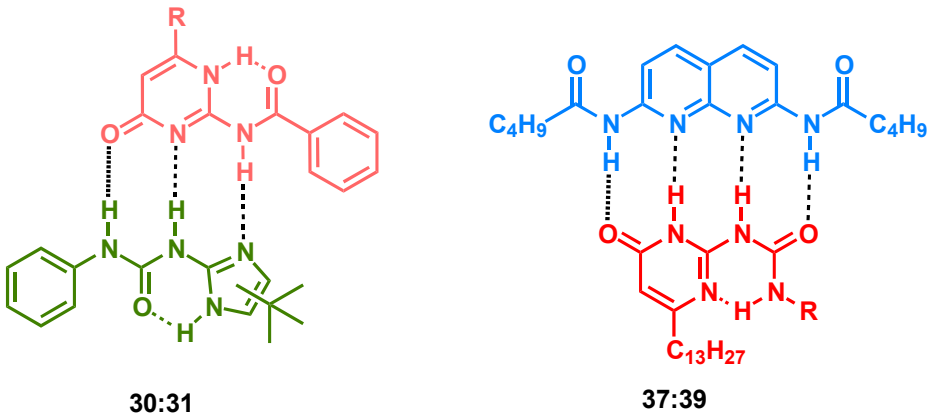

Figure 2.5 Proposed end-stage of self-sorting system investigated, using linear hydrogen bonding motifs. R on UPy 39 denotes *p*-ethyl benzoate. AIC 31 (pink), UIM 30 (green), DAN 37 (blue) and UPy 39 (red). R denotes Me for AIC

As documented by a previous member of the Wilson group (M. L. Pellizzaro), by carefully controlling the order of addition of four different components **Figure 2.5**, the specific complexes formed could be controlled.[106]

It was found that whilst AIC **31** shows high-fidelity behaviour by only associating with UIM **30**, the remaining components of the system display promiscuous

behaviour (**Figure 2.6**). Paths i and iii consider the effect on the system if addition of components is altered. Indeed, M. L. Pellizzaro found that by adding DAN **37** prior to AIC **31** results in the formation of an additional intermediate complex DAN:UIM **37:30**, which is not accessed *via* path ii. By employing path ii, the infidelity of UPy **39** and UIM **30** was exploited to exemplify a successful sequential self-sorting system.

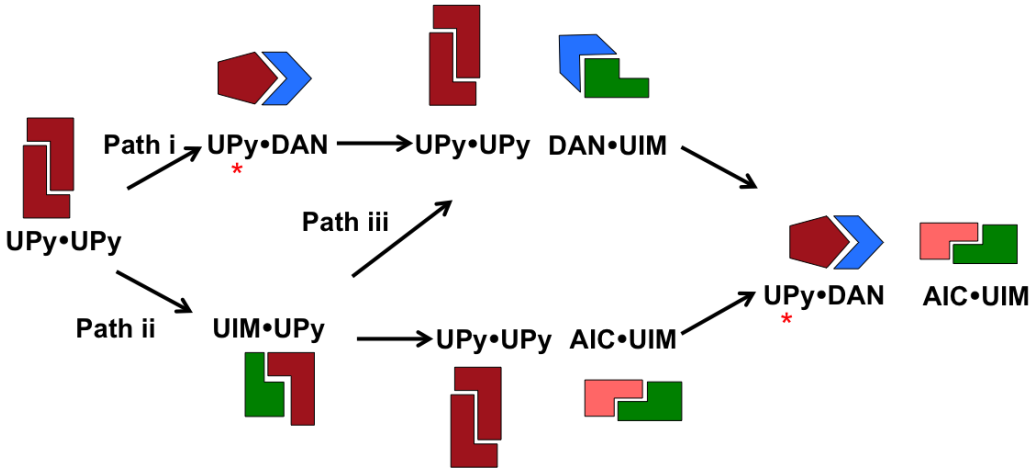

Figure 2.6. Schematic introducing the concept of dynamic orthogonal assembly. The complexes formed at each stage of addition are depicted. Red stars* indicate UPy 39 in tautomeric form

In path ii, the UPy homodimer **39:39** was broken upon addition of UIM **30**. Addition of AIC **31** regenerated the UPy homodimer **39:39** along with formation of the UIM:AIC **30:31** heterodimer. Addition of DAN **37** disrupts the UPy homodimer **39:39** to provide the UPy:DAN **39:37** heterodimer, whilst leaving the UIM:AIC **30:31** heterodimer undisrupted. The self-sorting system was followed *via* ^{1}H-NMR spectroscopy, confirmed by the presence, or absence, of diagnostic -NH signals relating to the UPy homodimer **39:39**.

With a successful self-sorting cascade established, we appended a photosensitive group **75** to AIC **31**, masking the hydrogen bonding array. The light-induced cleavage of a photolabile *ortho*-nitro-4,5-dimethoxybenzyl **75** group from AIC* **78** enabled us to 'trigger' a change in product distribution.

Synthesis of the photosensitive motif AIC* **78** (**Scheme 2.1** and **Scheme 2.2**) was achieved by nucleophilic attack of the isocytosine amine **74** on 4,5-dimethoxy-2-nitrobenzyl bromide **75**. Subsequent amide formation with benzoyl chloride **77** provided the product **78** in low yield.

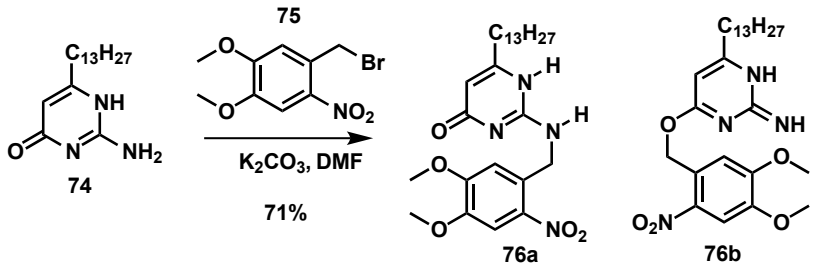

Scheme 2.1 –N and –O alkylation products 76a/b for the reaction between hydroxy pyrimidine 74 and *O*-nitro bromobenzene 75. 71% yield refers to recovery of –N and –O alkylation products *via* column chromatography. Ratio of –N and –O alkylated products was 50:50

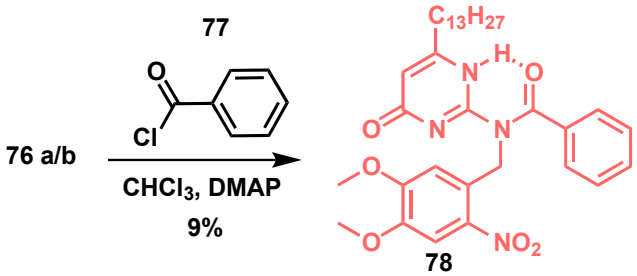

Scheme 2.2 Synthesis of light-sensitive AIC* 78 to be employed in the self-sorting cascade. 9% yield refers to using 1:1 equivalents of benzoyl chloride:–N and –O alkylated mixture

The low yield from this reaction originates from tautomerisation of amino-isocytosine **74a/b** (**Scheme 2.3**). A mixture of alkylation products was recovered from the first step, **Scheme 2.1**, which it was not possible to separate. Purification was therefore only possible after the amide formation step.

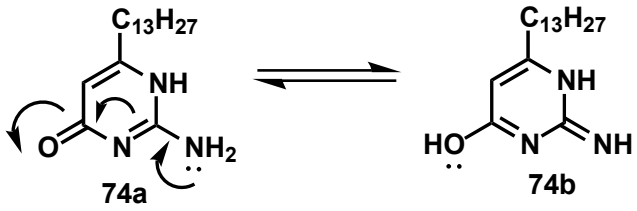

Scheme 2.3 Tautomerisation of amino-isocytosine 74a/b reveals a nucleophilic oxygen, resulting in a mixture of alkylation products

Alkylation products **76a** and **76b** could not be isolated individually by traditional column chromatography due to similar polarity. Amide formation only occurred with **76a**, enabling successful separation.

The Nuclear Overhauser effect (NOESY) spectrum of AIC* **78** shows that proton H_c (green), the benzyl -CH_2, has interactions with H_d and H_e, which correspond to the aromatic protons. The pyrimidine aromatic –CH, H_a (purple), shows interactions only with H_b, a proton of the solubilising -C_{13} alkyl chain. This indicates that the tertiary amide was the functional group isolated.

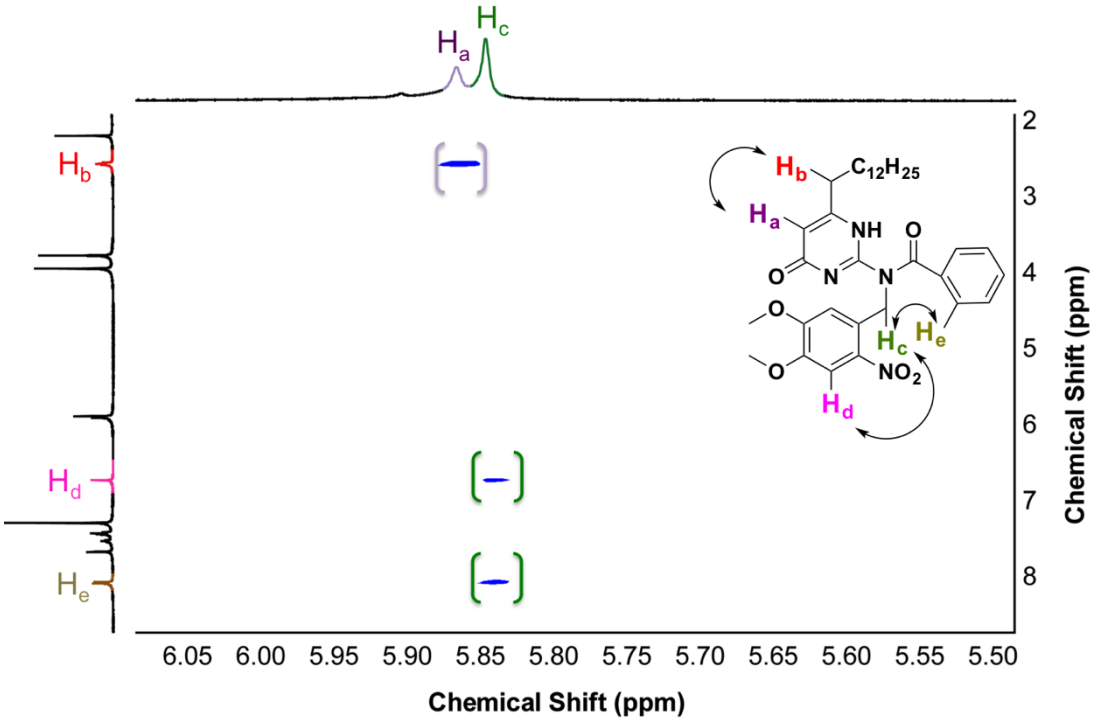

Figure 2.7 Partial ^{1}H NOESY spectrum of AIC* 78, showing the interactions through space of protons in proximity. Protons removed for clarity. $CDCl_3$ (10 mM), 293 K, 500 MHz

Cleavage of the photolabile group was achieved by irradiation with ultra- violet (UV) light. The UV spectrum of AIC* **78** (**Figure 2.8**) showed maximum absorbance between 250-300 nm. A solution of AIC* **78** in $CDCl_3$ (10 mM) was therefore irradiated at 254 nm for 4 hours under a lab-bench thin layer chromatography (TLC) lamp operating at this frequency.

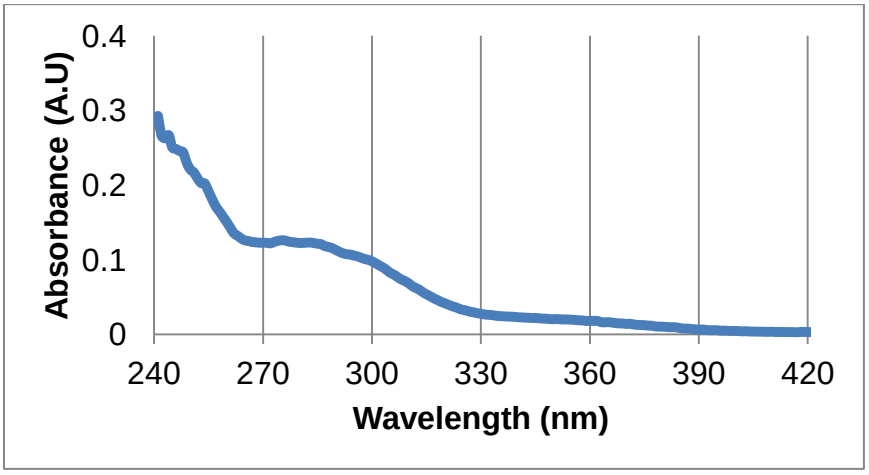

Figure 2.8 UV spectrum of AIC* (1 µM, $CDCl_3$)

After 4 hours irradiation time, the nitrobenzyl group was successfully cleaved as confirmed by liquid chromatography mass spectroscopy (LC-MS), **Figure 2.9**. The two degradation products, which are a consequence of radical formation in the nitro group, are the desired deprotected AIC triple hydrogen bonding array **79** and nitrosobenzaldehyde **80** (**Scheme 2.4**).

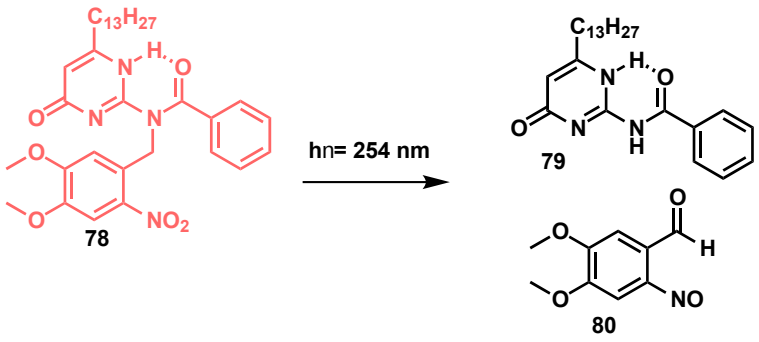

Scheme 2.4 Cleavage of the photolabile group by 254 nm UV irradiation. 2 hrs., 10 mM, $CDCl_3$

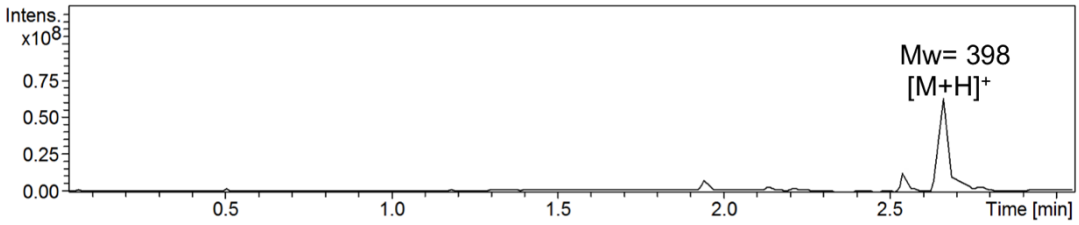

Figure 2.9 MS trace of the AIC* 78 solution post-irradiation. The molecular weight at 2.65 min corresponds to the mass of AIC hydrogen bonding unit 79

Only AIC unit **79** is seen in the LC-MS mass trace at 2.65 min, **Figure 2.9**, (labelled). After confirmation of the lability of the photosensitive group, the sequential self-sorting system developed (**Figure 2.5**), was recreated using AIC* **78** in place of AIC **31**.

As illustrated in **Figure 2.11**, incorporation AIC* **78** within the cascade to trigger product redistribution is successful. Addition of AIC* **78** to UPy **39** does not perturb the UPy homodimer **39:39**. This was unsurprising since AIC **31** has previously been shown to not to bind to UPy **39**.[106] Addition of UIM **30** to the mixture results in the disruption of the UPy homodimer **39:39** and formation of a UPy:UIM **39:30** heterodimer, demonstrating the success in masking of the AIC **31** hydrogen bonding array, as its preferred partner, UIM **30**, is present. After irradiation with UV light and hence removal of the protecting group, AIC **79** was liberated to sequester UIM **30** from UPy **39**, which is released to reform its homodimer **39:39**. Finally addition of DAN **37** breaks the UPy homodimer **39:39** to form an UPy:DAN **39:37** heterodimer, leaving AIC:UIM **79:30** intact.

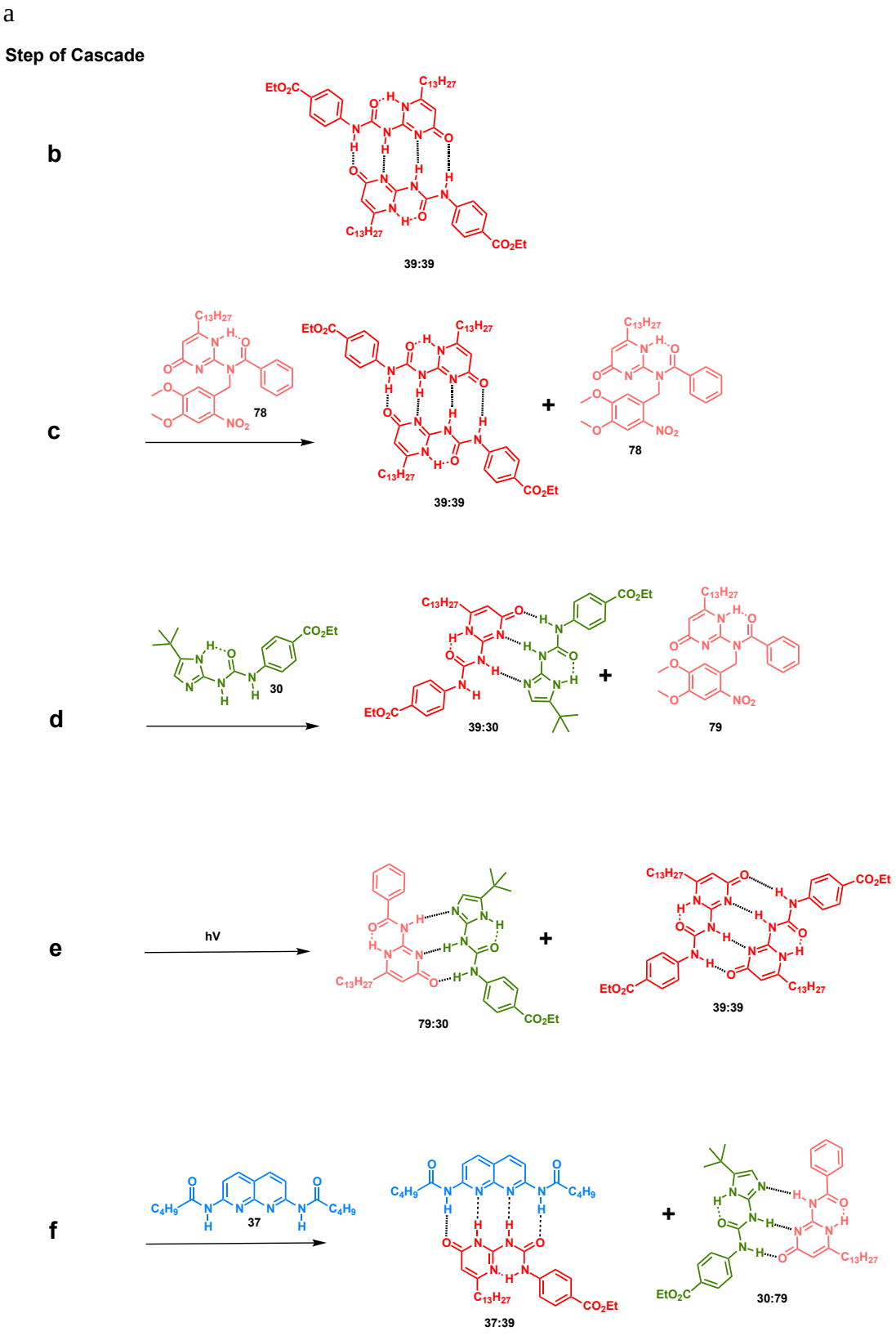

Figure 2.10 a) Signalling cascade using hydrogen bonding motifs 30, 79, 39 and 37. Step b) UPy homodimer 39:39 c) UPy 39 and AIC* 78 d) UPy 39 AIC* 78 and UIM 30 e) UPy 39, AIC 79, UIM 30 after irradiation for 4 hr., 254 nm and f) UPy 39, AIC 79, UIM 30 and DAN 37

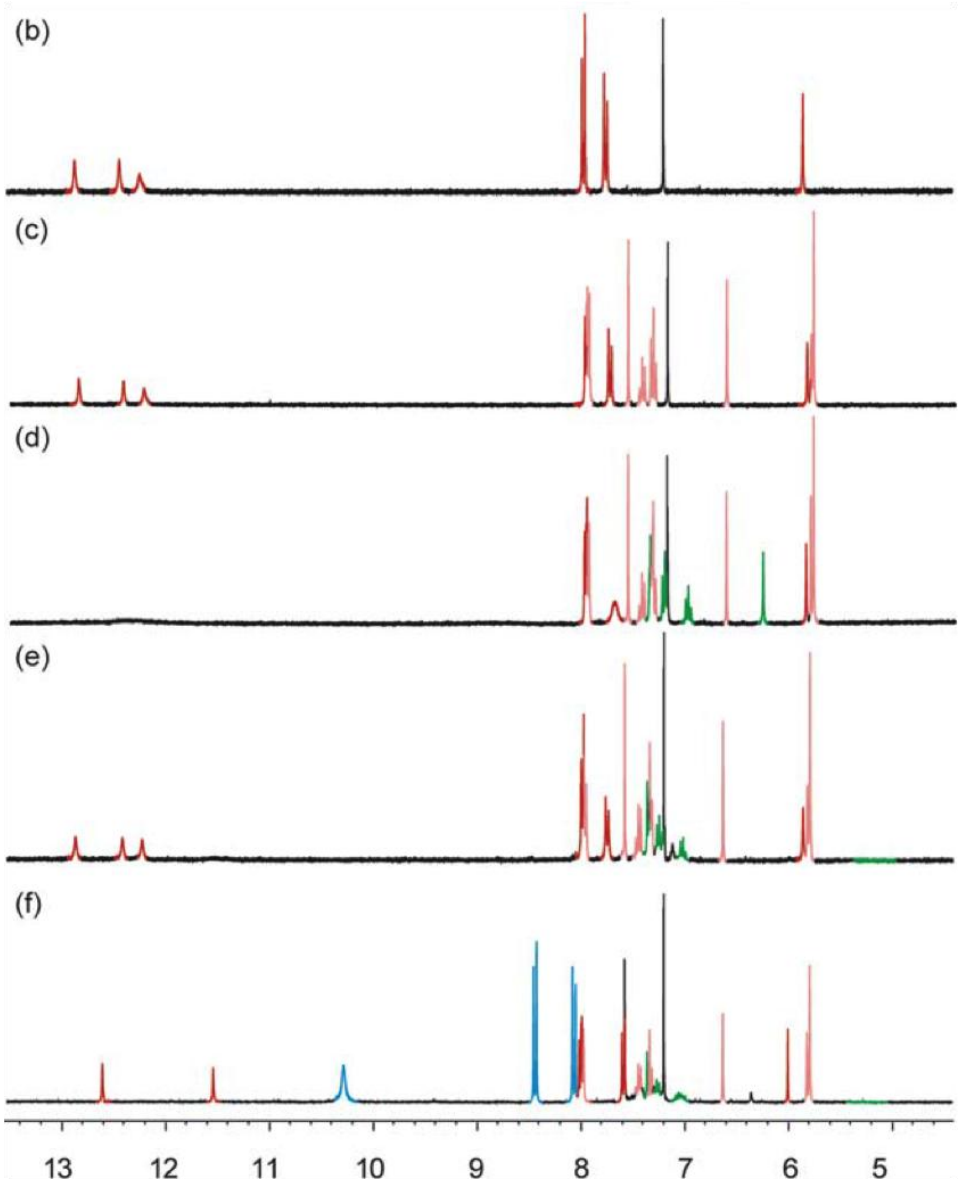

Figure 2.11 a) Signalling cascade using hydrogen bonding motifs 30, 79, 39 and 37. Step b) UPy homodimer 39:39 c) UPy 39 and AIC* 78 d) UPy 39 AIC* 78 and UIM 30 e) UPy 39, AIC 79, UIM 30 after irradiation for 4 hr., 254 nm and f) UPy 39, AIC 79, UIM 30 and DAN 37

2.3 Employment of orthogonal photo-labile protecting groups for application in extended self-sorting cascades

Successful (de) protection of the AIC unit **78/79** stimulated interest in the possibility of protecting another of the hydrogen bonding motifs *via* a similar strategy. Using two different light-sensitive appendages enables orthogonal deprotection and hence a well-controlled assembly mechanism.[107]

The photochemical behaviour of coumarin is a very well understood and explored.[108] It is known that substitutions on coumarin ring **81** (4' position), or at the 6' or 7' position (**Figure 2.12**) tune the absorption wavelength and hence the UV spectrum of the molecule.[109-113]

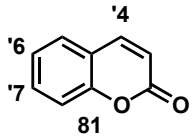

Figure 2.12 Available substitution positions on a coumarin molecule 81

The UV spectrum of AIC* **79** shows an absorbance between the wavelengths of 250-300 nm, hence for an alternative photolabile group to be orthogonal to AIC* **79**, the photoactive group would need to absorb in the region above 300 nm for selective cleavage. By functionalising coumarin **81** with –OH in the '7 position and –Br in the '6 position (bromohydroxycoumarin, BHC) **85**, λ_{max} is increased above 365 nm in comparison to unsubstituted coumarin.[110] Distefano and colleagues have shown uncaging of a bioactive molecule protected with BHC.[109] The wavelength required to cleave the BHC photolabile group was lengthened, and entered the infra-red (IR) region (**Figure 2.13**).

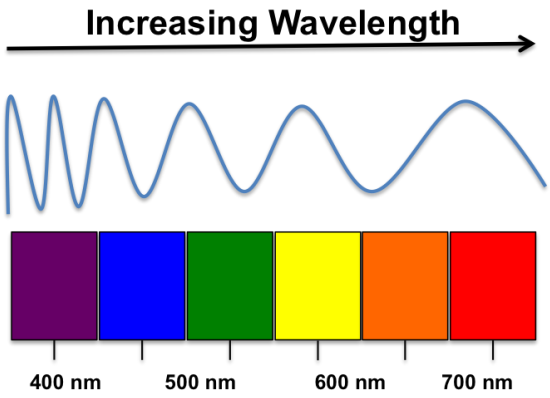

Figure 2.13 Wavelengths of light. The highest frequency, violet, is used for cleavage of the nitrobenzene group 75, whereas lower frequency could be used for BHC 85

Synthesis of a BHC **85** was attempted *via* a modified procedure reported by Tsien *et al*. **Scheme 2.5** [110, 111, 114]

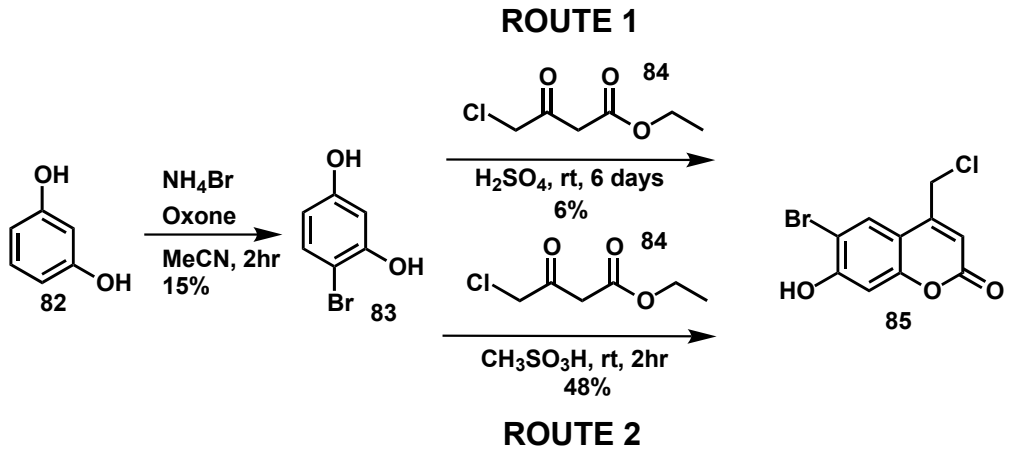

Scheme 2.5 Synthesis of BHC 85 reported by Tsien *et al*. (Route 1). Introducing Route 2 as an alternative, after low yielding Route 1, modified the procedure

Resorcinol **82** was subjected to oxybromination to afford the mono-brominated dihydroxyl compound **83**. Subsequent dissolution in sulfuric acid for 6 days gave low yields of the desired compound, in comparison to the 59% achieved in the literature preparation,[111] and hence an alternative was sought. It was found that condensation of the halogenated resorcinol **83** with 4-chloroacetoacetate **84** was more efficient in methane sulfonic acid,[110] yielding the desired product **85** in 48% yield.

With the BHC **85** in hand, we concluded that attachment of the photolabile group to a high-fidelity hydrogen bonding unit would be able to trigger successful product redistribution in the same way that AIC* **79** was able to in the original cascade (**Figure 2.11**). In the proposed cascade, the most suitable hydrogen bonding unit after AIC **79** was DAN **37**.

DAN **37** has a suitable potential substitution point for the photo labile group. The amide nitrogen could be alkylated to provide the desired target molecule **86** (**Figure 2.14**).

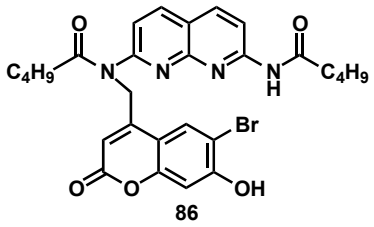

86

Figure 2.14 Proposed structure of DAN substituted with a photolabile coumarin

Several synthetic routes were proposed for coumarin functionalised DAN **86**. DAN **37** is accessed using a four-step synthesis (**Scheme 2.6**).[115]

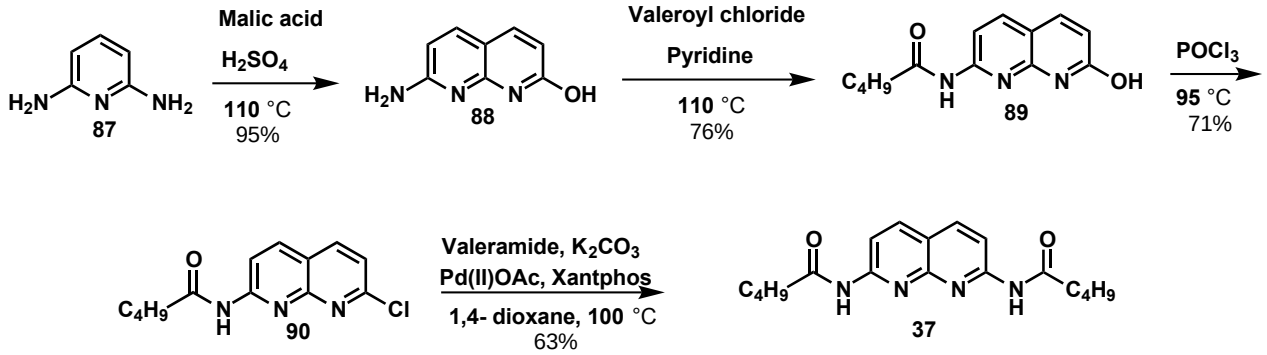

Scheme 2.6 Synthesis of DAN 37

There were three stages in the synthesis of DAN **37** at which functionalisation with the coumarin **85** was feasible. After the first amidation (**Scheme 2.7**), purified compound **89** was reacted in dimethylformamide using bases of differing strength.

When potassium carbonate did not yield any alkylation products, sodium hydride was tested.

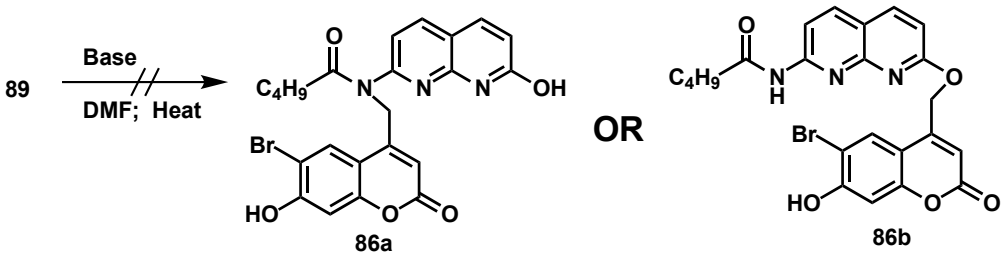

Scheme 2.7 Functionalisation of DAN 37 during synthesis. Base= NaH or K_2CO_3.

The reaction did not give the desired product, and starting material was recovered (100%). The same reaction was performed at two different points in the synthesis of DAN **37** (**Scheme 2.8**). These were also found to fail, and starting material was again recovered (100%) *via* column chromatography.

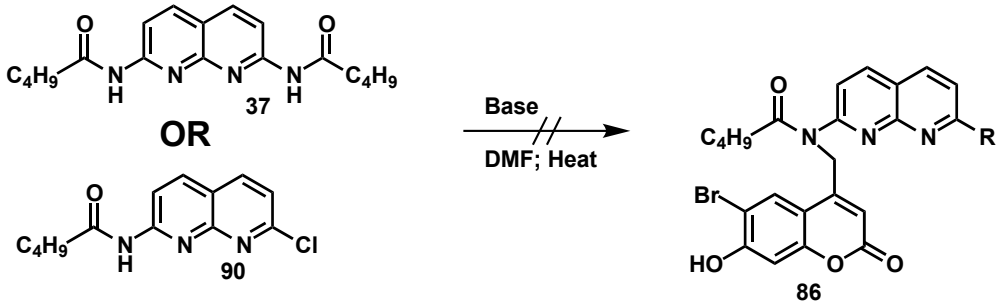

Scheme 2.8 Functionalisation of DAN 37 during synthesis. Base= NaH or K_2CO_3. R signifies Cl or C_4H_9.

Due to the aforementioned failure, it was postulated that the alkyl chloride group of the coumarin moiety was not an effective enough alkylating agent for the reaction to take place. By preparing alternative coumarin alkyl halides using the Finkelstein modification,[116, 117] replacing the chloride anion with bromine or iodine could result in successful functionalisation.

2.4 An alternative self-sorting cascade

Functionalisation of DAN **37** with a photolabile group was unsuccessful, so as a consequence an alternative hydrogen bonding unit was sought, which would be able to trigger successful product redistribution. Reported by Sijbesma and colleagues, functionalised naphthrydinones (NapyO) **89**, were shown to form homodimers with K_{dim}= 6 x10^3 M^{-1}, but even stronger heterodimers with UPy (K_a= 5 x10^5 M^{-1}), when UPy was functionalised with an electron donating group (in this instance dibutylamine) **91** at the 4- position (**Figure 2.15**).[118, 119]

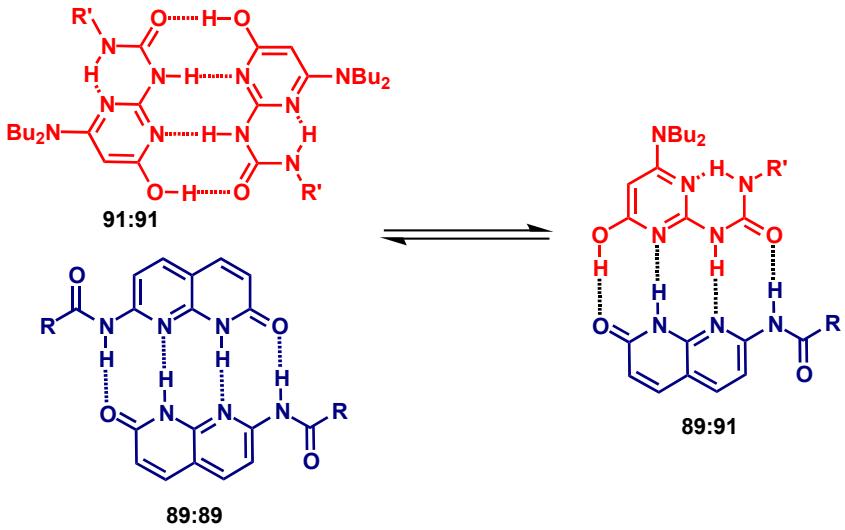

Figure 2.15 Equilibrium between UPy 91 and NapyO 89 homo- and heterodimers. R signifies C_4H_9, R' denotes $C_{12}H_{25}$

If we were to incorporate NapyO **89** into our self-sorting cascade, we firstly needed to see how NapyO **89** interacted with the other members of the cascade. NapyO **89** is one of the intermediate compounds from the synthesis of DAN **37** (**Scheme 2.9**).

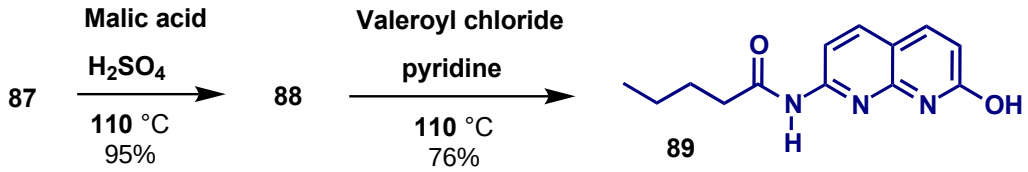

Scheme 2.9 Two-step synthesis of NapyO 89 from diaminopyridine 87 adapted from[115]

NapyO **89** is capable of tautomerising (**Figure 2.16**), presenting two different hydrogen bonding arrays. Only the keto- form **89b** is self-complementary, which could affect the recognition behaviour of NapyO in solution towards other hydrogen bonding arrays.

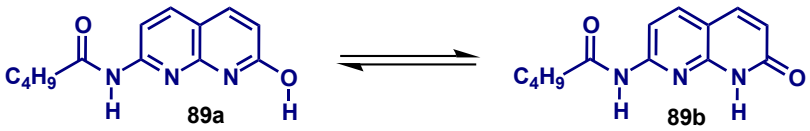

Figure 2.16 Tautomerisation of NapyO between enol 89a and keto 89b forms

A 10 mM solution of NapyO **89** in $CDCl_3$ enabled assignment of the tautomeric form *via* extensive 2D NMR experiments.

NOESY was used to explicitly assign the aromatic protons and the secondary amide proton, **Figure 2.17**. From this assignment, heteronuclear multiple-quantum correlation (HMQC) spectroscopy was used in conjunction with heteronuclear multiple-bond correlation (HMBC) spectroscopy to assign each carbon on the molecule.

Figure 2.17 shows interaction between H_a, which can be attributed to the alkyl –CH_2 and H_b, characteristic for –NH, as it is broad and shifted downfield. This can be assigned to interaction of the secondary amide nitrogen and the alkyl chain. H_c at 12.8 ppm is present due to the tautomerisation in the oxo-naphthrydine unit (**Figure 2.16**). Cross-peaks seen between H_b and H_c are indicative of the dimerisation of NapyO **89** (**Figure 2.17**). NapyO **89** can only self-associate as the keto tautomer **89b**, and hence at 10 mM in $CDCl_3$ at room temperature we can assume NapyO is present in this tautomeric configuration.

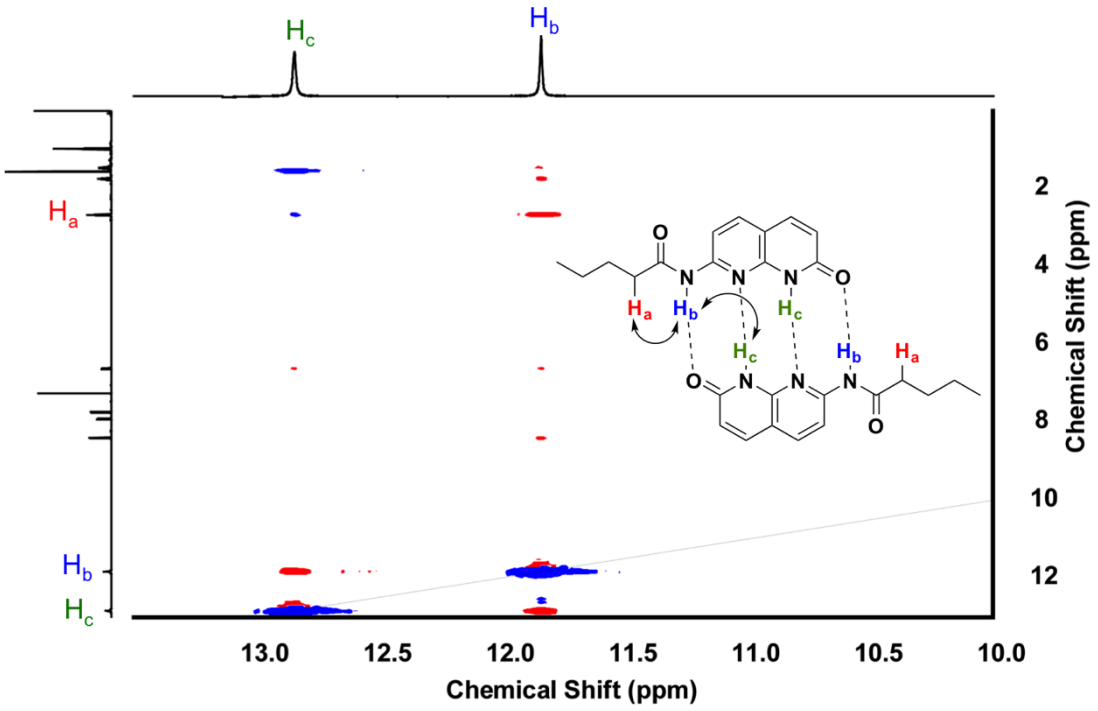

Figure 2.17 Partial ^{1}H NOESY NMR spectrum of NapyO 89b. Protons omitted for clarity. 300 MHz, 10 mM, $CDCl_3$, 293 K

From HMQC and HMBC NMR experiments, we could corroborate this assumption, by looking at the heteronuclear through-bond coupling in the molecule.

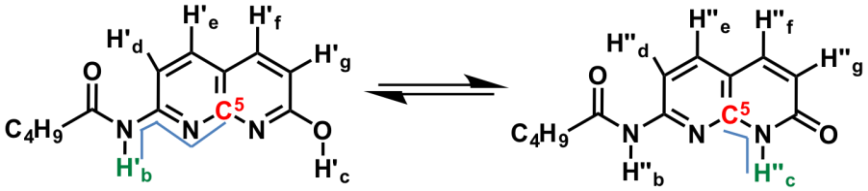

89a **89b**

Figure 2.18 Labelling of carbon and hydrogen atoms of NapyO 89a/b referred to below. *J* coupling shown by blue lines

HMBC confirmed the keto tautomer **89b** as H_c was shown to strongly couple with C_5, representing a $^{2}J_{CH}$ coupling. In the enol tautomeric form, this coupling would be from a $^{4}J_{CH}$ coupling, and would appear to be less intense, if the correlation could be seen at all.

With this information in hand, it was investigated if dissolution in $CDCl_3$ with some of the partners of cascade **Figure 2.11 31, 39, 92** and **37**, **Figure 2.19**, altered the preference for the keto, and hence dimeric form of NapyO **89b**.

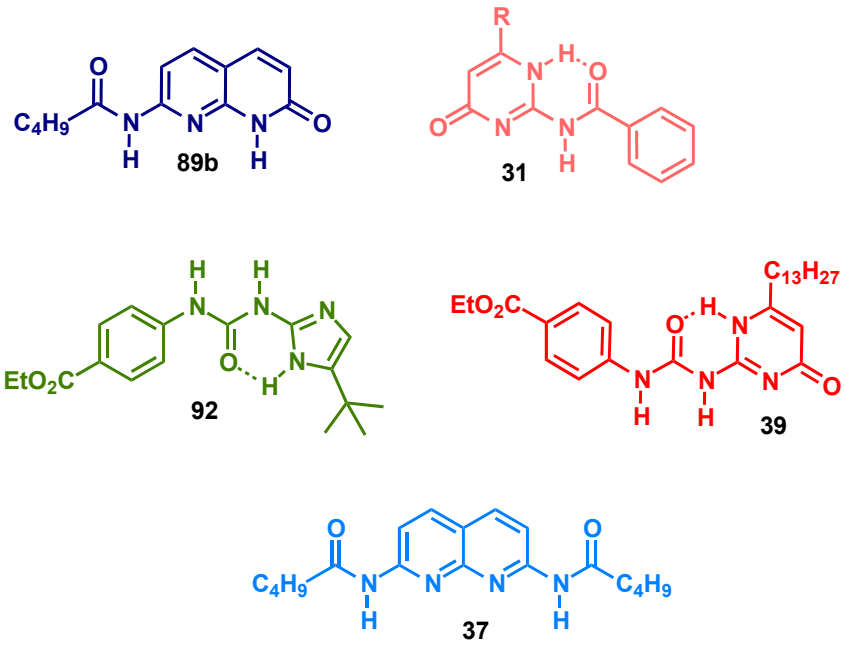

Figure 2.19 Hydrogen bonding motifs involved in the investigation of NapyO interactions. R is Me group

In line with the experiments conducted by Sijbesma and colleagues, we took 4-alkyl substituted UPy **39**, and recorded ^{1}H-NMR spectra, both with and without NapyO **89** in equimolar amounts.

Sijbesma and colleagues previously used an electron donating group at the 4-position, in which UPy favours the keto tautomeric form,[119] displaying a DADA hydrogen bonding array, which complements the ADAD array of NapyO **89** (**Figure 2.15**). In spite of the high number of disfavourable secondary interactions (**Figure 2.20**), the heterodimer was found to associate with 5 x 10^5 M^{-1}.[119] It was expected that NapyO would still be to be able to disrupt the UPy homodimer, when UPy was substituted with a less electron-donating group, **39**.

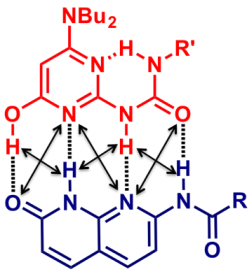

Figure 2.20 Secondary interactions arising from the formation of an UPy:NapyO heterodimer. Black solid double-headed arrows show unfavourable interactions. R signifies C_4H_9, R' is $C_{12}H_{25}$. NBu_2 is dibutylamine

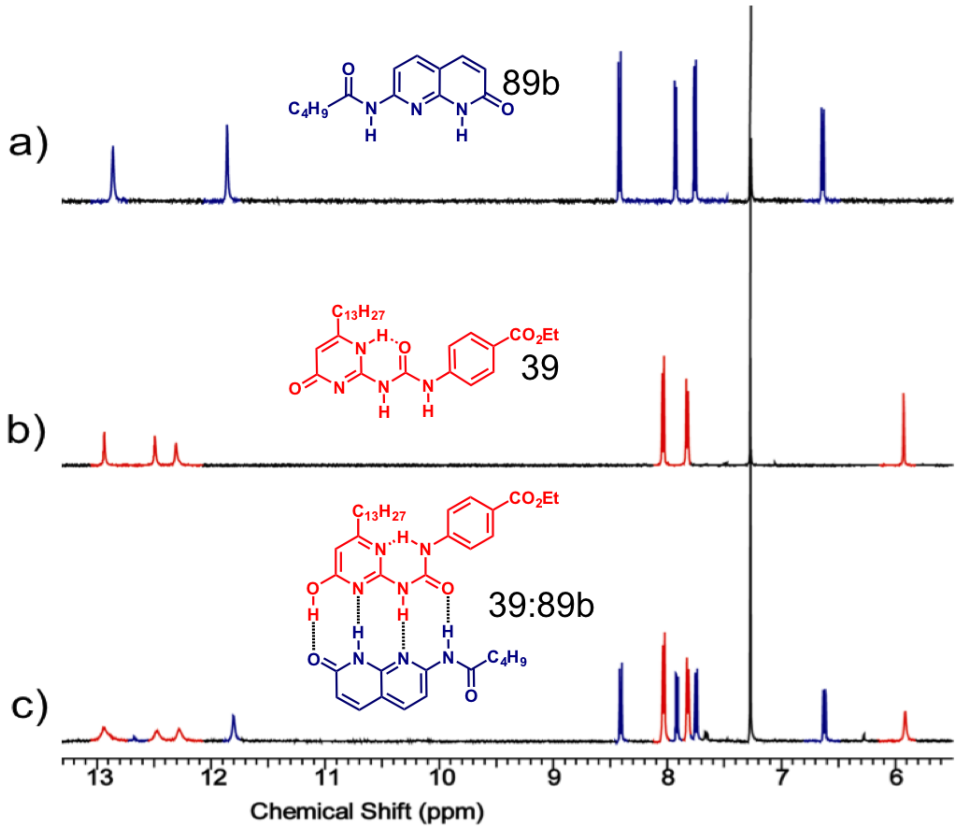

Figure 2.21 ^{1}H-NMR spectra, 300 MHz, 10 mM, $CDCl_3$, 293 K stackplot showing a) NapyO 89b, b) UPy 39 c) NapyO and UPy equimolar mixture

As we hypothesised, the –NH shifts for both NapyO **89** and UPy **39** were broadened and shifted, albeit not greatly, but was significant for the indication of complex formation (**Figure 2.21**). The pyrimidine proton of UPy **39** (5.9 ppm) was also seen

to shift and broaden, in good agreement with previous studies on the recognition behaviour of UPy.[45]

The NMR sample from **Figure 2.21** was subjected to ESI-HRMS to confirm the presence of UPy:NapyO **39:89** complex formation (**Figure 2.22**). The 10 mM mixture of NapyO **89** and UPy **39** showed both the presence of NapyO homodimers and **89:89** UPy:NapyO **39:89** heterodimers.

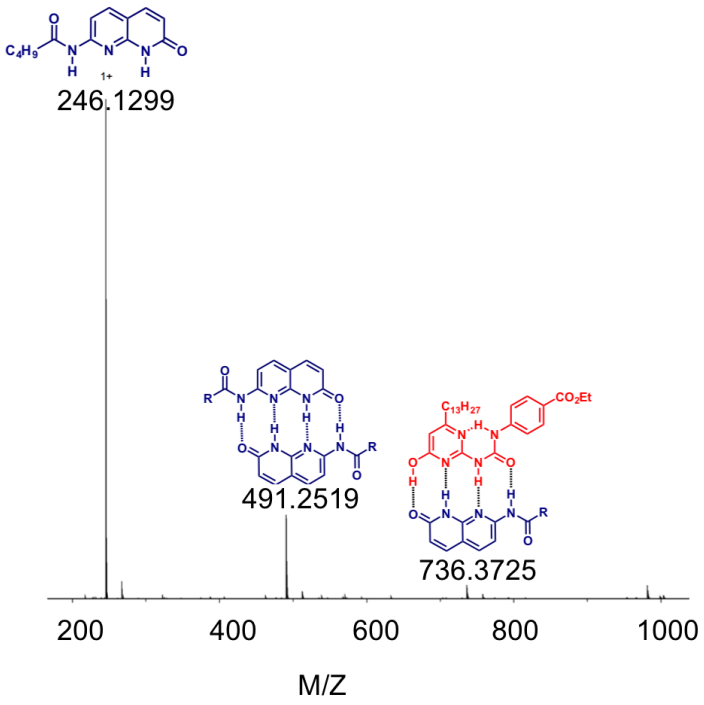

Figure 2.22 ESI-HRMS of a 10 mM solution of NapyO 89 and UPy 39 ($CDCl_3$, 293 K)

Because NapyO **89** was able to disrupt the UPy homodimer **39:39** to a degree, NapyO **89** was incorporated into a modified cascade (**Figure 2.23**). The pertinent association constants for all components of the cascade, which interact with NapyO **89** are on-going within the Wilson Group. All other association constants between the remaining members of the cascade had been previously measured by ^{1}H-NMR titrations, or taken from recent literature.

Table 2.1 Values for association constants for homo- and hetero- dimers (M^{-1}) of all molecules presents in the cascade

Complex	K_a/K_{dim} M^{-1}
AIC:AIC **31:31**	3.6 ± 0.3[120]
AIC:UIM **31:92**	$84 \times 10^3 \pm 22$[120]
AIC:UPy **31:39**	Negligible[64]
AIC:DAN **31:37**	Negligible[64]
UIM:UIM **92:92**	10 ± 2.2[120]
UIM:UPy **92:39**	$6.8 \times 10^4 \pm 9629$[64]
UIM:DAN **93:37**	$2 \times 10^3 \pm 40$[64]
UPy:UPy **39:39**	6×10^7 [121]
UPy:DAN **39:37**	4×10^5 [122]
DAN:DAN **37:37**	5[64]

NapyO **89** was introduced in step 1 of the cascade described in **Figure 2.23**, reproducing the broadening and shifting of all –NH peaks previously witnessed in **Figure 2.21** and possessed a similar HRMS pattern to **Figure 2.22**. Although a higher K_{dim} for UPy **39:39** is seen in comparison to the K_a of UPy:NapyO **39:89**,

UPy:NapyO **39:89** forms in addition to the UPy homodimer **39:39**. Heterodimerisation is favoured in this instance due to a higher number of hydrogen bonds being satisfied. During the cascade, the remainder of the self-sorting steps were also subjected to ESI-HRMS to inspect the complexed species present.

The addition of UIM **93**, showed NapyO **89** to be promiscuous, forming heterodimers with both UPy **39** and UIM **93** and a NapyO homodimer **89:89** as confirmed by electrospray ionisation high-resolution mass spectrometry (ESI-HRMS). (See Appendix 7.1)

Addition of AIC **31** promoted the formation of UIM:AIC **93:31** heterodimers as the major complexation product. Small amounts of UIM **93** were also seen to form heterodimers with UPy **39**, which returned to a mix of UPy:UPy **39:39** homodimer and UPy:NapyO **39:89** heterodimer.

Finally, addition of DAN **37** further altered the product distribution. AIC:UIM **30:93** and UPy:DAN **39:37** were seen as the major products by NMR, whilst ESI-HRMS showed small amounts of the UIM:DAN **93:37** heterodimer (See Appendix 7.1).

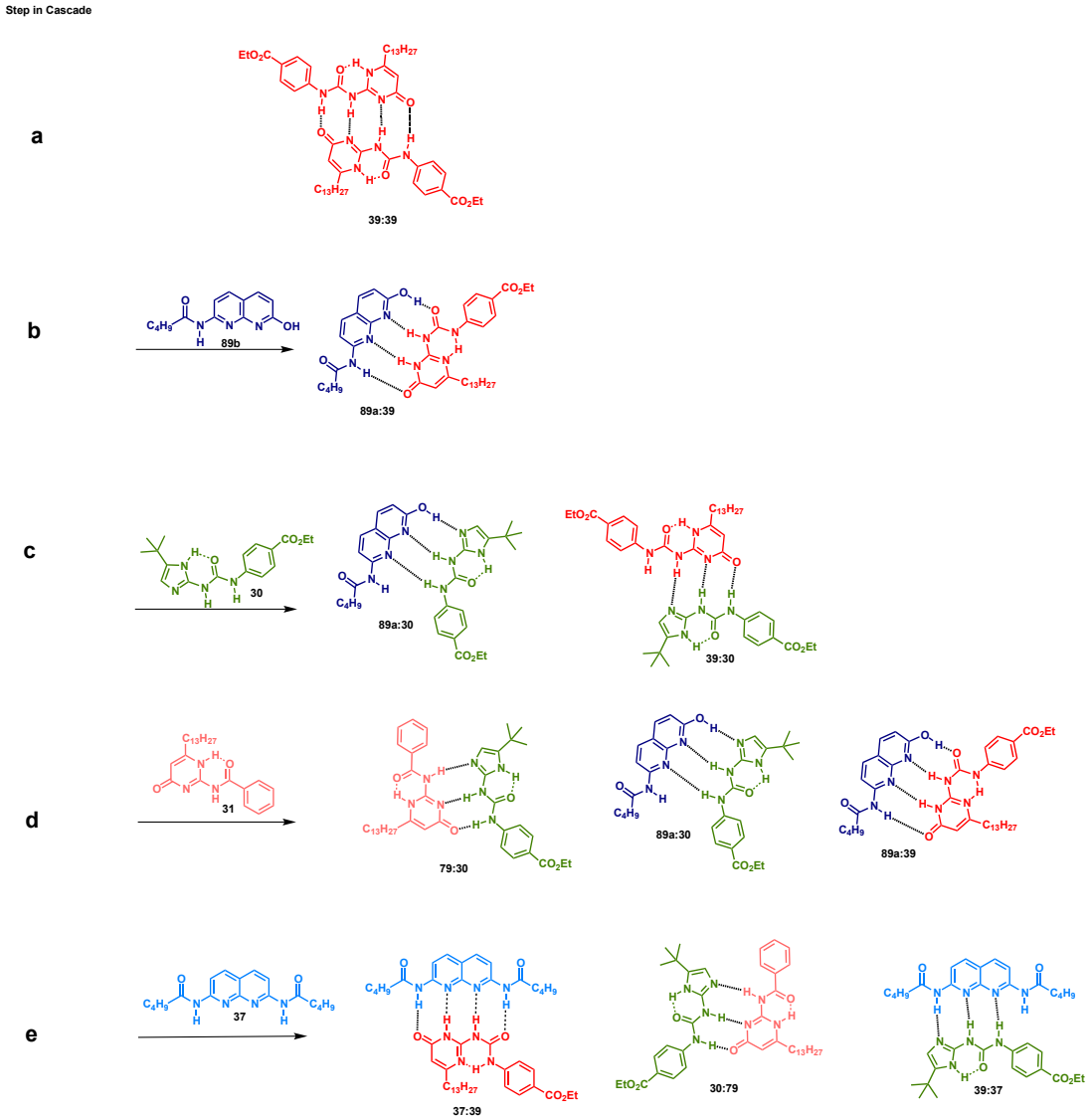

Figure 2.23 Schematic to illustrate the major hydrogen bonded complexes forming during the assembly process as seen by ^{1}H NMR and ESI-HRMS

The self-sorting behaviour of the cascade, *i.e.* the partners the system choses, shows that maximisation of non-covalent interactions; hydrogen bonds in particular, are what drive the changes in product distribution observed throughout the experiment.

It was shown in both the first cascade with photo cleavable AIC* **78** (**Figure 2.11**) and second cascade with an additional member (**Figure 2.24**), that these systems require components which are promiscuous in behaviour. When at least one member of the cascade has high-fidelity (*e.g.* AIC **31** in both of these cases), and can only recognise a limited number of components within the mixture, fidelity of the overall

system is increased,[64] in line with results observed by Zimmerman and colleagues.[123]

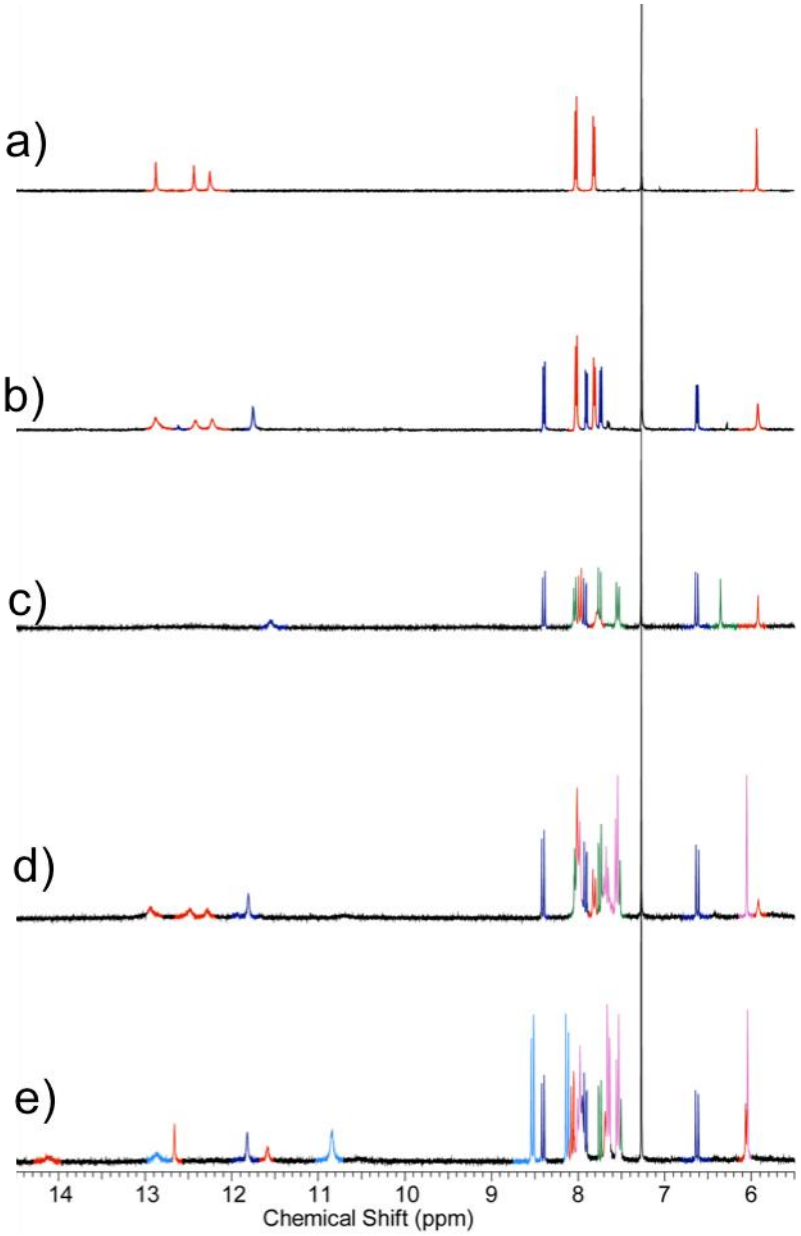

Figure 2.24 ^{1}H NMR spectra, 300 MHz, 10 mM, $CDCl_3$, 293 K stackplot showing a) UPy 39 b) NapyO 89 and UPy 39 c) NapyO 89, UPy 39 and UIM 93 d) NapyO 89, UPy 39, UIM 93 and AIC 31 e) NapyO 89, UPy 39, UIM 93, AIC 31 and DAN 37

2.5 Design of additional hydrogen bonding units for orthogonal self-assembly

Additional fidelity is imparted to a self-sorting system by a motif capable of recognising limited partners. Hydrogen bonds are already known to play a critical role in the function of proteins, for example in binding ligands and in folding.[124] Strongly electronegative atoms, for example nitrogen and oxygen, are considered traditional hydrogen bond acceptors and donators. Sulfur is an overlooked hydrogen bond participant due to its low electronegativity, but it had been found to contribute to conformational properties found in some crystals.[125]

Using a modified procedure, an ureidothiazole (UTIZ) **97** was synthesised to probe the effects of exchanging hydrogen bond acceptors for other members of group 6 in the periodic table (**Scheme 2.10**).[126, 127]

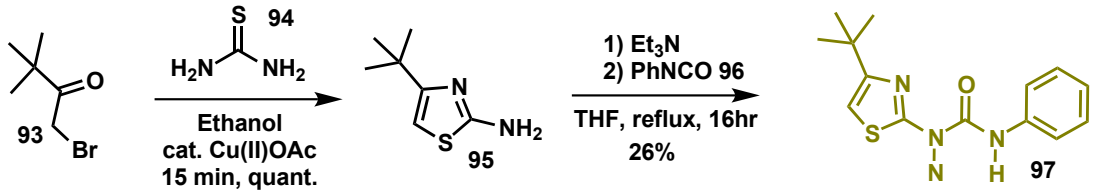

Scheme 2.10 Synthesis of thiazole urea 97 from a β-keto halide 93 catalysed by Cu(II)

The synthesis and isolation of UTIZ **97** was achieved in 26% yield and subsequently the recognition behaviour was investigated.

UIM **30** is known to make hydrogen bonding interactions with AIC **31**, UPy **39** and DAN **37**, which provided a starting point to study the association behaviour of UTIZ **97 Figure 2.25**.

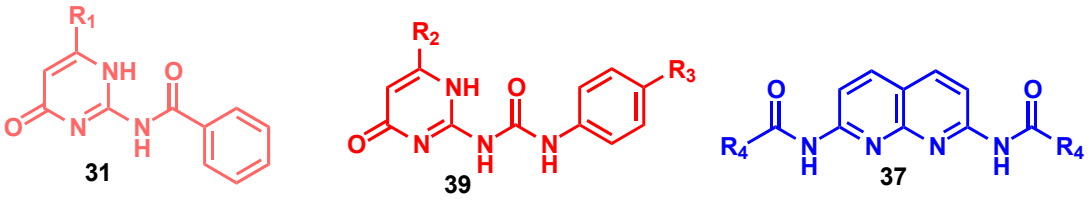

Figure 2.25 Known hydrogen bonding partners to UIM: - AIC 31, UPy 39 and DAN 37. R_1 denotes Me R_2 denotes $C_{13}H_{27}$, R_3 denotes ethyl benzoate and R_4 denotes C_4H_9

A 10 mM solution in $CDCl_3$ of each of the known hydrogen bonding partners, **Figure 2.25**, of UIM **30** was subjected to ^{1}H NMR. Subsequently, an equimolar amount of UTIZ **97** was added, and the ^{1}H NMR repeated to observe any complex formation induced shifts.

As shown in Appendix II: a-c, no complex formation was seen for any of the three proposed partners. This initial result was promising, as orthogonal assembly in a solution containing both UIM **30** and UTIZ **97** became a possibility.

The hydrogen bonding array of UTIZ **97** could not be identified through finding a binding partner. After crystallisation trials of UTIZ **97** failed, which would show the preferred conformation of the molecule, additional hydrogen bonding units in our library were assessed for complex formation with UTIZ **97**, DAP **98** and n-alkyl thymine (AThy) **99**. The library of molecules contains all hydrogen bonding motifs previously studied by the Wilson Group.

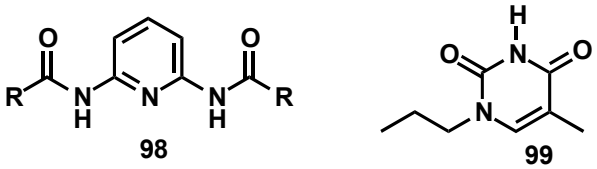

Figure 2.26 Structures of two additional hydrogen bonding units assessed for complex formation with UTIZ 97. R denotes C_6H_{13}

DAP **98** is structurally close to DAN **37**, but possesses a different hydrogen bond array (DAD, as opposed to DAAD). Hydrogen bonded complexes are governed not only by hydrogen bonding itself, but also by additional non-covalent forces, such as secondary interactions. Removal of the fourth donor/acceptor unit present in both

UPy **39** and DAN **37**, could avoid the occurrence of an additional destabilising secondary interaction with a heterocomplementary partner, increasing the stability of the system by approximately 3 kJ mol^{-1}.

As shown in Appendix 7.2, no association was seen as no complexation-induced shifts were observed for UTIZ:DAP **97:98**.

The final hydrogen bonding unit tested for association to UTIZ **97** was AThy **99**. Thymine **22** is known to hydrogen bond to adenine **21** *via* two hydrogen bonds, remaining selective during DNA transcription with other hydrogen bonding motifs present.

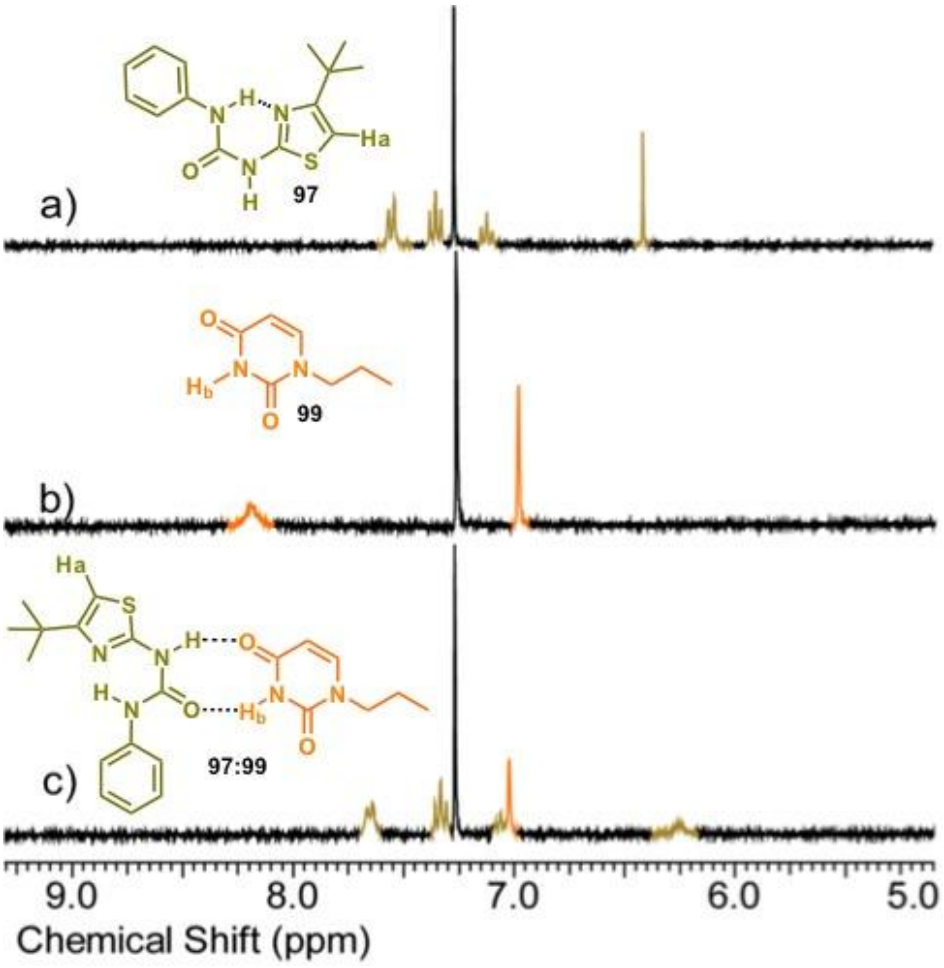

Figure 2.27 ^{1}H NMR spectra, 300 MHz, 10 mM, $CDCl_3$, 293 K stackplot showing a) UTIZ 97 b) AThy 99 c) UTIZ 97 AThy 99 equimolar mixture.

Comparison of the individual ^{1}H-NMRs with equimolar solution showed complexation induced shifts (**Figure 2.27**). The thiazole ring proton at ~6.5 ppm

shifted upfield indicating an increase in electron density and broadened substantially upon addition of AThy **99**. The AThy **99** –NH (~8.2 ppm) broadened and disappeared into the baseline, suggesting a substantial change in proton environment.

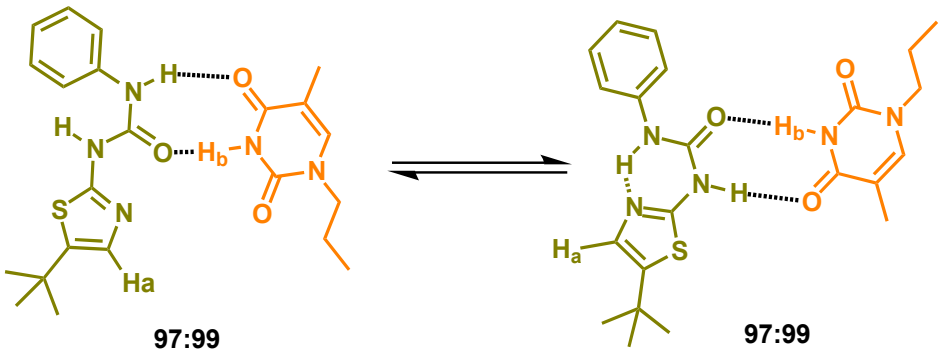

Figure 2.28 Proposed structures of the UTIZ-AThy 97:99 complex

Figure 2.28 proposes a structure for the complexation of **97:99**. UTIZ **97** adopts a trans-urea conformation to display a complementary AD array comparable to that shown by adenine **21**. To investigate assembly of the complex, small aliquots of a concentrated solution of AThy **99** in $CDCl_3$ were added to UTIZ **97**. After each aliquot addition, a ^{1}H-NMR was acquired, and the extent of complexation induced shifts observed (**Figure 2.29**).

As increasing amounts of guest were added, a substantial broadening was seen in H_a after 0.25 equivalents of AThy **99**. This could result from a change in conformation, or proximity to the guest molecule. Proton H_b of the guest was not seen as small aliquots are added, in line with previously observed, upon direct equimolar mixing of the host and guest molecules. As the guest concentration reached two equivalents, H_b was seen to increase in intensity and was shifted by 1 ppm downfield compared to that observed in the individual molecule. Such a large downfield shift is indicative of decrease of electron density on the proton, in accordance with shifts observed for AThy **99** with other hydrogen bonding molecules.[128]

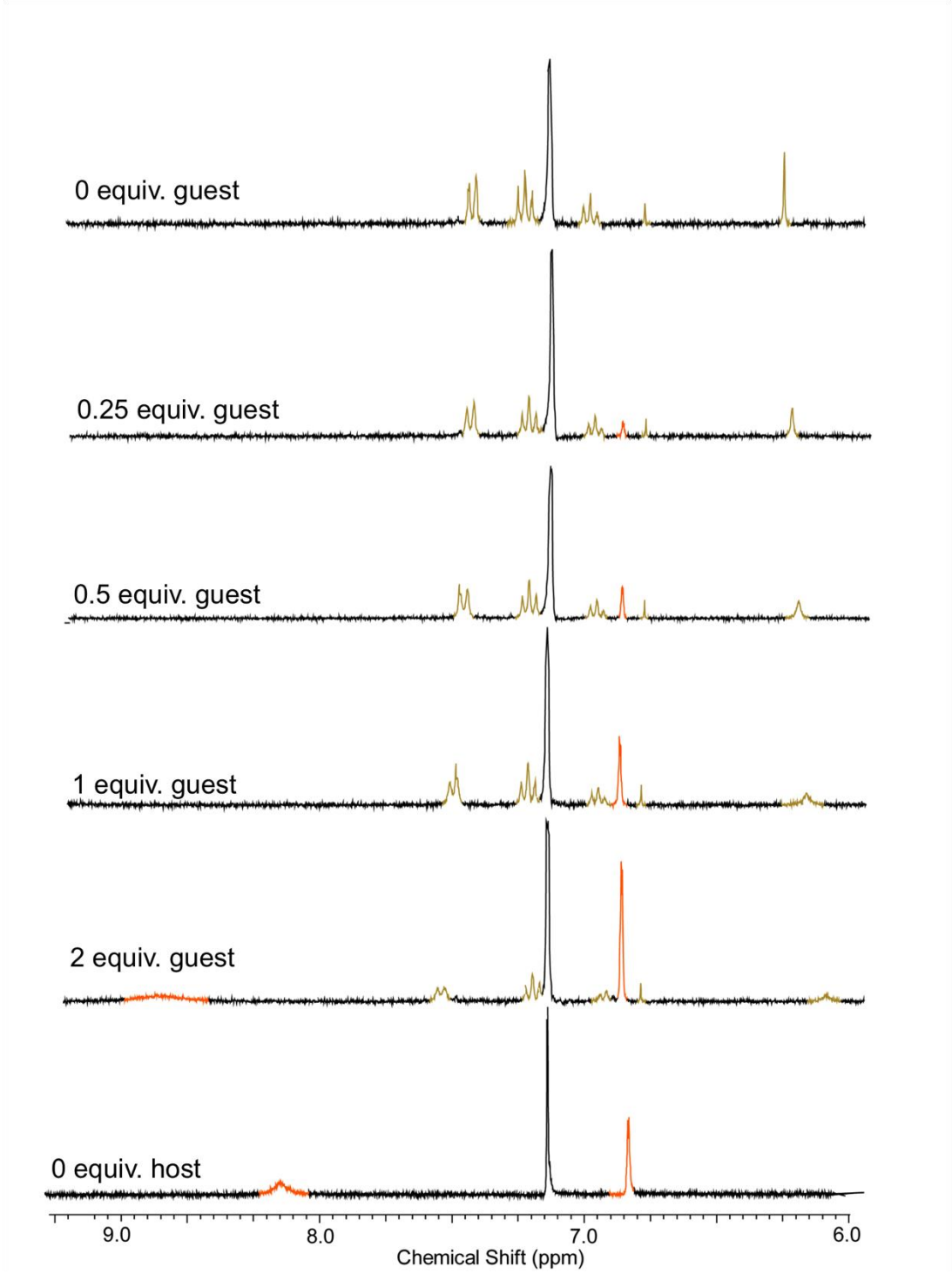

Figure 2.29 ^{1}H NMR spectra, 300 MHz, 10 mM, $CDCl_3$, 293 K stackplot showing the spectrum of UTIZ 97 after adding aliquots of AThy 99 as a guest. Complexation induced shifts were observed.

The binding strength of the UTIZ:AThy **97:99** complexation is currently under investigation within the Wilson Group.

2.6 Conclusions

It has been shown that simple hydrogen bonding motifs can be used in concert to perform complex behaviour, and are able to self-sort in a sequential manner based on the composition and order of addition to the system. It has also been shown that it was possible to alter the product distribution in the system by appending a photolabile group to one of the recognition motifs and cleaving it.

We extended this self-sorting cascade by introducing a new motif, based on DAN. NapyO showed promiscuous behaviour, associating with two other hydrogen bonding motifs as well as homodimerising. As a result, broadening in the ^{1}H-NMR was caused due to the large mix of conformational states and chemical environments.

The idea of orthogonal recognition was further advanced during this chapter, by the observation that UTIZ does not follow similar association behaviour to its sister molecule UIM. The level of association between UTIZ and AThy is significant, and this pairing could be included in future research for further modification of self-sorting cascades.

Chapter 3

Self- assembled supramolecular polyurethanes

3 Chapter 3

3.1. Self Assembled Thermoplastic Polyurethanes Using UIM and AIC Hydrogen Bonded Arrays

Traditional covalent polymers have diverse application, evidenced in everyday life. Thermoplastic polyurethanes (TPUs) in particular, due to their modular synthesis, exhibit a varied array of properties based on the components used for synthesis.[6]

TPUs benefit from the alternating nature of AB block copolymer morphologies, where strongly interacting crystalline segments containing hydrogen bonding units alternate with weakly interacting amorphous segments to produce phase separated materials. Recent focus has turned to synthesising crystalline segments functionalised with motifs that are capable of hydrogen bonding through linear arrays. Progress in this field is reliant on the development of these motifs to produce supramolecular thermoplastic polyurethanes (STPUs) with novel, predictable architectures.

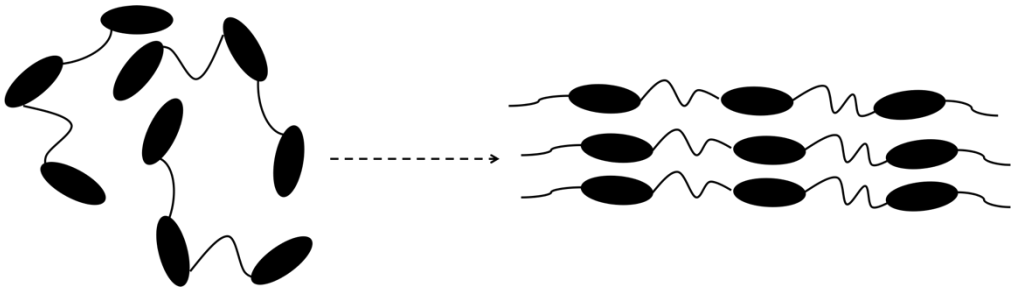

Figure 3.1 Assembly of covalent PUs into phase separated materials, where crystalline segments strongly interact. Black ovals represent the covalent bond between monomer units

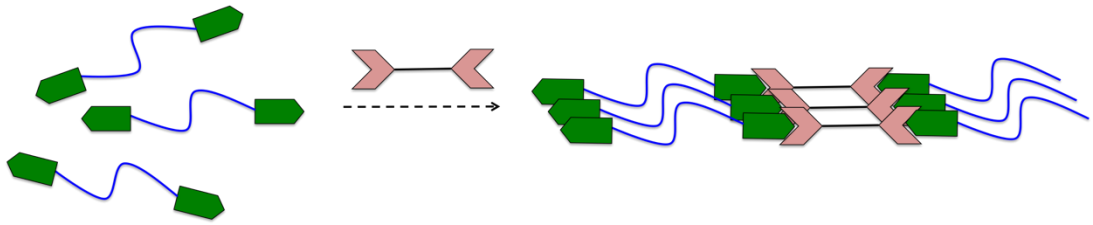

Figure 3.2 Assembly of non-covalent SPUs using heterocomplementary hydrogen bonding motifs (green and pink)

Using heterocomplementary arrays such as those shown in **Figure 3.2** could result in a non-covalent mimic of AB block copolymer type covalent TPUs, **Figure 3.1**.

The amorphous segment (blue lines, **Figure 3.2**) lends itself to deformation of the material; allowing elasticity and stretch, whilst the crystalline (aromatic and hydrogen bonding unit) portions provide mechanical integrity. The development of STPUs has seen the reproduction of mechanical properties of high-molecular-weight polymers whilst retaining the ability to dramatically reduce in viscosity when the melting temperature is reached.

The two heterocomplementary hydrogen bonding units AIC **31** and UIM **30** described in Chapter 2 were used to investigate the assembly of a supramolecular polymer.

Previously, the association constant for the heterodimerisation of UIM:AIC **30:31** was found to be approximately 3 x 10^4 M^{-1} in $CDCl_3$, which was considered insufficient in strength to form linear supramolecular polymers with a high degree of polymerisation in dilute solution. This was, however deemed to be sufficient in combination with lateral hydrogen bonding between amide, urea and urethane moieties. These play an active role in the self-assembly process in the bulk state, promoting interaction between polymer chains, as the groups of Hayes and Chien have both reported. [76, 77, 129]

With this in mind, attention was devoted to the synthesis of heterocomplementary hydrogen bonding macromonomers for supramolecular polyurethane elastomers, and the characterisation of their subsequent materials properties.

3.2. Characterisation of SPUs

3.2.1. Thermal Analysis

Differential Scanning Calorimetry

DSC is useful for determining the thermal transitions in polymers.

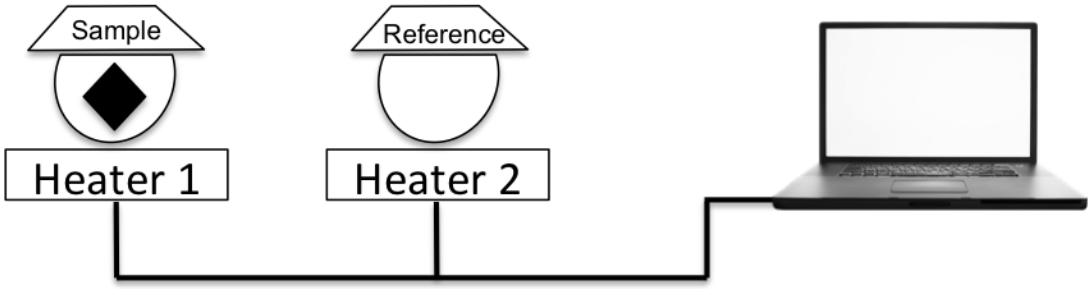

Figure 3.3 Cartoon of the experimental set-up of a differential scanning calorimeter. The computer program logs the change of heat flow to the reference cell and the sample cell

Figure 3.3 illustrates the basic experimental set-up for a DSC experiment. Up to 10 mg of polymer sample is placed in a non-hermetically sealed aluminium pan, whilst the reference pan is kept empty. Heat flow is recorded for each of the samples, and it is this difference in heat flow, which is translated to the thermal characteristics of the polymer.

DSC is especially useful for determining the T_g of a polymer. Described as the reversible transition in (semi) amorphous materials from a hard, brittle state into a rubber-like one, it can define the range of usefulness of an object in terms of temperature. Polymers have a higher heat capacity above their T_g than below it, which manifests itself as an increase in heat flow in a DSC curve.

To visualise the crystalline and amorphous portions of our supramolecular polymers, the samples are firstly cooled down inside the calorimeter to -90 ºC. Polyurethanes are known to undergo degradation from as low as 220 ºC[130] so analysis must be performed under nitrogen purge. After equilibration for 5 minutes at -90 ºC, the pans are heated at 10 ºC min^{-1} up to 210 ºC. Further equilibration is performed at 210 ºC (5 min), before the temperature is brought back down at the same rate to -90 ºC. The process is then repeated for as many cycles as required **Figure 3.4**.

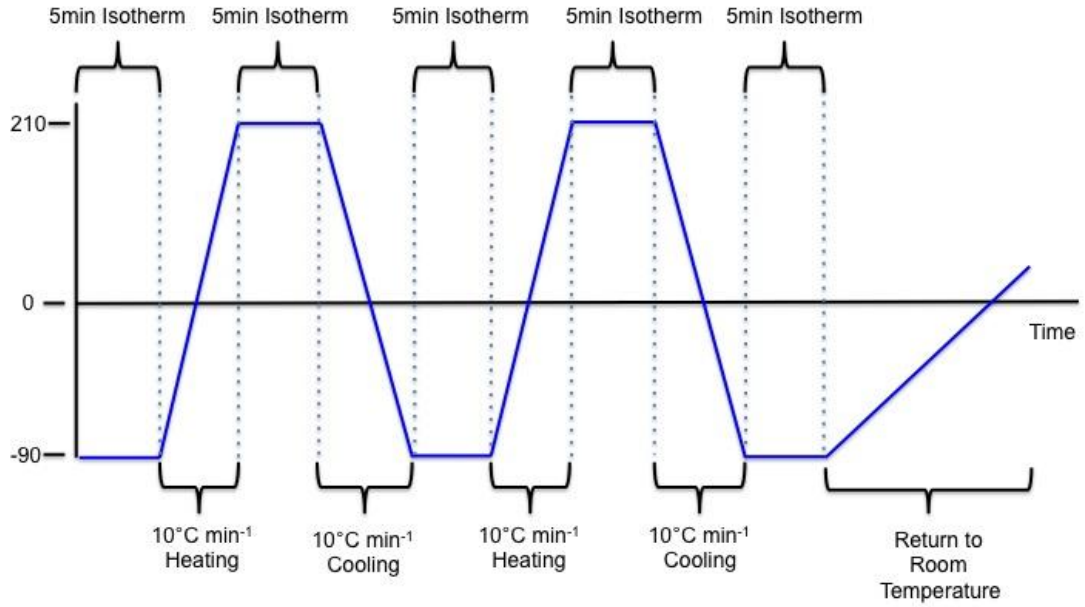

Figure 3.4 Schematic of the heating and cooling cycles employed during DSC analysis of supramolecular polymers

DSC however has its limitations. Whilst analysis uses a small amount of sample (~10 mg), it is also a destructive technique, meaning the sample cannot be recovered. Sensitivity is also relatively low in comparison to dynamic mechanical thermal analysis (DMTA), where sample size and heating rate are increased resulting in greater resolution. It is also difficult to pinpoint a T_g in highly crystalline polymer systems where the T_g is a relatively minor event.[131]

Dynamic Mechanical Thermal Analysis

The thermal transitions observed for the SPUs using DSC can be corroborated by DMTA. The machine applies a sinusoidal stress to the material being tested and records the resulting strain of the sample.

At the T_g of the material, several physical properties change abruptly; sample volume, viscosity and specific heat capacity to name a few. Whilst DSC can accurately measure the heat capacity of a sample, DMTA is equipped to measure dynamic elastic loss modulus (E") and dynamic elastic storage modulus (E'), which are indicators for changes in viscosity of the sample.

The response of the material to the applied stress is measured by the division of E" by E' giving a tan(∂) value, which can indicate the level of flexibility or stiffness that characterises the material. DMTA is therefore also useful for judging the material response of the SPUs over a wide range of temperature and informs on the mechanical properties of the material.

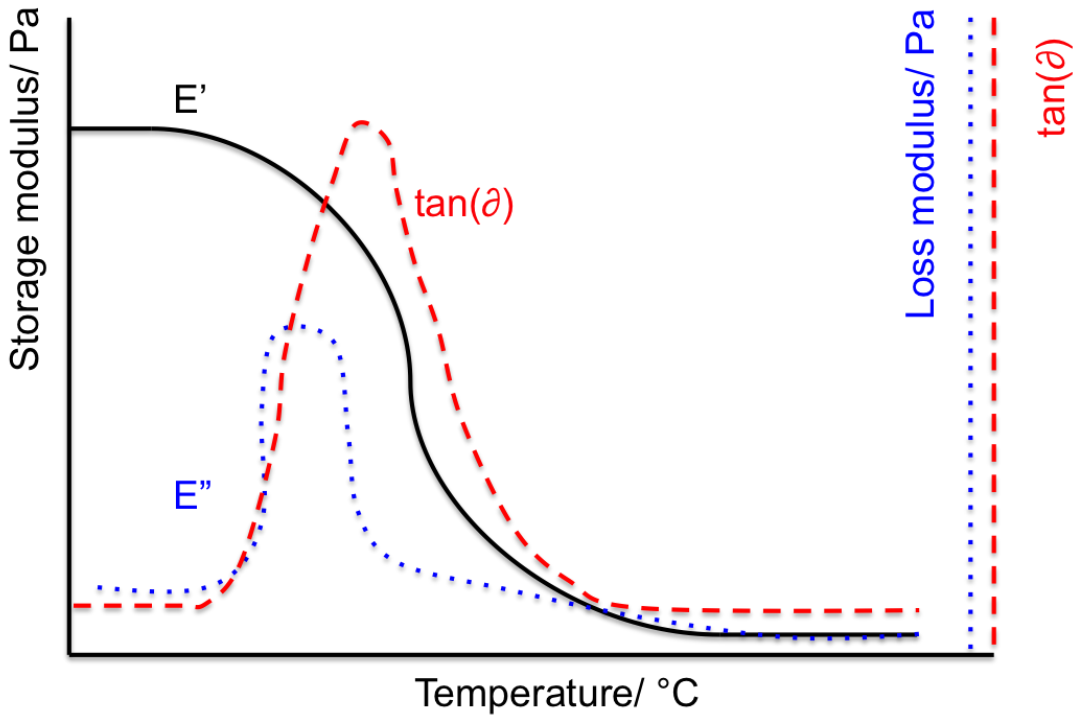

Figure 3.5 Schematic of the three materials properties indicating T_g measurable by DMTA

A typical DMTA trace is shown in **Figure 3.5**. The T_g is indicated by either the dramatic reduction in E', or the peak maxima of tan(∂) or E". Because tan(∂) relates to energy lost and energy stored in the material, it is not really associated with the traditional definition that T_g is the onset of segmental motion.[132] The peak maxima of E" is therefore more reliable, when compared to DSC data.

Wide-Angle and Small-Angle X-ray Scattering

Small- and wide- angle X-ray scattering (SAXS and WAXS) are useful for providing information on the structures of large assemblies in an environment with low order. The scattering of X-rays to these wide angles implies sub-nanometer structures. The segmented nature of SPUs means microphase separation will directly effect the interdomain spacing and hard block ordering[133], which should be visible using X-ray scattering. Highly ordered domains resulting from phase separation within the material give rise to maxima in the SAXs data. The dimensions of the ordered arrays can hence be estimated.[134]

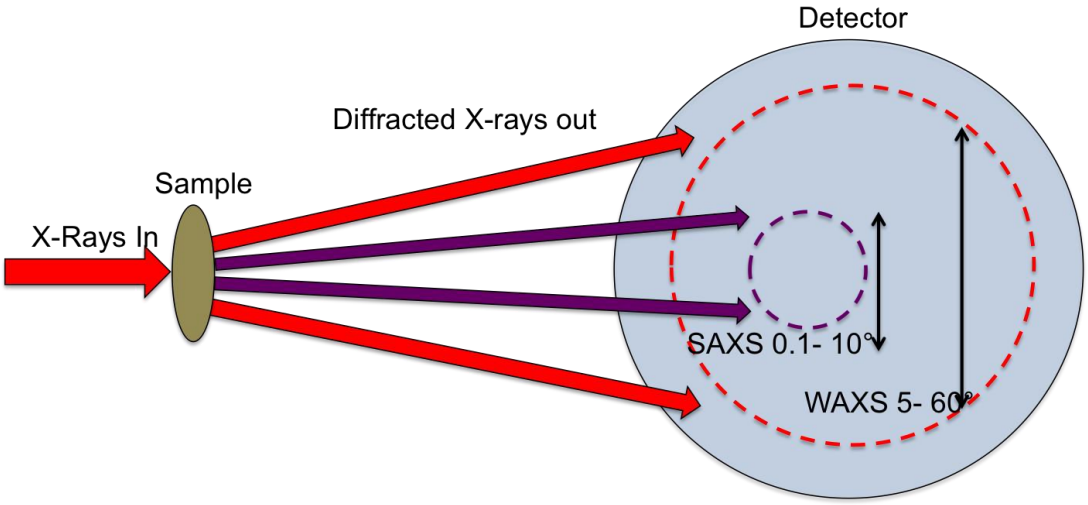

Figure 3.6 Cartoon depicting the basic uses of SAXS and WAXS. SAXS is limited to between 0.1 and 10º, whereas WAXS has a larger range; up to 60º

WAXS is used as an indicator of crystallinity of the polymer and of lateral packing in the polymer system between urea and urethane groups. The 'amorphous halo', which is common to many hydrogen bonded systems, often refers to a lattice spacing of between 4-5 Å.[22, 75, 77, 129]

3.3. Design of triple hydrogen bonded supramolecular polymers

As discussed in Chapter 1, the balance between the crystalline and amorphous regions within the microstructure of a polymer will define the materials properties.

Polyurethanes in particular are amenable to thermoplastic and elastomeric behaviour due to the chemical structure. When a stress is applied, the amorphous region of the polymer can elongate, allowing deformation, whilst the crystalline domain imparts structural and mechanical strength. Because of the wide application of covalent polyurethanes in industry,[6] which use phase separation to attain these properties, supramolecular polyurethanes can be exploited as a means of achieving highly ordered structures, forming phase separated materials with wide application potential.

3.4. Synthesis of heterocomplementary supramolecular polymers

The recognition behaviour between a ditopic version of UIM and AIC **62:100** by NMR was investigated by a former PhD student in the Wilson group, A. Gooch.[79] Complexation induced shifts were observed, suggesting assembly through the intended triple hydrogen bonding array to form dimers **Figure 3.7**.

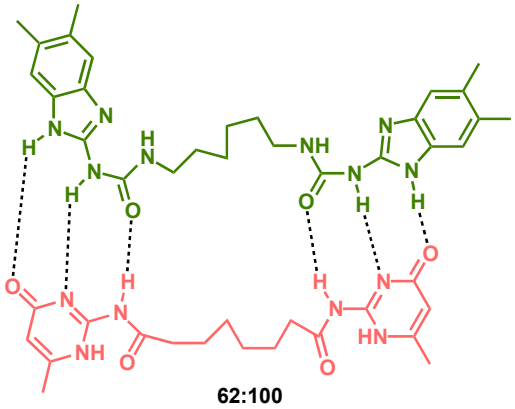

Figure 3.7 Cyclic dimer formed by ditopic AIC 62 and UIM 100 investigated by Gooch *et al*.

Constructing a high-molecular-weight analogue of the ditopic UIM, DUM **100** represented a means to explore the mechanical and structural properties of self-assembled polyurethanes.[135]

The synthetic route for a high-molecular-weight analogue is a one-pot procedure comprising two steps. The so-called ‘prepolymer’ method is widely used in industry,[7] permitting easy synthesis which is amenable to scale up.

Commercially available starting materials were used to obtain the macromonomer in high yield and quantity.

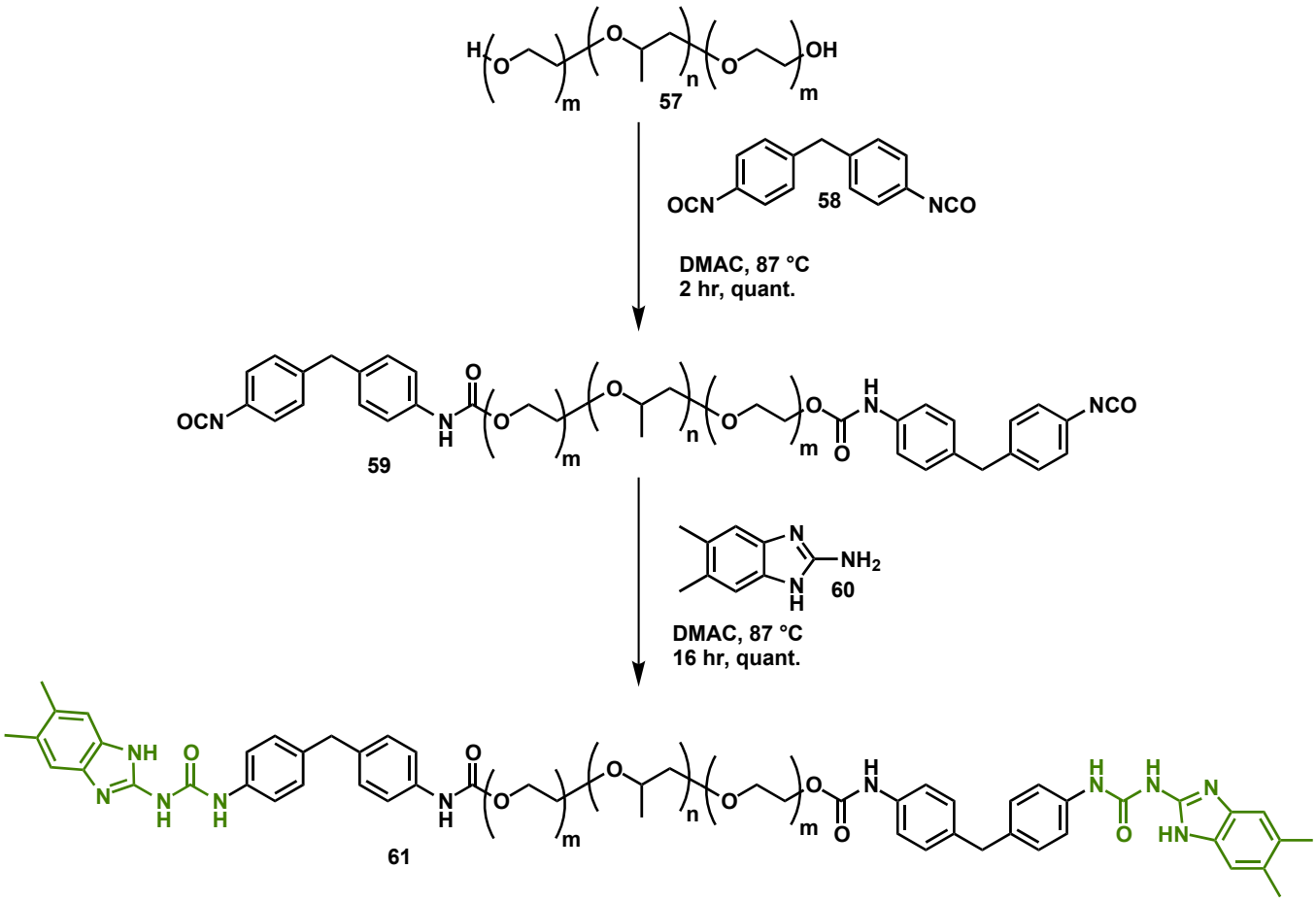

Scheme 3.1 Synthesis of a polyurethane 59 from a 2000 $gMol^{-1}$ PEG diol 57 and MDI 58, end-capped with hydrogen bonding moieties to form the macromonomer 61

The advantage of the 'one-pot' synthesis in this instance is that after consumption of the isocyanate functionalities upon addition of the aromatic amine **60**, the heterocomplementary ditopic AIC unit DAC **62** can be added without handling of the reaction mixture. Addition of this complementary unit provides the required supramolecular polymer, following removal of the solvent.

The ditopic unit AIC **62** was synthesised from commercially available starting materials **101** and **102** in one-step, **Scheme 3.2**.

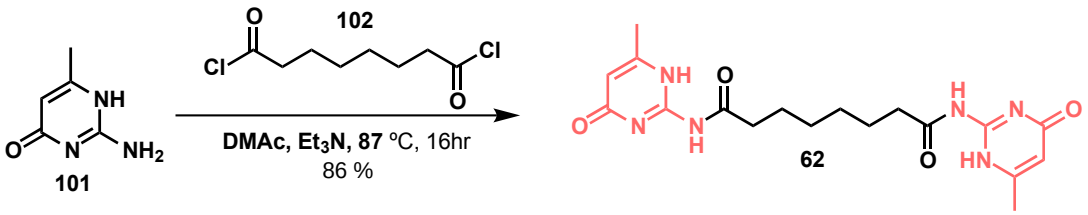

Scheme 3.2 Synthesis of supramolecular chain extender DAC 62, in a one-pot one step process from an isocytosine 101 and acyl chloride 102

A. Gooch further investigated the manipulation of heterocomplementary components (**Scheme 3.1** and **Scheme 3.2**) used for assembly of SPU **103**, (Figure 3.8), which is a mimic of a conventional AB-type co-block polymer.[80]

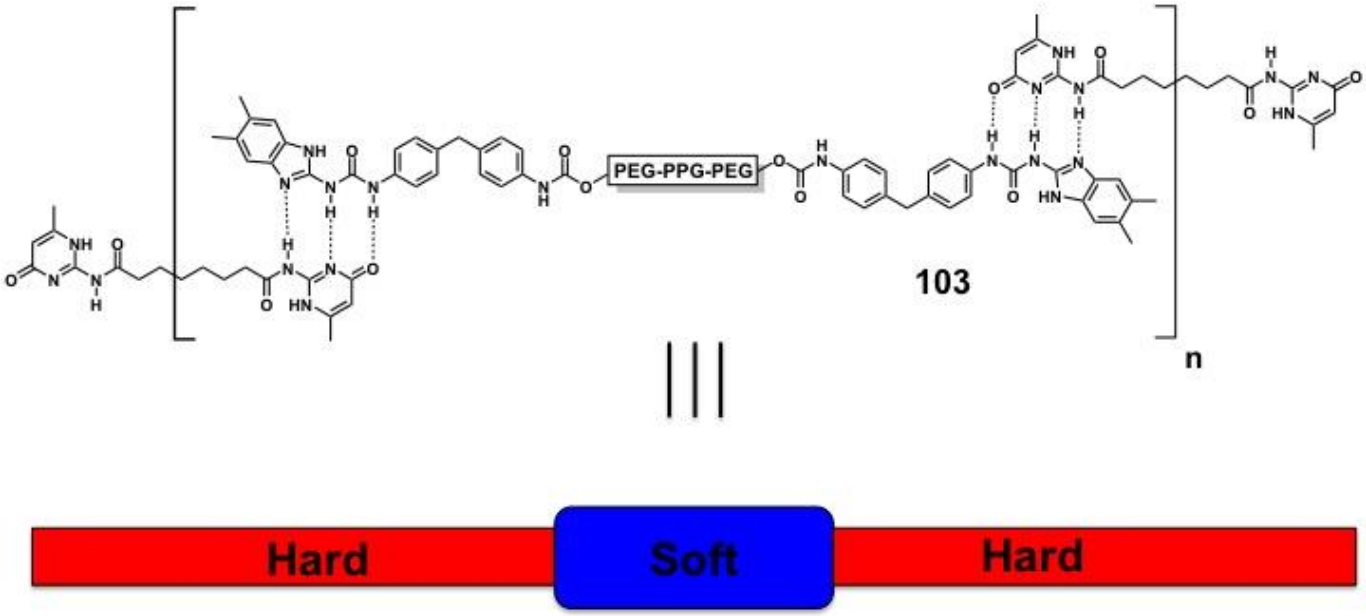

Figure 3.8 Proposed linear supramolecular polymer 103 formed from heterocomplementary units 62 and 61. Aromatic units contribute to the hard block, and the amorphous core polyol creates the soft block, forming phase-separated materials

Percentage hard block can be calculated from;

$$\frac{(moles\ of\ MDI\ \mathbf{58}) + (moles\ of\ DAC\ \mathbf{62}) + (moles\ of\ benzimidazole\ \mathbf{60})}{(moles\ of\ MDI\ \mathbf{58}) + (moles\ of\ DAC\ \mathbf{62}) + (moles\ of\ benzimidazole\ \mathbf{60}) + (moles\ of\ polyol\ \mathbf{57})} \times 100$$

Equation 3.1 Calculation required for percentage hard block for all supramolecular polymers. Moles refers to molar amount used during reaction

In this published work, by controlling the molar ratio of reaction components, different percentage hard block SPUs were obtained. In this instance, the ratio of MDI **58** to polyol **57** was controlled to introduce different hard: soft segment ratios into the SPU **103**, to gauge the effect on bulk state properties. The subsequent materials properties and appropriate mechanical responses were measured and investigated.

The ditopic natures of the polyol **57** and MDI **58** components dictate that the reaction product is comprised of a statistical mixture of capped and chain extended polyol species. When two equivalents of diisocyanate are used for every polyol, only 50% of the polyol becomes capped at both ends with MDI **58**. This rises to 75% when four equivalents of diisocyanate are used for every polyol. (Appendix 7.3 for a detailed statistical analysis). Hayes and colleagues have also previously reported on similar findings.[24]

The excess, unreacted MDI **58** left in solution forms a bisurea **104** with benzimidazole amine **60**, **Figure 3.9**, to display the same triple hydrogen bonding array as presented by the macromonomer **61** and acts as a supramolecular chain extension unit. The aromatic nature of this unit contributes to the crystalline, hard segment of the supramolecular polymer, maximising phase separation and potentially changing mechanical properties.

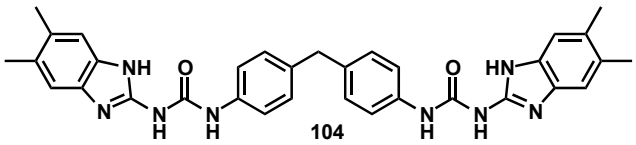

Figure 3.9 Structure of supramolecular chain extension unit 104 formed from the reaction of MDI with benzimidazole amine

Four SPUs, **Table 3.1**, were synthesised using the methodology in **Scheme 3.1**. They are referred to as ratios of MDI:Polyol so that 2:1 refers to a macromonomer, which is synthesised from two equivalents of MDI **58** for every equivalent of polyol **57**.

Table 3.1 Feed ratios during the synthesis of four different supramolecular polymers with different crystallinity

Ratio	*Equiv. polyol*	*Equiv. MDI*	*Equiv. Amine*	*Equiv. DAC*
2:1 **103a**	1	2	2	1
4:1 **103b**	1	4	6	3
6:1 **103c**	1	6	10	5
8:1 **103d**	1	8	14	7

A. Gooch previously synthesised all ratios of SPU shown in **Table 3.1**, but only entries 1 (2:1 **103a**) and 2 (4:1 **103b**) of **Table 3.1**, were fully characterised by DMTA and DSC.[80] For the purposes of this thesis, all SPUs mentioned hitherto were resynthesised for further materials characterisation.

From visual evaluation of the four supramolecular polyurethanes (SPUs) **103a-d**, it could be seen the morphology changed from a tacky brown very viscous liquid, to static, brown powder. With this promising starting point of ability to control the appearance of this supramolecular polymer system, materials analysis was used to provide more detailed physical properties.

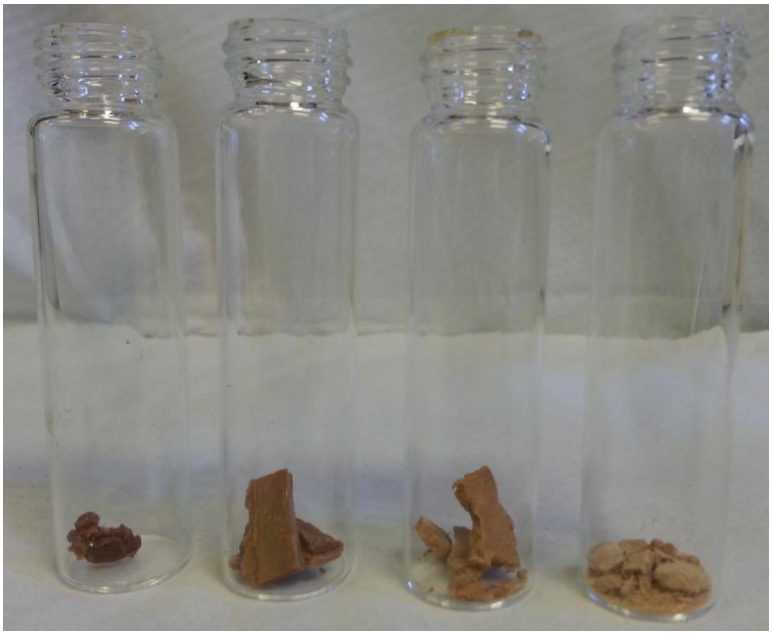

Figure 3.10 Visual inspection of SPUs L-R **103a, 103b, 103c** and **103d**, **Table 3.1**

3.5. Confirmation of association *via* triple-hydrogen bonding arrays

A. Gooch used a series of controls, which presented incomplete hydrogen bonding arrays, which were designed to show that the materials behaviour was not due to increase of molecular weight caused by covalent chain extension, but was due to the intended supramolecular polymerisation. **Figure 3.11**.[128]

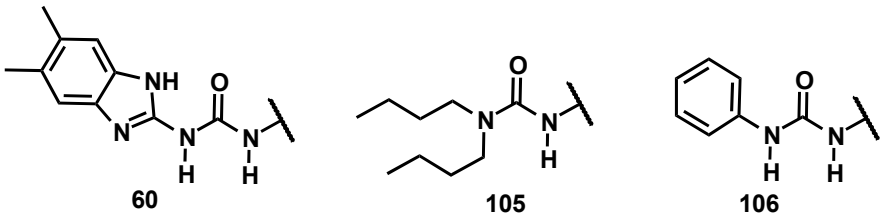

Figure 3.11 60 left- terminal urea of the macromonomer displaying the full triple hydrogen bonded array. 105 middle- displaying a 'blocked' urea, which could participate only with 1 hydrogen bond. 106 right- displays an incomplete triple hydrogen bonding array

Macromonomers terminated with amines, which did not present the full heterocomplementary array, were shown to not form materials with substantial

mechanical properties. Aniline moiety **106** is capable of participating in both hydrogen bonding and π-π stacking, but was not able to form a self-supporting material.

Heterocomplementary DAC **62** and macromonomer **61** units can interact laterally *via* hydrogen bonding and π-π stacking of end-groups, which contribute to materials properties in the bulk state. A negative control was synthesised, which lacked the ability to engage in triple-point hydrogen bonding in the same way as DAC **62**, but was still able to participate in lateral non-covalent interactions. Bis(amido) pyridine (BAP) **109** was synthesised in two steps from diaminopyridine **87** and valeroyl chloride **107 Scheme 3.3**.

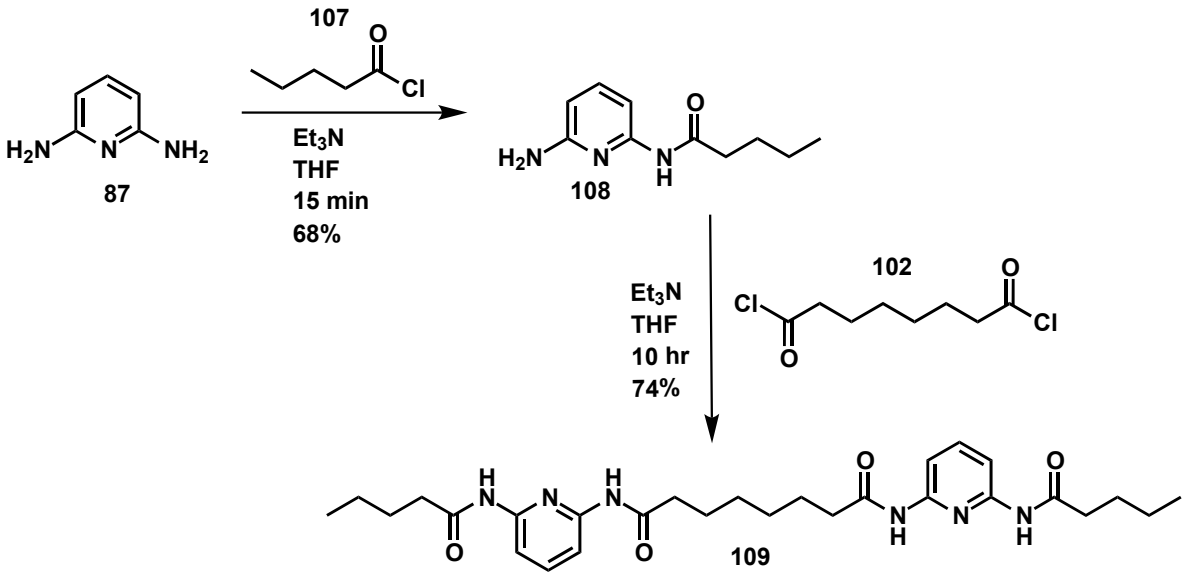

Scheme 3.3 The synthesis of bis(amido)pyridine (BAP) 109 from diamino pyridine 87 and valeroyl chloride 107

BAP **109** displays a DAD triple hydrogen bonding array, which is mismatched to the intended UIM macromonomer partner **61**, ADD. Addition of BAP **109** to the macromonomer afforded a polymer mixture. The materials properties observed for the polymer mixture with mismatched supramolecular chain extension unit **109** versus **62** were markedly different. Visual inspection alone confirmed formation of a SPU for **103b** based on the formation of a mechanically deformable solid. The negative control sample did not display similar materials properties, and it should be

noted that it did not form a solid material capable of supporting its own weight, **Figure 3.12**. This indicated that the materials properties of the SPU benefit significantly from complementary hydrogen bonding from both heterocomplementary partners.

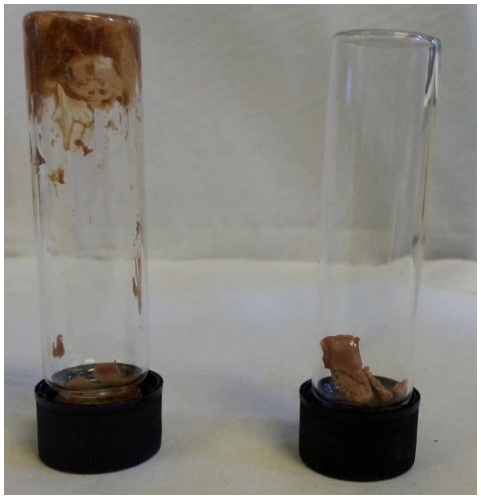

Figure 3.12 Visual inspection of polymer with mismatched BAP 109 (left) and SPU 103b with heterocomplementary hydrogen bonding unit DAC 62 (right)

Materials assembly and hence materials properties are therefore dependent on the presence and subsequent interaction of heterocomplementary hydrogen bonding motifs, amongst a plethora of other competitive non-covalent interactions, such as urea and urethane interaction between lateral chains and π-π stacking. This gives the added advantage over homocomplementary hydrogen bonded systems, as both partners must be present for supramolecular chain extension and hence supramolecular assembly to occur.

3.6. Mechanical analysis of heterocomplementary supramolecular polymers

3.6.1. Preparation of samples for materials analysis

Because some of the polymer products are brittle in nature, there was a necessity to mould them prior to analysis, minimising handling time, and as a result any breakage of samples.

The isolated SPUs **103a-d** were redissolved in hot dimethylacetamide (DMAc), before pouring the solutions into a Teflon mould. The DMAc solvent was evaporated slowly at room temperature then placed in a vacuum to ensure full removal of solvent. Once dry, the materials form a thin layer, which can be scratched from the mould. The SPUs **103a-d** were subsequently subjected to compression moulding at the temperatures found in **Table 3.2** for 3 minutes, which was dependent on percentage hard block **Table 3.2**.

Table 3.2 Compression moulding temperatures of each ratio supramolecular polymer correlated to percentage hard block

Ratio	*Percentage Hard Block*[#]	*Mould Temperature/ °C*
2:1 **103a**	37.7	120
4:1 **103b**	61.0	140
6:1 **103c**	71.7	160
8:1 **103d**	77.7	180

[#] Hard block percentage corresponds to the molecular weight, which comprises the hard block, divided by total molecular weight of the constituents of the polymer

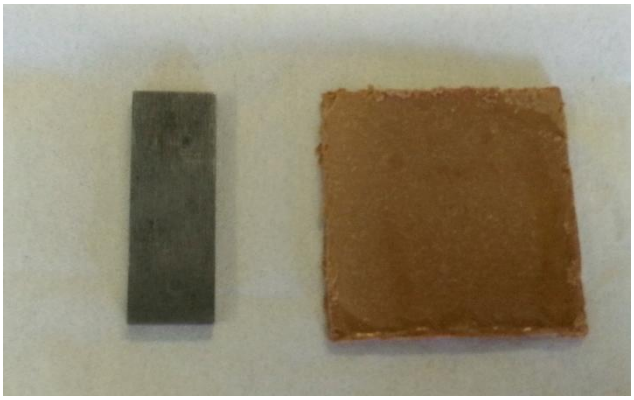

Figure 3.13 Compression moulded SPU 103b right. Left- steel standard used for calibration of the DMTA machine

The resultant compression moulded SPU **103b** was further cut into three pieces based on a steel standard used to calibrate the DMTA machine, **Figure 3.13** left.

Each of the four moulded supramolecular polymers were then subjected to DSC analysis.

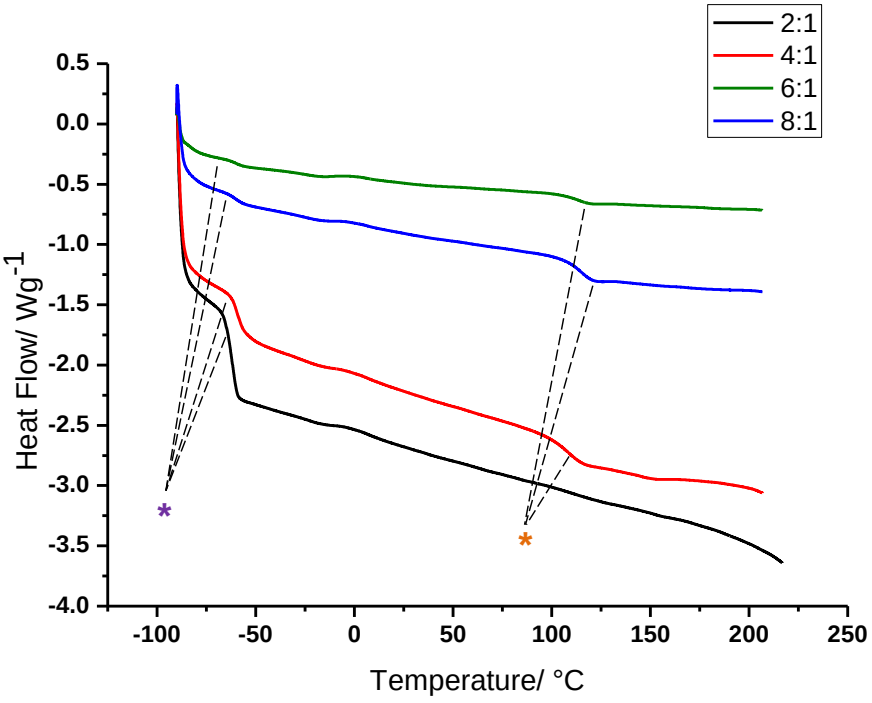

Figure 3.14 Second heating DSC trace of four supramolecular polymers 103a-d heated between -90 and 220 ºC at a rate of 10 ºC min^{-1}. Endotherm up. * Indicates T_g whilst * indicates hard block transition

Two transitions were expected in the DSC trace because of the phase separated morphology SPUs exhibit. Firstly the T_g of the amorphous core polyol, followed by the disruption of the ordered, hard phase at a higher temperature. **Figure 3.14** shows that the T_g for each NCO:OH ratio was seen around the same point; rising from -50 ºC for **103a**, to an average of -43 ºC for **103b, 103c** and **103d**. This increase in T_g was attributed to the increase in percentage hard block within the material. A greater percentage hard block will increase the ability of the polymer to form more ordered crystalline areas and as a result, enforces more order upon the amorphous phase, pushing the T_g to higher a temperature.[133, 136]

The subsequent hard block transition was observed at 124 ºC for **103d**, and 118 ºC for **103b**. Definition of the transition and temperature at which it occurred decreases as the NCO:OH ratio is also decreased. This is in line with our previous observations, as a lower percentage hard block will evidently require a lower melting temperature. These results also confirm a phase-separated morphology.

Table 3.3 Summary of hard and soft block transitions found in Figure 3.14 for SPUs 103a-d

NCO:OH Ratio	*Soft Block Transition Temperature/ ºC*	*Hard Block Transition Temperature/ ºC*
2:1 **103a**	-50	Broad❖
4:1 **103b**	-42	118
6:1 **103c**	-41	120
8:1 **103d**	-43	124

Full DSC data is available in Appendix 7.4, which shows recrystallisation of the hard block, T_c, at approximately 110 ºC for **103a-d**, which is just below the T_m. The T_m endotherm is still present after the third heating cycle, suggesting that disruption and reorganisation in the hard block is reversible- and stimuli responsive- based on the heat put into the polymer system.

DMTA was subsequently used to corroborate the data above. The DMTA curve for **103b** only was obtained. This was due to the fragile nature of materials **103c** and **103d**, and the high adhesiveness of materials **103a,** so adequate samples for testing could not be obtained.

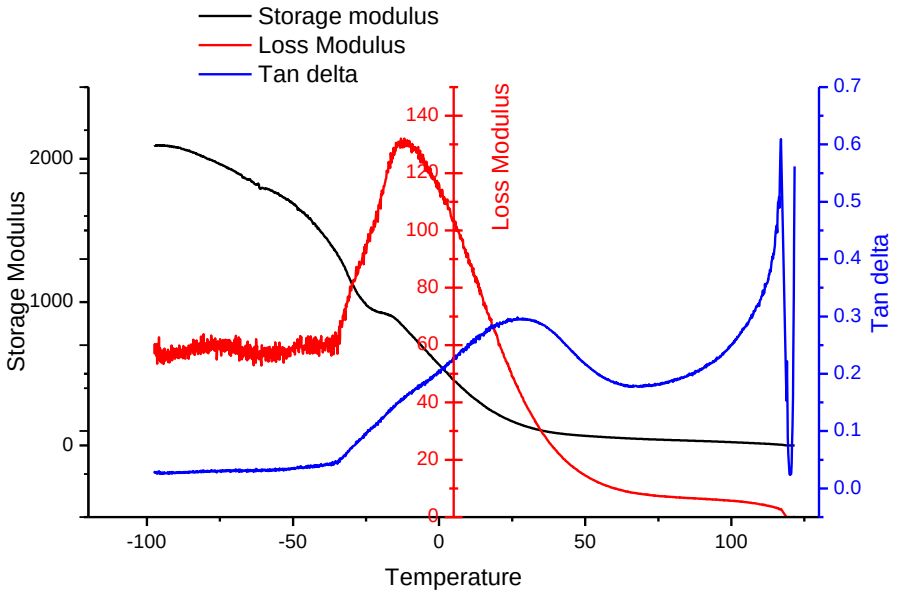

Figure 3.15 Storage and loss modulus of SPU 103b when subjected to DMTA between -100 to 120 ºC

The material response to temperature and deformation is visualised in **Figure 3.15**. Storage modulus, which refers to the strength of the SPU, shows a transition at 1000 MPa, indicative of the T_g of the SPU at -31 ºC. The storage modulus always gives the lowest value for T_g, and relates to mechanical failure. The loss modulus shows T_g at -15 ºC, and refers to the mid-point of the transition. The tan(∂) of the SPU shows onset of the T_g at -30 ºC and is the value historically used in the literature to describe the glass transition of polymers.[137] The amorphous content of polymers dramatically broadens the tan(∂) curve, often witnessed as a sharp peak, which explains the large range over which thermal transitions are occurring in the SPU. It is well known that the T_g of polymers appear to be increased from those measured using other methods such as DSC. As with any non-Newtonian fluid, the material requires more energy (i.e. more heat) to respond to the higher frequency of oscillation imposed for short periods of time. This is reflected in as much as a 30 ºC deviation upwards from the T_g seen *via* DSC.[138]

The tan(∂) curve in this instance is also particularly useful in displaying the melting transition of the material. At 120 ºC, the tan(∂) sharply drops, indicating the melt and flow of the polymer and hence loss of mechanical integrity. The behaviour seen was in in-line with that reported previously from the Wilson group.[80, 128]

Table 3.4 Comparison and deviation of glass transition temperature measured by DSC and DMTA

NCO:OH Ratio	*T_g / ºC measured by DSC*	*T_g / ºC measured by DMTA*	*Deviation in temperature / ºC*
2:1 **103a**	-50	N/A	-
4:1 **103b**	-42	-15	+27
6:1 **103c**	-41	N/A	-
8:1 **103d**	-43	N/A	-

With the mechanical properties determined, the level of crystallinity of the SPU samples was measured by WAXS and SAXS.

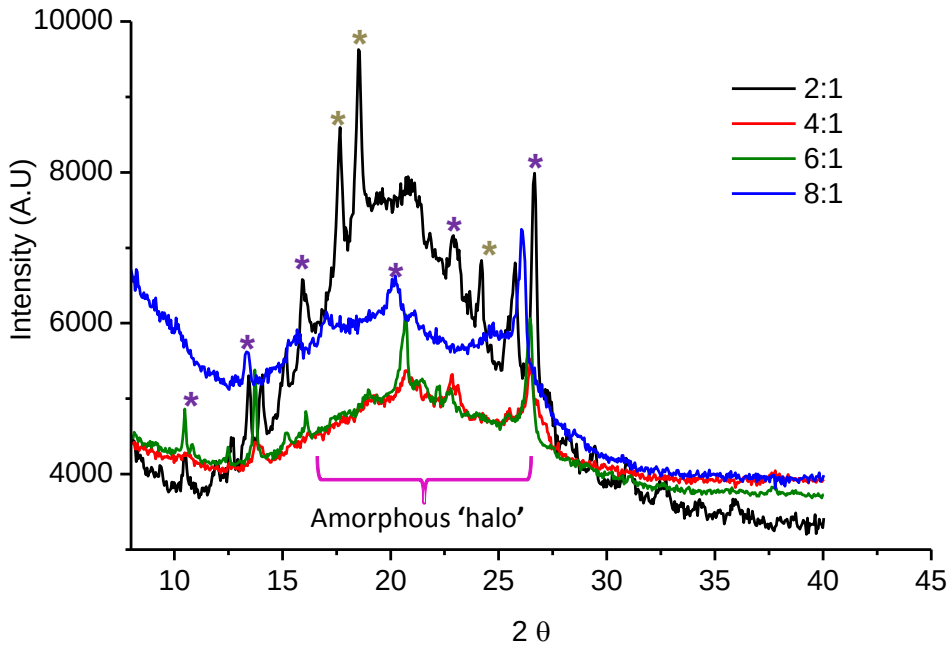

Figure 3.16 Diffraction data for SPUs 103a-d. The 'amorphous halo' is indicated with a pink parenthesis. * Refers to diffractions, which are unique, or have higher intensity for 103a. * Refers to diffractions common to SPUs 103b,c and d

Table 3.5 Bragg diffractions and d spacings from WAXS data

NCO:OH Ratio	*Bragg Diffraction/ 2θ*	*D spacing/ Å*
2:1, 4:1, 6:1 **103a, b, c**	10.3	8.6
All **103a, b, c** and **d**	13.8	6.4
2:1, 4:1 and 6:1 **103a, b, c**	15.7	5.6
2:1 **103a**	17.5	5.0
2:1 **103a,**	18.4	4.8
4:1, 6:1, 8:1 **103b, c** and **d**	20.8	4.3
4:1, 6:1, 8:1 **103b, c** and **d**	24.0	3.7
2:1 **103a**	25.6	3.5
All **103a, b, c** and **d**	26.5	3.4

It is clear from **Figure 3.16** that different hard block percentages have a direct effect on crystallinity. SPUs 103b, c and d all show additional diffractions at 21 and 24 2θ, corresponding to d spacings of 4.3 and 3.7 Å respectively and is much more pronounced in the SPU with higher hard block content. All samples exhibit a strong diffraction at 26 2θ, corresponding to a d spacing of 3.4 Å. These numbers are important because in combination with the amorphous halo, (maxima exhibited at 4.3 Å), which becomes broader and smoother as hard block percentage is increased, each of these diffractions are characteristic of a phase separated morphology within the SPU. Bonart elucidated that the smallest d spacings seen in their phase separated PU were due to the repeating unit of the poly(THF) backbone[139]. Whilst poly(THF) itself is a semi-crystalline polymer, it is feasible that crystallisation in the hard block enforces order in the PEG-PPG-PEG soft block, which means the diffraction seen at 2.7 Å (at 33 2θ in 103a only) may be attributable to the repeating units of the PEG-PPG-PEG structure. Reflections corresponding to 3.4 Å and 4.3 Å are due to the short-range ordering in between the hard blocks.[140, 141] This is indicative of π-π stacking and hydrogen bonding between ureas and urethane moieties, leading to urea tape formation and eventually lamella formation, which gives the SPU stereotypical phase separated morphology, **Figure 3.18**. The presence of a phase-separated morphology was further evidenced for all ratios with SAXS, **Figure 3.17**. A single scattering peak was seen for all ratios at 0.5 q, corresponding to value of 1.3 nm.[80]

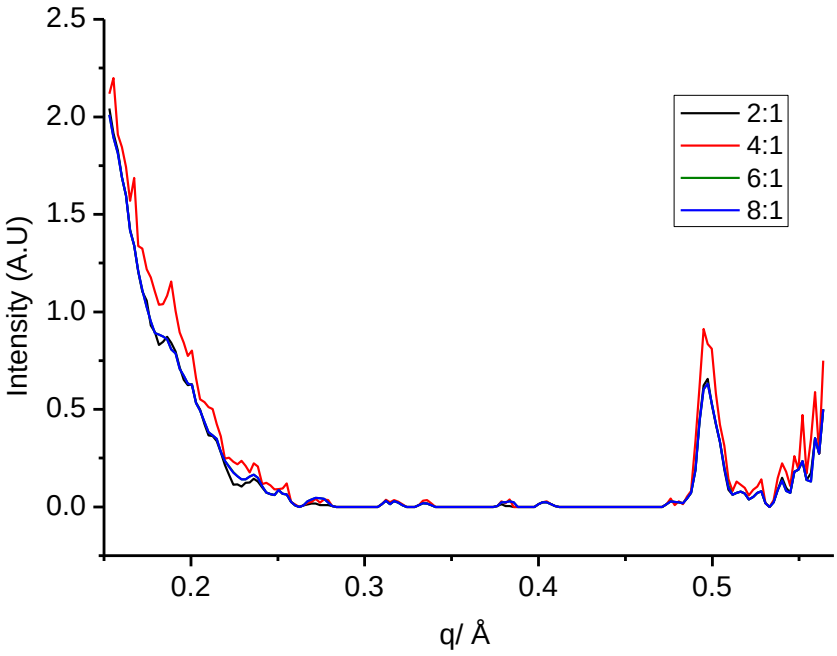

Figure 3.17 SAXS intensity profile for all NCO:OH ratios 103a-d

Koberstein and colleagues have previously reported that the single, broad scattering maximum that is observed can be associated with the interdomain domain spacing of the phase separated segments in PU block copolymers.[142, 143] Lower intensity reflections are seen for SPUs with higher MDI content between 0.3 and 0.4 $Å^{-1}$, this is an increased interdomain spacing of 4 nm, and indicates incorporation of supramolecular chain extender units which "lengthen" the hard phase, **Figure 3.19**.[80]

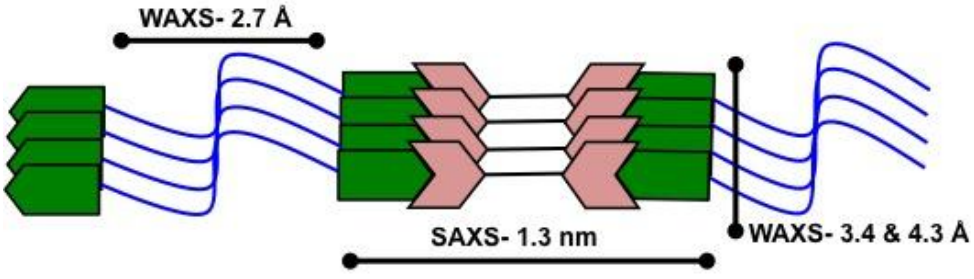

Figure 3.18 Cartoon of measurements acquired by using x-ray scattering methodology. The repeating ethylene units of the PEG polyol are seen at 2.7 Å, lamella formation at 3.4 & 4.3 Å, and interdomain distances of 1.3 nm

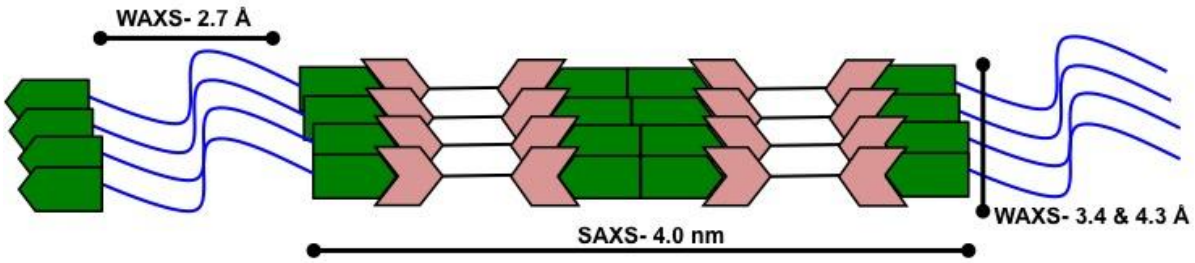

Figure 3.19 Cartoon of measurements acquired by using x-ray scattering methodology. The repeating ethylene units of the PEG polyol are seen at 2.7 Å, lamella formation at 3.4 & 4.3 Å, and interdomain distances of 4.0 nm

The level of crystallinity exhibited for these SPUs is typical of covalent PU elastomers,[144, 145] and phase separation at all percentages of hard block investigated was evidenced.

These data illustrate that the supramolecular chain extension within these SPUs is a key factor for control over mechanical properties. The supramolecular chain extension units are responsible for the higher degree of separation, which leads to a higher level of phase separation and hence different mechanical properties.

3.7 Thermal Analysis of Supramolecular Pseudo Block Polyurethanes

The desirable physical properties of PUs; strength and elasticity, are commonly attributed to their phase-separated morphology originating from the incompatibility of the soft and hard segments.[144] The thermal behaviour of the materials described earlier in Chapter 3 has been shown to be dependent on hard block content. The most intriguing DSC traces come from SPUs, which possess a high percentage of aromatic content. Several other groups have reported on the origins of the endotherms observed in our experiments.[132, 142-149] Saiani *et al.* proposed a two-phase morphology for PUs which are synthesised from an amorphous telechelic diol and aromatic diisocyanate.[144, 145, 150] Penetration of the hard phase by the soft phase occurs through quick cooling and other events, which do not allow the system to self-organise. Hence mixed phase morphology is produced which reduces the

crystallinity of the hard phase. Through annealing, phase separation occurs in the mixed phase, forming defined areas of crystalline order.

In the following section, the effect of annealing SPUs **103a-d** at temperatures above and below the hard block transition (T_m) was investigated. Using the T_m reported earlier in Chapter 3, each NCO:OH ratio from 2:1 to 8:1 was annealed at both 90 and 120 °C for 24 hours, and subsequently studied by DSC, SAXS and WAXS.

3.7.1. Annealing effect on SPU thermal transitions with different thermal histories

A comparison was drawn between the behaviour of soft and hard segments when annealed straight from synthesis and when annealed from quenching the melt state, **Table 3.6**. These were then compared to the melting transitions recorded when the samples were not subjected to annealing. All heating and cooling stages were performed under a nitrogen purge inside the DSC instrument. Samples were annealed in an oven at the given temperature.

Table 3.6 Summary of annealing conditions using DSC equipment

ORDER OF PROCESSING	**1**	**2**	**3**	**4**	**5**	**6**	**7**
Method 1 (Control)	-	-	-	Cool to -90 °C	Heat -90 to 210 °C	Cool to -90 °C	Heat -90 to 210 °C
Method 2 (Removal of thermal history)	Melt at 210 °C	Quench to r.t	Anneal at 90 °C, 24 hr.	Cool to -90 °C	Heat -90 to 210 °C	Cool to -90 °C	Heat -90 to 210 °C
Method 3	-	-	Anneal at 90 °C, 24 hr.	Cool to -90 °C	Heat -90 to 210 °C	Cool to -90 °C	Heat -90 to 210 °C

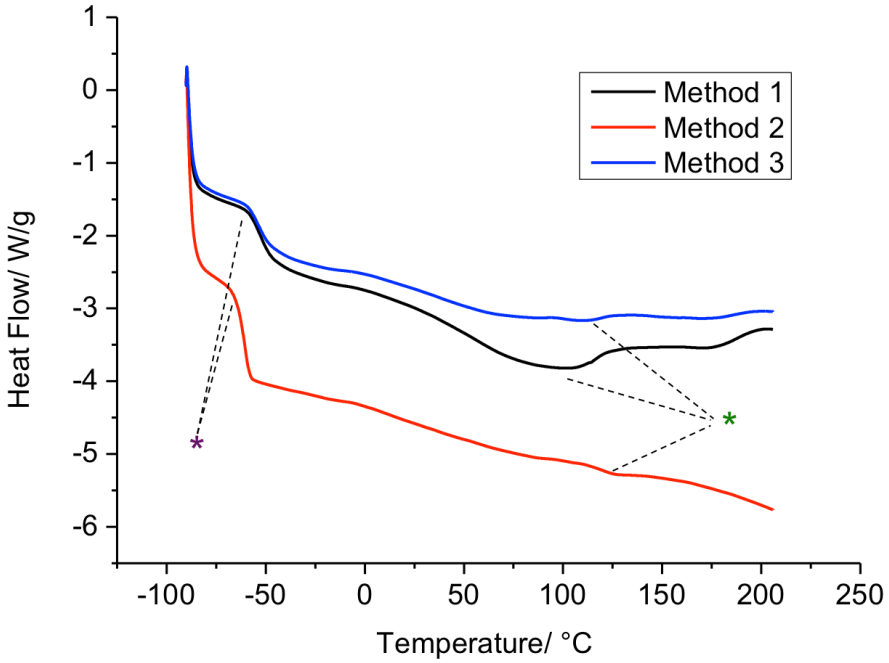

Figure 3.20 First DSC heating run of NCO:OH SPU = 2:1 103a after following the methods described in Table 3.6. * Indicates T_g, * indicates hard block transition

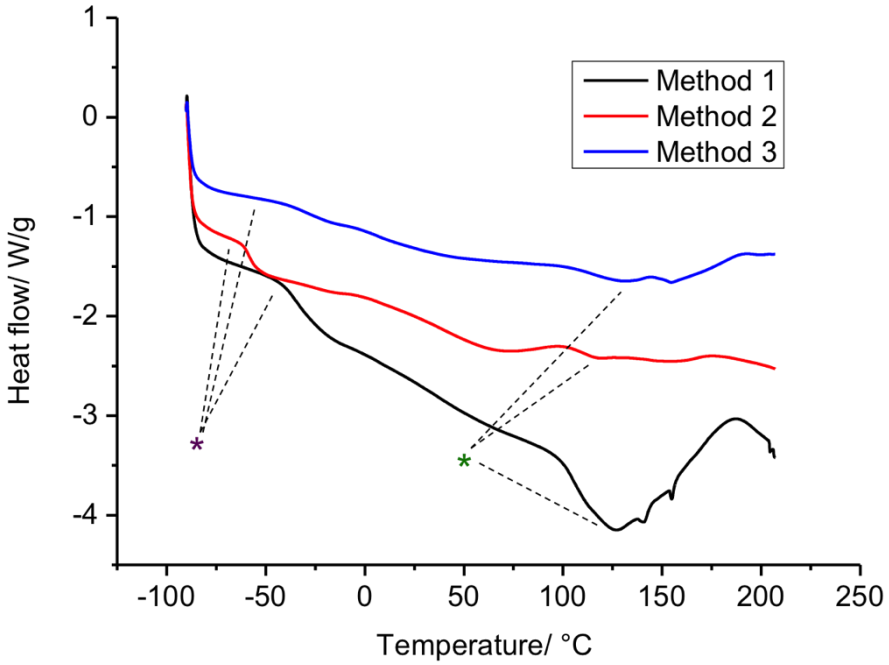

Figure 3.21 First DSC heating run of NCO:OH SPU = 4:1 103b after following the methods described in **Table 3.6**. * Indicates T_g, * indicates hard block transition

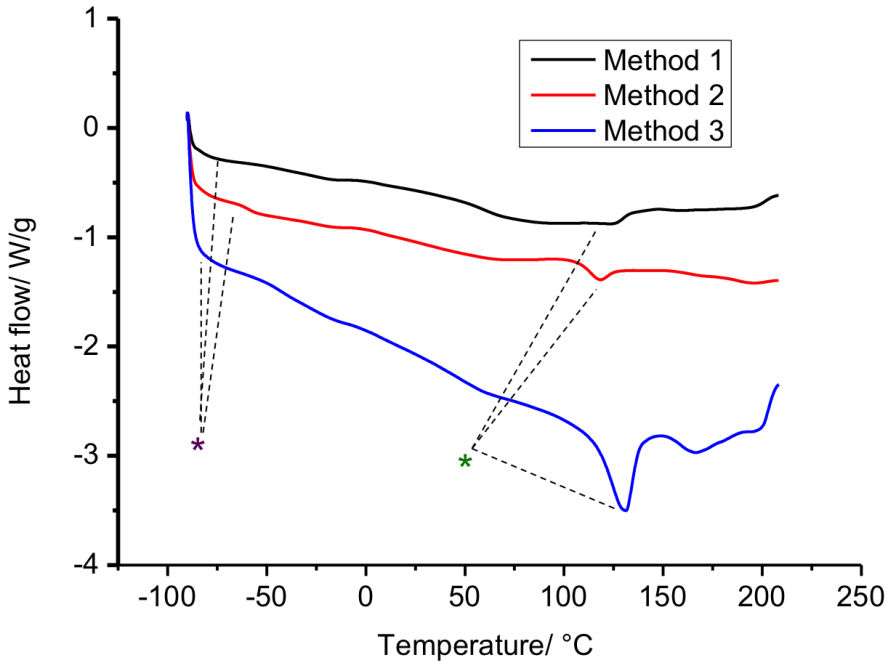

Figure 3.22 First DSC heating run of NCO:OH SPU = 6:1 103c after following the methods described in **Table 3.6**. * Indicates T_g, * indicates hard block transition

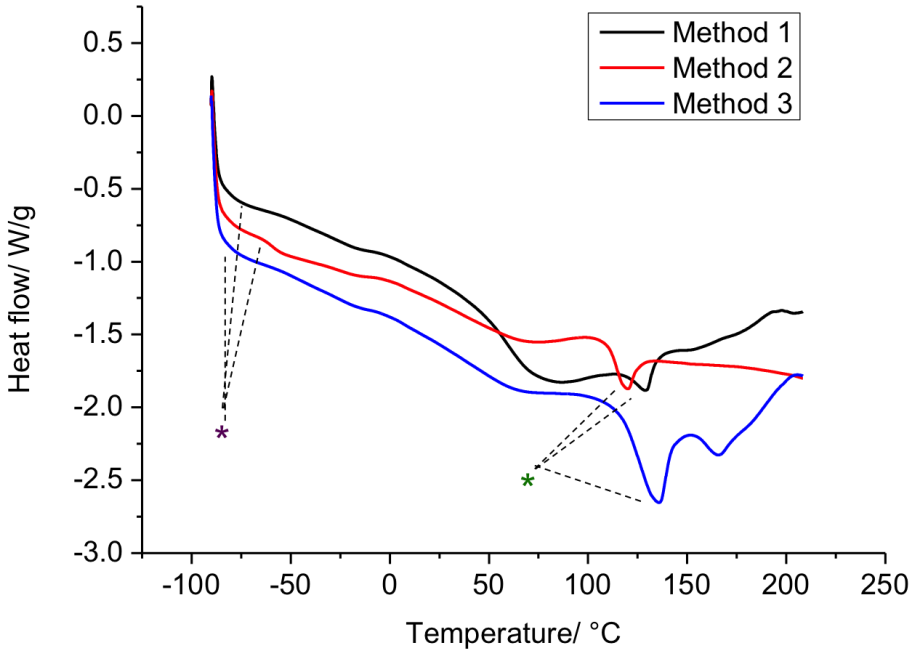

Figure 3.23 First DSC heating run of NCO:OH SPU = 8:1 103d after following the methods described in **Table 3.6**. * Indicates T_g, * indicates hard block transition

Figure 3.20 - **Figure 3.23** demonstrate variation in the thermal behaviour of both the soft and hard blocks, dependent upon thermal history of the material. Method 2 erases all thermal history of the SPU by melting the sample before annealing below the T_g of the material for 24 hours.

Using method 2, all NCO:OH ratios show clear transitions for both T_g and T_m, with an increasing intensity for T_m as hard block increases. In comparison to method 1 for NCO:OH = 8:1 **103d**, **Figure 3.23**, which shows a broad melting endotherm between 70 °C and 120 °C, T_m is presented as a sharp endotherm at 125 °C. This suggests that melting the material before annealing provided samples in a similar thermodynamic state[144] and hence the formation of 1 ordered hard phase.

By annealing for 24 hours before subjecting the samples to DSC (method 3), for SPUs with a hard block content higher than 60% (**103b, c** and **d**; **Figure 3.21**, **Figure 3.22** and **Figure 3.23**), a distinctive 'double' endotherm was exhibited, the first with higher intensity at ~120 °C and the second at 170 °C. By comparing these transitions to those seen using method 2, we can attribute the most intense endotherm at ~120 °C to the melting transition of the highly ordered hard block. The endotherm at ~170 °C indicates a similar morphology described by Saiani *et al.*.[145] Phase separation of the 'mixed phase' is stimulated by physical aging of the sample (*i.e.* annealing time), and this transition becomes more pronounced for increased percentage hard block, presumably due to an increased amount of hard block solubilised in the soft phase. This transition is not present in any DSC traces for method 2, which implies the occurrence of a mixed phase is not a thermodynamically preferable state for the microstructure of the material.[150-155] The second heating run of all annealing methodologies produced identical results, which duplicate the DSC trace for method 2 at all NCO:OH ratios (Appendix 7.5). This reinforces the occurrence of a phase-separated morphology of the SPUs at the nanometre scale.

3.7.2. Effect on SPU thermal transitions when annealed above their T_m

To further investigate the effect of physical aging by annealing, the materials were annealed above their T_m at 120 °C after melting and quenching to room temperature, following method 2, **Table 3.6**, and the results compared to those annealed at 90 °C after melting by DSC following method 2, **Table 3.6**.

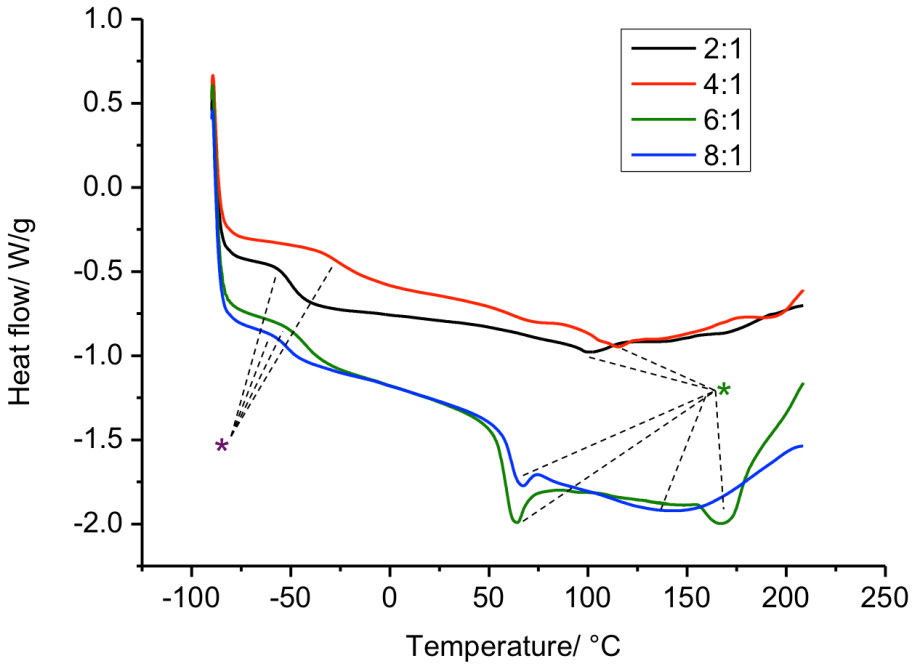

Figure 3.24 First DSC heating run of NCO:OH SPU 103a-d after annealing at 120 °C. * indicates T_g, * indicates hard block transition

DSC traces of the SPUs annealed above their T_m show the T_g is present at all ratios when samples are annealed above or below the T_m, indicating complete phase mixing does not occur at these temperatures, which has been observed for other PU systems.[156] Intriguingly, annealing above the T_m produces profound changes in the location of T_m for SPUs with a hard block ratio of more than 71% (**103c** and **d**). An additional endotherm is seen at ~60 °C and ~175 °C for these hard block values. **Table 3.7**. The endotherm observed at ~175 °C can be attributed to the 'annealing endotherm', a phenomenon which occurs up to 50 °C above the annealing temperature.[145] Attributed to the disruption of long-range ordering in the hard

segments, the location of the annealing endotherm can be shifted based on the temperature at which the samples are annealed.[157] Annealing below the T_m at 90 °C produces an annealing endotherm at roughly the same temperature the T_m is seen (~125 °C) and as such, this transition cannot be definitively assigned.[158] The reduction of T_m to ~75 °C at higher annealing temperatures can be attributed to partial melting of the hard phase, which increases the solubility into the soft phase (phase mixing).[159] The reduced order in the phase mixed portion of the microstructure is reflected in the reduced temperature observed by DSC.

Table 3.7 Summary of glass and hard block transitions found in SPUs after annealing at different temperatures above and below the hard block transition temperature. Taken from the first heat from DSC traces

NCO:OH Ratio	*Annealed*		*Observed T_g/ °C*	*Observed T_m/ °C*
	>Tm	<Tm		
2:1 **103a**	X		-50	113
2:1 **103a**		X	-52	117
4:1 **103b**	X		-27	98
4:1 **103a**		X	-58	71
6:1 **103c**	X		-43	59, 180
6:1 **103c**		X	-57	69, 161
8:1 **103d**	X		-52	63
8:1 **103d**		X	-48	140

3.7.3. Comparison of level of crystallinity visualised by DSC to that found by wide- angle X-ray scattering

WAXS measurements can provide data on phase separation and polymer chain structure.[78] In combination with the DSC experiment above, the level of crystallinity and hence change in microstructure upon annealing can be gauged.

Each NCO:OH ratio was subjected to WAXS after being annealed above and below the T_m.

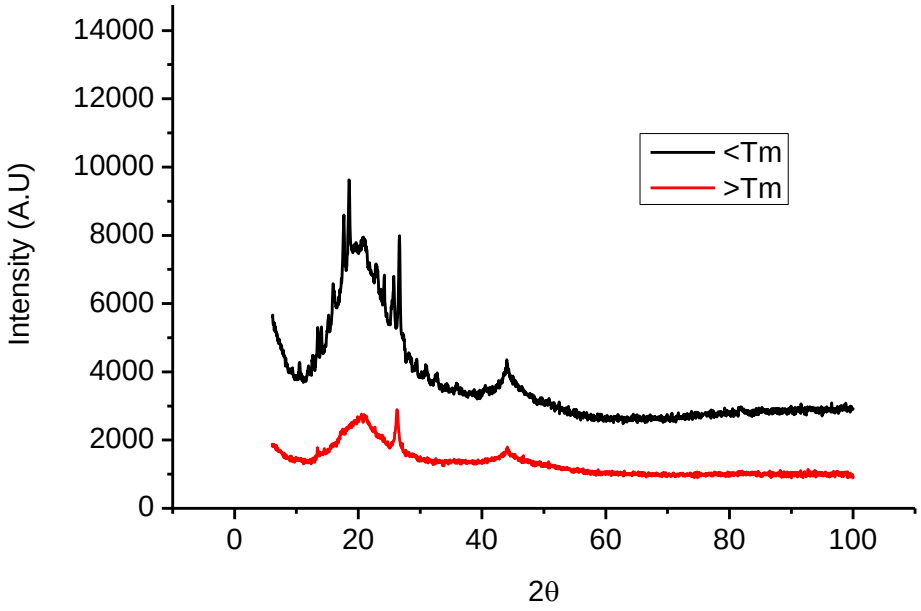

Figure 3.25 WAXS data of NCO:OH SPU = 2:1 103a after following the methods described in **Table 3.6**

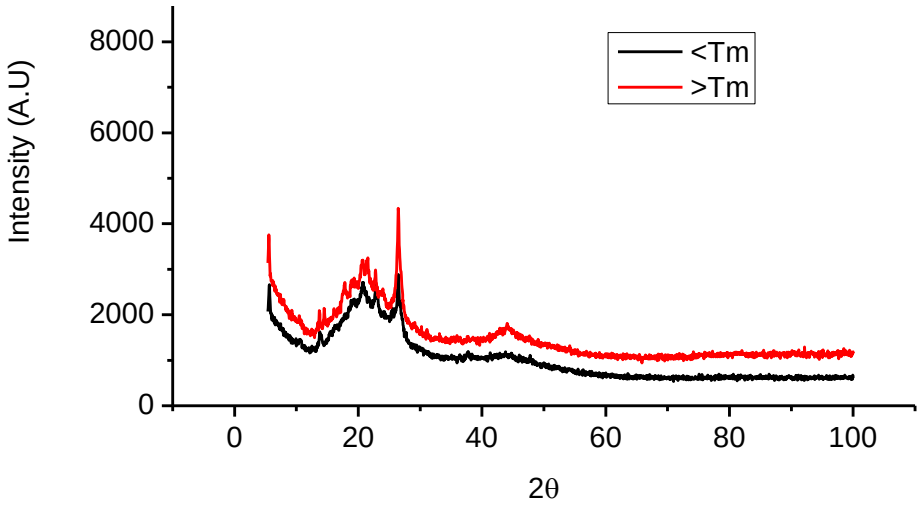

Figure 3.26 WAXS data of NCO:OH SPU = 4:1 103b after following the methods described in **Table 3.6**

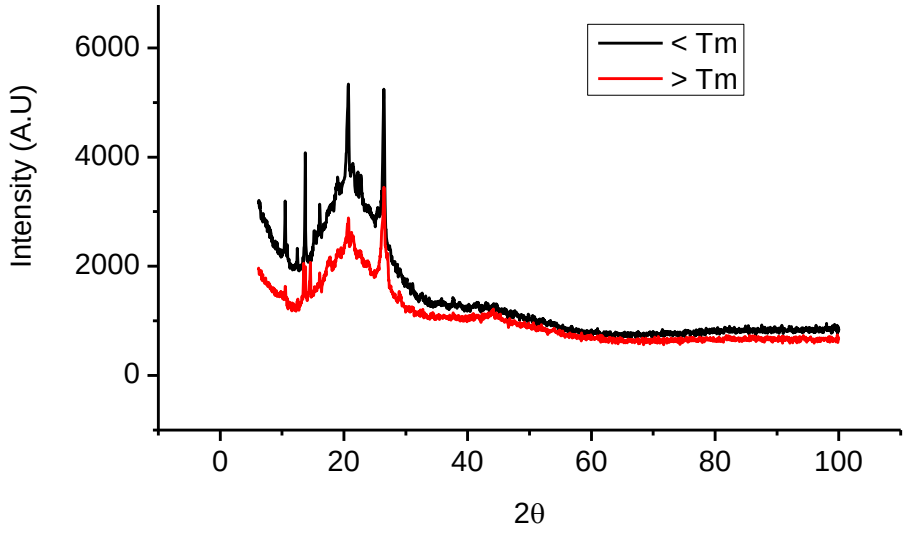

Figure 3.27 WAXS data of NCO:OH SPU = 6:1 103c after following the methods described in **Table 3.6**

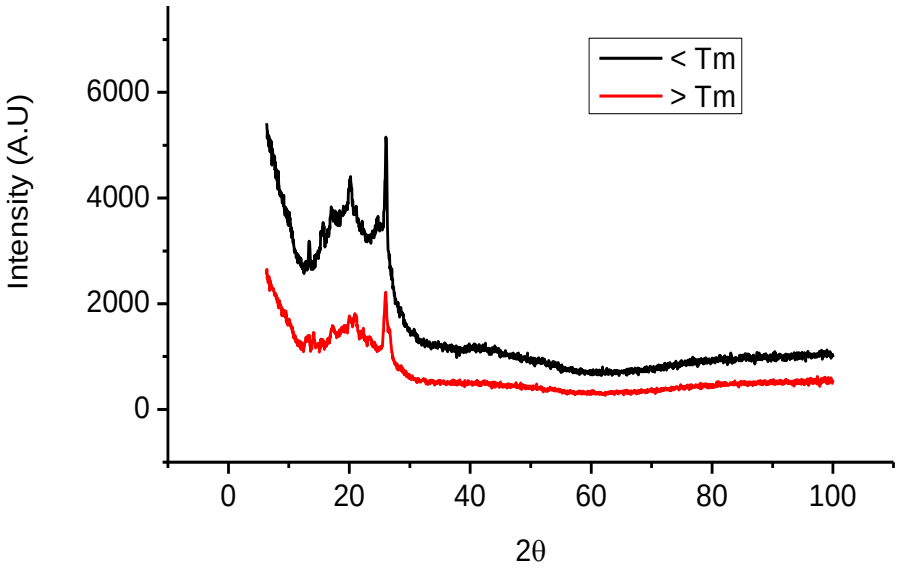

Figure 3.28 WAXS data of NCO:OH SPU = 8:1 103d after following the methods described in **Table 3.6**.

As NCO:OH ratio increases, the intensity of the reflection seen at 26 2θ is also seen to increase. This reflection can be attributed to scattering from the hard segments[160] which has been observed in various polymer systems.[78, 161-163]

As the NCO:OH ratio increases, crystalline peaks contained within the amorphous halo centred at 20 2θ for all ratios emerge. This is in line with observations by Samuels *et al.* and Miller and colleagues, who noted similar reflections for polyurethanes synthesised from PEG and MDI. This was attributed to increased phase separation as hard block percentage was increased.[163, 164] The amorphous halo becomes broader when the SPU was annealed above the T_m. As annealing temperature is increased, the lower molecular weight hard segments (*i.e.* supramolecular chain extension units) become increasingly dissolved in the soft phase, promoting a reduction in T_m. This is a common theme observed in the literature for covalent polyurethanes,[146, 156, 160, 162, 164-167], which has also been reported for supramolecular polymers.[24, 77, 78, 80, 168]

3.8. Variation of supramolecular polyurethane synthetic components to control materials properties

In Chapter 3.5- 3.7 it was shown that it is possible to control the level of crystallinity within SPU samples, and hence their mechanical responses and physical properties. With this in mind, it was decided to change the components of the macromonomer or supramolecular chain extender in the synthetic procedure.

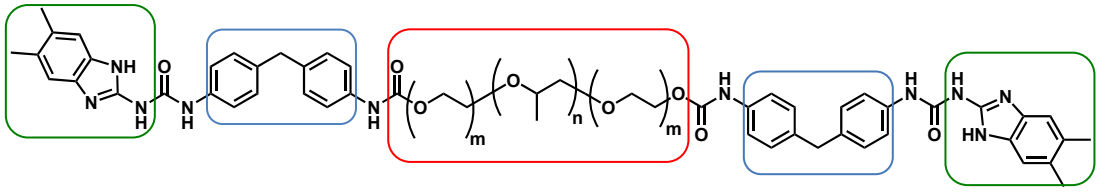

Figure 3.29 Cartoon representing the potential substitution points in the macromonomer 61. Green box signifies variation in amine starting material, blue box signifies variation in diisocyanate starting material and red box signifies variation in core telechelic polyol

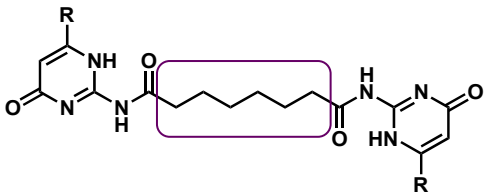

Figure 3.30 Cartoon representing a potential substitution point in the supramolecular chain extender 62. Purple box signifies variation in acid chloride used to form the chain linker between isocytosine units. R denotes Me

Based on the research using PEG-PPG-PEG **57** as the telechelic diol, it was assumed that to achieve adequate phase separation in our SPUs, the diol must be amorphous. To test this assumption, an SPU was synthesised using 2 kg mol^{-1} poly(THF) as the telechelic diol. Poly(THF) is a semi-crystalline polymer and hence has a higher tendency to crystallise than PEG-PPG-PEG **57**, and is used in PU products such as lycra, and in PU resins.[169]

The macromonomer **110** was formed using poly(THF), MDI **58** and 2-amino- 5,6-dimethylbenzimidazole **60 Scheme 3.4**.

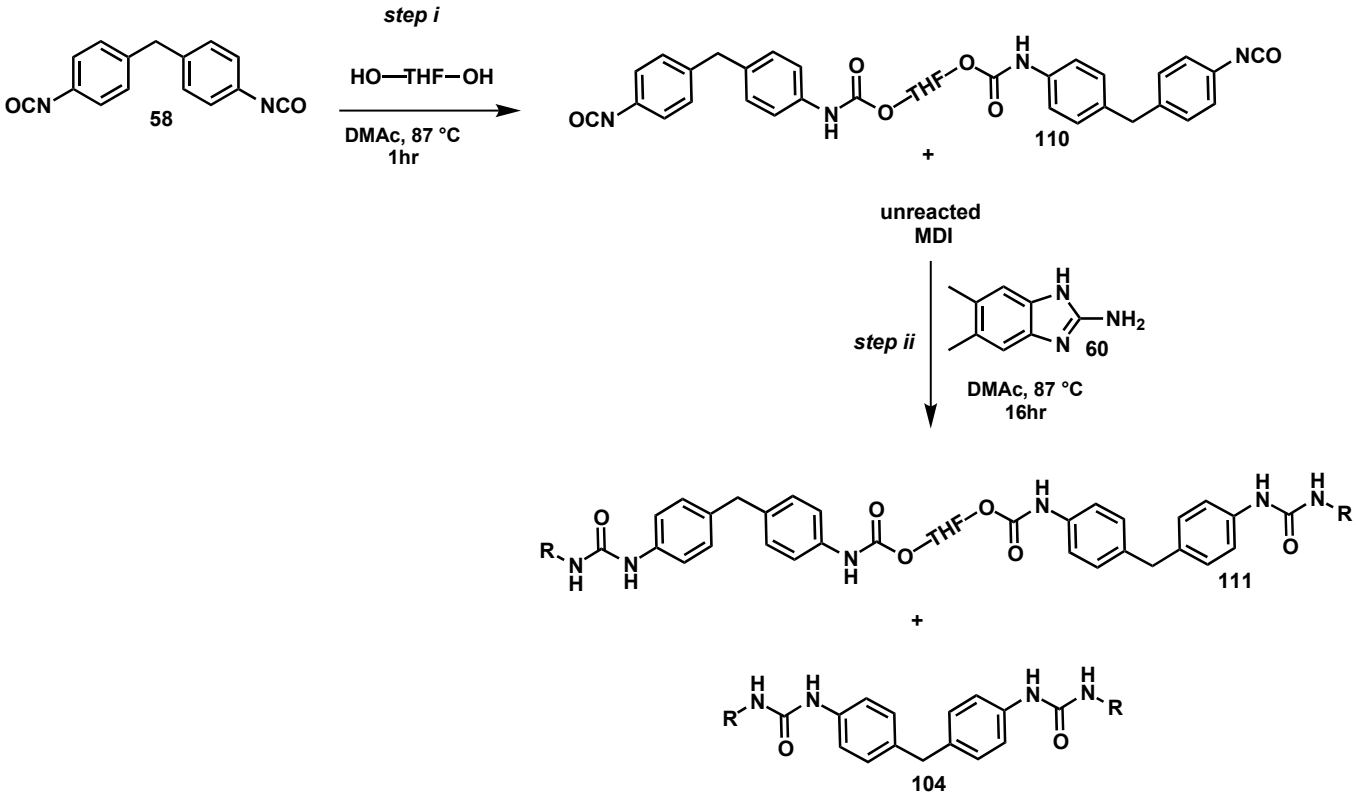

Scheme 3.4 Synthesis of triple hydrogen bonding array containing macromonomer 110. Using poly(THF) as telechelic diol. R denotes benzylimidazole

DAC **62** was added to the product in **Scheme 3.4** to form the SPU as a tacky brown solid and the isolated solid was subjected to DSC.

Pure poly(THF) has a T_g of 28 – 40 ºC[170]. The DSC trace shows a sharp melting transition of 13 ºC for the polyol core. This is reduced in temperature from the T_g of pure poly(THF). The melting transition of the hard block, seen at 73 ºC, is also reduced from that seen using PEG-PPG-PEG as telechelic diol, **Figure 3.31**. On the cooling cycles, endotherms are seen for both recrystallisations of the hard and soft blocks; something, which is absent for the soft, blocks in PEG-PPG-PEG SPUs.

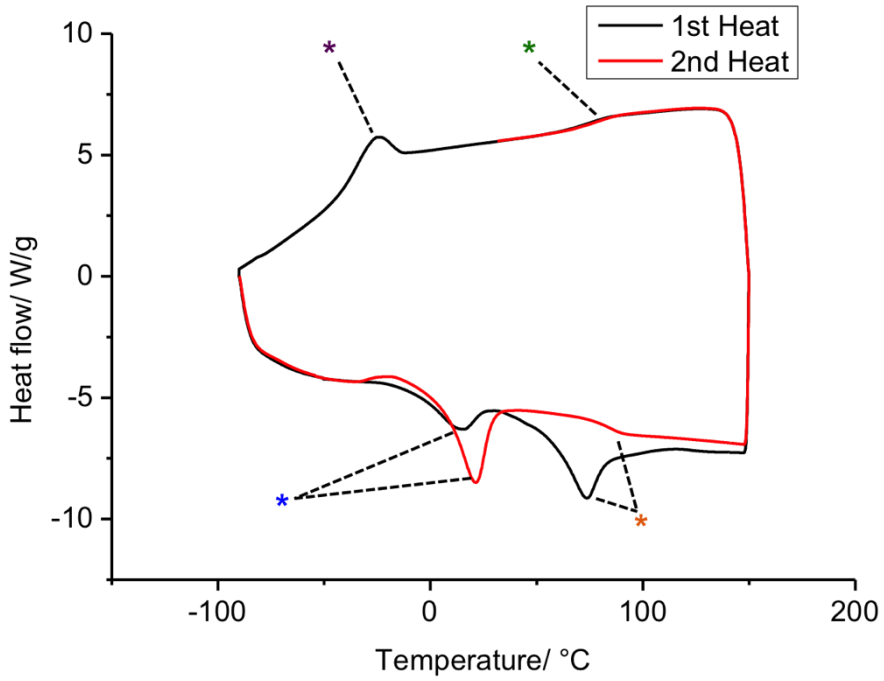

Figure 3.31 DSC trace of supramolecular polymer heated between -90 and 150 ºC at a rate of 10 ºC min^{-1}. Endotherm is up. * Indicate T_g whilst * indicates hard block transition. * Indicates recrystallization of hard block * indicates soft block recrystallization

Decreases in the transition temperatures seen in **Figure 3.14** indicate a high level of phase mixing as opposed to phase separation; an increase in relative free volume of the polymer chains and chain flexibility act to lower the T_g of the SPU. Because of the semi-crystalline nature of the poly(THF) core polyol, solute-solute interactions will be high, enabling efficient phase-mixing[171]. WAXS of the SPU showed decreased crystallinity in comparison to its PEG-PPG-PEG based parallel (**62b**). Notable peaks are starred, **Figure 3.32**. A minor diffraction peak at 15 2θ preceded a broad amorphous halo at 20 2θ, followed by a diffraction peak at 26 2θ corresponding to a distance of 3.4 Å. This confirms interactions between the hard blocks through π-π stacking and urea tape formation *cf*. PEG-PPG-PEG based SPUs **103a-d**. SAXS, **Figure 3.33**, revealed a single diffraction peak at 0.50 $Å^{-1}$, corresponding to a distance of 13 Å. This is the same distance as measured for PEG-PPG-PEG based SPUs, probably due to the similar molecular weight of telechelic diol.[142, 143]

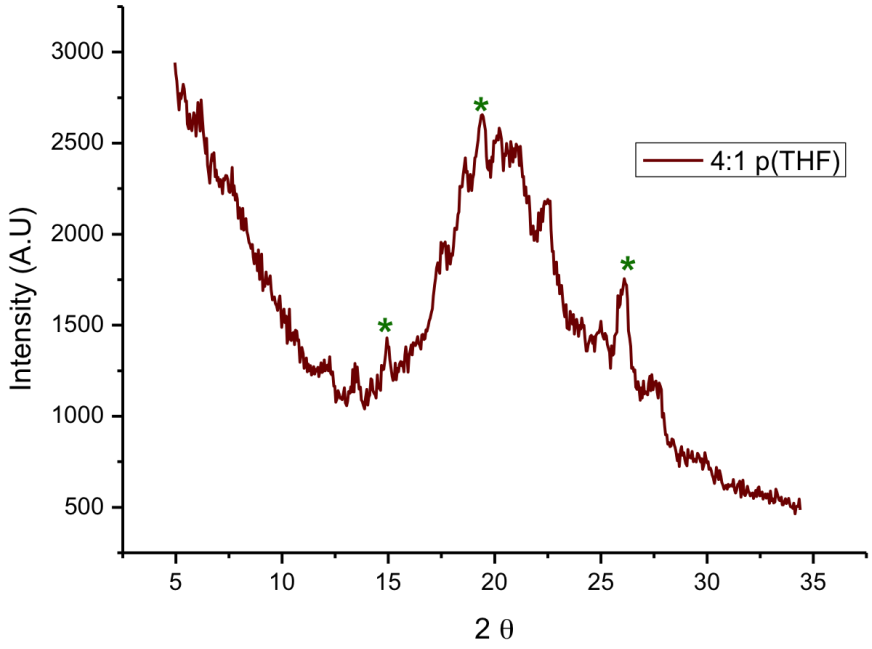

Figure 3.32 Diffraction data for SPU with NCO:OH 4:1. * Refers to reflections of interest

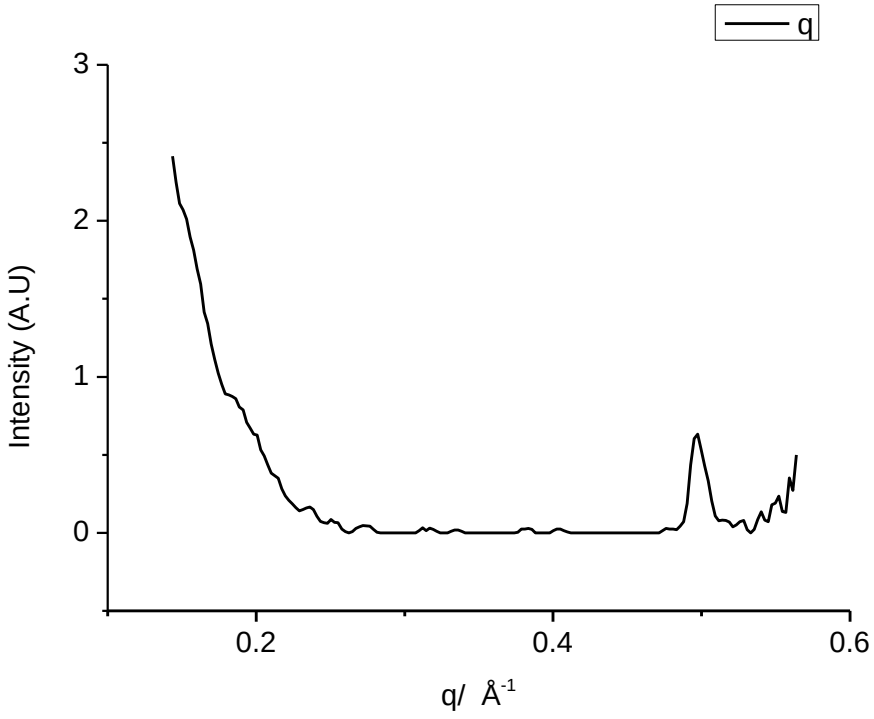

Figure 3.33 SAXS intensity profile for p(THF) SPU with NCO:OH= 4:1

Synthetic changes in the soft phase (*i.e.* PEG-PPG-PEG), showed a similar diffraction peak as reported by SAXS. Synthetic changes in the hard phase were therefore contemplated as alternatives to modulate phase separation. Three different supramolecular chain linkers were synthesised to study effect on hard phase, and as a direct result, soft phase.

Three alternative supramolecular chain linkers **112-114** were synthesised from 2-amino-4-hydroxy-6-methylpyrimidine **101**, **Figure 3.5**.

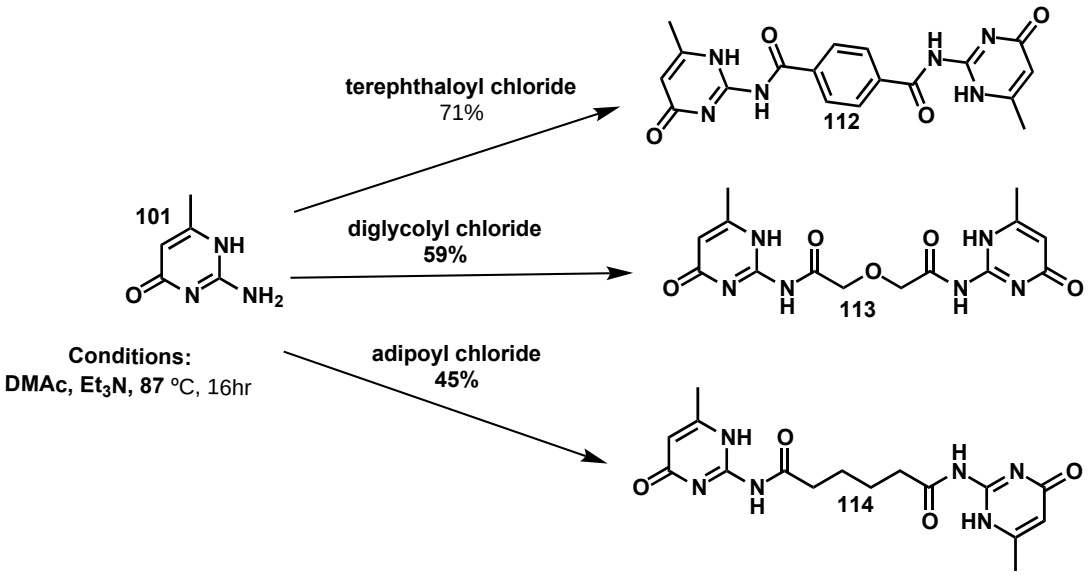

Scheme 3.5 Synthesis of three alternative supramolecular ditopic chain extenders 112-114 complementary to the macromonomer 61

The isolated pure compounds above were each added to the macromonomer to form three supramolecular polymers, **115, 116** and **117** respectively, **Figure 3.34**.

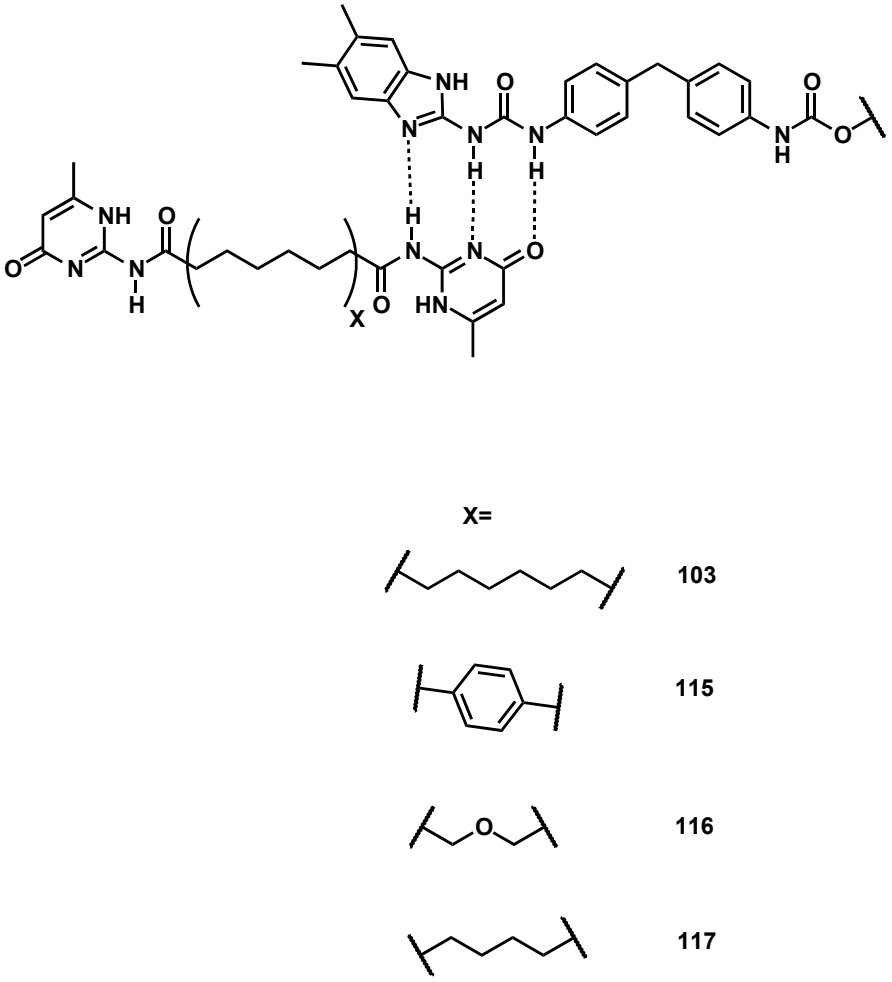

Figure 3.34 Synthesis of three alternative supramolecular polymers to 103, 115-117

All SPUs were synthesised at a ratio of NCO:OH = 4:1 to study structure function relationships with this new family of compounds. This is due to the ability of the suberoyl containing SPUs **103b** to be fully thermally and mechanically characterised at this ratio.

The study of the materials properties led to each of the samples being subjected to DSC and DMTA for quantification.

DSC analysis gave the T_g and T_m for the soft and hard blocks contained within each SPU, **Figure 3.35**.

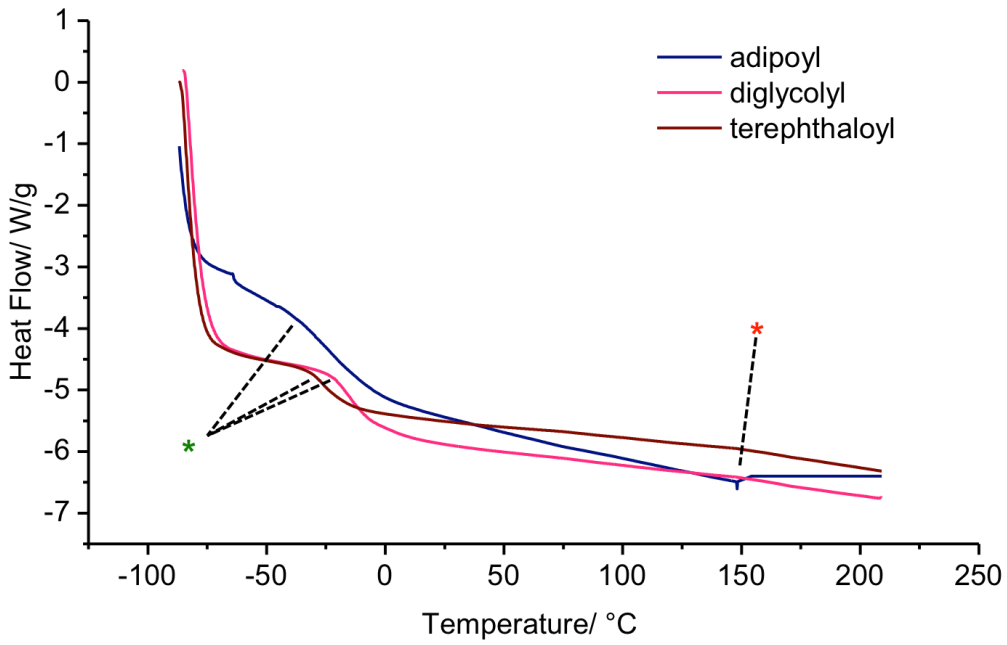

Figure 3.35 DSC trace of the second heating cycle of SPUs 115-117. Cycled between -90 and 200 ºC at a rate of 10 ºC min^{-1}. Endotherm is up. * Indicates T_g whilst * indicates hard block transition.

The aromatic nature of the terephthaloyl moiety in **112** and subsequent SPU **115** stimulated interest into whether an increase in π-π stacking could be effected and hence change hard phase order through enhancement of phase separation within the material.[172] On visual inspection alone, **115** formed a harder material, which was tougher to deform mechanically in comparison to **103b**. The DSC records an increased T_g over all other SPUs of -11 ºC, and has no obvious melting transition, suggesting that it has been shifted to a much higher temperature, in agreement that order has been enforced on both the soft and hard phases. Wilkes and colleagues previously ascertained that by observing the T_g, the level of any potential phase mixing could be determined. They concluded that any small amount of hard phase which becomes mixed into the soft phase can restrict chain mobility of the urethane chain, increasing T_g.[173]

Ether based linkers **113**, have previously been used in covalent PUs as they are known to aid phase separation in PU elastomers as they are incompatible with MDI and MDI oligomers.[174] They are also known to increase flexibility of alkyl chains in comparison to methylene due to the increase in free volume surrounding the oxygen linker, providing greater degrees of freedom.[175] Compound **116** was the most

malleable of all SPUs and showed some remarkable shape retention properties after deformation. The T_g for **116** is decreased by 40 ºC from terephthaloyl containing SPU **115** to -51 ºC. The ether linkage provides the flexibility so that the soft block components are more mobile and less hindered and hence does not crystallise sufficiently to promote high order in this phase. This behaviour could also explain the very wide T_g, which is exhibited for this SPU.

The third novel SPU **117**, was very similar to compound **103b**, from which is was derivatised, in that it formed a tacky brown soft solid. **117** shows deviation in both T_g and in T_m from **103b** suggesting chain length does have an effect on the ability for the SPU to produce order in the soft and hard phase. SPU **117** exhibits a clear melting transition at 150 ºC, which is an increase in temperature from original NCO:OH = 4:1 SPU **103b**, which shows T_m at ~125 ºC. This transition can be attributed to the dissociation of interurethane hydrogen bonding produced by complex domain structure.[136]

Much like SPU **116**, the T_g for **117** has a wide range in temperature over which it occurs. The onset temperature for the T_g of **117** is 15 ºC below the midpoint, which gives a T_g in-line with the traditional literature definition of – 20 ºC. The onset temperature for **103b** is only 3 ºC below the midpoint value, which is – 59 ºC. The higher temperature for the shorter alkyl chain containing SPU **117** is indicative that alkyl chain length does impact the ability for the polyurethane to self assemble. The T_m of both SPUs **103b** and **117** are different, signifying order is enhanced in the soft and hard phase of the phase separated PU. This enhanced order could again come from minimal phase mixing at phase boundaries, which rigidifies the urethane chains. Petrović commented that hard segments at chain ends (which our system relies upon) exacerbates phase mixing.[176] The butyl- methylene chain of **117** as opposed to the hexyl- methylene of **103b** may also permit the MDI units to π-π stack in a way, which permits higher crystalline order.[75, 177]

Table 3.8 Summary of soft and hard block transitions for alternative supramolecular chain linkers

Supramolecular chain linker and SPU	*T_g / ºC measured by DSC*	*T_m / ºC measured by DSC*
Suberoyl **103b**	-42	125
Terephthaloyl **115**	-11	-
Diglycolyl **116**	-51	Broad
Adipoyl **117**	-20	150

DMTA studies were instigated to further study the mechanical properties of each of these materials.

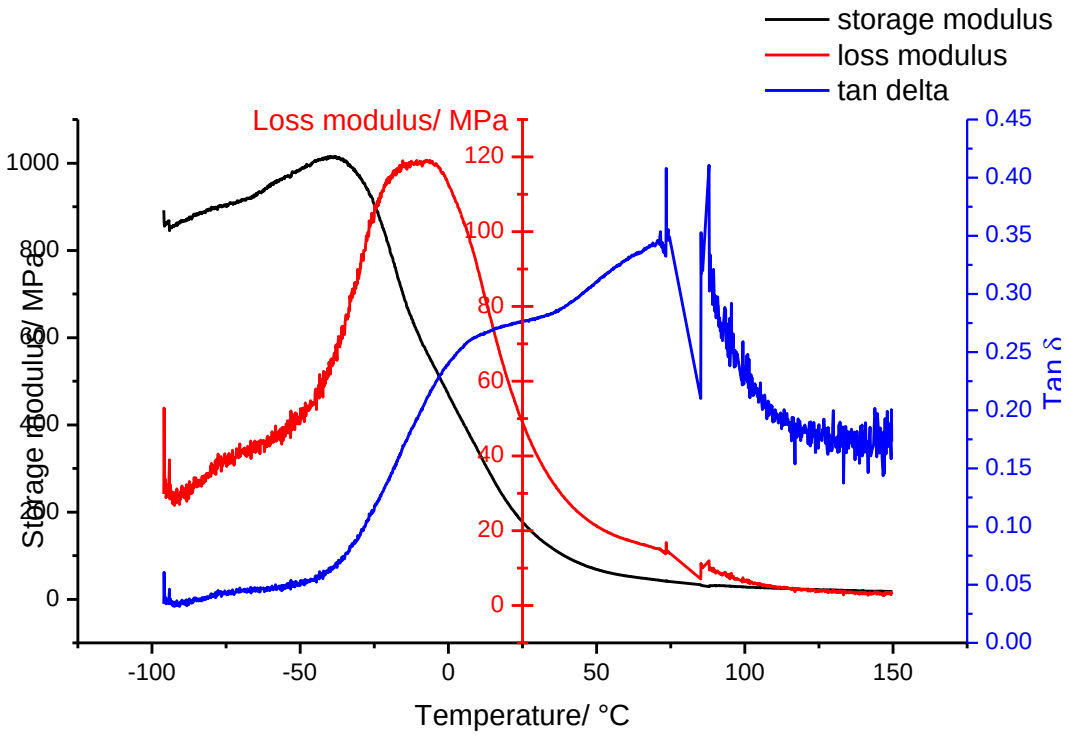

Figure 3.36 DMTA curves of SPU 115

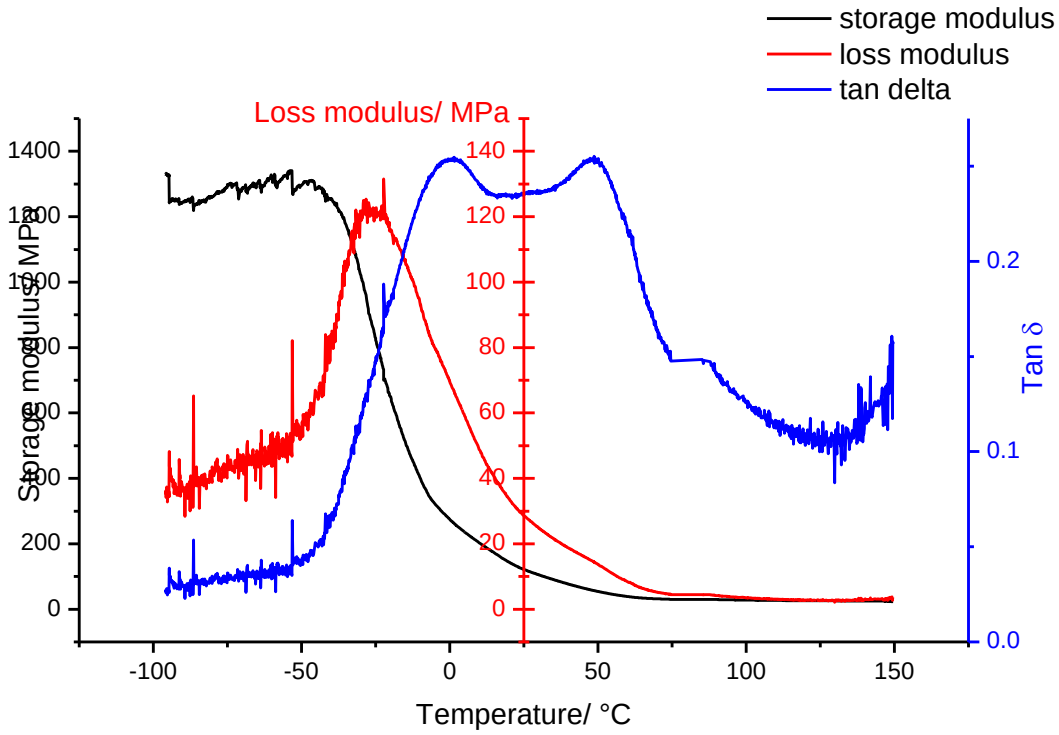

Figure 3.37 DMTA curves of SPU 116

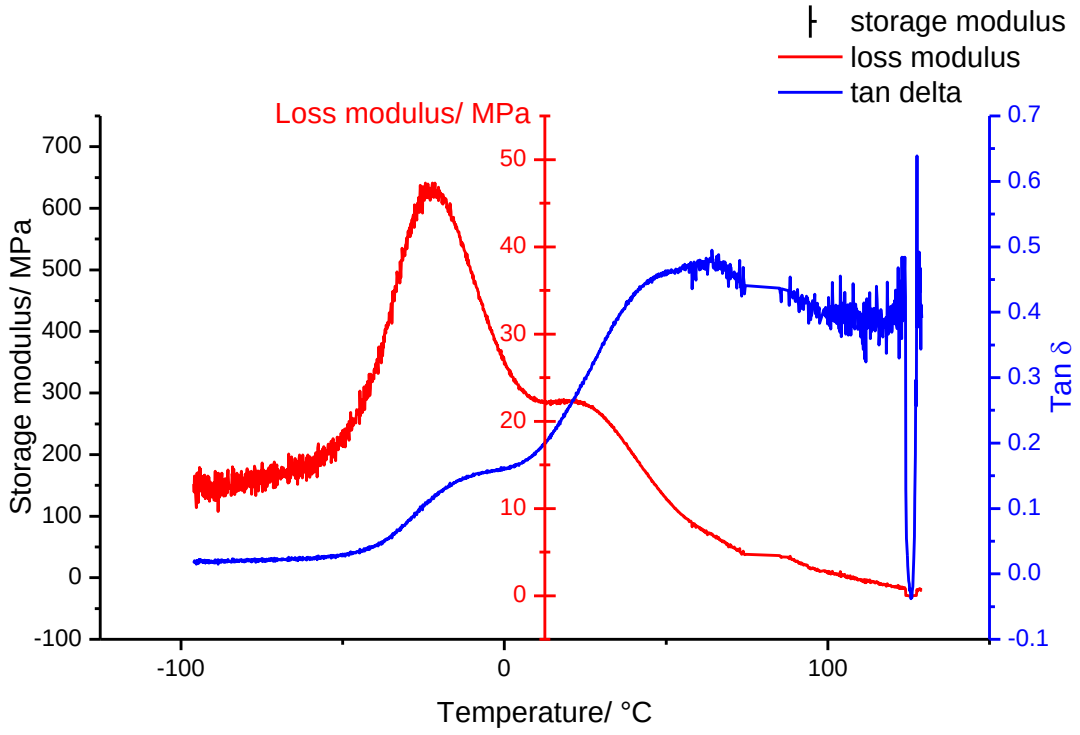

Figure 3.38 DMTA curves of SPU 117

The T_g recorded for DMTA of the SPU is designated by the loss modulus reaching a maximum. In agreement with that seen for the suberoyl chain linked SPU **103b**, the T_g are shifted upwards from the value obtained by DSC. DMTA alone has variations on the value of the Tg, based on the peak value of loss modulus or tan(∂) and the plateau region of the storage modulus. In-depth studies have concluded the most accurate way of defining the T_g from DMTA is from the peak value of loss modulus.[132, 149] As a consequence, it can be seen, **Figure 3.38**, **Figure 3.36** and **Figure 3.37**, that SPUs **116** and **117** have the lowest T_g, -30 ºC. This is a deviation from the values obtained by DSC of 21 ºC and 10 ºC respectively. Original suberoyl chain linker **103b** suffers the largest deviation of 27 ºC. Aromatic terephthaloyl linker produces concordant results, with a deviation of only 1 ºC. The thermal properties of the SPUs depend upon the thermal and mechanical history and this deviation in temperature between DSC and DMTA could arise from an increased level of cross-linked (*i.e.* hydrogen bonded) polymer chains when being subjected to the DMTA procedure.[178] Changes in the heating rate, sample size and the dynamic nature of DMTA as opposed to static nature of analysis used in DSC, have also been reported to effect the agreement of values.[147, 178, 179]

Because of the viscoelastic nature of the SPUs, storage modulus is an important component of their elastic properties. T_g in this instance is typified by a dramatic decrease in stiffness, as viscosity of the SPU increases.[22] The T_g found by analysis of the storage modulus in these cases roughly agrees with the values found from the loss moduli. As the temperature increases, all of the SPUs behave in a similar manner, retaining a storage modulus of ~100 MPa up to 50 ºC. Storage modulus is generally proportional to molecular weight, as longer chains result in the formation of more entanglements, rigidifying the PU.[146, 180] With this in mind, the trend followed by this series of SPUs is generally in agreement. The anomaly is the diglycolyl containing chain linker; it has the lowest percentage hard block, yet the second highest storage modulus. Additional stiffness in SPU **116** could be attributed to the supplementary level of hydrogen bonding capability from the ether group at these low temperatures, providing a higher number of physical cross-links between

lateral chains of polymers. These cross-links are readily breakable, affording SPU **116** with the lowest T_g as observed *via* DSC.

Table 3.9 Summary of soft and hard block transitions for alternative supramolecular chain linkers

Supramolecular chain linker and ***SPU***	*T_g / ºC DMTA E"*	*Deviation from DSC / ºC*	*T_m /ºC DMTA E'*	*Deviation from DSC / ºC*
Suberoyl **103b**	-15	+27	120	0
Terephthaloyl **115**	-10	+1	100	N/A
Diglycolyl **116**	-30	+21	-	N/A
Adipoyl **117**	-30	+10	120	0

3.9. Conclusions

It has been shown that the assembly of a supramolecular linear polyurethane is controlled principally by the presence of heterocomplementary hydrogen bonds. When complementary partners were absent, the materials formed were not capable of self-support, and hence could not be mechanically or thermally characterised. With the additional support of other non-covalent interactions, such as π-π stacking and urea/urethane tape formation between lateral chains, the triple hydrogen bond array formed selectively between a low-molecular-weight polyurethane and a supramolecular chain extender showed materials properties, that are reminiscent of covalent analogues.

It was also shown that these properties are controllable and tuneable. By increasing the ratio of hard block to soft block, crystallinity of the SPU was increased, in turn increasing crystalline order and hence T_g of the soft phase. Increasing crystallinity also encourages greater phase separation, which bestows the SPUs with the desirable properties of malleability and shape retention.

It was found that treatment of SPUs based on their thermal history directly impacted the thermal transitions of the materials as evidenced by DSC, SAXS and WAXS.

By removing the previous thermal history of the materials by melting, the most thermodynamically favourable state was formed, demonstrated in DSC as the display of one endotherm each for T_g and T_m. Analysis of untreated samples and samples which were annealed without first melting revealed a mixed phase morphology postulated by Saiani *et al*. The melt of the 'pure' hard block was seen to occur as a separate event from phase separation of the mixed phase, which was evidenced at higher temperatures. A relatively low crystallinity was observed for all SPUs *via* WAXS, however this crystallinity was reduced when the samples were annealed above T_m. This is seen as a broadening of the amorphous halo and a decrease in the number of reflections seen.

Thermally treating the samples is relevant to the behaviour of the materials in bulk state, as the temperatures of the soft and hard block transitions are greatly affected, which would in turn effect the application of the material as a polymer. Increased phase separation by annealing below T_m resulted in the presentation of one endotherm when the sample was subjected to DSC. Increased phase mixing occurred when heating above the T_m, evidenced as a lowered T_m and a raised T_g.

To investigate the tuneabilty of the SPUs, we studied the effect of changing parts of the SPU structure. Exchanging PEG-PPG-PEG for p(THF) resulted in an increase in phase mixing, resulting in reduced crystallinity and T_m in the overall SPU. By changing the molecular structure of the supramolecular chain linker, we found that aromatic cross-links provide additional stability, presumably through π-π stacking and greater ability to hydrogen bond. In contrast, by elongating the supramolecular chain extender, order in the soft phase is decreased, evidenced by a reduction in T_g in comparison to a linker two carbons shorter. The glycol supramolecular chain extender provides additional flexibility to the SPU and hence develops reduced melting temperatures of soft block. Increased phase separation raises the T_m to 30 ºC above the suberoyl based SPU. Surprisingly, the ability of the glycol group to participate in hydrogen bonding could explain the increased initial storage modulus of the SPU of over 1300 MPa, showing a higher stiffness than that achieved by the aromatic chain linker.

Chapter 4

Alternative synthetic routes to polyurethanes

4 Chapter 4

4.1 Development of alternative synthetic routes for polyurethane synthesis and supramolecular polymer formation

The demand on the performance and longevity of PUs is high because of the diverse applications in which they are used.[6] Industrially, synthetic processes used to access PUs are carried out under bulk conditions (*i.e.* absence of solvent). Viscosity control is necessary when using bulk conditions, as reaction products are susceptible to aggregation and premature crystallization during synthesis.[181] On laboratory scale, solution phase syntheses are carried out in polar, high boiling point solvents to counteract the decrease in solubility, which is aggravated by an increase in molecular weight as the polymer chain grows.

It is therefore desirable to look for cheaper, more economical and efficient ways of producing novel PUs with unique properties,[69] which exploit undemanding processing and the utilisation of renewable materials.

Supramolecular polymers offer opportunities for the design of novel synthetic methods, given that synthesis of the low molecular weight building blocks may be more amenable to common strategies employed to limit environmental impact.[18]

4.2 Statistical reaction products from di-functionalised alcohols and isocyanates

Flory's principle of equal reactivity states that the chemical reactivity of a functional group does not necessarily depend on the size of the molecule to which it is attached. Therefore at each stage of a polymerisation, the reactivity of every like functional group is assumed to be the same.[182] The principle allows the application of simple statistical models to describe the distribution of statistical products.

The reaction of diisocyanate MDI **58** and telechelic diol PEG-PPG-PEG **57** described in Chapter 3 follows Flory's theory, indeed producing a distribution of statistical products, described in Appendix iii. For brevity, as the ratio of MDI:OH is

increased, statistical models show an increased percentage of polyol end-capped at both ends with MDI units, *i.e*. the level of covalent chain extension is decreased.

A goal in synthetic PU chemistry is to eliminate the statistical distribution of products and hence form perfectly end-capped telechelics. In this work, several methods to this end were explored, including using heavily hindered ureas as masked isocyanates.

4.3 Using masked isocyanates for polyurethane and carbamate synthesis

Masked, or blocked, isocyanates have been the subject of a major review by Ganachaud and colleagues.[10] Hutchby *et al*. reacted an arylisocyanate **96** with a secondary amine **120** to form a trisubstituted hindered urea **121**, Scheme 4.1.[183]

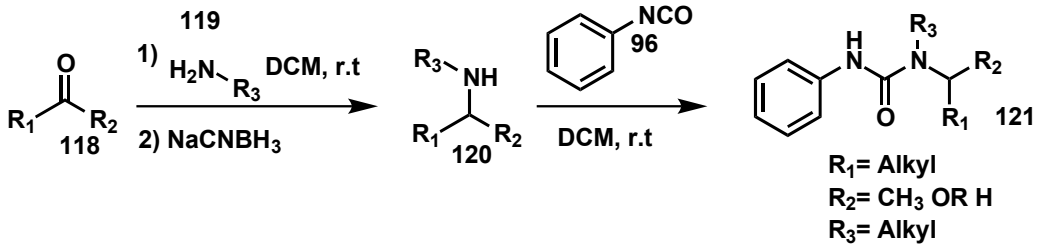

Scheme 4.1 Formation of a hindered urea 121 described by Hutchby et al.

Hindered ureas are usually inert to nucleophilic amines and alcohols, making them efficient masking groups for isocyanates. Hutchby *et al.* demonstrated very labile aniline-based ureas, which were capable of undergoing substitution with select small chain alcohols, at reduced temperatures, without catalysis. The solvolysis of hindered urea **121** in methanol resulted in formation of the methyl carbamate **123** after 1 hour at 20 °C in more than 99% yield, **Scheme 4.2**.

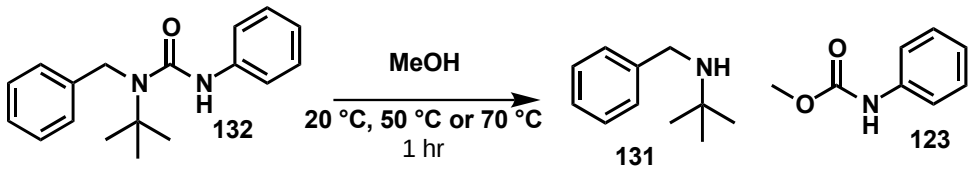

Scheme 4.2 Methanolysis of hindered urea 122 as described by Hutchby *et al.*

The carbamate formation demonstrated in **Scheme 4.2** represents a model reaction for urethane formation. Masking the isocyanate groups of MDI **58** to produce an unsymmetrical bisurea **124**, **Scheme 4.3**, would enable the selective mono-substitution reaction with a nucleophile for urea or urethane formation with milder reaction conditions in comparison to the reaction conditions previously reported by Gooch *et al.*.[80] It would also allow for selective capping of telechelics.

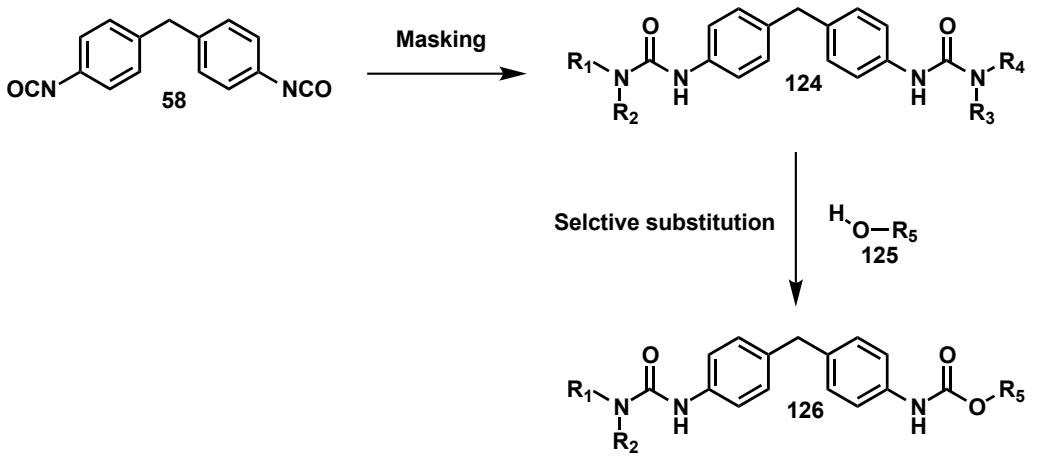

Scheme 4.3 Masking of isocyanate functionality of MDI 58 to form unsymmetrical ureas 124, followed by subsequent selective substitution with an alcohol nucleophile to form the corresponding urethane 126. $R_{1\text{-}5}$ denotes any alkyl or aryl unit

The synthesis outlined in **Scheme 4.1** was replicated using the reported conditions, but it was not possible to reproduce the disubstituted amine.

An alternative route to secondary amines was employed using the procedure reported by Taylor and colleagues.[184] An *in situ* oxidation- imine formation-reduction sequence utilising manganese dioxide and sodium borohydride produced an array of secondary amines **128**, **Scheme 4.4**.

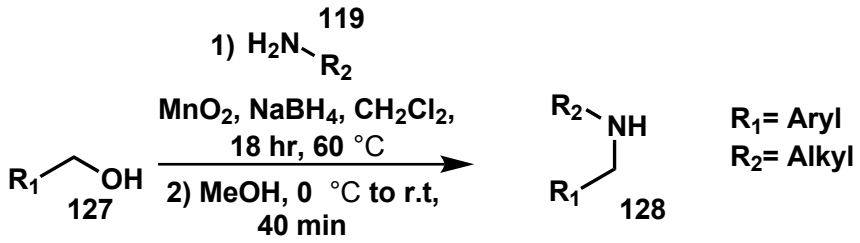

Scheme 4.4 Secondary amine synthesis reported by Kanno *et al.*

Compound **132** was prepared by further reaction of secondary amine **131** with phenylisocyanate **96**, **Scheme 4.5**, after following the procedure outlined in **Scheme 4.4**.

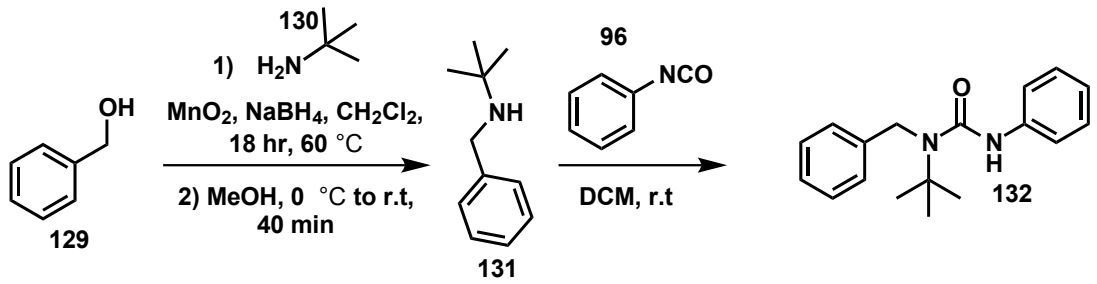

Scheme 4.5 Synthesis of a hindered urea 132 using the method reported by Kanno *et al.*

Successful isolation of the hindered urea **132** allowed subsequent methanolysis studies at a range of temperatures, to be performed in order to gauge whether nucleophilic substitution and hence carbamate formation **123** was possible, **Scheme 4.6**.

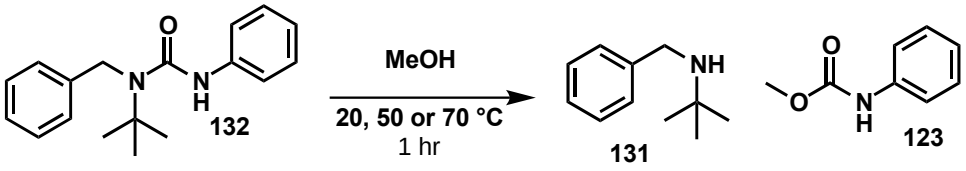

Scheme 4.6 Methanolysis study of hindered urea 132

Table 4.1 Summary of conversion of hindered urea 132 to methyl carbamate 123

Entry	*Temperature/ °C*	*Conversion to carbamate **123**/ %* *
1	20	0
2	50	100
3	70	100

*Conversion to carbamate as determined by crude ^{1}H NMR in combination with LC-MS traces of the reaction mixture

As seen in **Table 4.1**, **132** was not as susceptible to nucleophilic substitution as the urea reported by Hutchby *et al.*, but underwent complete carbamate formation at 50 °C. During purification of the desired carbamate shown in **Scheme 4.6**, it was possible to isolate the blocking amine **131**. Due to low volatility, the amine **131** is not lost during purification and hence could be recycled for subsequent blocking reactions.

Consequently, the *N*, *N*- *tert*-butyl *iso*propyl amino phenyl urea **122** in **Scheme 4.2**, isolated by Hutchby *et al*. was synthesised in a similar manner to that in **Scheme 4.5**. Methanolysis of this compound revealed conversion to carbamate **123** in more than 96% isolated yield at 20 °C for 1 hour, confirming the results found by Hutchby and co-workers.

Since a viable synthetic route to hindered amines was identified, reaction with MDI **58** to form an unsymmetrical urea **134** was attempted, **Scheme 4.7**.

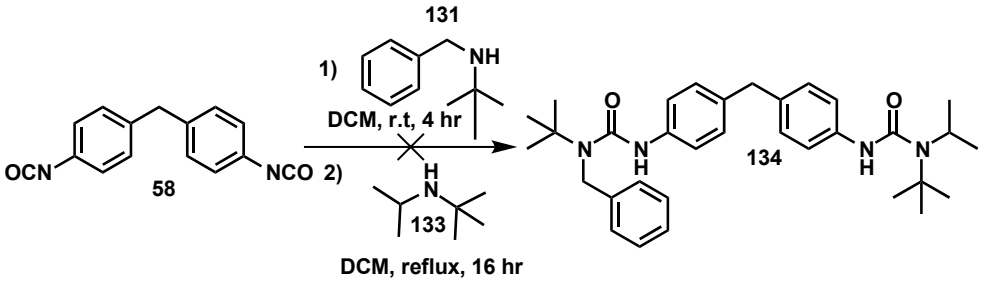

Scheme 4.7 Failure of the reaction of MDI 58 with two secondary amines 131, 133 to form a disubstituted unsymmetrical urea 134

After Step 1, **Scheme 4.7**, the monosubstituted urea was seen *via* liquid chromatography- mass spectrometry (LC-MS), and TLC plates of the reaction mixture stained with ninhydrin and potassium permanganate gave negative results for presence of the secondary amine. The presence of a disubstituted symmetrical urea was not seen at this stage. Step 2 did not yield the desired unsymmetrical urea **134**. Formation of the first urea and loss of the first isocyanate group negates its influence on reactivity of the second isocyanate group. The *para*-methylene bridge between the aryl rings has a deactivating effect on the remaining isocyanate, hence decreasing its reactivity as documented by Spaunburgh and colleagues, **Figure 4.1**.[185]

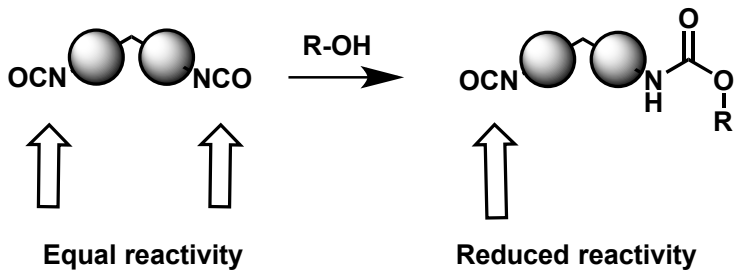

Figure 4.1 Effect of carbamate formation on the reactivity of the second isocyanate group in an aromatic diisocyanate

Because of the low reactivity of the amine **133** towards the remaining isocyanate functionality combined with the manganese dioxide waste, which occurs from synthesis of the secondary amines, an alternative was sought to form hindered ureas.

Commercially available amines were used to form hindered ureas, namely di*iso*propylamine, **Scheme 4.8**.

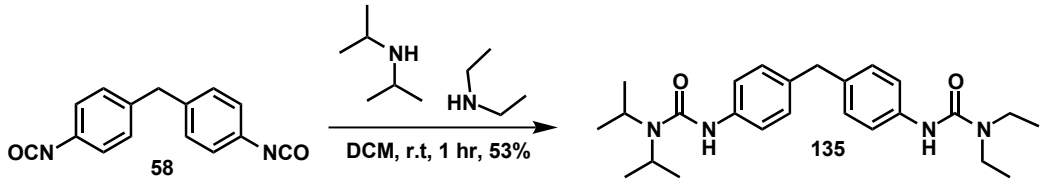

Scheme 4.8 Reaction of MDI 58 with commercially available amines to form a bisurea 135 for solvolysis studies. 53% pure product is isolated after separation of undesired products *via* column chromatography

Compound **135** synthesised in **Scheme 4.8** is unique in its design in that one of the ureas is more sterically hindered than the other. It was postulated that the most strained urea, *i.e.* the most sterically hindered, would undergo solvolysis with a nucleophile. To test this hypothesis, **135** was subjected to solvolysis, firstly with methanol at different temperatures, then with different alcoholic solvents, **Table 4.2**.

Table 4.2 Summary of conditions for solvolysis of hindered urea 135 for 2 hr.

Entry	*Temperature/ °C*	*Solvent*	*Conversion to carbamate/ % * 135*
1	20	Methanol	0
2	50	Methanol	20
3	70	Methanol	100
4	70	Ethanol	100
5	70	1-Propanol	0
6	70	2-Propanol	0
7	70	Ethylene glycol	0

*Conversion to carbamate as determined by crude ^{1}H NMR in combination with LC-MS traces of the reaction mixture

It was found that the di*iso*propyl urea only was substituted at each temperature, making the reaction selective, **Scheme 4.9**.

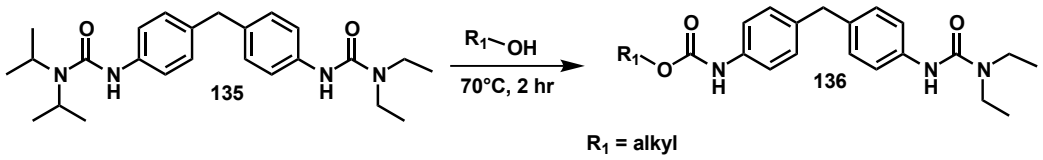

Scheme 4.9 Selective solvolysis of hindered bisurea 135 with nucleophilic solvent to form mono-carbamate 136. R_1 denotes alkyl chain

By gradually increasing the molecular weight and/or complexity of the alkyl chain, *i.e.* branching, the alcohol became less proficient at solvolysis. PEG-PPG-PEG analogue ethylene glycol did not react to form a carbamate, suggesting that a 2000 $gmol^{-1}$ diol terminated polymer would also be incapable of reaction. The increased viscosity associated with a 2 $Kg\ mol^{-1}$ polyol presumably decreases the effectiveness of smaller molecules to diffuse through the polymer solution, resulting in a slower reaction rate.

Low-molecular-weight alcohols were found to promote solvolysis of the unsymmetrical diurea, **135**. However, as the carbon chain was increased above 2, no conversion to carbamate **136** was seen. The use of hindered ureas as masked isocyanates was therefore deemed as an unviable option for controlled end-capping of a PEG-PPG-PEG **57** diol.

4.4 Solution phase catalysis

Failure to employ masked isocyanates for the synthesis of polyurethanes resulted in returning to the original reaction, and implementing changes to the reaction conditions.

The one-pot synthesis of the macromonomer **61** described in Chapter 3 is amenable to reaction condition changes, such as solvent, temperature and catalyst. Industrially, it is typical to synthesise PUs in the presence of a catalyst, which generally falls into two categories- organotin or amine based.[10, 75, 186, 187] Dibutyltin dilaurate is extensively used on an industrial scale.[188] A fast reaction time is offset by residual amounts of the compound affecting the lifetime of the polymer product.[189] The toxicological consequence of heavy metals leaching into the surrounding environment are also very complex.[190]

Non-nucleophilic organic bases have also been shown to catalyse urethane formation. Steinle *et al.* documented the reaction between MDI **58** and butanediol, noting the decrease in activation energy of the reaction by half using diazabicyclo[2.2.2]octane (DABCO) **141**, in comparison to the uncatalysed

reaction.[191] Reduced usage of DABCO **141** however is desirable, as this too exhibits environmental toxicity.[10, 75]

4.4.1 Catalysis of carbamate formation

Burkus previously reported conditions for triethylamine (Et_3N) **140** catalysed carbamate formation between isocyanates and various alcohols, **Scheme 4.10**.[192, 193]

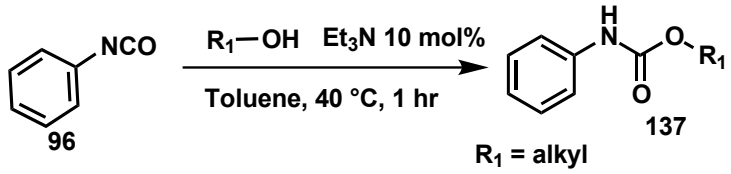

Scheme 4.10 Investigation of catalysed carbamate formation by Burkus *et al.* R_1 denotes alkyl chain

Et_3N **140** is more desirable as a catalyst than DABCO **141** due to reduced toxicity and cost, and because low volatility means it can be removed from reaction vessels separate to the PU product, and recycled.

The reaction conditions in **Scheme 4.10** were applied to a model reaction between 1-propanol **138** as a PEG-PPG-PEG low-molecular-weight analogue, and MDI **58**.

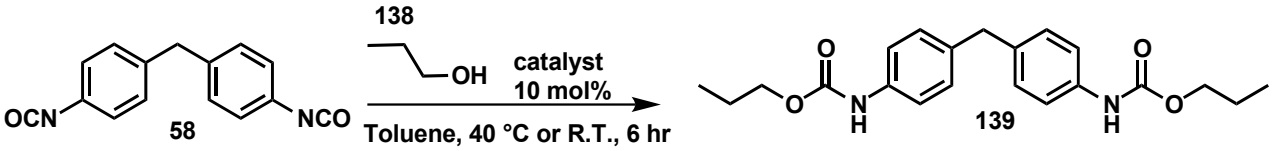

Scheme 4.11 Reaction of MDI 58 with 1-propanol 138 to form biscarbamate 139 using 10 mol% of basic catalyst in toluene at room temperature or 40 °C for 6 hours. See Table **4.3** for yields under various conditions

Using one equivalent of Et_3N **140**, precipitation of the biscarbamate **139** from the solution was evident after 1 hour and afforded product in ~60% yield. The promising results from using Et_3N **140** as a catalyst for carbamate formation prompted a more extensive study. The effect of different catalysts, catalyst p*K*a and reaction temperature on **Scheme 4.11** were considered. Triazabicyclo[4.4.0]dec-5-

ene (TBD) **143** and DABCO **141** were also used in comparison to the uncatalysed reaction.

Table 4.3 Summary of conditions[#] for the study of carbamate synthesis using 1-propanol 138 and MDI 58

Entry	Catalyst	pKa	Temperature/°C	Conversion to carbamate* **139**
1	None	-	r.t	29
2	None	-	40	29
3	Et_3N	10.8	r.t	75
4	Et_3N	10.8	40	74
5	DABCO	8.9	r.t	91
6	DABCO	8.9	40	97
7	TBD	22	r.t	67
8	TBD	22	40	66

*****Conversion is based on the integration of product signals against starting materials from crude ^{1}H NMR. [#] General conditions; 10 mol % catalyst in toluene for 6hr, 1 equiv. MDI, 2 equiv. 1-propanol.

DABCO **141** and Et_3N **140** were found to be superior catalysts in comparison to the uncatalysed reaction. The crude yield was greatly increased from 29% uncatalysed to 97% and 74% for DABCO **141** and Et_3N **140** respectively at 40 °C. Temperature does not affect the crude conversion for all catalysts. This reaction can therefore be conducted without heating, which is significant for the environmental aspect of this investigation.

Appendix 7.6 exemplifies the crude ^{1}H NMR of products obtained from each catalyst in comparison to that of pure biscarbamate **139** (Appendix figure VI-b). The additional –NH resonance at 8.5 ppm (starred green) is indicative of formation of a urea by-product from the foaming reaction, where MDI **58** has reacted with water in the atmosphere, **Scheme 4.12**.

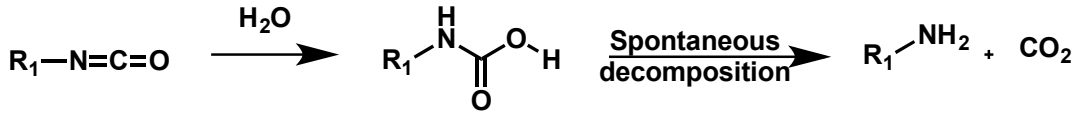

Scheme 4.12 Foaming reaction between an isocyanate and water, producing an amine and carbon dioxide. R_1 denotes any alkyl or aryl unit

DABCO **141** has previously been shown to catalyse the NCO/-OH reaction as opposed to the detrimental foaming reaction,[194] which may also apply to the high catalytic activity of Et_3N **140**. The difference in rate of these two catalysts has been rationalised by Burkus and co-workers. With a highly basic tertiary amine, such as Et_3N **140**, the mechanism of catalysis first involves the formation of a base-alcohol hydrogen bonded complex, **Figure 4.2**a. In toluene, the complex formed with Et_3N **140** is stable and hence prevents reaction with the isocyanate.[192] DABCO **141**, on the other hand is less basic and therefore favours base-isocyanate complex formation, **Figure 4.2**b, which minimises base-alcohol interaction.[195] The extra step in the Et_3N **140** mechanism could account for the lower catalytic ability in comparison to DABCO **141**.

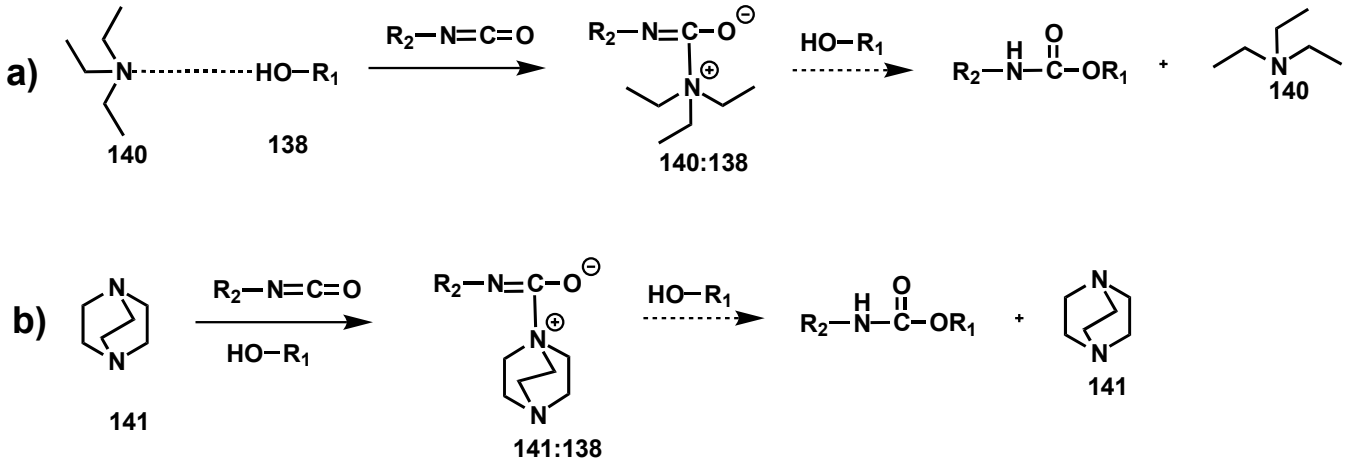

Figure 4.2 Two schemes exemplifying the difference between the catalytic effect of DABCO 141 and Et_3N 140. $R_{1\text{-}2}$ denotes any alkyl or aryl unit

Alsarraf *et al.* also observed reduced catalysis when using TBD **143**. They found that instead, the corresponding urea **154** from TBD **143** and benzylisocyanate **142**, **Scheme 4.13**, was rapidly formed, retarding the conversion to carbamate.[186]

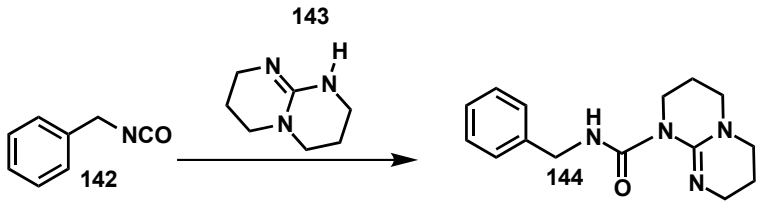

Scheme 4.13 Reaction of benzylisocyanate 142 with TBD 143 catalyst to form a stable urea 144, which hinders reaction progress

In addition, there was a clear correlation between the p*K*a of the catalyst and crude conversion. As p*K*a of the catalyst was increased, crude conversion was seen to decrease. It has been previously reported that as p*K*a of the tertiary amine conjugate acid increases, so does the foaming reaction, **Scheme 4.12**, hence this may contribute to the decrease in crude conversion.[196]

The reaction between diisocyanate MDI **58** and 1-propanol **138** with Et_3N **140** catalyst was subsequently monitored by IR spectroscopy, so as to probe the reaction dependence on time. Isocyanate reactions are amenable to monitoring by IR spectroscopy, as the isocyanate absorption at ~2200 cm^{-1} is sharp, strong and distinguishable from other functional groups. Carbamate formation of **139** is also indicated by the appearance of absorptions at ~1640 cm^{-1} and ~1540 cm^{-1} for the carbonyl functionality.

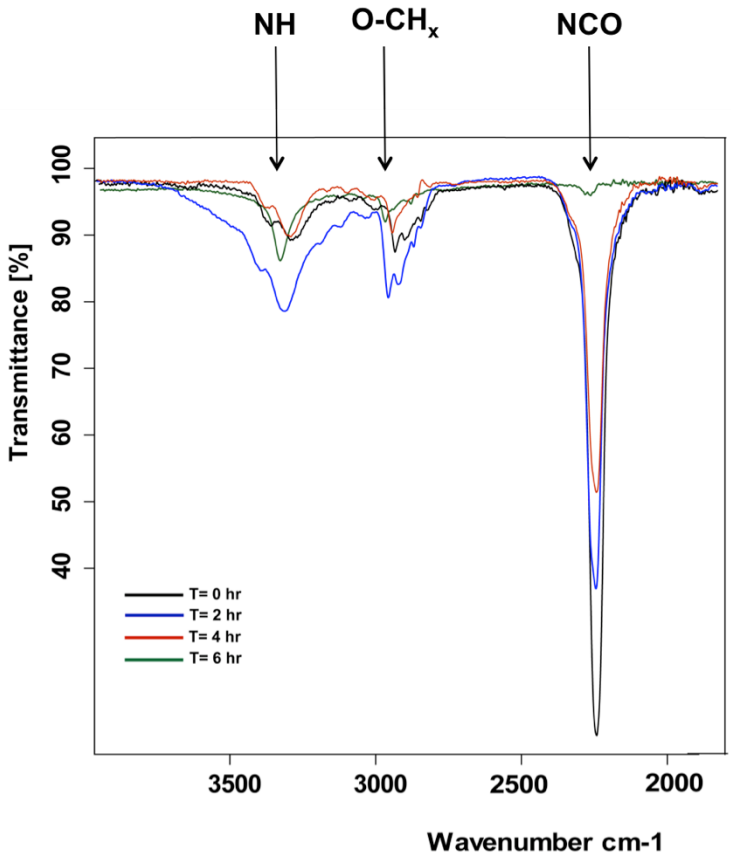

Figure 4.3 Overlaid IR spectra of the reaction between MDI 58 and 1-propanol 138 at different time points. General conditions; 10 mol % Et_3N 140 catalyst in toluene, 1 equiv. MDI, 2 equiv. 1-propanol

As time progresses, it can be seen in **Figure 4.3** that the absorption at ~2200 cm^{-1}, responsible for isocyanate stretching, decreases in intensity relative to other discernible absorptions. This suggests consumption of the starting material and conversion to carbamate **139**, which is confirmed by the shifting and sharpening of absorptions at ~2900 cm^{-1} and ~ 3300cm^{-1}, due to the –NH and O-alkyl stretching in the carbamate functionality. Mesrobian and colleagues noted the autocatalytic effect of carbamate formation due to the weakly basic character of carbamate. The rate at which MDI **58** is consumed appears to increase with time which is consistent with autocatalysis of the reaction.[197]

The synthetic procedure developed by Burkus using Et_3N **140** was subjected to a solvent and concentration screen to study to establish if the reaction could be optimised. Stebner and colleagues built on the previous mechanism postulated by Burkus for base catalysed urethane formation *via* hydrogen bond activated

complexes.[192, 198] Such complexes will be more prevalent in non-polar solvents, leading to the identification of hexane, 1,4-dioxane, diethyl ether and chloroform as lower-boiling-point solvents as alternatives, **Table 4.4**.

Table 4.4 Summary of conditions[#] for the solvent screen of carbamate synthesis using 1-propanol 138 and MDI 58

Entry	Solvent	Conversion to carbamate*/ %
1	Toluene	74
2	Hexane	46
3	1,4-Dioxane	18
4	Diethyl ether	52
5	Chloroform	45

*****conversion is based on the integration of product signals against starting materials from crude ^{1}H NMR. [#] General conditions; 10 mol % Et_3N for 6hr, 40 °C, 1 equiv. MDI, 2 equiv. 1-propanol.

Toluene was recognised as the most suitable solvent for the catalysis of carbamate formation **139** in this instance, as it gave the highest crude conversion of 74%. **Figure 4.4** visualises the extent of conversion of isocyanate to carbamate for the alternative solvent systems. Isocyanate starting material is evident in each solvent, whereas these signals are virtually absent in reactions run in toluene under the same conditions. The shift at ~8.5 ppm for the urea side product is also more prominent for the other solvents used in the solvent screen, most notably 1,4-dioxane.

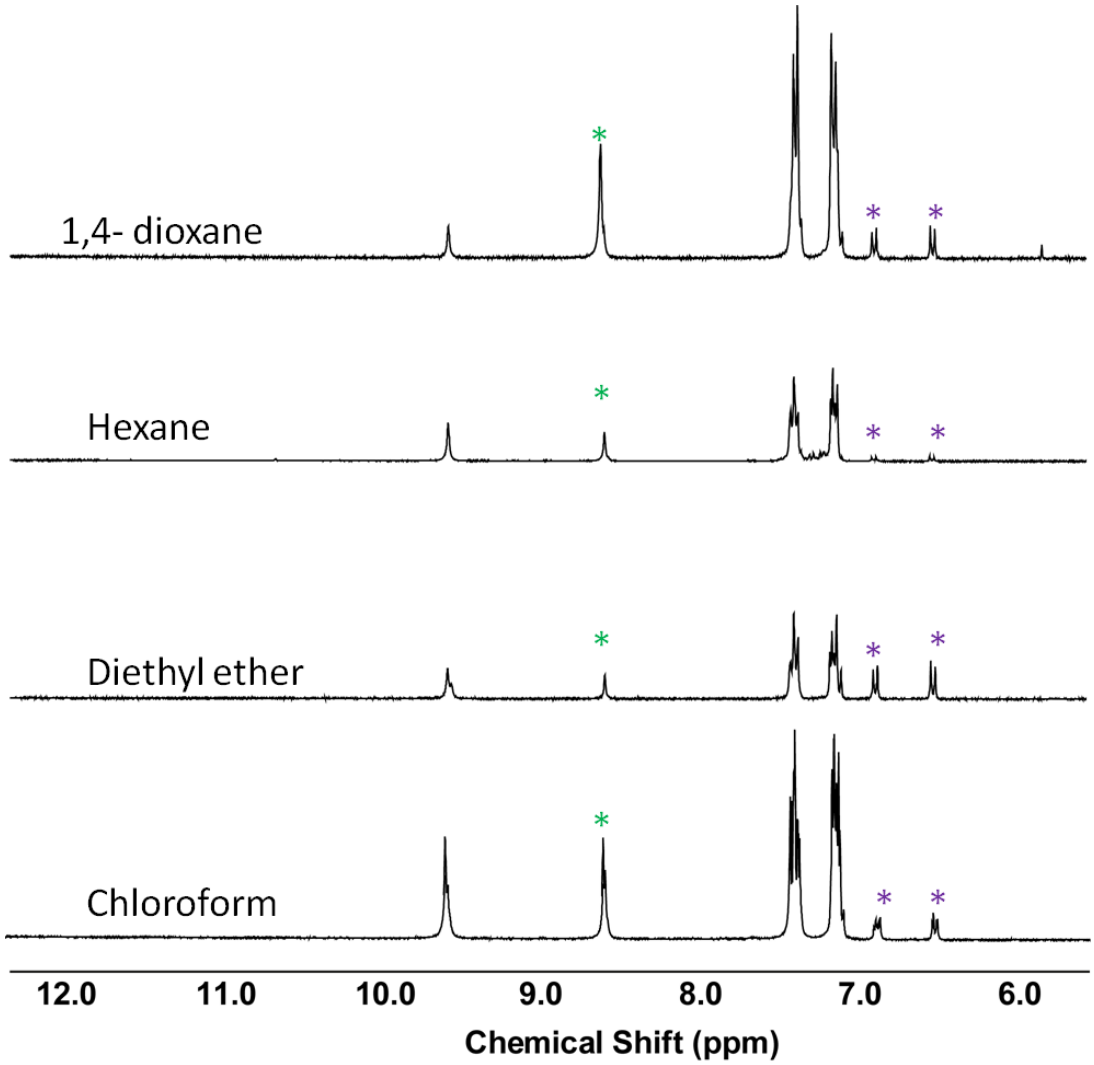

Figure 4.4 Partial crude NMR (DMSO-d_6, 500 MHz); 10 mol% Et_3N, 40 °C, 6 h. [0.05 M], 1 equiv. MDI, 2 equiv. 1-propanol. * indicative of MDI urea side product, * indicative of starting material

It was also found that concentration of the reaction impacts crude reaction conversions. At higher concentrations, gelation of the solvent occurred after 10 minutes preventing further conversion of starting materials. Gelation is indicative of formation of a highly cross-linked network, potentially through lateral hydrogen bonding of carbamate groups, which has previously been described in the literature.[199] The lowest concentration of MDI **58**, 0.01 M gave 100% conversion to product from crude NMR analysis, **Table 4.5**.

Table 4.5 Summary of conditions[#] for the concentration study of carbamate 139 synthesis using 1-propanol and MDI

Entry	*Concentration/ M*	*Conversion to carbamate*/ %*
1	0.1	12
2	0.05	87
3	0.01	100

*****Conversion is based on the integration of product signals against starting materials from crude ^{1}H NMR. [#] General conditions; 10 mol % Et_3N in toluene, 40 °C, 1 equiv. MDI, 2 equiv. 1-propanol.

In summary, the best conditions that were found for carbamate formation using the least toxic catalyst (Et_3N) were 10 mol% of catalyst at a reaction concentration of 0.01 M in toluene for 6 hours at 40 °C.

4.4.2 Catalysis of urethane formation

The optimisation of the model reaction conditions prompted the move to investigate the synthesis of the PU macromonomer **61**, reported in Chapter 3. Reaction progress was monitored with IR spectroscopy, used to follow the disappearance of the –OH stretch of the polyol **57** starting material. Temperature and effect of catalyst was used to probe the extent of reaction.

Changing the temperature from room temperature to 40 °C did show an increase in crude conversion to polyurethane, the most notable examples are Entries 3 and 4 of **Table 4.6**, where Et_3N **140** catalysed crude conversion increased by 10%.

Table 4.6 Summary of conditions[#] for the study of PU synthesis using PEG-PPG-PEG (2000 $gMol^{-1}$) 57 and MDI 58

Entry	*Catalyst*	*pKa*	*Temp/°C*	*Conversion to urethane*[#]
1	None	-	r.t	47
2	None	-	40	53
3	NEt_3	10.8	r.t	54
4	NEt_3	10.8	40	65
5	DABCO	8.9	r.t	Not Soluble❖
6	DABCO	8.9	40	43
7	TBD	22	r.t	Not Soluble❖
8	TBD	22	40	Not Soluble❖

*****Conversion is based on the integration of product signals against starting materials from crude ^{1}H NMR. [#] General conditions; 10 mol % catalyst in toluene for 6hr, 2 equiv. MDI, 1 equiv. polyol. ❖Solubility in DMSO-d_6 was not achieved

The activity of the catalyst followed the trend set by the model reaction for carbamate synthesis, in that the highest p*K*a value regarding the base used resulted in the lowest crude reaction conversion. The use of TBD **143** as a catalyst at both temperatures, and DABCO **141** at room temperature (Entries 5, 7 and 8, **Table 4.6**), resulted in a product that was insoluble in DMSO-d_6. Observation of gelation during these reactions and hence subsequent insolubility could suggest a *pseudo* Tromsdorff effect (auto-acceleration), which is common in other polymerisation procedures.[200]

Urethane catalysis, in similarity to carbamate catalysis, found the best conditions were using Et_3N **140** catalysis at 10 mol% of catalyst, a reaction concentration of 0.01 M in toluene for 6 hr. at 40 °C. These conditions replace the use of carcinogenic, teratogen DMAc with toluene and reduce the temperature required for carbamate **139** and PU **59** formation relative to the conditions used for

macromonomer synthesis in Chapter 3, which is likely to reduce side reactions, such as transcarbamoylation, which is facile at high temperatures.[187]

4.5 Catalysis in mechanochemical systems

Solvent-free synthesis is attractive in the polymer industry due to the difficulty in obtaining a solvent that can solubilise high percentage hard block polymers.[201] Polymers that have high urea content are also prone to gelation and premature precipitation, and hence require high reaction temperatures and highly polar solvents.

Mechanochemical organic synthesis,[202-204] has been used to promote Knoevenagel condensations,[205] aldol reactions[206] and Michael additions[207] amongst many other synthetically important organic transformations.[208] Organic frameworks[209, 210] and crystalline materials[210, 211] have also been obtained.

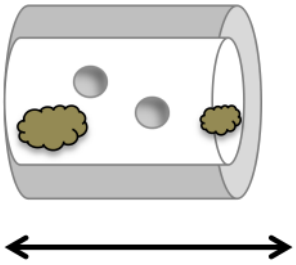

Figure 4.5 Internal view of a ball-milling cup with reactants (olive) inside. Stainless steel balls act to crush and mix the material (silver) by mechanical agitation

Figure 4.5 gives the internal view of a ball milling reaction vessel. A mechanical arm in the horizontal position oscillates 10 mL stainless steel cups containing loose stainless steel balls. Inertia causes the balls to crush and grind the sample with high energy, which is then transferred to the material facilitating a reaction.

Whilst reviewing the literature, limited evidence was found for urea/ carbamate synthesis[212] using this technique. It has, however been shown by Tan and colleagues that thioisocyante and symmetrical thioureas can be synthesised.[213, 214]

Using Et_3N catalysis, which was identified from solution phase investigations, solvent-free synthesis using a ball mill was investigated.

4.5.1 Mechanochemical carbamate catalysis

The model reaction of MDI **58** and 1-propanol **138** was again used to explore whether biscarbamate **139** formation was possible using mechanochemical methods. For this study, the ball mill was set to a vibrational frequency of 20 Hz for three minute intervals and the reaction monitored by IR, following loss of the isocyanate stretch at ~2200 cm^{-1}. Catalysts Et_3N **140**, DABCO **141** and TBD **143** were again tested for activity in the bulk state and compared to the uncatalysed reaction under the same reaction conditions.

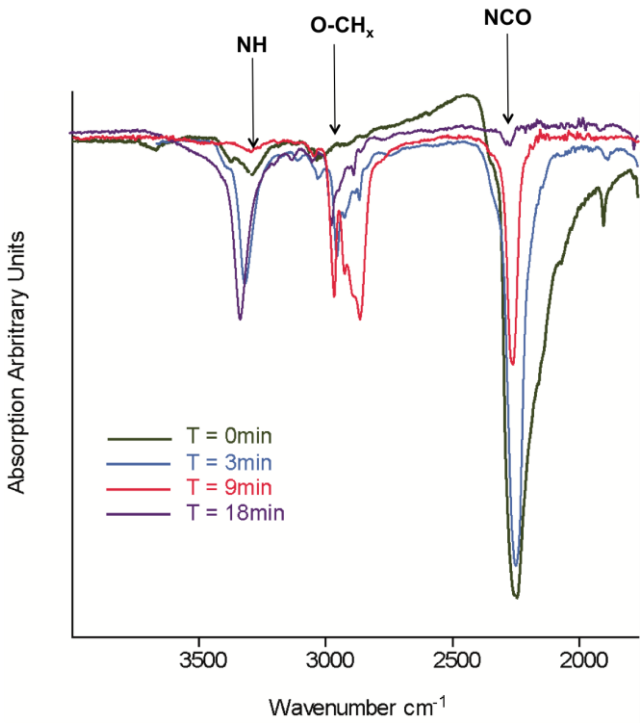

Figure 4.6 Partial IR spectra showing the effect of ball milling at three-minute intervals on biscarbamate 139 formation in the bulk. 10 mol % Et_3N, 18min, 1 equiv. MDI, 2 equiv. 1-propanol

As shown in **Figure 4.6**, for Et_3N catalysis after three minutes, a decrease in isocyanate absorbance was seen at 2200 cm^{-1}, indicative of consumption of starting material. Sharpening of the stretch at ~3300 cm^{-1} and shifting to a lower frequency was also observed, consistent with loss of alcohol and formation of the biscarbamate **139**. After eighteen minutes of milling, there was no IR absorption for the isocyanate stretch at ~2200 cm^{-1}. All catalysts were subjected to the same reaction conditions as above, and two additional reactions were also seen to be complete after this time period, highlighting similar reactivity for the Et_3N, DABCO and uncatalysed reactions, **Table 4.7**. This would suggest that in the bulk state, the catalyst does not impact carbamate **139** formation. TBD was again detrimental to biscarbamate formation.

Table 4.7 Summary of conditions[#] for the study of biscarbamate 139 synthesis using 1-propanol and MDI

Entry	**Catalyst**	**pKa**	**Conversion to carbamate[♯]**
1	None	-	93
2	Et_3N	10.8	95
3	DABCO	8.9	93
4	TBD	22	80

Conditions: 10 mol% catalyst (Entries 2-4) used, 1 equiv of MDI, 2 equiv. of 1-propanol, vibrational frequency was 20 Hz, 18 min. [♯] Conversion to biscarbamate is based on comparison of NMR signals of crude reaction mixture

Because **Table 4.7** shows conversion to carbamate **139** is effective in the bulk state without a catalyst, substrate tolerance to the reaction conditions was assessed for urea and carbamate formation without a catalyst. An isocyanate and either an amine or alcohol was tested for reaction, **Scheme 4.14**.

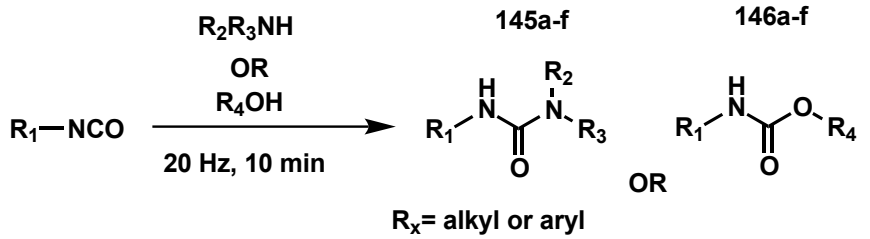

Scheme 4.14 Reaction of an isocyanate with either a substituted amine or alcohol to form the corresponding ureas 145 a-e and carbamates 146 a-f in the ball mill. $R_{1\text{-}4}$ denotes any alkyl or aryl unit

Isocyanates with both electron withdrawing and donating substituents were used to assess if electronic effects affected the crude conversion. Generally, electron withdrawing substituents in the *para*- position to the isocyanate increased reactivity whereas electron donating substituents reacted more slowly, due to the inductive effect of the alkyl group, **Table 4.8**.[215] NMRs including relevant protons are present in Appendix 7.7.

Table 4.8 Substrate Tolerance for Solvent Free carbamate/ urea synthesis

Entry	*R_2 or R_4*	*R_3*	*R_1*	*Crude Conversion[♯] / %*
1 **145a**	2-benzimidazyl	H	*p*-cyano phenyl	46*
2 **145b**	*iso*propyl	*iso*propyl	*p*-nitro phenyl	99
3 **145c**	*iso*propyl	*iso*propyl	*p*-ethyl phenyl	100
4 **145d**	2-benzimidazyl	H	1-adamantyl	60*
5 **145e**	*iso*propyl	*iso*propyl	1-adamantyl	100
6 **146a**	propyl		*p*-nitro phenyl	79
7 **146b**	propyl		1-adamantyl	100
8 **146c**	*o*-nitrobenzyl		1-adamantyl	100*
9 **146d**	*o*-nitrobenzyl		*p*-cyano phenyl	50*
10 **146e**	*o*-nitrobenzyl		*p*-nitro phenyl	75*
11 **146f**	*o*-bromobenzyl		*p*-ethyl phenyl	55*

Conditions: No catalyst, 1 equiv. of isocyanate, 1 equiv. of amine/ alcohol, vibrational frequency was 20 Hz, 10 min. ♯Conversion to product is based on comparison of NMR signals of crude reaction mixture. *donates a solid-solid reaction

Many of the ureas synthesised in **Table 4.8** using this method are hindered and could not to be obtained *via* traditional solution methodology (see Chapter 4.2). Solid amines, isocyanates and alcohols in addition to liquid counterparts were tested. All substrates were found to be amenable to these conditions indicating that liquid assisted grinding (LAG) effects[216] are negligible in promoting the reaction. This is important given that both the reaction between MDI **58** and 1-propanol **138** and MDI **58** and the polyol **57** are both reactions that involve a liquid component.

4.5.2 Mechanochemical synthesis of urethanes

Because of the success seen with small molecular weight carbamate **146a-f** and urea **145a-e** syntheses, the milling methods were applied to the synthesis of SPUs **103a/b** described in Chapter 3. MDI **58** and PEG-PPG-PEG **57** were initially subjected to milling at 20 Hz for three-minute intervals inside the ball mill, the same conditions established for 1-propanol **138** and MDI **58**. By following the reaction by IR, urethane formation appeared to be slower than carbamate formation, noted by retention of the free –OH peak at ~3300cm^{-1}. The vibrational frequency of ball mill was hence increased to 25 Hz for five-minute intervals for a total time of thirty minutes.

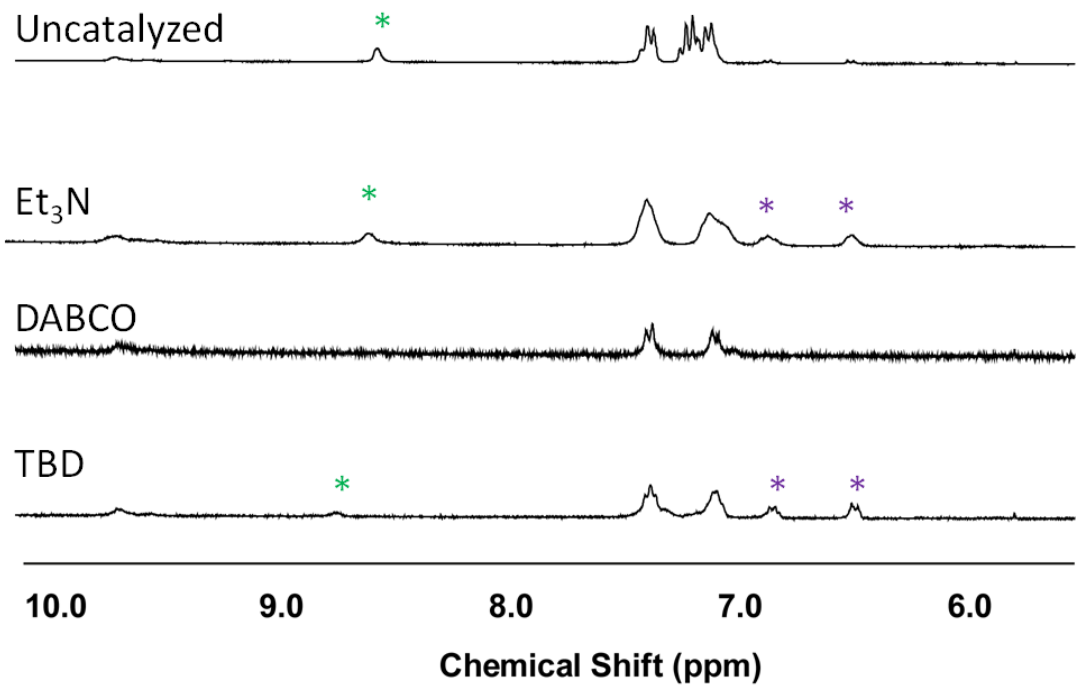

Figure 4.7 Partial crude NMR (DMSO-d_6, 500 MHz); 10 mol% catalyst, 40 °C, toluene, 6 h. 2 equiv. MDI, 1 equiv. PEG-PPG-PEG. * indicative of MDI urea side product, * indicative of starting material

PU **59** formation was found to rely on the catalyst. DABCO **141** was the most efficient catalyst, and produced the cleanest crude NMR spectrum, with no apparent side products, **Figure 4.7**. This contrasts carbamate formation in the model system, where catalyst did not affect the crude yield to any great extent. TBD **143** for PU **59**

formation was an effective catalyst, with a high crude conversion and purity, similar to that obtained using Et_3N as catalyst,Table **4.9**.

Table 4.9 Effect of catalyst on conversion of the PEG diol to urethane

Entry	Catalyst	pKa	Crude Conversion[♯] / %
1	None	-	70
2	NEt_3	10.8	78
3	DABCO	8.9	100
4	TBD	22	93

Conditions: 10 mol% catalyst (Entries 2-4) used, 1 equiv of polyol, 2 equiv. of MDI, vibrational frequency was 25 Hz, 30 min. [♯] Conversion is based on comparison of NMR signals of crude reaction mixture

The PU **59** was then reacted further with 2-amino-5,6-dimethylbenzimidazole **60** to produce the complete macromonomer **61** displaying triple hydrogen bonding units as in previous work described by Gooch *et al.* **Scheme 4.15**. [80]

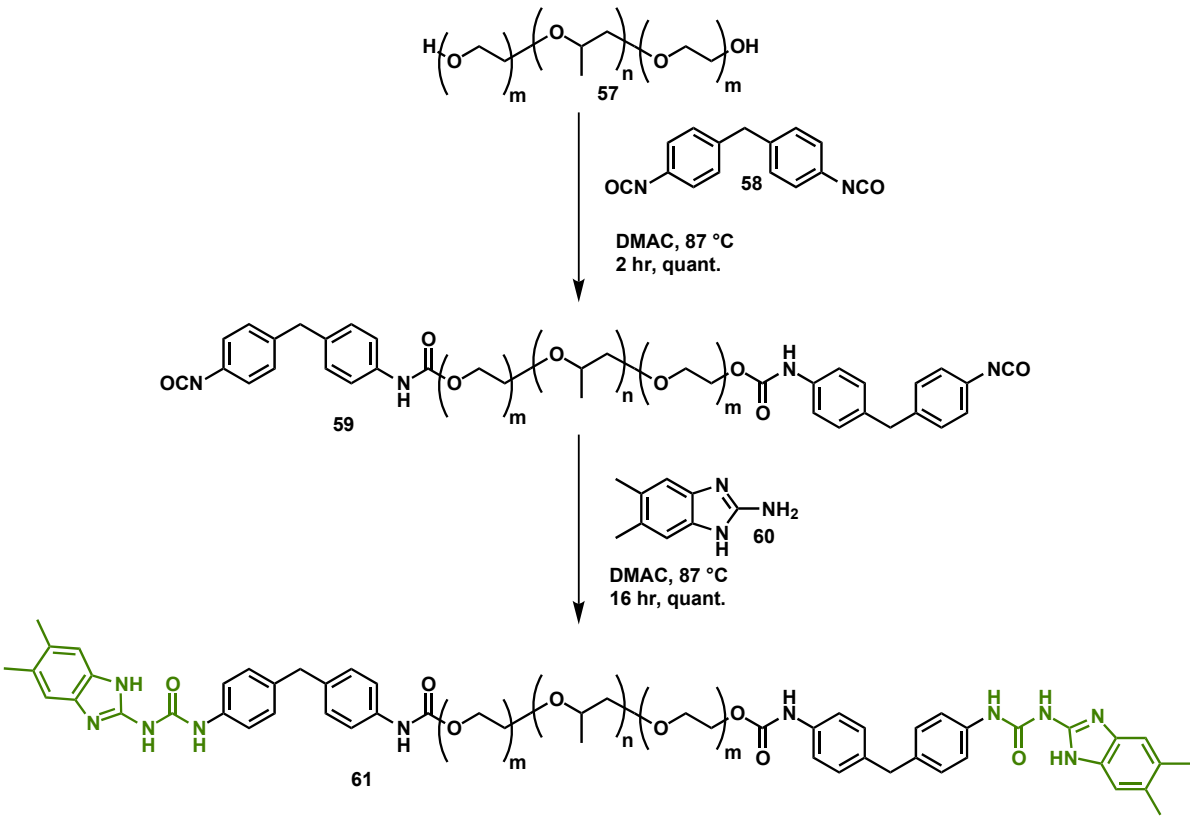

Scheme 4.15 Supramolecular macromonomer 61 synthesised by Gooch *et al.*

IR analysis of the material both before and after reaction, **Figure 4.8**, illustrated the disappearance of remaining isocyanate groups within 10 minutes.

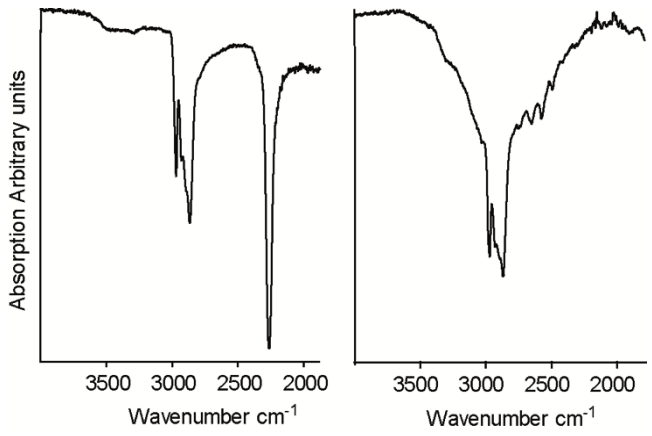

Figure 4.8 IR spectrum showing reaction of the MDI end-capped PU 59 (left), which shows free isocyanate at 2200 cm^{-1}. Reaction with 2-amino-5,6-dimethylbenzimidazole 60 (right) shows that after ten minutes of milling, this absorption has disappeared suggesting urea 61 formation with the amine

Subsequent addition of heterocomplementary supramolecular chain extension unit DAC **62**, followed by grinding for a further 30 minutes until a homogenous powder was obtained, generating supramolecular polymers with a 2:1, **Figure 4.9**, and 4:1 NCO:OH ratio as in our previous work.[80]

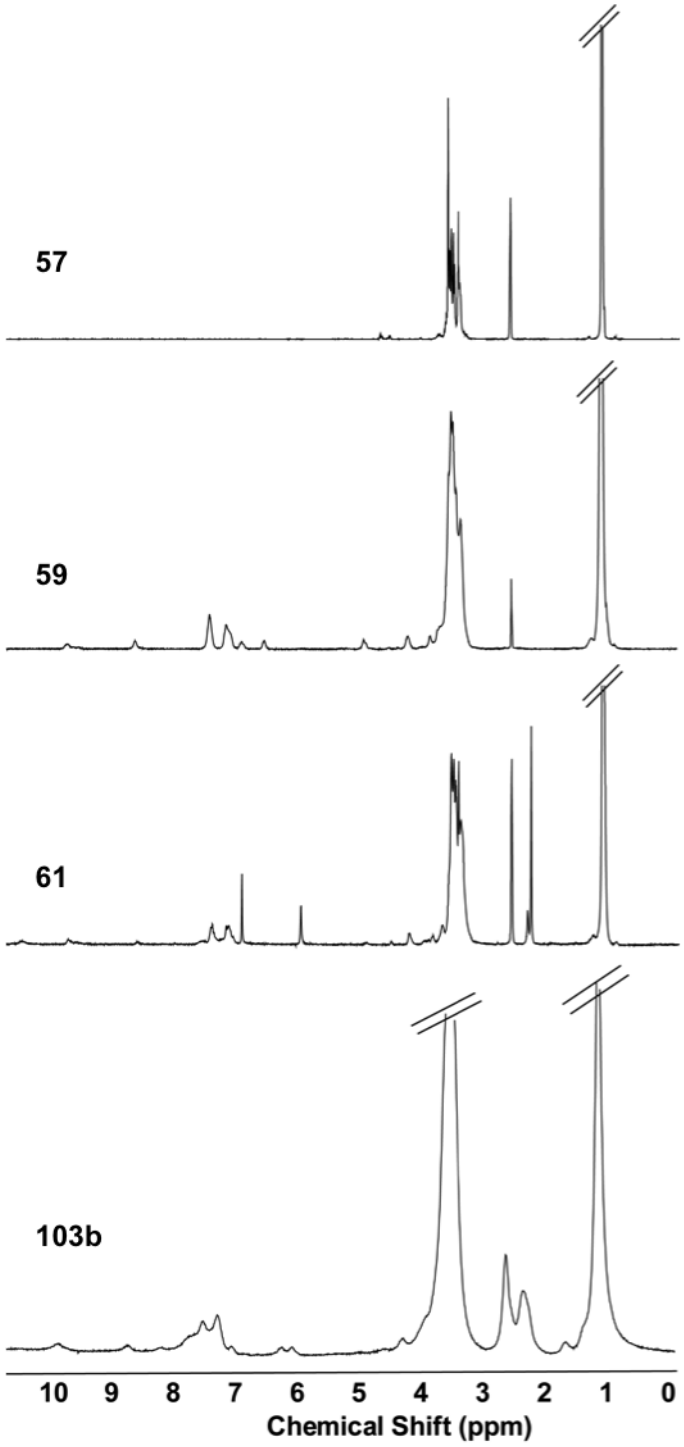

Figure 4.9 Partial crude NMR (DMSO-d_6, 500 MHz); PEG-PPG-PEG 57, -NCO terminated polyurethane 59, macromonomer 61 and subsequent SPU 103a/b

^{1}H NMR of each stage of the synthetic sequence illustrated formation of a carbamate as evidenced by the appearance of a resonance at ~ 4.2 ppm, expected for the OC**H**$_2$-CO-NH group. Loss of the unreacted aromatic isocyanate resonances, ~ 6.5 & 6.8 ppm, on reaction with 5,6-dimethyl-2-aminobenzimidazole **60** confirmed urea **61** formation by the emergence of the characteristic –NH urea resonance at ~ 6 ppm. ^{1}H NMR of SPU **103b** was broad and indistinctive, although the aromatic resonance for pyrimidine **62** is visible adjacent to that of the urea –NH (~ 6 ppm).

Supramolecular polymer **103a/b** formation was hence assessed by DSC by comparison of defined glass transitions located in those synthesised in the solution phase, and described, in Chapter 3.

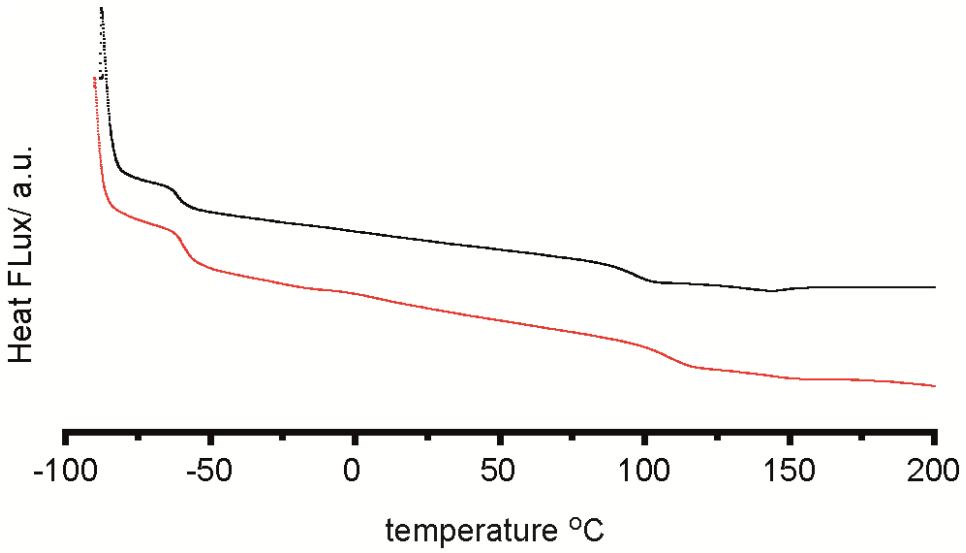

Figure 4.10 DSC traces of MDI 58 and PEG-PPG-PEG 57 based supramolecular polymer 103b (NCO:OH = 4:1) synthesised by traditional solution phase (red) and in bulk state in a ball mill (black)

The broad exotherm shown at ~ -50 °C, **Figure 4.10**, can be attributed to the T_g of the PEG based polymer backbone. A further transition ~120 °C is common in the traces for all methodologies and can be attributed to transitions in the hard blocks of the polymer. These properties are similar to those we previously observed for the range of SPUs **103** prepared shown in Chapter 3.[80]

4.6 Conclusions

The possibility of masking diisocyanates and hence desymmetrising them would allow the controlled reaction with a telechelic diol. The polyurethane synthetic product would not be subject to statistical models, and hence confidence in product identification results. Due to Flory's rule of equal reactivity, a desymmetrised diisocyanate would possess two different reaction rates, making product identification simple. Attempts to create an unsymmetrical MDI *via* reaction with hindered amines failed, as the conversion of the first isocyanate led to greatly decreased reactivity of the second. Further attempts to synthesise MDI ureas with hindered amines was successful, and the hindered ureas showed reaction with low-molecular-weight alcoholic solvents, such as methanol and ethanol, resulting in *trans*-carbamoylation. n-Propanol and *iso*propanol, however, resulted in no reaction, suggesting larger molecular-weight molecules such as diols would also prove futile.

As a result, focus shifted instead to the selective catalysis of polyurethane formation, and hence an improved synthetic approach than that described at the start of Chapter 3 (DMAc, > 30 hrs. at 87 °C) for SPU synthesis. Catalyst, temperature, solvent and reaction concentration were optimised for the synthesis of a *bis*carbamate model compound, which was than applied to urethane formation.

Solvent free method syntheses of the same molecules were then investigated using ball milling. The method was found to be applicable to a wide range of low-molecular-weight urea and carbamates, which were efficient enough to proceed without a catalyst. This methodology was then applied to the synthesis of PUs **59**, macromonomer **61** and assembly of an SPU with NCO:OH = 4:1 **103b** in one pot.

Gelation occurred in reactions with higher concentrations in the solution phase, whereas no such problems were observed with ball milling. As a result, application of this method to the synthesis of a previously described SPU[80] was successful. This method is important for environmental impact and could be elaborated further, to operate in tandem with phosgene-free routes to isocyanates.[69]

Chapter 5

Thesis Summary

5 Chapter 5

5.1 Thesis Summary

Hydrogen bonding plays an important role in recognition between self and non-self, and hence assembly of complex structures. The assembly of the DNA double helix requires orthogonal recognition, which is modulated by relative strength of the hydrogen bonded complexes.[101, 118, 217] Because linear arrays of hydrogen bonds are so easily incorporated into structures, their synthesis, highly directional behaviour and easily controllable strength has been the focus of this project.

Homocomplementary hydrogen bonding motifs such as UPy have stimulated great advances in this area of supramolecular chemistry,[46] but do not facilitate controlled assembly of SMPs. Molecular weight has been shown to be controllable only be dilution, or by including chain termination sequences, which consist of mono-functionalised UPy units.[46, 50] Hence, the development of heterocomplementary hydrogen bonding motifs for both small molecule and polymer assembly represents a powerful strategy for the controllable assembly of complex architectures.

The behaviour of several hydrogen bonding motifs that are able to form hetero- and homo- complementary complexes in the presence of each other was investigated (Chapter 1). The UIM and AIC motifs, designed within the Wilson research group[79, 106, 120] were investigated for orthogonal assembly with other motifs, which have been reported. Meijer and co-workers have previously investigated the heterocomplementary assembly mechanism for the UPy and DAN motifs, but had not studied this in the presence of molecules also capable of hydrogen bonding.[105, 118, 122]

Previous work carried out in the Wilson group involving orthogonal assembly pathways presented the starting point for this thesis.[64, 106]

Appending a light-cleavable protecting group to the AIC motif ‘masked’ the triple hydrogen bonding array, facilitating assembly using a stimulus (*i.e.* light). It was

shown that when the masked unit was present in solution with it's preferred hydrogen bonding partner, UIM, complexation did not occur. This was indicative of successful masking of the triple hydrogen bonding array, and that the ability to hydrogen bond was necessary to perform molecular recognition. Upon cleavage of the light sensitive *O*-nitro benzyl group, the presence of the AIC:UIM heterodimer was evidenced though complexation induced shifts in the ^{1}H NMR spectra. The use of promiscuous hydrogen bonding units in the cascade allowed certain complexation products to be observed, before switching to a different product when a more preferred binding partner was introduced to the solution. It was found that this was due to satisfaction of a greater number of hydrogen bonds in the overall system.

Two of the hydrogen bonding motifs were then taken forward and further studied as building blocks for the assembly of heterocomplementary supramolecular polymers (Chapter 3). In-depth mechanical and structural analysis of supramolecular polymers constructed from a high-molecular-weight analogue of UIM, and a ditopic version of AIC, DAC was investigated. Studies previously reported by the Wilson group,[128] provided the preliminary work for this study. Focus on phase separation, which plays a large part in structure and subsequent materials properties,[77] was controlled by increasing the crystalline composition of building blocks used in synthesis. Flexibility and toughness of the material was found to increase with hard block content, before the materials became too crystalline and very brittle at high hard block percentage content. Mechanical characterisation of the higher percentage hard block supramolecular polymers was challenging, but the crystalline nature was studied in-depth using SAXS and WAXS. Thermal transitions for all polymers were studied using DSC, highlighting an increase in T_m with hard block percentage.

An intermediate hard block percentage (NCO:OH= 4:1), proved the best material due to ease of processability for characterisation. This material was therefore subjected to further thermal testing, mainly through annealing, which has previously been shown to maximise phase separation due to thermal motion in the hard blocks.[144, 145] Annealing of samples showed higher intensity transitions in the DSC for hard block melting endotherms. This is inline with thermal motion enabling the hard blocks to align themselves in the preferred conformation, providing the material with a higher level of phase separation.

Because control over materials properties based solely on hard block content had been shown,[80] variation on the structure of the supramolecular polymers was investigated. A more flexible ether linkage was introduced into the DAC unit, producing a substantial decrease in T_g of the soft block, indicating phase mixing. On the other hand, replacing the ditopic linker in DAC with a benzyl group increases the T_g of the soft block. The ability of the DAC unit to π-π stack promotes order in the hard phase, rigidifying the whole system, which reinforces order in the soft phase. We have thus been able to demonstrate in Chapter 3 control over the mechanical and materials properties of heterocomplementary hydrogen bonding systems in bulk state.

Chapter 4 introduces synthetic processes for polyurethanes synthesis in industry, and the need to eliminate solvents or toxic waste. The original synthesis of the SPUs reported in this thesis used a high boiling point, teratogenic solvent, which requires heating at high temperatures over several days to afford the SPU. A reduction in reaction temperature and time using a tertiary amine as a catalyst for urethane formation was first shown, before removing solvent from the reaction system altogether, presenting the first synthesis of a supramolecular polymer in its entirety using solvent-free methods in a ball mill. Thermal characterisation using DSC showed that glass transitions for both the hard and soft blocks of the polymer synthesised in the bulk state were identical to those exhibited from polymers synthesised in solution phase.

In summary, this thesis has shown the importance of defining orthogonal hydrogen bonding units, which can be applied to supramolecular polymer systems with the vision of creating stimuli responsive, 'living' systems, which react to a change or absence of a binding partner.

Characterisation of a heterocomplementary supramolecular polymer formed from two of these hydrogen bonding motifs showed that control over materials properties is possible, contributing to a 'toolbox' for supramolecular chemists. It has also been shown that synthesis of supramolecular polymers is possible in the solid state, which is unprecedented in this field.

5.2 Future Directions

Research efforts in the Wilson group utilising hydrogen bonding motifs for orthogonal assembly behaviour are currently on-going. Association constants for complexes formed with the NapyO moiety using NMR titrations are being investigated. Continuing the work developed on sulfur derivatives of the hydrogen bonding motifs reported in this thesis, *e.g.* UTIZ, are under investigation by S. Parker. UTIZ revealed exciting behaviour, in that it did not recognise the same hydrogen bonding partner as its imidazole sister, UIM, showing promise for these molecules to be used in orthogonal recognition sequences.

The binding strength of complexation can be assessed by ^{1}H-NMR titration. The change in chemical shift is proportional to the strength of the interaction, allowing calculation of the strength of interaction in the complex.

$$UTIZ.UTIZ + ATHy.ATHy \rightleftharpoons UTIZ + ATHy \rightleftharpoons UTIZ.ATHy$$

Equation 5.1 Equilibrium bewteen UTIZ and AThy hydrogen bonded complexes

$$\therefore K_a = \frac{[UTIZ.ATHy]}{[UTIZ.UTIZ][ATHy.ATHy][UTIZ][ATHy]}$$

Equation 5.2 Association constant of the UTIZ:AThy complex, based on the concentrations of the above determined by ^{1}H NMR

The equilibrium position for the desired complex is shifted if self-association between the individual monomers is high. Dimerisation constants for homoassociation is hoped to be negligible, for successful self-sorting behaviour. The titration is performed by adding aliquots of a concentrated solution of guest into a solution of host molecule. After each aliquot, a ^{1}H-spectrum is recorded, allowing logging of the change in chemical shift of key protons. Change in chemical shift can be plotted against number of equivalents of guest, and HypNMR is used to calculate the resulting K_a of the homo- or heterodimer. Subsequently, ΔG can be calculated using equation **Equation 5.3**.

$$\Delta G = -RTlnK_a$$

Equation 5.3 Gibb's free energy of the hydrogen bonded system

Future work should be focused on ascertaining the hydrogen bonding ability of the sulfur derivatives of hydrogen bonding units in the presence of each other and with their oxygen/nitrogen siblings.

Further modification of the supramolecular polymers in Chapter 3 could also be introduced. The design of the DAC unit means such modification in chain spacer is synthetically simplistic, and different chain lengths including C_3 and C_7 have already been synthesised to see if carbon chain length is a factor for regulation of supramolecular properties, which has previously been observed for C_4 and C_6 carbon chains. Further materials characterisation of the SPUs reported in Chapter 3 would rationalise the behaviours and trends observed. Performing melt rheology could strengthen the link between the DMTA and DSC results. Molecular weight impacts the polymer flow behaviour at temperatures above the T_g and T_m, therefore rheological measurements could study the effects of molecular weight differences in the SMPs. Differences in molecular weight are manifested in large changes in viscosity, which would indicate the extent of supramolecular polymerisation in the bulk state of each SPU. This would circumvent the solubility and practical issues related to measure molecular weight of dynamic supramolecular polymer *via* gel permeation chromatography (GPC).

By producing additional polymers end-capped with the hydrogen bonding units in Chapter 2 *via* the same route as the original family (Chapter 3), 'living' supramolecular polymers, **Figure 5.1**, which choose a complementary partner dependent on the presence of preferred partners, can be realised.

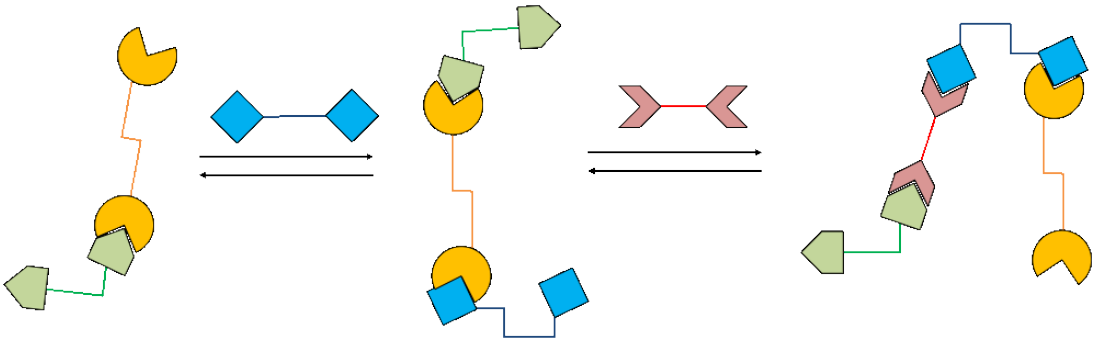

Figure 5.1 Cartoon representative of 'living' supramolecular polymers, which adapt and change structure based on the presence or absence of specific ditopic hydrogen bonding partners

Since the solvent free synthetic method developed is robust, producing supramolecular polymers on a larger scale could be investigated. The ball mill reactions cups are available in a range of sizes and industrial processes such as hot melt or twin screw extrusion could be amenable synthetic processes.

Chapter 6

Experimental

6 Experimental

6.1 General materials and methods for organic synthesis

All reactions were carried out in clean and oven-dried glassware under a nitrogen atmosphere unless otherwise stated. Solvents and reagents were purchased from Sigma Aldrich or Fisher and used without further purification unless otherwise stated. Anhydrous dichloromethane, tetrahydrofuran, chloroform, toluene, acetonitrile, methanol and ethanol were obtained from the in-house solvent purification system from Innovative Inc. PureSolv®. Anhydrous dimethylformamide, dimethylacetamide and chloroform-*d* were obtained from Sigma Aldrich equipped with Sure/Seal™. Mixtures of solvents are quoted as ratios and correspond to a volume: volume ratio. Triethylamine was distilled before use from calcium hydride and stored under nitrogen over potassium hydroxide pellets. Analytical thin layer chromatography was performed on Merck Kieselgel 60 F_{254} 0.25 mm pre-coated aluminium plates. Product spots were visualised under UV light (λ_{max} = 254 nm). Flash chromatography was carried out using Merck Kieselgel 60 silica gel. Nuclear magnetic resonance spectra were obtained using a Bruker AMD300 or Bruker DMX500 spectrometer operating at 300 MHz or 500 MHz for ^{1}H spectra and 75 MHz or 125 MHz for ^{13}C spectra as stated. Melting points were determined using a Griffin D5 variable temperature apparatus and are uncorrected. Infra-red spectra were obtained using a Perkin-Elmer FTIR spectrometer where absorption maxima ($\bar{\upsilon}_{max}$) are quoted in wavenumbers (cm^{-1}) and only structurally relevant absorptions have been included. Ultra-violet spectra were recorded using a Varian Cary spectrophotometer; where absorption maxima (A) are quoted in wavelengths (nm). High Resolution Mass Spectra (HRMS) were recorded on a BrukerDaltonicsmicroTOF using electrospray ionisation (ESI).

Molecules numbered: **37** and **39** were previously prepared by Wilson Group member M. L. Pellizzaro.

Molecules numbered: **98** and **99** were previously prepared by Wilson Group member A. Gooch.

All compounds used from the group compound database were first subjected to ^{1}H NMR to check for degradation and/or impurities. Compounds were then recrystallized ($MeOH/CH_2Cl_2$) and dried before NMR studies.

6.2 Experimental Section for Chapter 2

N-tert-Butoxycarbonylguanidine[42]

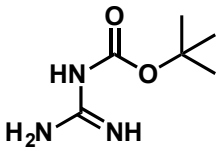

Guanidine hydrochloride (26.2 g, 275 mmol) was dissolved in milli-Q H_2O (200 mL). Sodium hydroxide (22 g, 550 mmol) was added in portions with stirring. Di-*tert*-butyl dicarbonate (20 g, 92 mmol) in acetone (200 mL) was added at 0 °C and the reaction mixture was left to stir, once reaching room temperature, for 20 hr. The volatiles were removed *in vacuo* to provide an aqueous suspension, which was extracted into ethyl acetate (2 x 150 mL). The organic layer was dried ($MgSO_4$), filtered and evaporated *in vacuo*. The resultant solid was triturated (75:25 hexane − ethyl acetate) to provide the *title compound* (7.6 g, 52%) as a colourless powder; m.p: 165-168 °C (lit.[42] decomp > 350 °C); δ_H (500 MHz, DMSO-d_6): 6.81 (4H, br s, $\underline{H_2}$NC and 2xN$\underline{H}$C), 1.34 (9H, s, $\underline{^{t}Bu}$); δ_C (125 MHz, DMSO-d_6): 163.0, 162.1, 77.4, 28.3; $\bar{\upsilon}_{max}/cm^{-1}$ (solid state) = 3332, 2263 and 1602; ESI-HRMS found mass 160.1086 $[M + H]^+$ $C_6H_{14}N_3O_2$ requires 160.1086.

Tert-Butyl 4-*tert*-1*H*-imidazol-2-yl-carbamate[42]

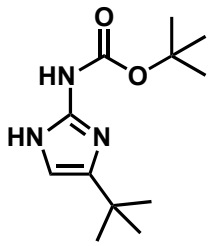

1-Bromopinacolone (1.7 mL, 12.6 mmol) was added to a solution of *N-tert*-Butoxycarbonylguanidine (6.0 g, 38 mmol) in anhydrous dimethylformamide (40 mL). The reaction was stirred at room temperature for 72 hr. The solution was filtered and the precipitate was dried providing the *title compound* (0.99 g, 57%) as a colourless powder; m.p: decomp. > 150 °C (lit.[42] decomp. > 163 °C); δ_H (500 MHz, $CDCl_3$): 6.38 (1H, s, imidazole-H), 5.70 (2H, br s, 2xNHC), 1.52 (9H, s, ^{t}Bu-OCO), 1.15 (9H, s, ^{t}Bu-CCH); δ_C (75 MHz, $CDCl_3$): 151.3, 149.5, 147.9, 104.1, 84.7, 36.5, 29.2 and 28.0; $\bar{\upsilon}_{max}/cm^{-1}$ (solid state) = 3437 and 3285-2733; ESI-HRMS found mass 240.1710 $[M + H]^+$ $C_{12}H_{22}N_3O_2$ requires 240.1712.

4-(*tert*-Butyl)-1*H*-imidazol-2-amine hydrochloride[42]

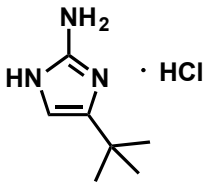

Tert-Butyl 4-tert-1H-imidazol-2-yl-carbamate (1 g) was dissolved in 100 mL 1 M hydrochloric acid in ethanol. The reaction mixture was refluxed for 3 hr. Once cooled to room temperature, the volatiles were evaporated *in vacuo* to provide the *title compound* (quant.) as a pungent orange oil, which was used immediately; δ_H (500 MHz, $CDCl_3$): 6.12 (1H, s, imidazole-H), and 1.10 (9H, s, ^{t}Bu); δ_C (75 MHz, $CDCl_3$): 147.5, 136.7, 105.3, 30.3 and 29.2; $\bar{\upsilon}_{max}/cm^{-1}$ (solid state) = 3411-3314, 1755, 1682; ESI-HRMS found mass 140.1134 $[M + H]^+$ $C_7H_{14}N_3$ requires 140.1188.

1-(5-*tert*-Butyl-1*H*-imidazole-2-yl)-3-phenylurea[42] **31**

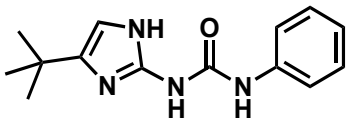

Anhydrous triethylamine (15 mL, 108 mmol) was added drop wise with stirring to a solution of deprotected tert-butyl 4-tert-1H-imidazol-2-yl-carbamate (10 g, 72 mmol) in anhydrous tetrahydrofuran (60 mL). After 10 min, a solution of phenylisocyanate (8.6 mL, 79 mmol) in anhydrous tetrahydrofuran (20 mL) was added drop wise. The reaction mixture was heated to reflux for 24 hr. After cooling to room temperature, the organics were evaporated *in vacuo*. The resulting solid was dissolved in ethyl acetate (500 mL) and the organic layer subsequently washed with H_2O (2 x 150 mL), 10 % aqueous hydrochloric acid (2 x 150 mL), saturated aqueous sodium bicarbonate solution (2 x 150 mL) and dried ($MgSO_4$) before the solvent was evaporated *in vacuo*. The resulting solid was triturated with chloroform and the filtrate was evaporated *in vacuo*. The resultant solid was crystallised (50:50 acetonitrile − methanol) to give the *title compound* (1.7 g, 10 %) as colourless needles; m.p: 241-247 °C (lit.[79] decomp > 147 °C); δ_H (500 MHz, $CDCl_3$): 7.91 (1H, s, imidazole-H), 7.41 (2H, d, *J*= 7.8 Hz, Ar-H), 7.22 (2H, m, *J* = 7.8 Hz, Ar-H), 6.95 (1H, t, *J* = 7.3 Hz, Ar-H), and 1.10 (9H, s, ^{t}Bu); δ_C (125 MHz, DMSO-d_6): 180.6, 152.5, 139.7, 128.7, 121.7, 118.1, 91.4, 45.7, 39.0 and 8.6; $\bar{\upsilon}_{max}/cm^{-1}$ (solid state) = 3333-3060, 2797, 1686, 1594, 1549; ESI-HRMS found mass 259.1543 $[M + H]^+$ $C_{14}H_{19}N_4O$ requires 259.1559.

Ethyl-3-(3-(4-*tert*-butyl-1*H*-imidazol-2-yl)ureido)benzoate[120] **92**

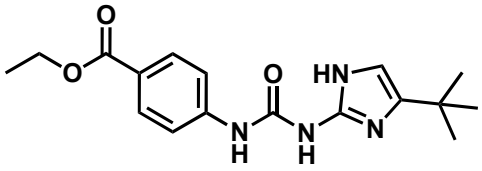

Anhydrous triethylamine (3.38 mL, 24 mmol) was added drop wise with stirring to a solution of deprotected tert-butyl 4-tert-1H-imidazol-2-yl-carbamate (2.25 g, 16 mmol) in anhydrous tetrahydrofuran (100 mL). After 10 min, 4-ethoxycarbonyl

phenylisocyanate (3.05 g, 16 mmol) was added in portions. The reaction mixture was heated to reflux for 24 hr. After cooling to room temperature, the volatiles were evaporated *in vacuo*. The resulting solid was suspended in ethyl acetate (500 mL) and the organic layer subsequently washed with saturated ammonium chloride solution (2 x 50 mL), saturated aqueous sodium bicarbonate solution (2 x 50 mL), saturated aqueous sodium chloride (2 x 50 mL) and dried ($MgSO_4$) before the solvent was evaporated *in vacuo*. The resulting solid was triturated with chloroform and the filtrate was evaporated *in vacuo*. The resultant solid was purified by column chromatography (5:95 methanol−dichloromethane) to give the *title compound* (0.74 g, 15%) as an off-white powder; m.p: 241-247 °C (lit.[120] not reported); δ_H (300MHz, $CDCl_3$): 8.03 (2H, d, *J* = 8.7 Hz, Ar-H) 7.63 (2H, d, *J* = 8.7 Hz, Ar-H) 6.50 (1H, s, imidazole-H) 4.38 (2H, q, *J* = 6.9 Hz, O-CH_2-CH_3) 1.41 (3H, t, *J* = 6.9 Hz, O-CH_2-CH_3) 1.36 (9H, s, ^{t}Bu); δ_C (125 MHz, $CDCl_3$): 186.1, 177.2, 131.0, 125.4, 121.2, 118.6, 77.0, 60.7, 45.9, 34.9, 29.7, 14.4 and 8.6; $\bar{\upsilon}_{max}/cm^{-1}$ (solid state) = 3332, 3075, 1715, 1699, 1550; ESI-HRMS found mass 331.1765 $[M + H]^+$ $C_{17}H_{23}N_4O_3$ requires 331.1770.

Ethyl-3-oxodecanoate[218]

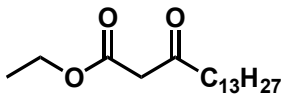

Potassium ethyl malonate (20.4 g, 120 mmol) was suspended in anhydrous acetonitrile at 0 °C. Anhydrous triethylamine (25 mL, 180 mmol) was added drop wise and stirred at 0 °C for 15 min. A solution of magnesium chloride (14.8 g, 156 mmol) in anhydrous acetonitrile (100 mL) was added as slurry and the reaction mixture allowed to reach room temperature. After stirring for an additional 2 hr., myristoyl chloride (16.5 mL, 60 mmol) was added drop wise at 0 °C and stirred at room temperature for an additional 16 hr. After this time, the volatiles were removed *in vacuo* and the resulting solid dissolved in diethyl ether (200 mL). The solution was washed with 30% aqueous hydrochloric acid (100 mL) and saturated aqueous sodium bicarbonate (100 mL) solution before the organics were dried ($MgSO_4$) and evaporated *in vacuo* to give *title compound* as a colourless oil (5.6 g, 31%); m.p:

241-247 °C (lit.[218] not reported); δ_H (300 MHz, $CDCl_3$): 4.18 (2H, q, *J* = 7.1 Hz, CH_3-C<u>H</u>$_2$-O), 3.42 (2H, s, CO-C<u>H</u>$_2$-CO), 2.52 (2H, t, J = 7.4 Hz, CO-C<u>H</u>$_2$-$C_{12}H_{25}$), 1.57 (2H, m, CO-CH_2-C<u>H</u>$_2$-$C_{11}H_{23}$), 1.26 (23H, m, COO-CH_2-C<u>H</u>$_3$ and C_9<u>H</u>$_{18}$), 0.86 (3H, t, *J* = 7.0 Hz, $C_{12}H_{24}$-C<u>H</u>$_3$); δ_C (75 MHz, $CDCl_3$): 206.3, 167.3, 61.3, 49.3, 42.3, 33.8, 29.7, 29.6-29.4 m, 27.5, 27.3, 23.2, 22.7, 14.1; $\bar{\upsilon}_{max}/cm^{-1}$ (solid state) = 2925, 2954, 1747, 1720, 1233; ESI-HRMS found mass 321.2413 $[M + Na]^+$ $C_{18}H_{34}NaO_3$ requires 259.1559.

2-Amino-6-tridecylpyrimidin-4(1*H*)-one[218] **74**

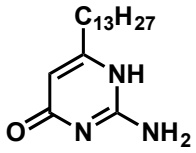

To a stirring solution of ethyl-3-oxodecanoate (5 g, 16.8 mmol) in anhydrous ethanol (70 mL) was added guanidine carbonate (2.3 g, 25 mmol) and potassium *tert*-butoxide (1.90 g, 17 mmol) and the reaction mixture was heated to reflux for 48 hr. After this time, the reaction mixture was cooled and filtered and the solvent evaporated *in vacuo*. The resulting solid was dissolved in H_2O (500 mL) and acidified to pH 6 with glacial acetic acid. The resulting solid was filtered and triturated (acetone then diethyl ether) before recrystallisation (2-propanol) to give the *title compound*, (4.9 g, 54%) as a cream coloured powder. m.p: 127-129 °C (lit.[218] not reported); δ_H (500 MHz, DMSO-d_6): 10.56 (1H, br s, N<u>H</u>C), 6.43 (2H, br s, N<u>H</u>$_2$), 5.38 (1H, s, pyrimidyl-H), 2.23 (2H, t, *J* = 7.6 Hz, CO-C<u>H</u>$_2$-$C_{12}H_{25}$), 1.53 (2H, m, CO-CH_2-C<u>H</u>$_2$-$C_{11}H_{23}$), 1.25 (20H, app. s, C_{10}<u>H</u>$_{20}$-CH_2-CH_3), 0.85 (3H, t, *J* = 6.9 Hz, $C_{12}H_{24}$-C<u>H</u>$_3$); The molecule was insufficiently soluble to obtain ^{13}C NMR spectra; ESI-HRMS found mass 294.2526 $[M + H]^+$ $C_{17}H_{32}N_3O$ requires 294.2545.

N-(4-Oxo-6-tridecyl-1,4-dihydropyrimidin-2-yl)benzamide **79**

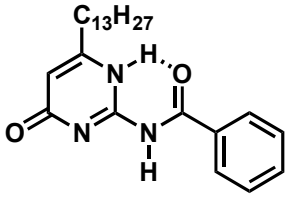

Benzoyl chloride (0.2 mL, 1.6 mmol) was added drop wise to a stirred solution of **74** (0.4 g, 1.7 mmol) and 4-dimethylaminopyridine (2 mg, 0.2 mmol) in anhydrous chloroform (50 mL). The reaction mixture was heated to reflux for 16 hr. The reaction was cooled to room temperature and the solvent was removed *in vacuo*. The recovered solid was purified by column chromatography (60:40 hexane−ethyl acetate) to give the *title compound* (0.21 g, 33%) as a colourless powder; m.p: decomp. > 175 °C; δ_H (300 MHz, $CDCl_3$): 7.88 (2H, d, *J* = 7.7 Hz, Ar-H), 7.59 (1H, t, *J* = 7.7 Hz, Ar-H), 7.45 (2H, t, *J* = 7.7 Hz, Ar-H), 5.95 (1H, s, pyrimidyl-H), 2.38 (2H, t, *J* = 7.7 Hz, pyrimidyl-CH_2CH_2), 1.57 (2H, m, pyrimidyl-CH_2CH_2), 1.18 (20H, m, alkyl-CH_2), 0.81 (3H, t, *J* = 7.1 Hz, alkyl-CH_3); δ_C (75 MHz, $CDCl_3$): 163.4, 150.8, 145.5, 133.7, 132.1, 129.0, 127.9, 94.9, 36.7, 31.9, 29.7 x2, 29.6 x2, 29.5 x2, 29.4 x2, 29.1, 27.7, 22.7, 14.1; $\bar{\upsilon}_{max}/cm^{-1}$ (solid state) =3193, 3066, 2850, 1644, 1470, 1263; ESI-HRMS found mass 398.2809 $[M + H]^+$ $C_{24}H_{36}N_3O_2$ requires 398.2808.

2-((4,5-Dimethoxy-2-nitrobenzyl)amino)-6-tridecylpyrimidin-4(1*H*)-one **76**

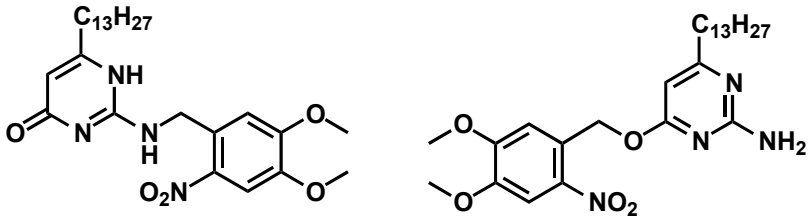

74 (0.5 g, 1.7 mmol) and potassium carbonate (0.47 g, 3.4 mmol) were suspended in anhydrous dimethylformamide. With stirring, 4,5-dimethoxy-2-nitrobenzyl bromide (0.47 g, 1.71 mmol) was added and the reaction mixture subsequently protected from light with aluminium foil and heated to 50 °C for 18 hr. After cooling, the reaction mixture was filtered and the solvent removed under reduced pressure. The recovered solid was purified by column chromatography (60:40 hexane−ethyl

acetate) to give a mixture of the O- and N- alkylated products (0.59 g, 71%) as a yellow powder. These could not be separated so were both taken on to the next step; ESI-HRMS found mass 489.3074 $[M + H]^+$ $C_{26}H_{41}N_4O_5$ requires 489.3077. Melting points and IR spectra were not obtained due to the light sensitive nature of this compound.

N-(4,5-dimethoxy-2-nitrobenzyl)-*N*-(4-oxo-6-tridecyl-1,4-dihydropyrimidin-2-yl)benzamide **78**

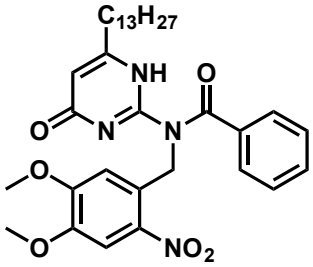

76 (0.5 g, 1.0 mmol) and 4-dimethylaminopyridine (0.01 g, 0.10 mmol) were dissolved in anhydrous chloroform (50 mL). Benzoyl chloride (0.12 mL, 1.0 mmol) was added drop wise with stirring and the reaction mixture subsequently heated to reflux for 20 hr. After cooling to room temperature, the solvent was removed *in vacuo* and the recovered solid was purified twice by column chromatography (60:40 hexane – ethyl acetate, then dichloromethane) to provide the *title compound* (50 mg, 9%) as a white powder. δ_H (500 MHz, $CDCl_3$): 7.97 (2H, d, J = 7.3 Hz, benzoyl-Ar-H), 7.57 (1H, s, nitrobenzyl-Ar-H), 7.43 (1H, t, J = 7.3 Hz, benzoyl-Ar-H), 7.33 (2H, t, J = 7.3 Hz, benzoyl-Ar-H), 6.63 (1H, s, nitrobenzyl-Ar-H), 5.81(1H, s, pyrimidyl-H), 5.79 (2H, s, nitrobenzyl-CH_2), 3.85 (3H, s, nitrobenzyl-O-CH_3), 3.67 (3H, s, nitrobenzyl-O-CH_3), 2.47 (2H, t, J = 7.8 Hz, pyrimidyl-CH_2CH_2), 1.66 (2H, quin, J = 7.3 Hz, pyrimidyl-CH_2CH_2-), 1.19 (20H, m, alkyl-CH_2) and 0.81 (3H, t, J = 7.3 Hz, alkyl-CH_3); δ_C (75 MHz, $CDCl_3$): 193.2, 187.5, 184.9, 172.9, 153.3, 147.8, 142.4, 137.3, 136.4, 132.6, 129.4, 128.3, 127.0, 126.6, 109.1, 108.1, 103.0, 56.2, 42.1, 33.1, 29.6, 33.1, 31.9, 29.6, 29.5, 29.4, 28.9, 22.7 and, 14.1 multiple resonances overlap; ESI-HRMS found mass 615.3146 $[M + Na]^+$ $C_{33}H_{44}N_4O_6Na$ requires 615.3159; UV-Vis: A = 223 nm. Melting points and IR spectra were not obtained due to the light sensitive nature of this compound.

7-Amino-1,8-naphthridin-2-ol[219] **88**

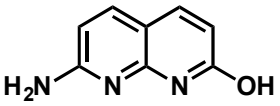

Concentrated sulfuric acid (10 mL), was added drop wise at 0 °C to a ground mixture of 2,6-diaminopyridine (1.83 g, 15 mmol) and D-malic acid (2.5g, 19 mmol). The reaction mixture was then heated to 110 °C for 3 hr. before being cooled back to 0 °C. Saturated aqueous ammonium hydroxide solution was then added drop wise to pH 9, before the reaction mixture was filtered and subsequently washed with water and diethyl ether, to give the *title compound* (2.33 g, 97%) as an olive green solid. m.p: decomp. > 300 °C (lit.[219] decomp. > 360 °C); δ_H (500 MHz, DMSO-d_6): 7.67 (2H, m, Ar-H), 6.99 (2H, s, NH_2), 6.37 (1H, d, J = 8.5 Hz, Ar-H), 6.14 (1H, d, J = 9.2 Hz, Ar-H); δ_C (75 MHz, DMSO-d_6): 164.1, 160.9, 150.7, 140.1, 137.7, 115.2, 105.6, 105.4; $\bar{\upsilon}_{max}/cm^{-1}$ (solid state) = 3500-2500 (broad), 1617, 1513, 1375, 1138, 831; ESI-HRMS found mass 162.0679 $[M + H]^+$ $C_8H_8N_3O$ requires 162.0667.

N-(7-Hydroxy-1,8-naphthyridin-2-yl)pentamide[61] **89**

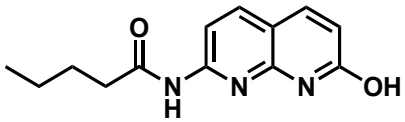

The compound was synthesised *via* a modified procedure.[220] Valeroyl chloride (2.5 ml, 21 mmol) was added drop wise to a solution of **88** (2.00 g, 12 mmol) in pyridine (20 mL). The reaction mixture was subsequently heated to 110 °C for 20 hr. After this time, the pyridine was removed under reduced pressure, and then co-evaporated *in vacuo* with toluene. The resulting black liquid was dissolved in a minimum of hot chloroform, where hexane (100 mL) was added. The precipitate was filtered and subsequently triturated with methanol to give the *title compound* (2.29 g, 78%) as a brown powder. m.p: decomp. > 300 °C; δ_H (500 MHz, DMSO-d_6): 10.51 (1H, S, -NH), 8.07 (1H, d, J = 8.5 Hz, Ar-H), 7.97 (1H, d, J = 8.5 Hz, Ar-H), 7.86 (1H, d, J = 9.4 Hz, Ar-H), 6.44 (1H, d, J = 9.4 Hz, Ar-H), 2.37 (2H, t, J = 7.4 Hz, CO-CH_2), 1.61 (2H, m, CO-CH_2CH_2), 1.36 (2H, m, CO-$CH_2CH_2CH_2$), 0.92 (3H, t, J = 7.4 Hz,

$CH_2C\underline{H}_3$); δ_C (125 MHz, DMSO-d_6): 172.1, 163.2, 152.1, 148.2, 138.6, 138.1, 120.4, 110.1, 108.7, 36.6, 26.9, 21.7, 13.4; $\bar{\upsilon}_{max}/cm^{-1}$ (solid state) = 3200-2872 (broad), 1661, 1532; ESI-HRMS found mass 168.1047 $[M + Na]^+$ $C_{13}H_{16}N_3O_2Na$ requires 168.1062.

4-*tert*-Butylthiazol-2-amine[126] **95**

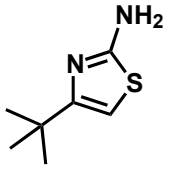

Thiourea (1.00 g, 13 mmol) was stirred in anhydrous ethanol. Copper-(II) acetate (24 mg, 10 mol%) was then added in one portion. 1-Bromopinacolone (1.8 mL, 13 mmol) was subsequently added drop wise. Following completion (monitored by TLC) after 3 hr., the reaction was quenched with water (10 mL). The aqueous phase was extracted with ethyl acetate, dried ($MgSO_4$) and the solvent removed *in vacuo* to give the *title product* (2.36 g, quant.) as a brown oil. δ_H (300 MHz, DMSO-d_6): 8.51 (2H, s, -$N\underline{H}_2$), 6.41 (1H, s, thiazole-$\underline{H}$), 1.19 (9H, s, $^t\underline{Bu}$); δ_C (125 MHz, DMSO-d_6): 169.9, 99.5, 33.2 28.6, 25.8; $\bar{\upsilon}_{max}/cm^{-1}$ (solid state) = 3440, 3383, 3096, 1626, 1563; ESI-HRMS found mass 157.0820 $[M + H]^+$ $C_7H_{13}N_2S$ requires 157.0799.

1-(4-*tert*-Butylthiazol-2-yl)-3-phenylurea **97**

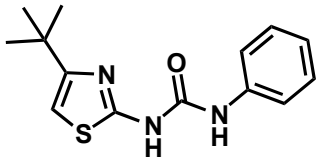

Anhydrous triethylamine (67 µL, 0.48 mmol) was added drop wise with stirring to a solution of 4-*tert*-butylthiazol-2-amine **95** (50 mg, 0.32 mmol) in anhydrous tetrahydrofuran (50 mL). After 10 min, phenylisocyanate (38 µL, 0.32 mmol) was added in one portion. The reaction mixture was heated to reflux for 5 hr., where the reaction was seen to be complete by TLC. After cooling to room temperature, the organics were evaporated *in vacuo*. The resulting solid was suspended in ethyl acetate (100 mL) and the organic layer subsequently washed with H_2O (2 x 150

mL), saturated aqueous ammonium chloride (2 x 50 mL), saturated aqueous sodium bicarbonate solution (2 x 50 mL), saturated aqueous sodium chloride solution (2 x 50 mL) and dried ($MgSO_4$) before the solvent was evaporated *in vacuo*. The resultant solid was purified by mass directed HPLC (gradient 5-95 methanol – water + formic acid 0.01%) to give the *title compound* (23 mg, 26%) as colourless needles; m.p: 250-257 °C; δ_H (300 MHz, $CDCl_3$): 7.56 (2H, d, *J* = 7.8 Hz, Ar-H), 7.37 (2H, app. t, *J* = 7.8 Hz, Ar-H), 7.13 (1H, t, *J* = 7.8 Hz, Ar-H), 6.42 (1H, s, thiazole-H), 1.37 (9H, t, *J* = 7.3 Hz, ^tBu); δ_C (125 MHz, $CDCl_3$): 161.2, 152.3, 138.9, 134.1, 129.1, 123.9, 120.0, 103.1, 29.8 and 25.8; $\bar{\upsilon}_{max}/cm^{-1}$ (solid state) = 3060, 2790, 1681, 1594, 1533; ESI-HRMS found mass 276.1174 $[M + H]^+$ $C_{14}H_{18}N_3OS$ requires 276.1171.

4-Bromobenzene-1,3-diol[114] **83**

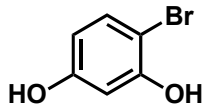

Resorcinol (0.44 g, 4.0 mmol) was dissolved in acetonitrile. Ammonium bromide (0.43 g, 4.4 mmol) and Oxone® (0.66 g, 4.4 mmol) were subsequently added in one portion. The reaction mixture was stirred for 24 hr., before filtration. The filtrate was concentrated *in vacuo* before purification *via* column chromatography (5:95 methanol−dichloromethane) to yield the *title compound* (0.75 g, 15%) as colourless crystals; m.p: 98-103 °C (lit.[114] not reported); δ_H (500 MHz, DMSO-d_6): 9.98 (1H, s, O-H), 9.46 (1H, s, O-H), 7.20 (1H, d, *J* = 8.7 Hz, Ar-H), 6.44 (1H, s, Ar-H), 6.19 (1H, d, *J* = 8.7, 2.5 Hz, Ar-H); δ_C (125 MHz, DMSO-d_6): 157.8, 155.2, 132.7, 108.1, 103.6, 97.7; $\bar{\upsilon}_{max}/cm^{-1}$ (solid state) = 3464, 1858, 1692, 1620, 1158; ESI-HRMS found mass 188.9375 $[M + H]^+$ $C_7H_5O_2Br$ requires 188.9551.

6-Bromo-4-(chloromethyl)-7-hydroxy-2*H*-chromen-2-one[110, 111] **85**

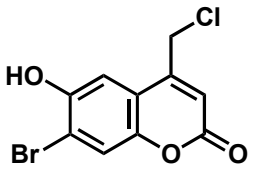

4-Bromobenzene-1,3-diol **83** (0.73 g, 3.9 mmol) was stirred in methane sulfonic acid (10 mL). Ethyl-4-chloroacetoacetate (0.79 mL, 5.8 mmol) was added drop wise and stirred for 2hr. The reaction mixture was poured over ice, and stirred for a further 0.5 hr. The suspension was filtered and dried before purification *via* column chromatography (10:90 methanol−dichloromethane) to yield the *title compound* (0.53 g, 48%) as colourless crystals; m.p: 98-103 °C (lit.[110] not reported); δ_H (500 MHz, DMSO-d_6): 7.98 (1H, s, Ar-H), 6.91 (1H, s, Ar-H), 6.46 (1H, s, Ar-H), 4.99 (2H, s, Cl-CH_2); δ_C (125 MHz, DMSO-d_6): 159.6, 157.5, 154.1, 150.1, 129.0, 112.1, 110.7, 106.1, 103.3, 41.2; $\tilde{\upsilon}_{max}/cm^{-1}$ (solid state) = 3564-2947 (broad), 1683, 1601, 1388; ESI-HRMS found mass 288.9097 $[M + H]^+$ $C_{10}H_7O_3BrCl$ requires 288.9267.

6.3 Procedure for testing the photolability of 78

A 10 mM solution of **78** was sealed inside a bench-top UV TLC visualising box, operating at 365 nm. The sample was irradiated for 2 hr. approximately 4 cm from the light source, before submitting the sample for ^{1}H NMR and LC-MS analysis in amber glassware. DAN **37** and UPy benzyl ester **39** were previously synthesised in the group by M. Pellizzaro.

6.4 Experimental section for Chapter 3

*N*1, *N*8-bis(6-methyl-4-oxo-1,4-dihydropyrimidin-2-yl)octanediamide[80] **62**

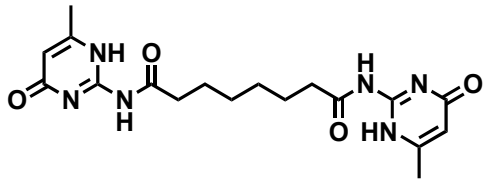

2-Amino-4-hydroxy-6-methylpyrimidine (6.0 g, 48 mmol) was suspended in anhydrous dimethylacetamide (50 mL). Anhydrous triethylamine (6.65 mL, 48 mmol) was added drop wise with stirring. Suberoyl chloride (4.33 mL, 24 mmol) was then added drop wise at 0 °C. The reaction mixture was subsequently heated to 87 °C and was left to stir for 16 hr. After cooling to room temperature, the solvent was removed under reduced pressure. The crude product was triturated (H_2O) followed by crystallisation (chloroform – hexane) to provide the *title compound* (8.03 g, 86%) as a colourless powder, m.p: 244–246 °C (Lit.[80] 180–182 °C); δ_H (300 MHz, DMSO-d_6): 11.80 (2H, br s, NHCO), 11.60 (2H, br s, NHC(CH)$_3$), 5.92 (2H, s, pyrimidyl-H), 2.38 (4H, t, J = 7.2 Hz, CH_2CO), 2.13 (6H, s, CH_3), 1.54 (4H, m, CH_2CH_2CO), 1.17 (4H, m, $CH_2CH_2CH_2CO$); δ_C (75 MHz, DMSO-d_6): 176.5, 165.1, 160.4, 150.4, 106.9, 35.8, 27.9, 24.1, 23.3; $\bar{\upsilon}_{max}/cm^{-1}$ (solid state) = 3162, 2850, 1711, 1643, 1561; ESI-HRMS found mass 389.1859 $[M + H]^+$ $C_{18}H_{25}N_6O_4$ requires 389.1937.

Pentanoic acid(6-amino-pyridin-2-yl)-amide **108**

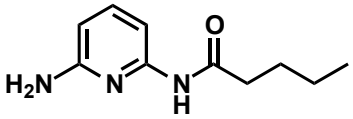

To a stirred solution of 2,6-diaminopyridine (0.21 g, 1.9 mmol) in anhydrous tetrahydrofuran (50 mL) and anhydrous triethylamine (0.28 mL, 1.9 mmol), was added pentanoyl chloride (0.21 mL,1.8 mmol) dropwise via cannula over 5 minutes at 0 ^oC. The remaining solvent was removed under reduced pressure to yield a yellow oil. The oil was dissolved in $CHCl_3$ (30 mL) and washed with water (5×100 mL). The organic portions were combined and dried over $MgSO_4$, filtered and

concentrated under reduced pressure. The product was purified by column chromatography (3:97 MeOH:$CHCl_3$) to yield the *title compound* as a brown solid (0.21 g, 68%); mp: 74 – 75 °C; δH (300MHz, $CDCl_3$): 7.72 (1H, br s, NHCO), 7.54 (1H, d, *J* = 7.8 Hz, Ar-H), 7.44 (1H, t, *J* = 8.1 Hz, Ar-H), 6.23 (1H, d, *J* = 7.8 Hz, Ar-H), 4.30 (2H, br s, NH_2), 2.34 (2H, t, *J* = 7.6 Hz, $CH_3CH_2CH_2CH_2$), 1.69 (2H, dt, *J* = 7.3, 7.6 Hz, $CH_3CH_2CH_2$), 1.38 (2H, sextet, *J* = 7.4 Hz, CH_2CH_3), 0.94 (3H, t, *J* = 4.2 Hz, Me); δC (300 MHz, $CDCl_3$): 172.1, 157.4, 150.2, 140.7, 104.5, 103.7, 37.9, 27.9, 22.7, 14.2; ν_{max} (neat) / cm^{-1}: 3412, 3328, 2962, 2871, 2453, 2261, 1967, 1846, 1669, 1527, 1436; ESI-MS: m/z = 278.3 [M+ H]+.

Octanedioic acid bis-[(6-pentanoylamino-pyridin-2-yl)-amide] **109**

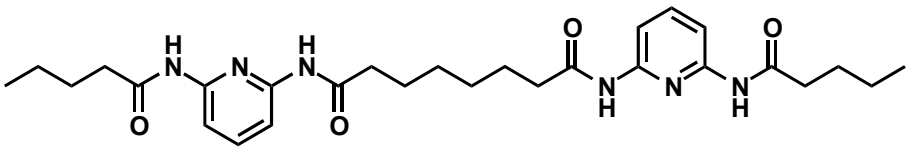

To a solution of pentanoic acid(6-amino-pyridin-2-yl)-amide (0.197 g, 0.71 mmol) in anhydrous tetrahydrofuran (25 mL), was added suberoyl chloride (0.06 mL, 0.33 mmol). The reaction was then heated under reflux for 60 hr. The reaction mixture was then concentrated under reduced pressure and the remaining residue was dissolved in $CHCl_3$ (30 mL) and washed with water (3 × 30 mL). The organic portion was collected and dried over Na_2SO_4, filtered and concentrated under reduced pressure. The remaining residue was purified by column chromatography (1:1 EtOAc:CH_2CH_2) and concentrated under reduced pressure to provide the *title compound* as a flocculent powder. (79 mg, 84%); mp: 182 – 183 ^oC; δH (300 MHz, CDCl3): 7.94 (2H, d, *J* = 8.0 Hz, Ar-H), 7.93 (2H, d, *J* = 8.0Hz, Ar-H), 7.73 (2H, t, *J* = 8.0 Hz, 2 × Ar-H), 7.60 (4H, br s, 4 × NH), 2.39 – 2.44 (8H, m, 4× CH_2CO), 1.70 – 1.81 (8H, m, 4 × CH_2), 1.30 – 1.51 (8H, m, 4 × CH_2), 0.99 (6H, t, *J* = 7.3Hz, 2 × Me); ν_{max}(neat): 3315, 2936, 2340, 1995, 1770, 1670; ESI-MS: m/z = 525 [M + H]+.

*N*1, *N*4-bis(6-methyl-4-oxo-1,4-dihydropyrimidin-2-yl)terephthalamide **112**

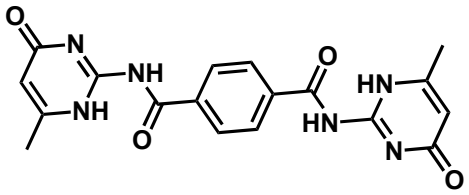

The compound was synthesised using a modified literature procedure.[80] 2-Amino-4-hydroxy-6-methylpyrimidine (6.0 g, 48 mmol) was suspended in anhydrous dimethylacetamide (50 mL). Anhydrous triethylamine (6.65 mL, 48 mmol) was added drop wise with stirring. Terephthaloyl chloride (4.86 g, 24 mmol) was added in one portion at 0 °C. The reaction mixture was subsequently heated to 87 °C and was left to stir for 16 hr. After cooling to room temperature, the solvent was removed under reduced pressure. The crude product was triturated (H_2O) and crystallised (chloroform – hexane) to provide the *title compound* (6.50 g, 71%) as a colourless powder; m.p: 155-158 °C; δ_H (300 MHz, DMSO-d_6): 12.30 (4H, br s, NHCO, NHC(CH)$_3$), 8.16 (4H, s, Ar-H), 5.93 (2H, s, pyrimidyl-H), 2.21 (6H, s, CH$_3$); δ_C (75 MHz, DMSO-d_6): 17.7, 106.9, 125.5, 137.4, 150.4, 165.2, 176.5, 187.6; ν_{max}/cm^{-1} (solid state) = 3165, 2831, 1701, 1635, 1557; ESI-HRMS found mass 381.1314 $[M + H]^+$ $C_{18}H_{17}N_6O_4$ requires 381.1311.

*N*1, *N*6-bis(6-methyl-4-oxo-1,4-dihydropyrimidin-2-yl)adipamide **113**

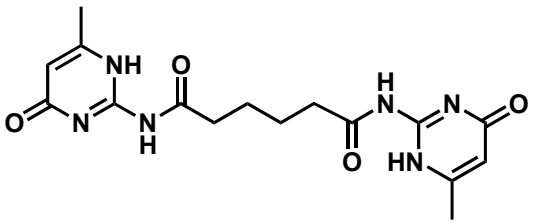

The compound was synthesised using a modified literature procedure.[80] 2-Amino-4-hydroxy-6-methylpyrimidine (6.0 g, 48 mmol) was suspended in anhydrous dimethylacetamide (50 mL). Anhydrous triethylamine (6.65 mL, 48 mmol) was added drop wise with stirring. Adipoyl chloride (3.49 mL, 24 mmol) was then added drop wise at 0 °C. The reaction mixture was subsequently heated to 87 °C and was left to stir for 16 hr. After cooling to room temperature, the solvent was removed under reduced pressure. The crude product was triturated (H_2O) and precipitated

(DMSO – H_2O) to provide the *title compound* (3.89 g, 45%) as a grey powder; m.p: decomp. > 200 °C; δ_H (300 MHz, DMSO-d_6): 11.94 (2H, br s, N<u>H</u>CO), 11.79 (2H, br s, N<u>H</u>C(CH)$_3$), 5.93 (2H, s, pyrimidyl-H), 2.43 (4H, s, $CH_2C\underline{H_2}CO$), 2.13 (6H, s, C<u>H</u>$_3$), 1.50 (4H, s, <u>C</u>H_2CH_2CO); δ_C (75 MHz, DMSO-d_6): 23.6, 35.6, 38.6, 107.0, 150.4, 160.3, 176.3 and 190.6; $\bar{\upsilon}_{max}/cm^{-1}$ (solid state) = 2724, 1737, 1619, 1512; ESI-HRMS found mass 383.1424 $[M + Na]^+$ $C_{16}H_{20}N_6NaO_4$ requires 383.1444.

2, 2'-oxy-bis(*N*-(6-methyl-4-oxo-1,4-dihydropyrimidin-2-yl)acetimide) **114**

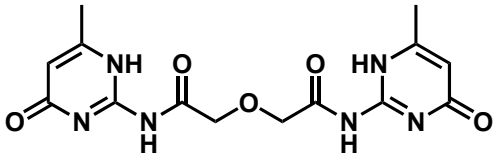

The compound was synthesised using a modified literature procedure.[80] 2-Amino-4-hydroxy-6-methylpyrimidine (6.0 g, 48 mmol) was suspended in anhydrous dimethylacetamide (50 mL). Anhydrous triethylamine (6.65 mL, 48 mmol) was added drop wise with stirring. Diglycolyl chloride (2.85 mL, 24 mmol) was added drop wise at 0 °C. The reaction mixture was subsequently heated to 87 °C and was left to stir for 16 hr. After cooling to room temperature, the solvent was removed under reduced pressure. The crude material was triturated (H_2O) to provide the *title compound* (4.92 g, 59%) as a cream powder; m.p: decomp. > 260 °C; δ_H (500 MHz, DMSO-d_6): 11.69 (2H, br s, N<u>H</u>CO), 11.52 (2H, br s, N<u>H</u>C(CH)$_3$), 5.96 (2H, s, pyrimidyl-H), 4.31 (4H, s, C<u>H</u>$_2$O), 2.13 (6H, s, C<u>H</u>$_3$); δ_C (75 MHz, DMSO-d_6): 17.5, 69.6, 106.2, 153.9, 169.0, 171.4, 189.9; $\bar{\upsilon}_{max}/cm^{-1}$ (solid state) = 2404, 1606, 1507, 1073; ESI-HRMS found mass 371.1084 $[M + H]^+$ $C_{14}H_{16}N_6NaO_5$ requires 371.1080.

1,1'-(Hexane-1,6-diyl)bis(3-(5,6-dimethyl-1*H*-benzo[d]imidazol-2-yl)urea)[79] **100**

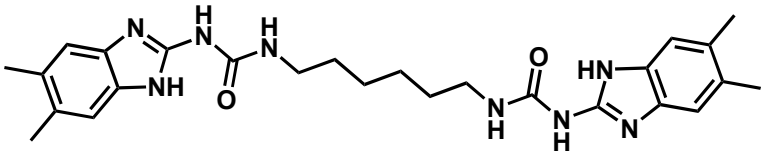

A solution of 1,6-diisocyanato hexane (0.49 mL, 3.1 mmol) in anhydrous dimethylacetamide (10 mL) was added drop wise with stirring to 2-amino-5,6-dimethylbenzimidazole (1.0 g, 6.2 mmol) in anhydrous dimethylacetamide (20 mL). The reaction mixture was subsequently heated to 87 °C for 16 hr. The reaction mixture was cooled to room temperature and the precipitate filtered, crystallised (dimethylacetamide), and washed (methanol) to provide the title compound (0.4 g, 24%) as dark pink flakes. m.p: decomp. > 250 °C; δ_H (500 MHz, DMSO-d_6): 7.11 (4H, s, Ar-H), 3.15 (4H, t, J = 7.3, NHCH_2), 2.21 (12H, s, CH_3), 1.50 (4H, m, CH_2-CH_2-NH), 1.26 (4H, m, CH_2- CH_2-CH_2-NH); $\bar{\upsilon}_{max}$/cm^{-1} (solid state) = 3350, 2970, 2939, 1701, 1554. The compound was insufficiently soluble for ^{13}C analysis.

6.5 General Synthetic Procedure for Synthesis of Telechelic Supramolecular Polymers[80]

The required amount of 4,4'-methylenediphenyldiisocyanate (MDI) was dissolved in anhydrous dimethylacetamide (5 mL g^{-1}) for 1 hr. A solution of the required polyol dissolved in anhydrous dimethylacetamide (30 mL g^{-1}) was added drop wise to the stirred solution of MDI over 30 min at 87 °C and stirred for an additional 1.5 hr. A solution of the required amine dissolved in anhydrous dimethylacetamide (10 mL g^{-1}) was then added drop wise over 30 min and the reaction mixture heated for a further 16 hr. After this time, the required amount of the chosen complementary hydrogen bonding unit was added in one portion and stirred for an additional 16 hr. The reaction mixture was then allowed to cool to room temperature, and the solvent removed under reduced pressure to provide the target material.

Polymer Macromonomer^{80}NCO:OH = 2:1

The general procedure for the synthesis of macromolecules was followed using MDI (0.50 g, 2.00 mmol), poly(ethylene glycol)-*block*- poly(propylene glycol)-*block*-poly(ethylene glycol) (PEG-PPG-PEG) (2.00 g, 1.00 mmol) and 2-amino-5,6-dimethylbenzimidazole (0.24 g, 1.50 mmol). The chosen DAC was not added on this occasion providing the title compound,[80] as a very viscous dark orange liquid; δ_H (300 MHz, DMSO-d_6): 7.35-7.29 (8H, MDI, Ar-H), 7.11-7.04 (8H, MDI, Ar-H), 6.82 (4H, s, diUIM-Ar-H), 4.19-4.10 (4H, m, MDI CH_2), 3.50-3.33 (44H, m, *block*-poly(ethylene) CH_2, CH_2, *block*-poly(propylene oxide) CH_2), 2.51 (12H, s, diUIM-CH_3) and 1.04-1.02 (31H, m, *block*- poly(propylene oxide) CH_3). ν_{max}/cm^{-1} (solid state) = 3448, 3311, 3124, 2971, 2873, 1728, 1642, 1543 and 1512.

Telechelic Supramolecular Polymer^{80}NCO:OH = 2:1 **103a**

The general procedure for the synthesis of macromolecules was followed using MDI (0.50 g, 2.00 mmol), PEG-PPG-PEG (2.00 g, 1.00 mmol), 2-amino-5,6-dimethylbenzimidazole (0.24 g, 1.50 mmol) and S- DAC (0.39 g, 1.00 mmol) providing the title compound, as a sticky, very viscous, brown liquid; δ_H (300 MHz, DMSO-d_6): 11.59 (4H, br s, S-DAC-NH), 7.37-7.30 (8H, MDI, Ar-H), 7.12-7.02 (8H, MDI, Ar-H), 6.87 (4H, s, benzimidazole-Ar-H), 5.92 (2H, s, S-DAC Ar-H), 4.18-4.14 (4H, m, MDI CH_2), 3.52-3.30 (144H, m, *block*-poly(ethylene) CH_2, CH_2, *block*-poly(propylene oxide) CH_2 and *block*-poly(propylene oxide) CH), 2.41 (4H, t, *J* = 7.2 Hz, S-DAC CH_2), 2.19 (12H, s, benzimidazole-CH_3), 2.10 (6H, s, S-DAC CH_3), 1.59-1.53 (4H, S-DAC, CH_2), 1.31-1.23 (4H, S-DAC CH_2) and 1.04-1.02 (99H, m, *block*- poly(propylene oxide) CH_3); δ_C (100 MHz, DMSO-d_6): 176.6, 158.8, 154.4, 150.2, 134.6, 131.1, 130.4, 128.7, 123.4, 118.2, 114.0, 106.9, 74.6, 72.4, 70.1, 69.8, 69.7, 41.2, 35.8, 27.9, 24.1, 20.3, 19.7, 17.9 and 17.2; ν_{max}/cm^{-1} (solid state) = 3311, 3124, 2971, 2873, 1728, 1642, 1539 and 1513.

Chain-Extended Telechelic Supramolecular Polymer[80] NCO:OH = 4:1 **103b**

The general procedure for the synthesis of macromolecules was followed using MDI (0.50 g, 2.00 mmol), PEG-PPG-PEG (1.00 g, 0.50 mmol), 2-amino-5,6-dimethylbenzimidazole (0.48 g, 3.00 mmol) and S-DAC (0.58 g, 1.50 mmol) providing the title compound, as a waxy brown solid; δ_H (300 MHz, DMSO-d_6): 11.79-11.62 (6H, br s, DAC-N<u>H</u>), 7.39-7.31 (32H, MDI, Ar-<u>H</u>), 7.12-7.06 (32H, MDI, Ar-<u>H</u>), 6.87 (16H, s, benzimidazole-Ar-<u>H</u>), 5.92 (6H, s, S-DAC Ar-<u>H</u>), 4.20-4.13 (16H, m, MDI C<u>H</u>$_2$), 3.53-3.35 (194H, m, *block*-poly(ethylene) C<u>H</u>$_2$, C<u>H</u>$_2$, *block*-poly(propylene oxide) C<u>H</u>$_2$ and *block*-poly(propylene oxide) C<u>H</u>), 2.40 (12H, t, *J* = 7.7 Hz, S-DAC C<u>H</u>$_2$), 2.19 (48H, s, benzimidazole-C<u>H</u>$_3$), 1.96 (24H, s, S-DAC C<u>H</u>$_3$), 1.60-1.52 (12H, S-DAC, C<u>H</u>$_2$), 1.31-1.22 (12H, S-DAC C<u>H</u>$_2$) and 1.04-1.02 (96H, m, *block*- poly(propylene oxide) C<u>H</u>$_3$); δ_C (100 MHz, DMSO-d_6): 176.5, 160.8, 155.7, 150.4, 134.3, 133.1, 131.3, 128.9, 126.3, 118.2, 114.0, 107.0, 74.6, 72.4, 69.8, 68.7, 68.3, 67.8, 40.8, 35.8, 28.0, 24.1, 23.4, 29.7 and 17.2; ν_{max}/cm^{-1} (solid state) = 3347, 3183, 2970, 2870, 1710, 1645, 1538 and 1512.

Chain-Extended Telechelic Supramolecular Polymer[80] NCO:OH = 6:1 **103c**

The general procedure for the synthesis of macromolecules was followed using MDI (0.38 g, 1.50 mmol), PEG-PPG-PEG (0.50 g, 0.25 mmol), 2-amino-5,6-dimethylbenzimidazole (0.32 g, 2.50 mmol) and S-DAC (0.49 g, 1.25 mmol) providing the title compound, as an orange waxy solid; δ_H (300 MHz, DMSO-d_6): 11.74-11.50 (10H, br s, DAC-N<u>H</u>), 7.35-7.30 (48H, MDI, Ar-<u>H</u>), 7.12-7.04 (48H, MDI, Ar-<u>H</u>), 6.88 (24H, s, benzimidazole-Ar-<u>H</u>), 5.92 (10H, s, S-DAC Ar-<u>H</u>), 4.20-4.11 (24H, m, MDI C<u>H</u>$_2$), 3.53-3.33 (292H, m, *block*-poly(ethylene) C<u>H</u>$_2$, C<u>H</u>$_2$, *block*-poly(propylene oxide) C<u>H</u>$_2$ and *block*-poly(propylene oxide) C<u>H</u>), 2.41 (20H, t, *J* = 7.3 Hz, S-DAC C<u>H</u>$_2$), 2.19 (48H, s, benzimidazole-C<u>H</u>$_3$), 2.13 (30H, s, S-DAC C<u>H</u>$_3$), 1.61-1.51 (20H, S-DAC, C<u>H</u>$_2$), 1.31-1.23 (20H, S-DAC C<u>H</u>$_2$) and 1.04-1.02 (142H, m, *block*- poly(propylene oxide) C<u>H</u>$_3$); δ_C (100 MHz, DMSO-d_6): 176.6, 162.4, 154.4, 151.4, 133.2, 131.2, 130.2, 128.9, 124.5, 118.3, 113.9, 106.9, 74.6, 72.4, 69.8, 68.3, 67.4, 67.1, 41.3, 35.8, 27.9, 24.1, 19.7, 19.0 and 17.2; ν_{max}/cm^{-1} (solid state) = 3353, 2966, 2871, 1899, 1642, 1504 and 1312.

Chain-Extended Telechelic Supramolecular Polymer[80] NCO:OH = 8:1 **103d**

The general procedure for the synthesis of macromolecules was followed using MDI (0.25 g, 1.00 mmol), PEG-PPG-PEG (0.25 g, 0.13 mmol), 2-amino-5,6-dimethylbenzimidazole (0.28 g, 1.75 mmol) and S-DAC (0.34 g, 0.88 mmol) providing the title compound,[80] as a waxy dark orange solid; δ_H (300 MHz, DMSO-d_6): 11.81-11.61 (28H, br s, DAC-NH), 7.36-7.32 (64H, MDI, Ar-H), 7.13-7.07 (64H, MDI, Ar-H), 6.88 (32H, s, benzimidazole-Ar-H), 5.92 (14H, s, S-DAC Ar-H), 3.82-3.76 (32H, m, MDI CH_2), 3.54-3.35 (250H, m, *block*-poly(ethylene) CH_2, CH_2, *block*-poly(propylene oxide) CH_2 and *block*-poly(propylene oxide) CH), 2.40 (28H, t, *J* = 7.9 Hz, S-DAC CH_2), 2.19 (96H, s, benzimidazole-CH_3), 2.13 (42H, s, S-DAC CH_3), 1.60-1.53 (28H, S-DAC, CH_2), 1.31-1.23 (28H, S-DAC CH_2) and 1.04-1.02 (113H, m, *block*- poly(propylene oxide) CH_3); δ_C (100 MHz, DMSO-d_6): 176.5, 155.7, 154.5, 151.2, 137.7, 134.2, 132.7, 128.9, 126.4, 118.3, 113.9, 106.9, 74.6, 72.4, 69.8, 67.8, 67.0, 64.9, 40.6, 35.8, 27.9, 24.1, 22.2, 19.72, 18.9 and 17.2; ν_{max}/cm^{-1} (solid state) = 2940, 2873, 1728, 1642, 1506 and 1462.

Chain-Extended Telechelic Supramolecular Polymer NCO:OH = 4:1 **115**

The general procedure for the synthesis of macromolecules was followed using MDI (0.50 g, 2.00 mmol), PEG-PPG-PEG (1.00 g, 0.50 mmol), 2-amino-5,6-dimethylbenzimidazole (0.48 g, 3.00 mmol) and T-DAC (0.57 g, 1.5 mmol) providing the *title compound*, as a very viscous and sticky dark orange liquid; δ_H (300 MHz, DMSO-d_6): 8.22-7.94 (12H, T-DAC Ph-H), 7.36-7.30 (32H, MDI, Ar-H), 7.12-7.04 (32H, MDI, Ar-H), 6.88 (16H, s, benzimidazole-Ar-H), 5.89 (6H, s, T-DAC Ar-H), 4.20-4.12 (16H, m, MDI CH_2), 3.53-3.30 (476H, m, *block*-poly(ethylene) CH_2, CH_2, *block*-poly(propylene oxide) CH_2 and *block*-poly(propylene oxide) CH), 2.28 (18H, s, T-DAC CH_3), 2.24 (48H, s, benzimidazole-CH_3), 1.60-1.52 (12H, S-DAC, CH_2), 1.31-1.22 (12H, S-DAC CH_2) and 1.04-1.02 (357H, m, *block*- poly(propylene oxide) CH_3); δ_C (100 MHz, DMSO-d_6): 185.9, 171.6, 154.3, 152.8, 146.6, 137.7, 137.1, 136.2, 131.5, 128.7, 126.7, 123.1, 118.2, 113.9, 112.3, 74.6, 72.4, 69.8, 68.7, 67.8, 63.3, 41.4, 19.7, 18.3, 17.2

and 15.0; ν_{max}/cm^{-1} (solid state) = 3312, 3124, 2971, 2873, 1722, 1642, 1546 and 1513.

Chain-Extended Telechelic Supramolecular Polymer NCO:OH = 4:1 **117**

The general procedure for the synthesis of macromolecules was followed using MDI (0.50 g, 2.00 mmol), PEG-PPG-PEG (1.00 g, 0.50 mmol), 2-amino-5,6-dimethylbenzimidazole (0.48 g, 3.00 mmol) and A-DAC (0.54 g, 1.5 mmol) providing the *title compound*, as a very viscous and sticky brown liquid; δ_H (300 MHz, DMSO-d_6): 11.72-11.14 (6H, br s, DAC-N<u>H</u>), 7.40-7.30 (32H, MDI, Ar-<u>H</u>), 7.13-7.02 (32H, MDI, Ar-<u>H</u>), 6.88 (16H, s, benzimidazole-Ar-<u>H</u>), 5.92 (6H, s, A-DAC Ar-<u>H</u>), 4.20-4.11 (16H, m, MDI C<u>H</u>$_2$), 3.53-3.29 (173H, m, *block*-poly(ethylene) C<u>H</u>$_2$, C<u>H</u>$_2$, *block*-poly(propylene oxide) C<u>H</u>$_2$ and *block*-poly(propylene oxide) C<u>H</u>), 2.46 (12H, bs, A-DAC C<u>H</u>$_2$), 2.24 (18H, s, A-DAC C<u>H</u>$_3$), 2.19 (48H, s, benzimidazole-C<u>H</u>$_3$), 1.59 (12H, bs, A-DAC, 2C<u>H</u>$_2$) and 1.04-1.02 (143H, m, *block*- poly(propylene oxide) C<u>H</u>$_3$); δ_C (100 MHz, DMSO-d_6): 190.6, 179.7, 176.3, 154.5, 152.1, 144.4, 136.3, 129.8, 128.7, 126.4, 118.2, 113.9, 106.9, 74.6, 72.4, 69.8, 69.8, 68.7, 67.8, 66.9, 40.3, 38.1, 35.6, 23.6, 19.7, 18.3 and 17.2; ν_{max}/cm^{-1} (solid state) = 3314, 3187, 2969, 2872, 1728, 1644, 1549 and 1513.

Chain-Extended Telechelic Supramolecular Polymer NCO:OH = 4:1 **116**

The general procedure for the synthesis of macromolecules was followed using MDI (0.50 g, 2.00 mmol), PEG-PPG-PEG (1.00 g, 0.50 mmol), 2-amino-5,6-dimethylbenzimidazole (0.48 g, 3.00 mmol) and D-DAC (0.52 g, 1.5 mmol) providing the *title compound*, as soft and rubbery light brown flakes; δ_H (300 MHz, DMSO-d_6): 10.74-10.50 (6H, br s, DAC-N<u>H</u>), 7.35 (4H, s, benzimidazole-Ar-<u>H</u>), 7.12-7.06 (32H, MDI, Ar-<u>H</u>), 6.49-6.42 (32H, MDI, Ar-<u>H</u>), 5.98 (6H, s, D-DAC Ar-<u>H</u>), 5.39 (12H, s, D-DAC C<u>H</u>$_2$), 4.19-4.12 (16H, m, MDI C<u>H</u>$_2$), 3.53-3.32 (307H, m, *block*-poly(ethylene) C<u>H</u>$_2$, C<u>H</u>$_2$, *block*-poly(propylene oxide) C<u>H</u>$_2$ and *block*-poly(propylene oxide) C<u>H</u>), 2.32 (18H, s, D-DAC C<u>H</u>$_3$), 1.98 (48H, s, benzimidazole-C<u>H</u>$_3$) and 1.04-1.02 (211H, m, *block*- poly(propylene oxide) C<u>H</u>$_3$); δ_C (100 MHz, DMSO-d_6): 194.7, 174.3, 169.9, 149.9, 148.1, 137.6, 132.1, 130.7,

128.8, 127.1, 118.0, 115.7, 100.2, 74.6, 72.2, 72.1, 69.8, 68.7, 67.8, 66.4, 41.2, 19.9, 17.2 and 14.9; ν_{max}/cm^{-1} (solid state) = 3313, 3183, 2971, 2868, 1728, 1647, 1543 and 1512.

Self-Assembly Control using *N*1,*N*8-*bis*(6-pentanamidopyridin-2-yl)octanediamide as the HCU^{80} NCO:OH = 4:1

*N*1,*N*8-bis(6-pentanamidopyridin-2-yl)octanediamide **108** was synthesised by previous member of the Wilson Group, Adam Gooch. An NMR was obtained to check any degradation of the molecule, which was then used without any further purification. The general procedure for the synthesis of macromolecules was followed using MDI (0.10 g, 0.40 mmol), PEG-PPG-PEG (0.40 g, 0.20 mmol), 2-amino-5,6-dimethylbenzimidazole (0.06 g, 0.40 mmol) and *N*1,*N*8-*bis*(6-pentanamidopyridin-2-yl)octanediamide (0.11 g, 0.2 mmol) providing the *title compound*, as a non-self-supportive dark yellow paste; δH (500 MHz, DMSO- d6): 7.69 (6H, s, Ar-H), 7.36-7.30 (8H, m, MDI-Ar-H), 7.10–7.03 (8H, m, MDI-Ar-H), 6.83 (4H, s, diUIM-Ar-H), 3.78 (4H, br s, MDI-CH_2), 3.50–3.30 (44H, m, *block*-poly(ethylene) CH_2, CH_2, *block*-poly(propylene oxide)-CH_2 and *block*-poly(propylene oxide) CH), 2.38 (8H, m, CH_2- CONH), 2.24 (12H, s, diUIM-CH_3), 1.54 (8H, m, CH_2-CH_2CONH), 1.30 (8H, m, CH_2- CH_2CH_2CONH), 1.27–1.02 (31H, m, *block*-poly(propylene oxide)-CH_3), 0.87 (8H, t, *J*= 7.3 Hz, $CH_2CH_2CH_2$-CH_3); δC (125 MHz, DMSO- d6): 169.5, 156.9, 150.3, 139.8, 137.8, 134.8,130.9, 128.8, 123.6, 118.2, 114.0, 111.9, 74.6, 72.4, 69.8, 68.2, 66.8, 65.0, 41.4, 37.4, 36.1,35.8, 27.1, 21.7, 19.6, 17.3 and 13.7; υmax/cm-1 (solid state) = 3319, 2870, 1726, 1633, 1539 and 1449.

Chain-Extended Telechelic Supramolecular Polymer NCO:OH = 4:1 **111**

The general procedure for the synthesis of macromolecules was followed using MDI (0.50 g, 2.00 mmol), poly(tetrahydrofuran) (1.00 g, 0.50 mmol), 2-amino benzimidazole (0.40 g, 3.00 mmol) and S-DAC (0.58 g, 1.5 mmol) providing the *title compound*, as a brittle light yellow solid; δ_H (500 MHz, DMSO-d_6): 7.37-7.32 (4H, s, benzimidazole-Ar-H), 7.11-7.09 (32H, MDI, Ar-H), 6.87-6.85 (32H, MDI,

Ar-H), 5.93 (6H, s, D-DAC Ar-H), 5.40 (12H, s, D-DAC CH_2), 4.15-4.01 (16H, m, MDI CH_2), 3.53-3.32 (156H, m, poly(tetrahydrofuran) CH_2), 2.43 (18H, s, D-DAC CH_3), 1.97 (48H, s, benzimidazole-CH_3) and 1.51 (68H, m, poly(tetrahydrofuran), m, *poly*(tetrahydrofuran) CH_2); δ_C (100 MHz, DMSO-d_6): 181.8, 160.4, 155.6, 134.1, 124.2, 123.5, 119.2, 116.8, 112.2, 74.9, 45.3, 45.2, 45.1, 44.9, 44.8 44.7, 44.6, 44.4, 44.3, 41.1, 39.7, 33.2, 31.1, 29.3 and 26.6.

6.6 Experimental section for Chapter 4

1,1'-(4,4'-Methylenebis(4,1-phenylene))-3-diethylurea-3-diisopropylurea **135**

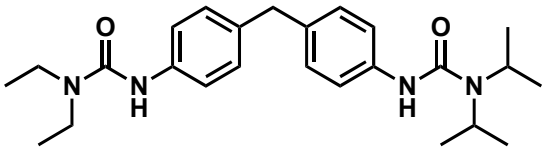

4,4'-Methylenediphenyldiisocyanate (0.5 g, 2 mmol) was dissolved in anhydrous dichloromethane (40 mL). Diethyl amine (0.2 mL, 2 mmol) and diisopropylamine (0.3 mL 2 mmol) were added drop wise simultaneously. After 1 hr. the reaction was complete by TLC. The solvent was removed *in vacuo* before purification *via* column chromatography (10:90 acetone−dichloromethane) to yield the *title compound* (0.23g, 53%) as a white solid; m.p: 164-166 °C; δ_H (500 MHz, $CDCl_3$): 7.28 (4H, m, Ar-H), 7.08 (4H, d, *J* = 8.2 Hz, Ar-H), 6.22 (1H, s, NH), 6.00 (1H, s, NH), 4.04 (4H, m, NCH$(CH_3)_2$), 3.86 (2H, s, Ar-CH_2-Ar), 3.37 (8H, q, *J* = 7.1 Hz, CH_2CH_3), 1.32 (24H, d, *J* = 6.9 Hz, NCH(CH_3)$_2$), 1.13 (12H, t, *J* = 7.1 Hz, CH_2CH_3); δ_C (125 MHz, $CDCl_3$): 154.7, 137.3, 135.9, 129.3, 119.9, 45.4, 21.6, 13.9; $\bar{\upsilon}_{max}/cm^{-1}$ (solid state) = 3304, 2966, 2924, 1904, 1634, 1515, 1242; ESI-HRMS found mass 447.2723 $[M + Na]^+$ $C_{25}H_{36}O_2N_4Na$ requires 447.2736.

Methyl-4(4-(3,3-diethylureido)benzyl)phenylcarbamate **136**

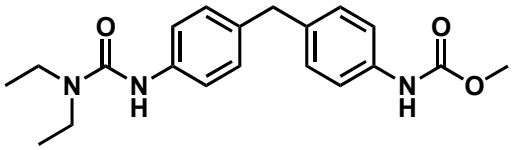

127 (20 mg, 0.04 mmol) was refluxed in methanol (10 mL) for 1 hr. The reaction was seen to be complete by TLC and the solvent was removed *in vacuo* before purification *via* column chromatography (10:90 acetone−dichloromethane) to yield the *title compound* (quant.) as a white solid; δ_H (500 MHz, $CDCl_3$): 7.33 (4H, m, Ar-H), 7.14 (4H, m, Ar-H), 6.59 (1H, s, NH), 6.24 (1H, s, NH), 4.00 (2H, s, Ar-CH_2-Ar), 3.79 (3H, s, O-CH_3), 3.40 (8H, q, *J* = 7.2 Hz, CH_2CH_3), 1.28 (12H, t, *J* = 7.1 Hz, CH_2CH_3); δ_C (125 MHz, $CDCl_3$): 154.7, 154.3 137.2, 135.6, 129.4, 129.3, 120.1, 52.1, 41.7, 40.6, 13.9; $\bar{\upsilon}_{max}/cm^{-1}$ (solid state) = 3411, 3266, 2976-2897, 1905, 1723, 1516, 1225; ESI-HRMS found mass 356.1973 $[M + Na]^+$ $C_{20}H_{26}O_3N_3$ requires 356.1973.

N-tert-butyl benzyl amine **131**

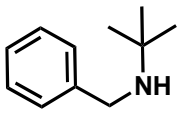

Benzyl alcohol (0.5 mL, 4.6 mmol) and *tert*-butyl amine (0.48 mL, 4.6 mmol) were stirred in anhydrous dichloromethane. Manganese dioxide (4.00 g, 46 mmol) and sodium borohydride (0.35 g, 9.3 mmol) were added in one portion before bringing the solution to reflux for 18 hr. At 0 °C, the reaction was quenched with methanol (10 mL). After 0.5 hr., the solution was filtered through celite and the filtrate removed *in vacuo*. The resultant solid was dissolved in diethyl ether and washed with water. The organic layer was dried ($MgSO_4$) and the solvent removed *in vacuo* to provide the *title compound* (0.15 g, 20%) as a yellow oil; δ_H (500 MHz, $CDCl_3$): 7.39-7.32 (4H, m, Ar-H), 7.27 (1H, m, Ar-H), 4.68 (1H, s, N-H), 3.77 (2H, s, Ar-CH_2), 1.26 (9H, s, NHCCH_3); δ_C (125 MHz, $CDCl_3$): 141.4, 128.5, 128.3, 126.8, 50.7, 47.3, 29.2; $\bar{\upsilon}_{max}/cm^{-1}$ (solid state) = 2964, 1605, 1388, 1230, 1027; ESI-HRMS found mass 164.1443 $[M + H]^+$ $C_{12}H_{17}N$ requires 164.1439.

1-Benzyl-1-*tert*-butyl-3-phenylurea **132**

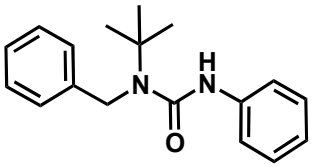

131 (200 mg, 1.2 mmol) was stirred in anhydrous dichloromethane. Phenylisocyanate (0.24 mL, 2.2 mmol) was added drop wise and the reaction mixture stirred for 1 hr. The solvent was removed *in vacuo.* Purification *via* column chromatography (10:90 acetone−dichloromethane) yielded the *title compound* (27 mg, 20%) as a yellow oil; δ_H (500 MHz, $CDCl_3$): 7.48-7.34 (5H, m, Ar-H), 7.24 (2H, t, *J* = 7.3 Hz, Ar-H), 7.10 (2H, app. t, *J* = 7.8 Hz, Ar-H), 6.99 (1H, t, *J* = 7.3 Hz, Ar-H), 5.24 (1H, s, N-H), 4.66 (2H, s, Ar-CH_2), 1.55 (9H, s, NCCH_3); δ_C (125 MHz, $CDCl_3$): 156.9, 139.2, 139.1, 129.3, 129.1, 128.7, 128.3, 125.7, 122.7, 56.9, 49.2, 29.1; $\bar{\upsilon}_{max}/cm^{-1}$ (solid state) = 3291, 2962, 1620, 1440 and 1244; ESI-HRMS found mass 283.1799 $[M + H]^+$ $C_{18}H_{23}ON_2$ requires 283.1810.

1-*tert*-Butyl-1-isopropyl-3-phenylurea **122**

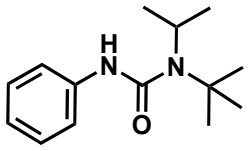

N-*tert*-butyl isopropyl-1-amine (0.84 mL, 5.5 mmol) was stirred in dry dichloromethane. Phenylisocyanate (0.5 mL, 4.6 mmol) was added drop wise and the reaction mixture stirred for 16 hr. The solvent was removed *in vacuo.* Purification *via* column chromatography (dichloromethane) yielded the *title compound* (0.79 g, 73%) as a colourless oil; δ_H (500 MHz, DMSO-d_6): 7.99 (1H, s, N-H), 7.46 (2H, t, *J* = 7.8 Hz, Ar-H), 7.25 (2H, t, *J* = 7.8 Hz, Ar-H), 6.94 (1H, t, *J* = 7.3 Hz, Ar-H), 3.65 (1H, m, C$H(CH_3)_2$), 1.31 (9H, s, CCH_3), 1.03 (6H, d, *J* = 6.6 Hz, CH(CH_3)$_2$); δ_C (125 MHz, DMSO-d_6): 152.3, 134.2, 124.3, 119.5, 113.7, 51.2, 41.2, 23.5, 18.4; ESI-HRMS found mass 235.1802 $[M + H]^+$ $C_{14}H_{23}ON_2$ requires 235.1810.

Methyl-phenylcarbamate **123**

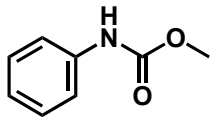

122 (30 mg, 0.13 mmol), was stirred in methanol at 20 °C for 1 hr. The solvent was removed *in vacuo* to yield the *title compound* (quant.) as a colourless oil; δ_H (500 MHz, DMSO-d_6): 9.59 (1H, s, N-H), 7.47 (2H, t, J = 7.9 Hz, Ar-H), 7.24 (2H, t, J = 7.9 Hz, Ar-H), 6.96 (1H, t, J = 7.9 Hz, Ar-H), 3.65 (3H, s, O-CH_3); δ_C (125 MHz, DMSO-d_6): 154.3, 138.2, 128.7, 122.3, 118.2, 51.5; ESI-HRMS found mass 151.0634 $[M + H]^+$ $C_8H_9NO_2$ requires 151.1626.

Dipropyl-4,4'-methylenebis(4,1-phenylene)dicarbamate[221] **139**

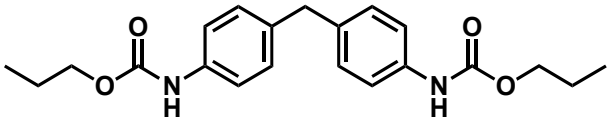

1-Propanol (0.15 mL, 2 mmol) and triethylamine distilled from calcium hydride (10 mol%) were stirred in anhydrous toluene (10 mL) for 10 minutes at 40 °C. 4,4'-Methylenediphenyldiisocyanate (0.25 g, 1 mmol) dissolved in anhydrous toluene (10 mL) was added drop wise. After 6 hr., the solvent was removed *in vacuo* to yield the *title compound* (quant.) as colourless flakes; m.p: 203- 206 °C; δ_H (500 MHz, DMSO-d_6); 9.47 (2H, s, N-H), 7.32 (4H, d, J = 8.3 Hz Ar-H), 7.08 (4H, d, J = 8.3 Hz, Ar-H), 4.00 (4H, t, J = 7.4 Hz, COO-CH_2), 3.85 (2H, s, Ar-CH_2), 1.62 (4H, sext., J = 7.4 Hz, COO-CH_2CH_2), 0.91 (6H, t, J = 7.4 Hz CCH_3); δ_C (125 MHz, DMSO-d_6): 153.6, 137.1, 135.4, 128.7, 128.4, 118.3, 65.5, 21.9, 10.2; $\bar{\upsilon}_{max}/cm^{-1}$ (solid state) = 3391, 2958, 1640, 1422, 1255; ESI-HRMS found mass 393.1794 $[M + Na]^+$ $C_{21}H_{26}O_4N_2Na$ requires 393.1790.

6.7 NMR Titration/Dilution Experiments

Anhydrous $CDCl_3$ was purchased from Sigma Aldrich equipped with Sure/Seal™. The $CDCl_3$ was stirred over K_2CO_3 prior to distillation from $CaCl_2$ to remove trace

amounts of HCl. For titrations, the ^{1}H NMR spectrum of host (2 – 10 mM) in $CDCl_3$ was recorded upon sequential addition of aliquots of guest (20 – 120 mM) in $CDCl_3$. The change in the chemical shift of key proton resonances was recorded for each addition point. The data was analysed with HypNMR using the appropriate model for stoichiometry. Dimerisation constants were calculated by taking ^{1}H NMR spectra of a solution of the desired molecule as it was diluted from 20 – 1 mM. The change in chemical shift of key resonances was recorded and analysed in HypNMR.

6.8 NOESY Data Acquisition

^{1}H-^{1}H NOESY data were recorded on a Bruker Avance 500 instrument operating at 293 K and a frequency of 500 MHz. Concentration of samples was 10 mM.

6.9 Mass-Directed HPLC Conditions

5:95 – 95:5 methanol:water, formic acid positive. Retention time: 3.58 min, with **compound 97, UTIZ**. With established procedure, injection volumes were 100 μL and fractions were collected automatically.

6.10 DSC Experiments

Measurements were performed on a DSC Q100 from TA Instruments equipped with an auto sampler and a liquid nitrogen cooling system. 10 mg of sample were placed in a standard aluminium pan that was not hermetically sealed. Experiments were performed under a nitrogen atmosphere, using a scanning rate of 10 °C min^{-1} in a cyclic manner between -90 °C and 210 °C. Data was analyzed using Universal Analysis 2000 software.

6.11 Solvent Casting and Compression Moulding of Polymer Samples

Samples were redissolved in DMAc at a concentration of 15 ml g^{-1} and stirred for 12 hr. to ensure full dissolution. The solutions were then spread in a PTFE mould and left at room temperature to enable slow evaporation. Vacuum was applied for the last 12 hr. to ensure full drying. The resultant solid was removed from the mould and broken into a fine powder. Solvent casted samples were placed between PET sheets in a 2 mm thick metal mould, which in turn was placed between two flat steel plates. The samples were then placed inside a pre-heated press at the required temperature. The samples were compression moulded for 3 min. The steel plates were cooled to room temperature by flow of cold water before removal from the press. The samples were then carefully cut out of the mould using a craft knife, and sealed in plastic under nitrogen.

6.12 DMTA Experiments

Measurements were performed using a TA Q800 DMTA instrument equipped with a liquid nitrogen-cooling accessory. Single cantilever mode was used for the characterization of the samples within a temperature range of -100 °C to 210 °C. The test frequency and amplitude used were 1 Hz and 10 μm, respectively.

6.13 WAXS Data Acquisition

Measurements were performed on a Philips X'Pert APD (PW 3710) instrument equipped with a copper anode source (generator settings: 40 mA, 50 kV). Scattering patterns were collected in the angular range: 2 ° - 70 ° (2θ). The scan type, step time, and step size used were continuous, 10 s, and 0.07 ° (2θ), respectively.

6.14 SAXS Data Acquisition

Measurements were performed using a Hecus S3-MICRO X-ray instrument equipped with a 2D Pilatus detector under vacuum. The scan time was 500 s per sample.

6.15 General procedure for solid phase carbamate synthesis

The alcohol (1.85 mmol), the required amount of catalyst (10 mol%) and the isocyanate or diisocyanate (1.85 mmol or 0.93 mmol) were added in one portion to the reaction cups (stainless steel, 10 mL) and the reaction mixture was ball-milled for 3 minute intervals at 20 Hz. The recovered solid was subjected to crude ^{1}H NMR and LC-MS analysis only. Retsch supplied the Retsch Mixer Mill 200.

6.16 General procedure for solid phase polyurethane synthesis

The polyol (2 mmol), the required amount of catalyst (10 mol%) and the diisocyanate (1.00 mmol or 0.50 mmol) were added in one portion to the reaction cups (stainless steel, 10 mL) and the reaction mixture was ball-milled for 5 minute intervals at 25 Hz for a total of 30 min. The recovered solid was subjected to crude ^{1}H NMR and IR analysis only.

6.17 General procedure for solid phase synthesis of the macromonomer 61

The recovered solid from 6.16 was subjected to further ball-milling with for 2-amino-5,6-dimethylbenzimidazole (4 mmol or 12 mmol) for 5 minute intervals at 25 Hz for a total of 10 min. The recovered solid was subjected to crude ^{1}H NMR and IR analysis only.

6.18 General procedure for the solid phase synthesis of supramolecular polyurethanes 103a and 103b

The recovered solid from 6.17 was subjected to further ball-milling with the chosen heterocomplementary unit (2 mmol or 3 mmol) for 5 minute intervals at 25 Hz for a total of 30 min. The recovered solid was subjected to crude ^{1}H NMR and IR analysis only.

Chapter 7

Appendix

7 Appendix

7.1 Appendix for Chapter 2.4- an alternative self-sorting cascade

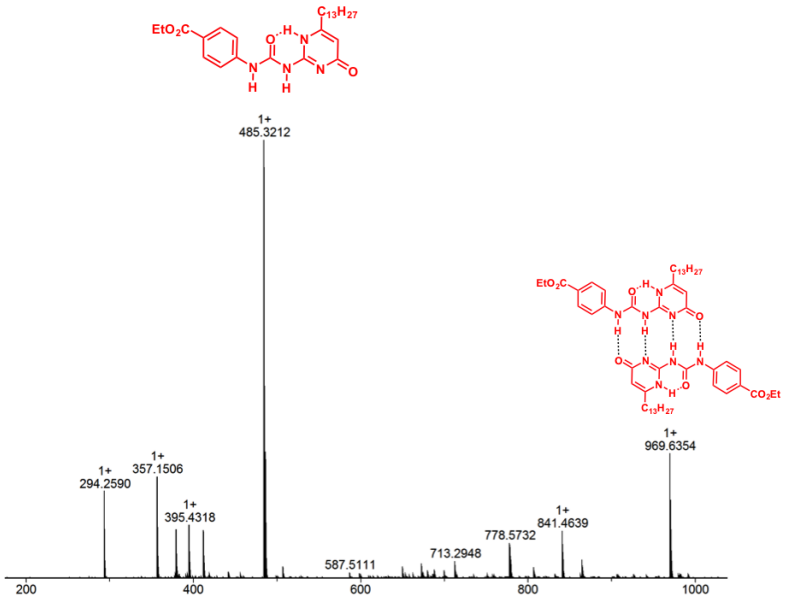

Figure 7.1 HRMS of UPy

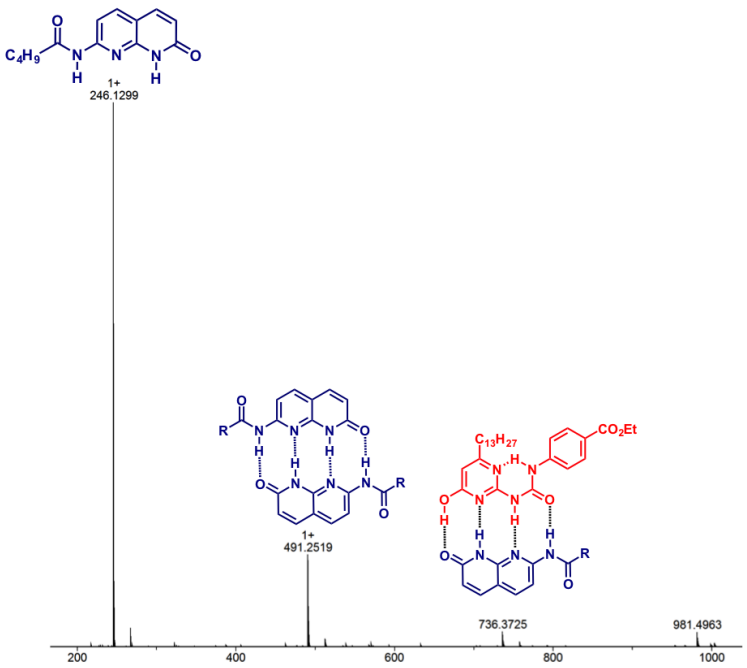

Figure 7.2 HRMS of UPy and NapyO

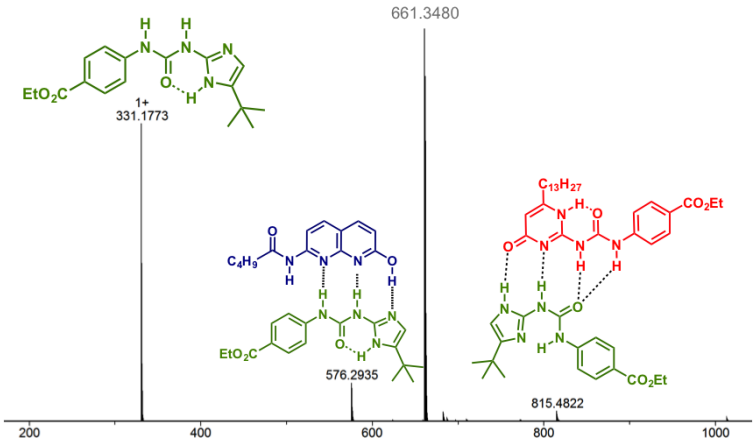

Figure 7.3 HRMS of UPy, NapyO and UIM

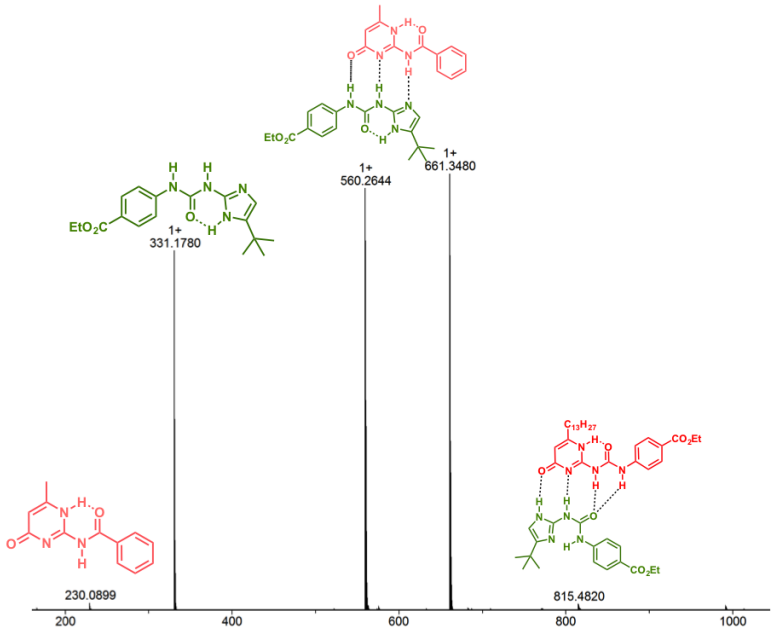

Figure 7.4 HRMS of UPy, NapyO, UIM and AIC

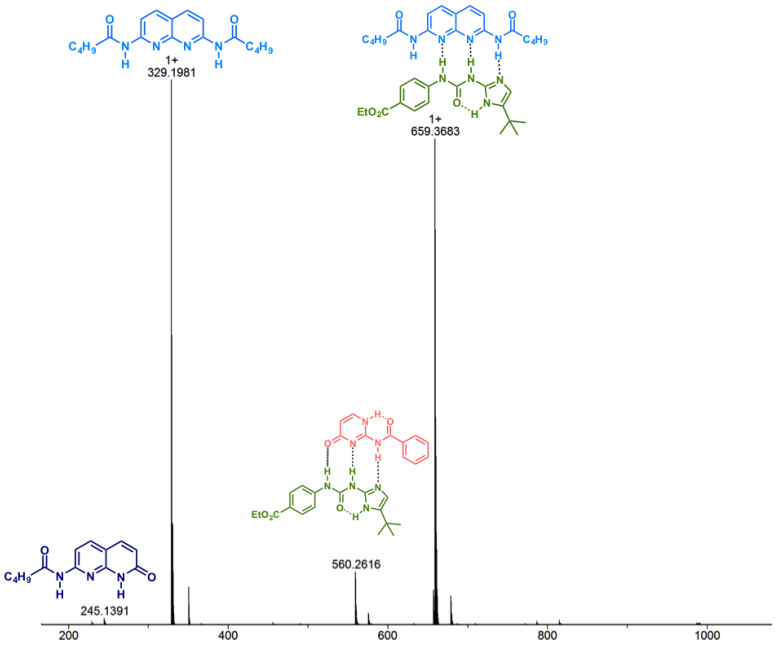

Figure 7.5 HRMS of UPy, NapyO, UIM, AIC and DAN

7.2 Appendix for Chapter 2.5- Design of additional hydrogen bonding units for orthogonal self-assembly

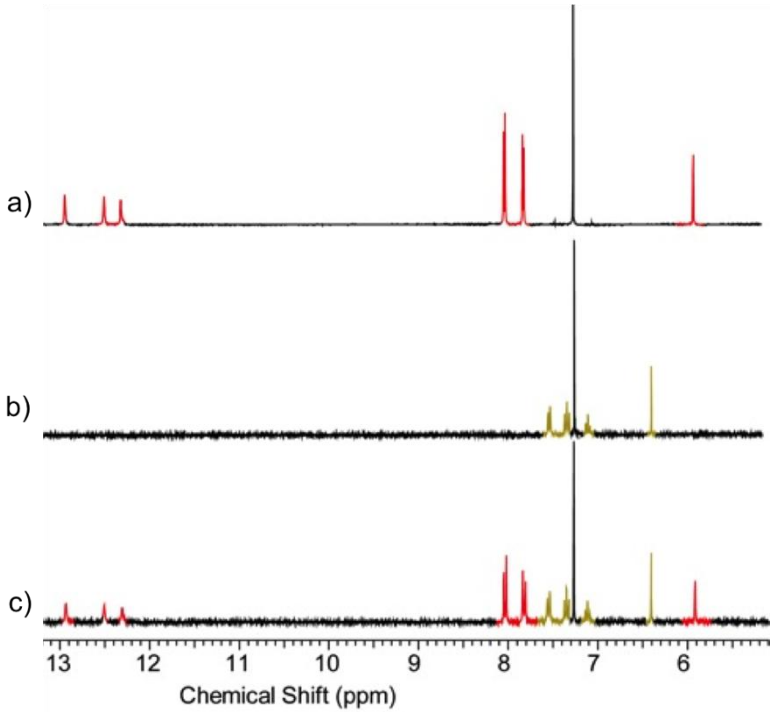

Figure 7.6 ^{1}H NMR spectra, 300 MHz, 10 mM, $CDCl_3$, 293 K. a) UPy, b) UTIZ c) UPy:UTIZ equimolar mixture

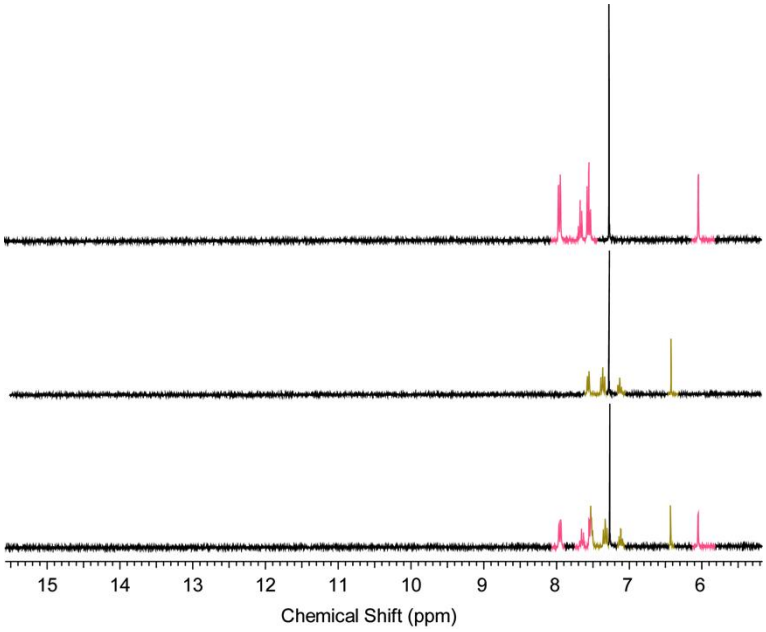

Figure 7.7 ^{1}H NMR spectra, 300 MHz, 10 mM, $CDCl_3$, 293 K. a) AIC, b) UTIZ c) AIC:UTIZ equimolar mixture

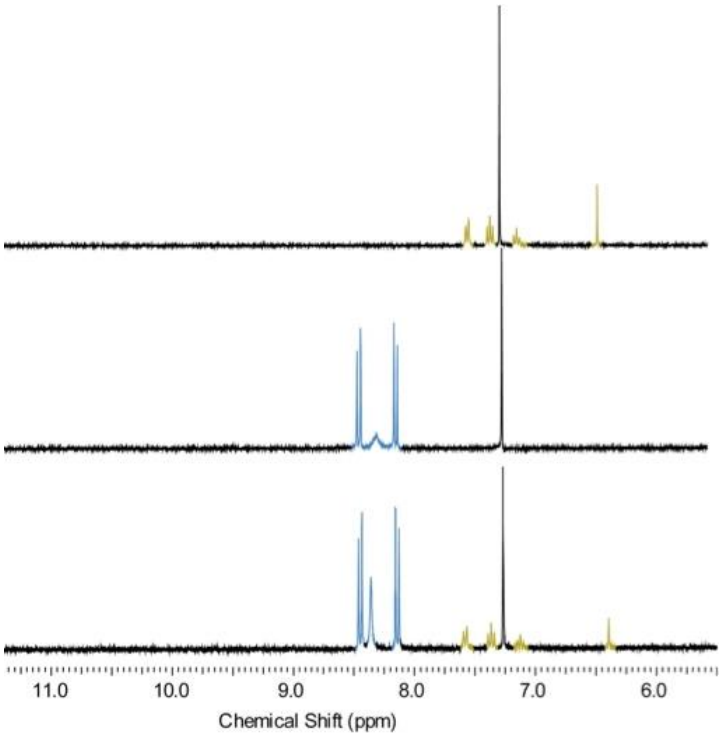

Figure 7.8 ^{1}H NMR spectra, 300 MHz, 10 mM, $CDCl_3$, 293 K. a) DAN, b) UTIZ c) DAN:UTIZ equimolar mixture

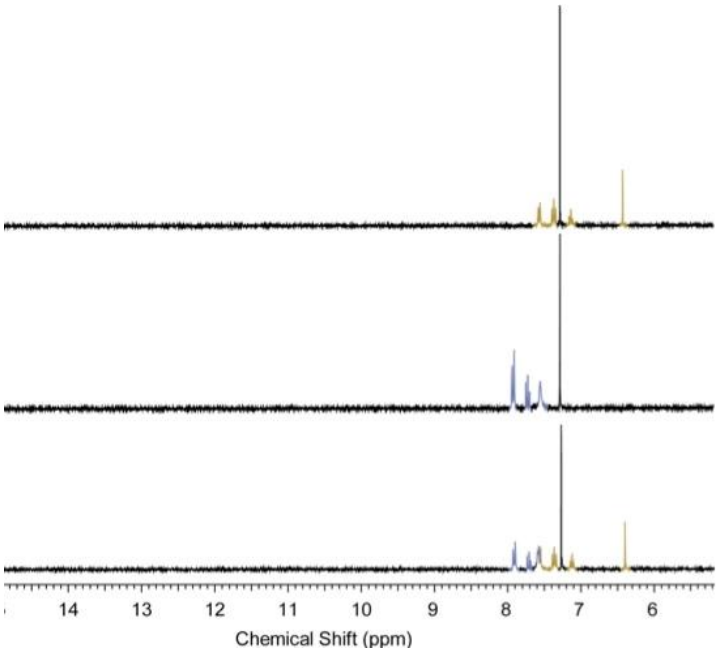

Figure 7.9 ^{1}H NMR spectra, 300 MHz, 10 mM, $CDCl_3$, 293 K. a) DAP, b) UTIZ c) DAP:UTIZ equimolar mixture

7.3 Appendix for Chapter 3.4- Synthesis of heterocomplementary supramolecular polymers. Supramolecular Chain-Extension Statistical Calculations

Statistical calculations were provided by Huntsman Polyurethanes and performed to predict the statistical proportions of covalently chain extended species during synthesis of polymers **62a-d**. The statistical model used was based upon previous studies on covalent chain extension of similar systems. As the proportion of diisocyanate is increased, the statistical model predicts that a lower percentage of covalently chain extended prepolymer species will be generated.

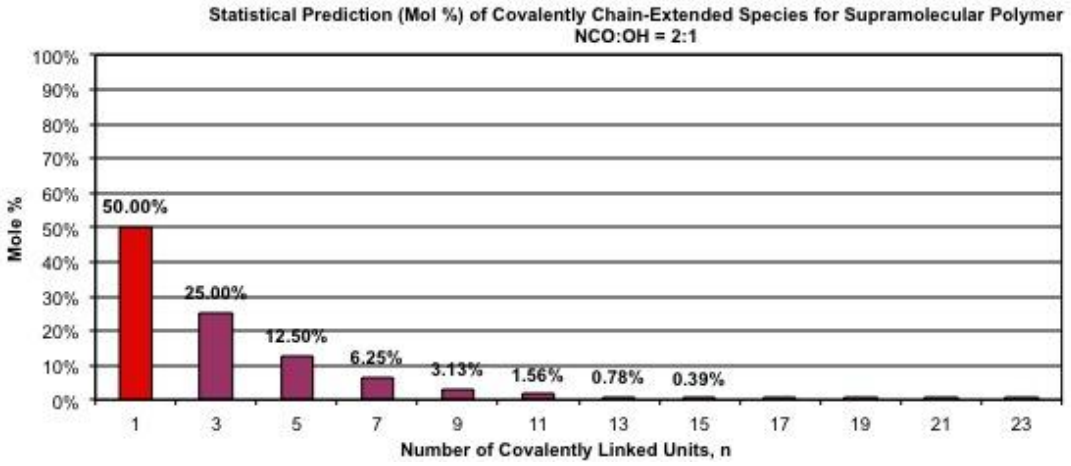

Figure 7.10 Statistical calculation of the mole percent of chain capped species present after the reaction of MDI and polyol at a molar ratio of 2:1

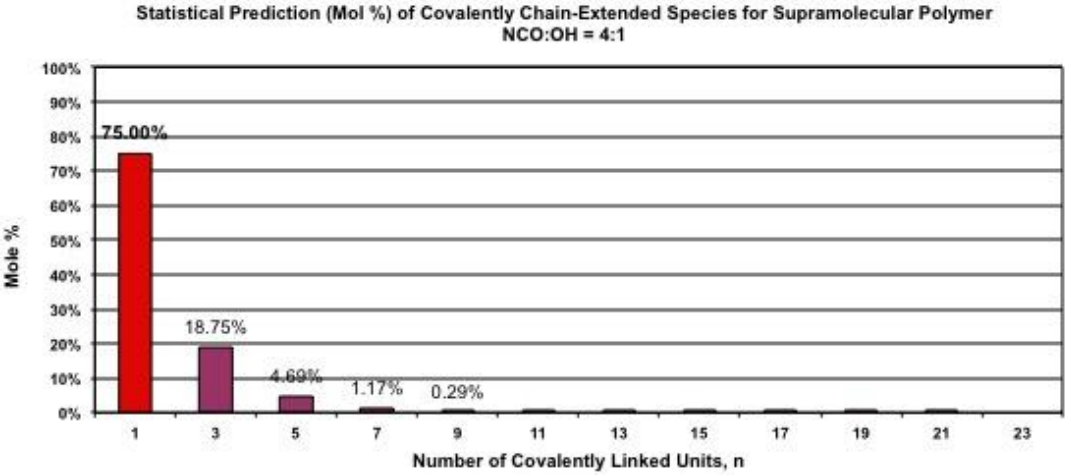

Figure 7.11 Statistical calculation of the mole percent of chain capped species present after the reaction of MDI and polyol at a molar ratio of 4:1

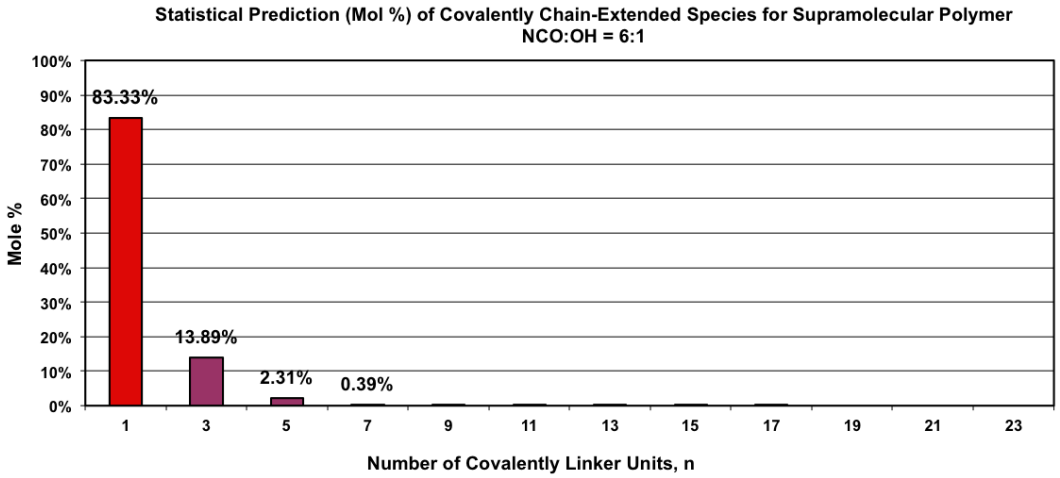

Figure 7.12 Statistical calculation of the mole percent of chain capped species present after the reaction of MDI and polyol at a molar ratio of 6:1

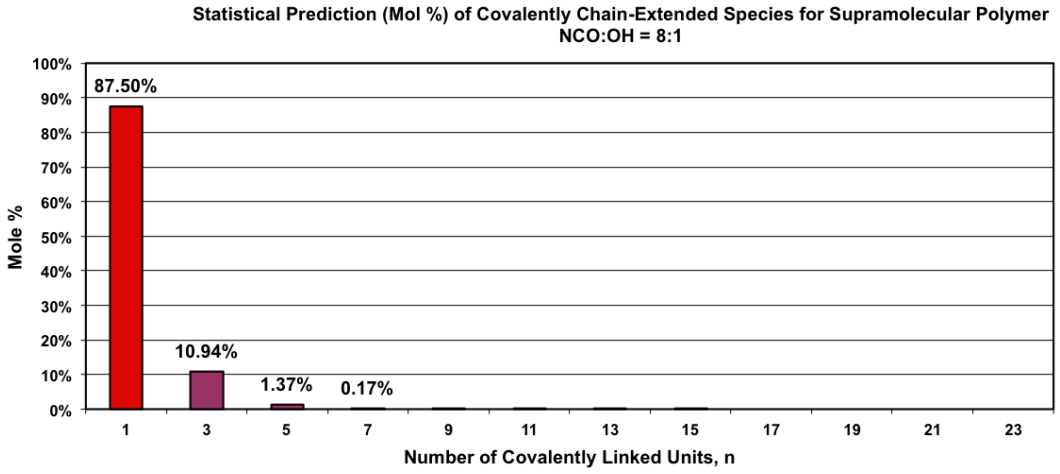

Figure 7.13 Statistical calculation of the mole percent of chain capped species present after the reaction of MDI and polyol at a molar ratio of 8:1

7.4 Appendix for Chapter 3.6- Mechanical analysis of heterocomplementary supramolecular polymers

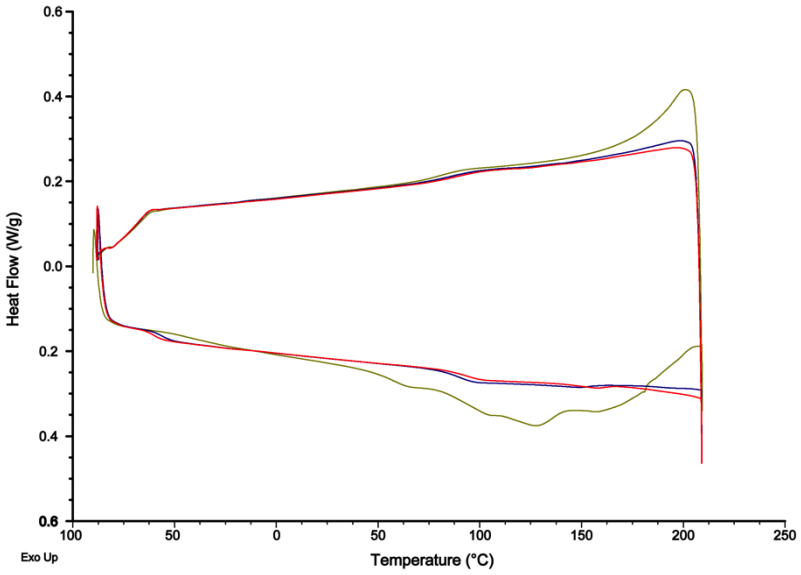

Figure 7.14 First (gold), second (blue) and third (red) heating traces of SPU 103a, NCO:OH = 2:1 heated between -90 and 220 ºC at a rate of 10 ºC min^{-1}

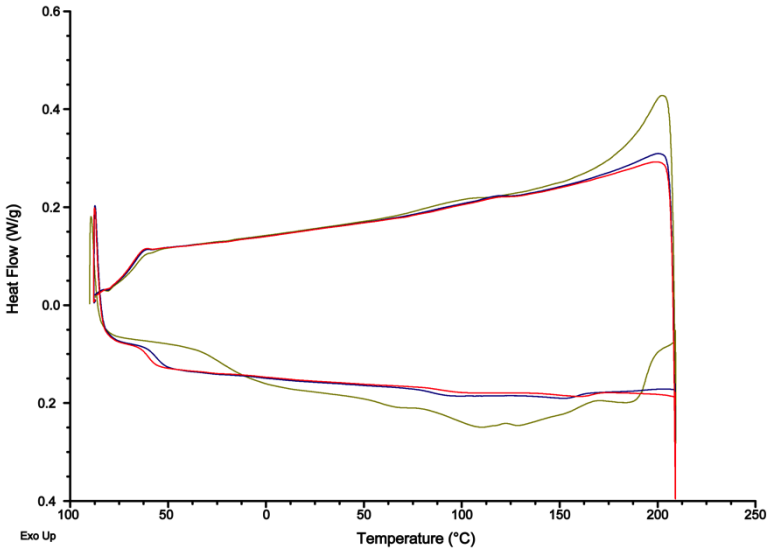

Figure 7.15 First (gold), second (blue) and third (red) heating traces of SPU 103b, NCO:OH = 4:1 heated between -90 and 220 ºC at a rate of 10 ºC min^{-1}

7.5 Appendix for Chapter 3.7.1- Annealing effect on SPU thermal transitions with different thermal histories

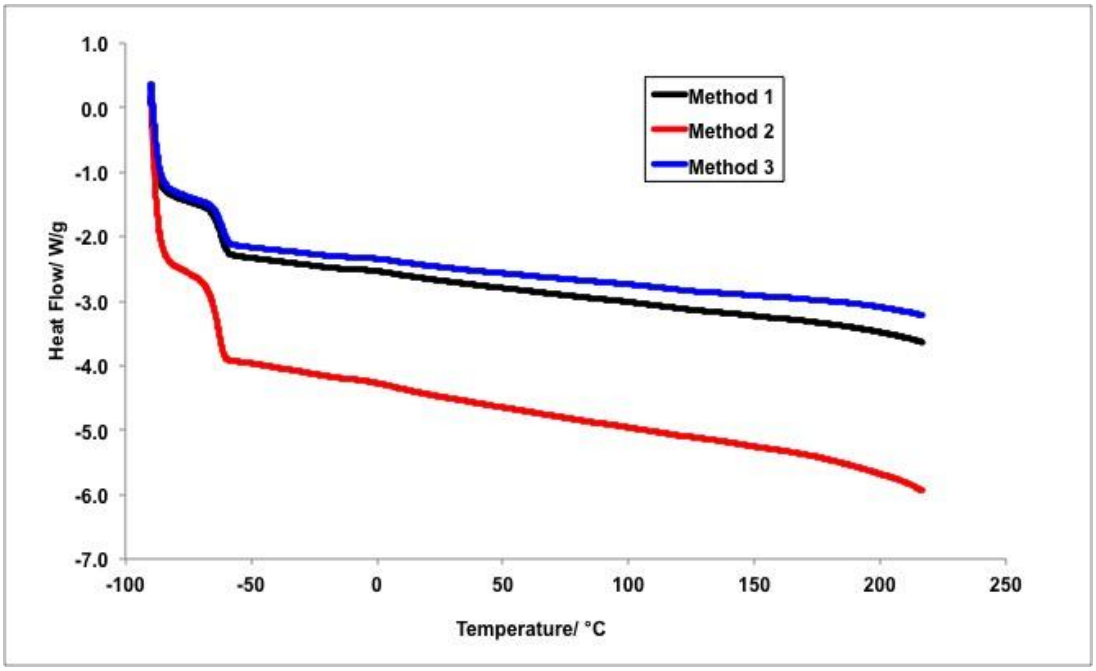

Figure 7.16 Second DSC heating run of NCO:OH SPU = 2:1

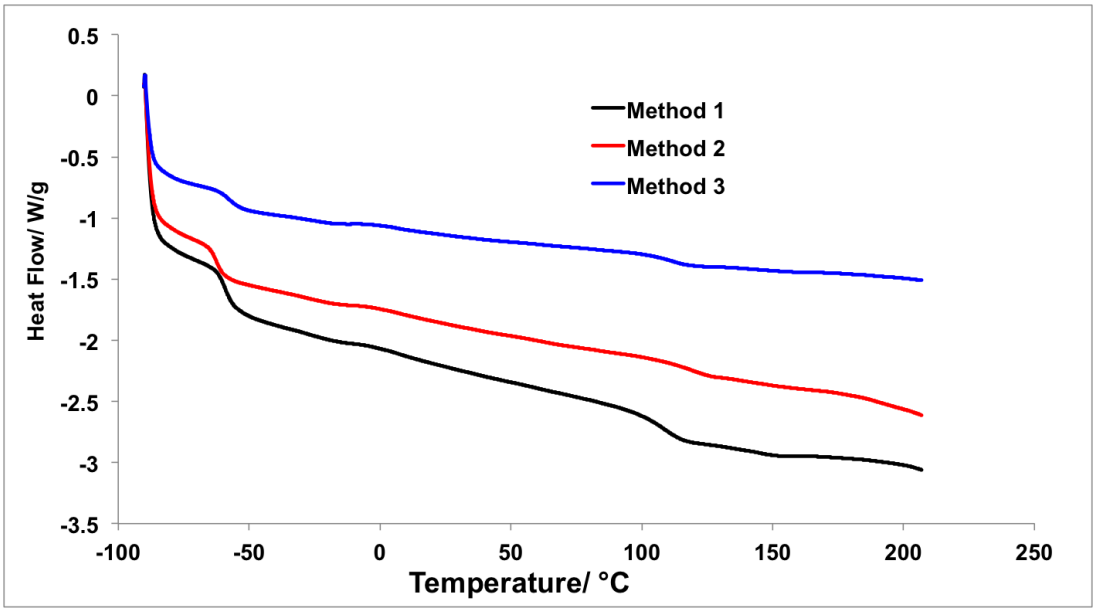

Figure 7.17 Second DSC heating run of NCO:OH SPU = 4:1

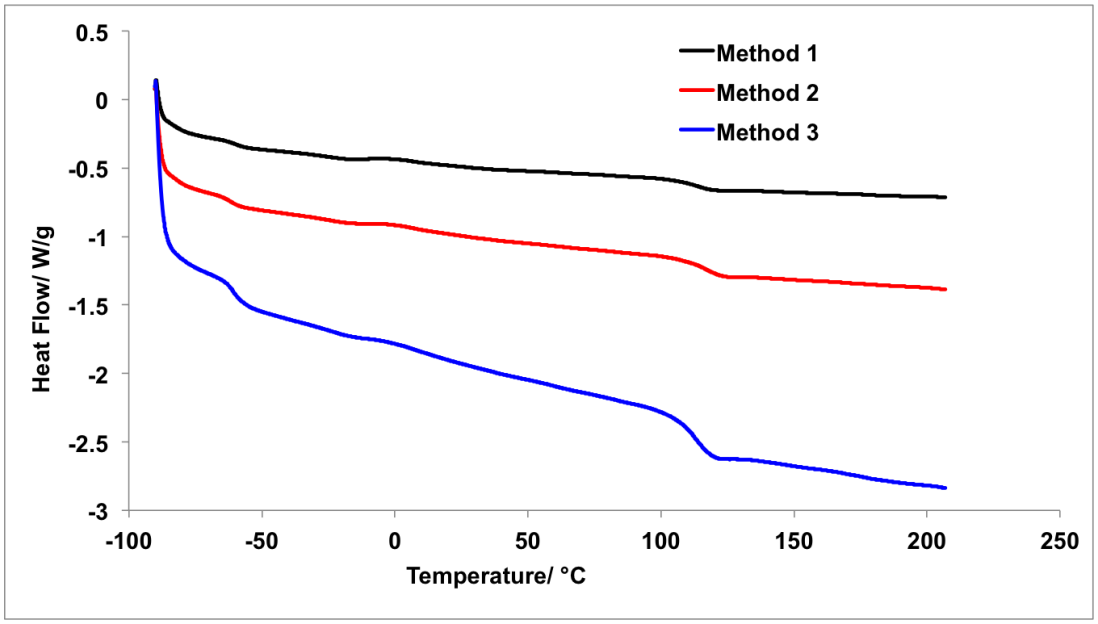

Figure 7.18 Second DSC heating run of NCO:OH SPU = 6:1

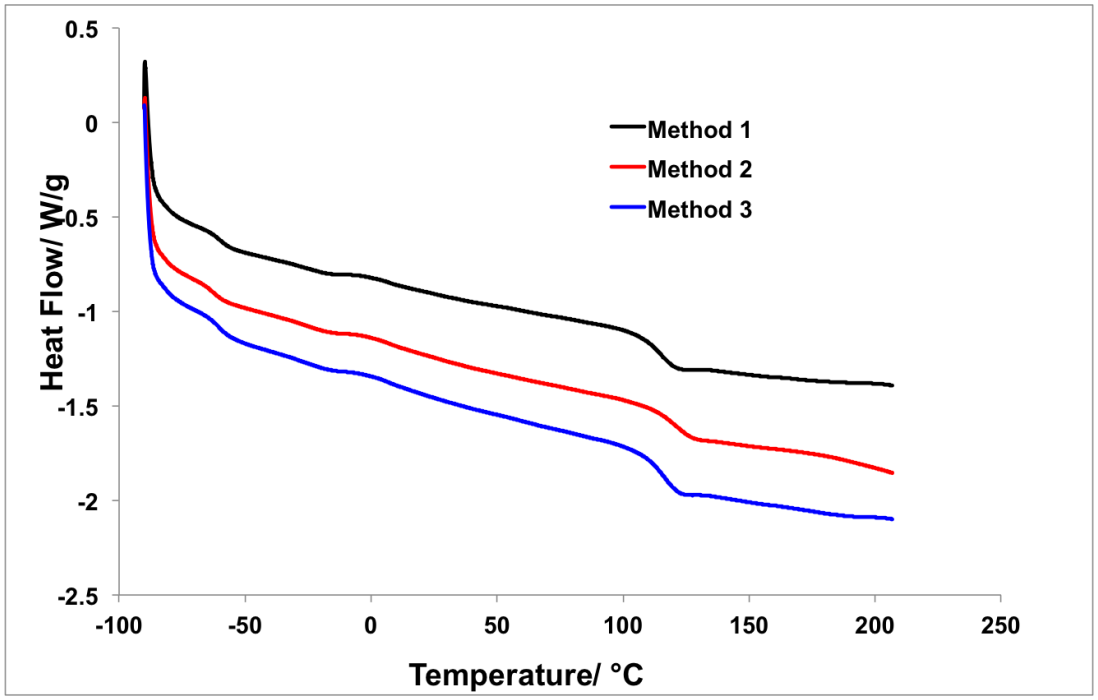

Figure 7.19 Second DSC heating run of NCO:OH SPU = 8:1

7.6 Appendix for Chapter 4.4.1- Catalysis of carbamate formation

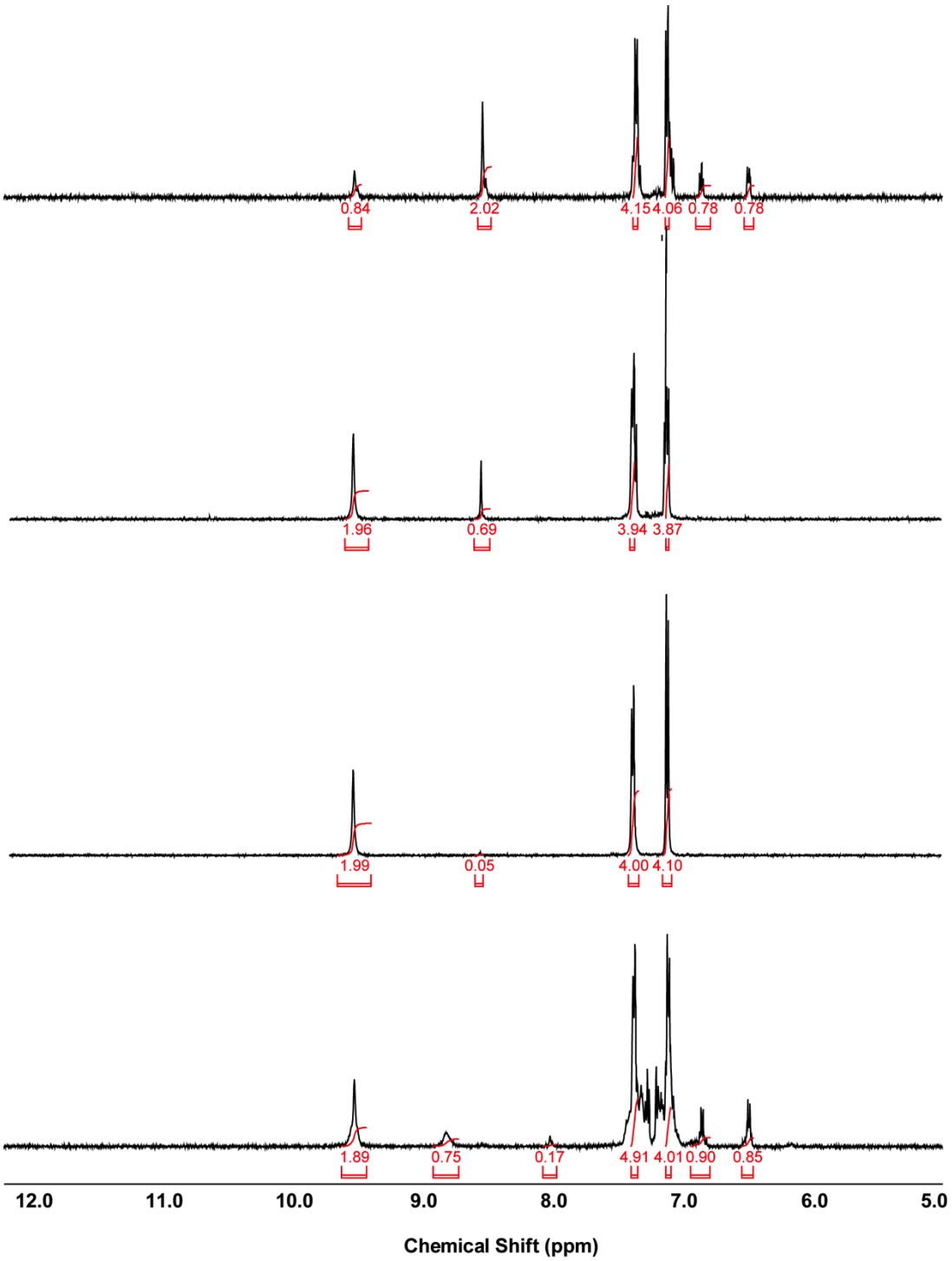

Figure 7.20 Partial crude NMR (DMSO-d6, 500 MHz); 10 mol% catalyst 40 °C, toluene, 6 h. [0.05 M], 1 equiv. MDI, 2 equiv. 1-propanol. No catalyst, Et3N, DABCO and TBD

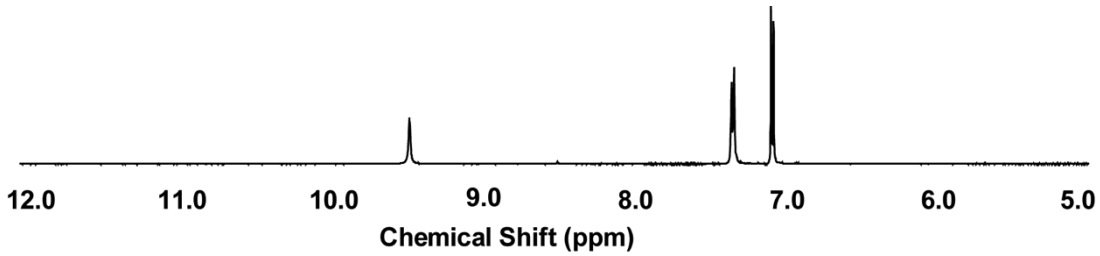

Figure 7.21 Partial NMR (DMSO-d6, 500 MHz) of pure biscarbamate 138; 10 mol% Et3N, 40 °C, toluene, 6 h. [0.05 M], 1 equiv. MDI, 2 equiv. 1-propanol

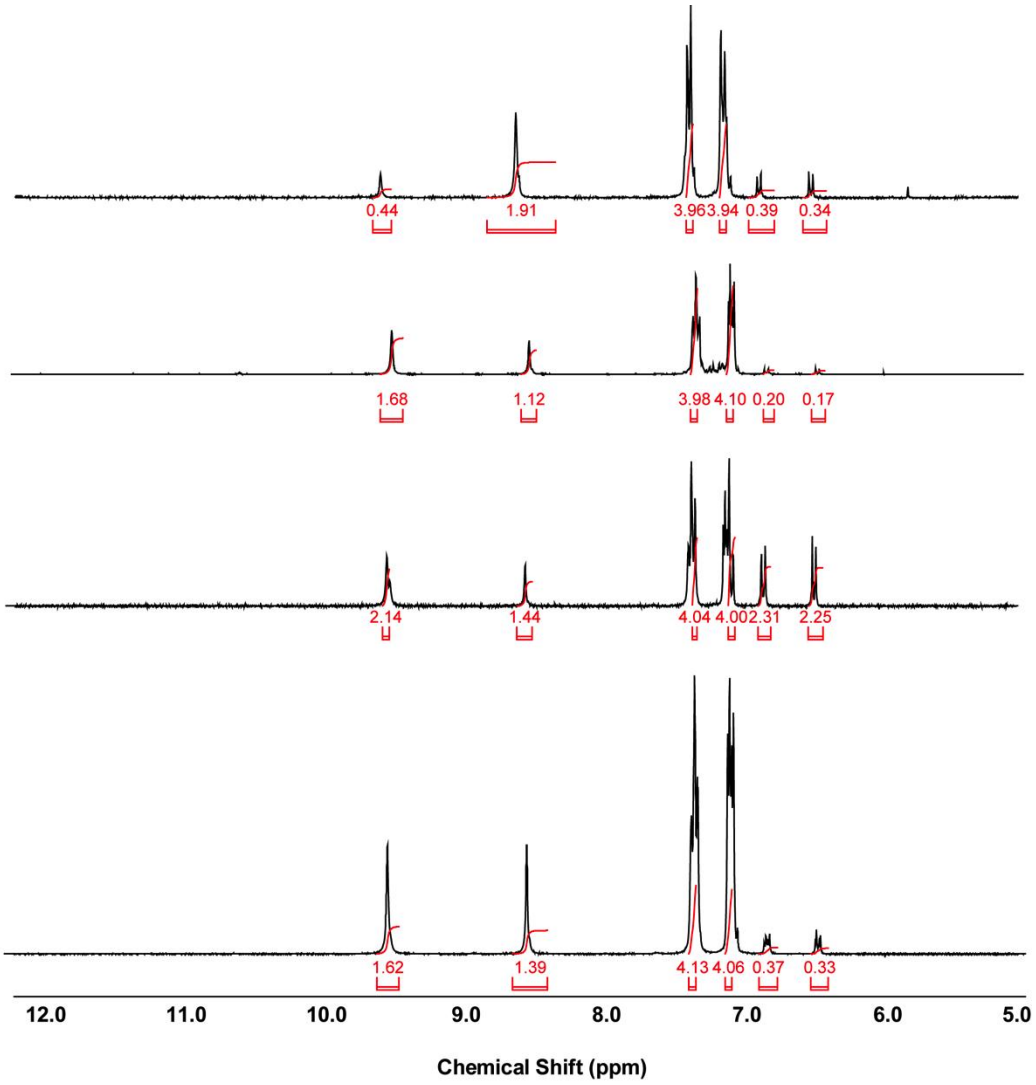

Figure 7.22 Partial crude NMR (DMSO-d6, 500 MHz); 10 mol% Et3N, 40 °C, 6 h. [0.05 M], 1 equiv. MDI, 2 equiv. 1-propanol. 1,4-dioxane, hexane, diethyl ether and chloroform

7.7 Appendix for 4.5.1- mechanochemical synthesis of small molecules

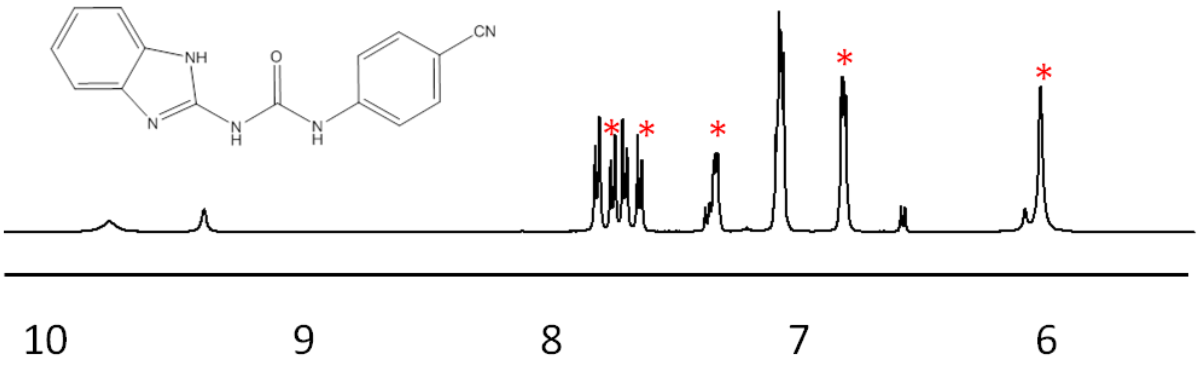

145a- reaction of p-cyano phenylisocyanate with 2-aminobenzimidazole in the ball mill for 10 minutes. Partial crude NMR (DMSO-d6, 500 MHz). Crude conversion was taken from integration of product protons (starred) against starting material.

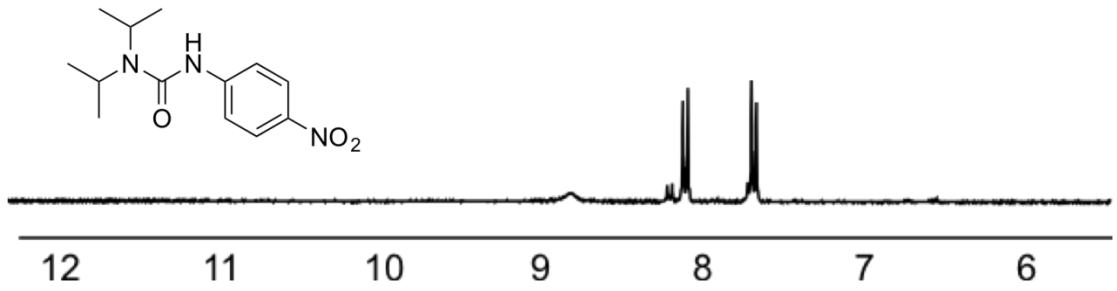

145b- reaction of p-nitro phenylisocyanate with diisopropylamine in the ball mill for 10 minutes. Partial crude NMR (DMSO-d6, 500 MHz).

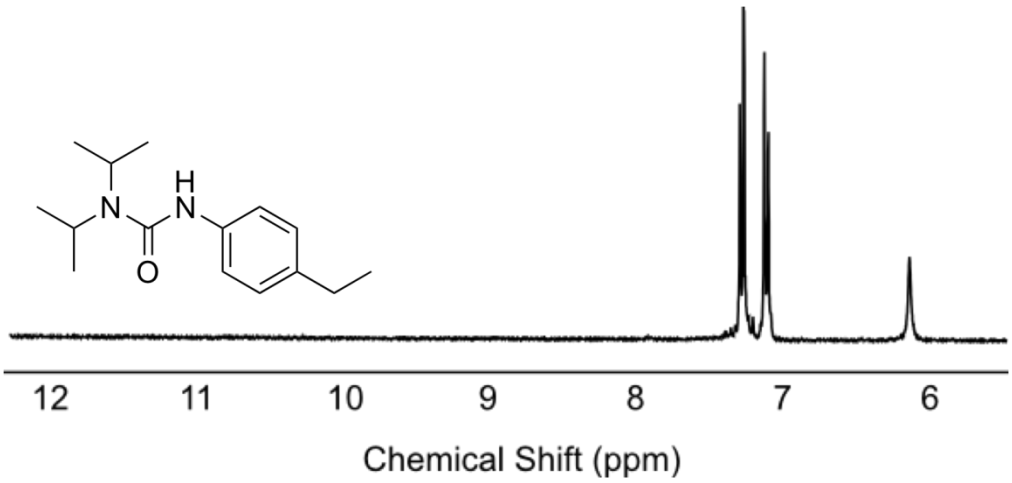

145c- Reaction of p-ethyl phenylisocyanate with diisopropylamine in the ball mill for 10 minutes. Partial crude NMR (DMSO-d6, 500 MHz)

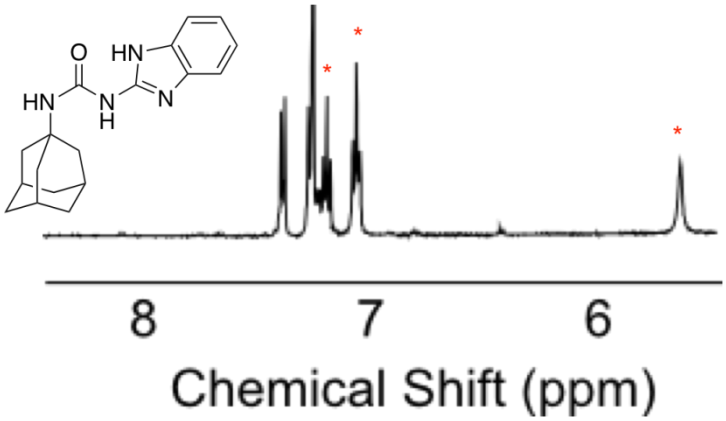

145d- Reaction of adamantyl isocyanate with 2-aminobenzimidazole in the ball mill for 10 minutes. Crude conversion was taken from integration of product protons (starred) against starting material.

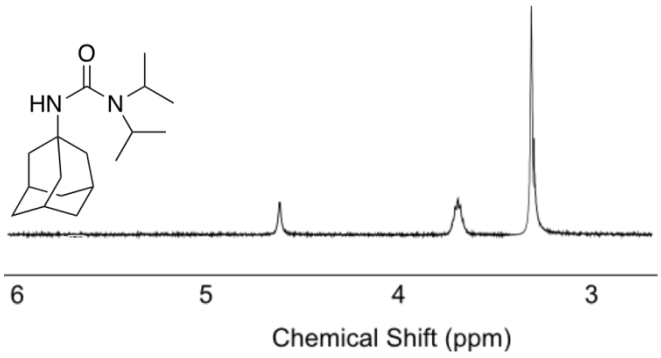

145e- Reaction of adamantyl isocyanate with diisopropylamine in the ball mill for 10 minutes. Partial crude NMR (DMSO-d6, 500 MHz);

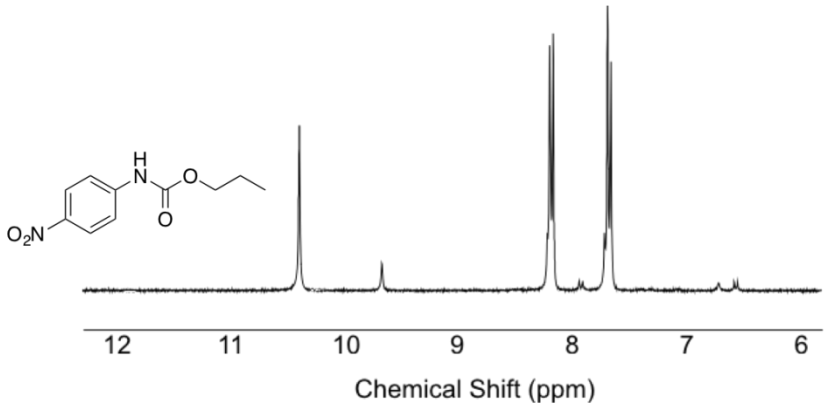

146a- Reaction of p-nitro phenylisocyanate with n-propanol in the ball mill for 10 minutes. Partial crude NMR (DMSO-d6, 500 MHz)

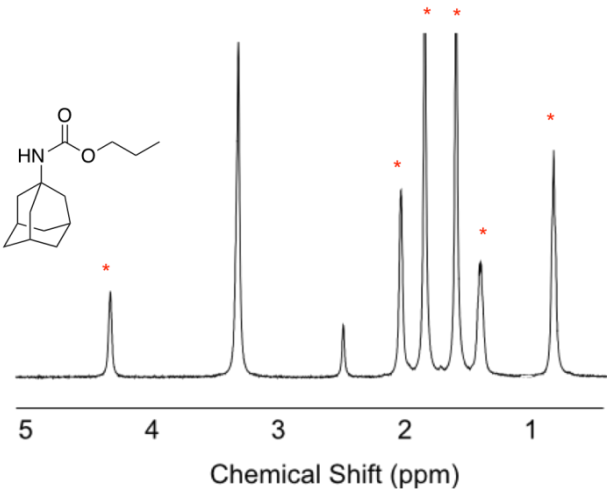

146b- Reaction of adamantyl isocyanate with n-propanol in the ball mill for 10 minutes. Partial crude NMR (DMSO-d6, 500 MHz); Crude conversion was taken from integration of product protons (starred) against starting material.

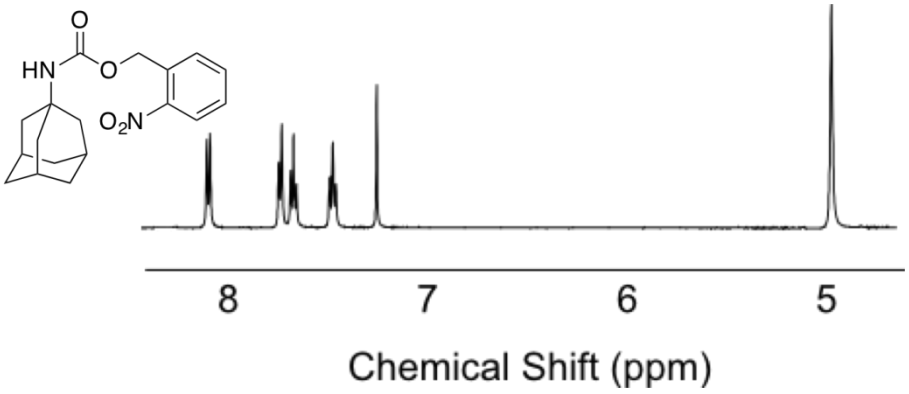

146c- Reaction of adamantyl isocyanate with O-nitro benzyl alcohol in the ball mill for 10 minutes. Partial crude NMR (CDCl3, 500 MHz).

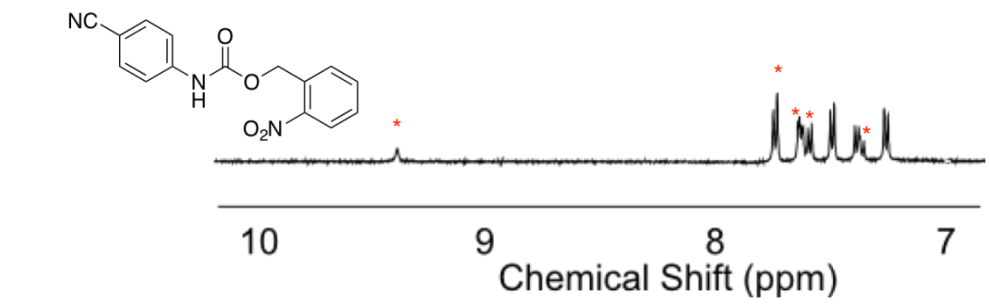

146d- Reaction of p-cyano phenylisocyanate with o-nitrobenzyl alcohol in the ball mill for 10 minutes. Partial crude NMR (DMSO-d6, 500 MHz): Crude conversion was taken from integration of product protons (starred) against starting material.

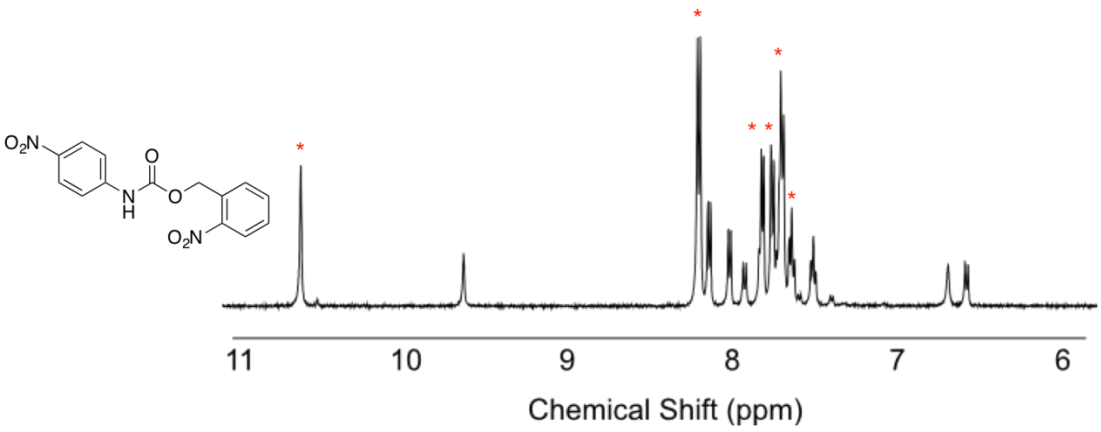

146e- Reaction of p-nitro phenylisocyanate with o-nitro benzyl alcohol in the ball mill for 10 minutes. Partial crude NMR (DMSO-d6, 500 MHz); Crude conversion was taken from integration of product protons (starred) against starting material.

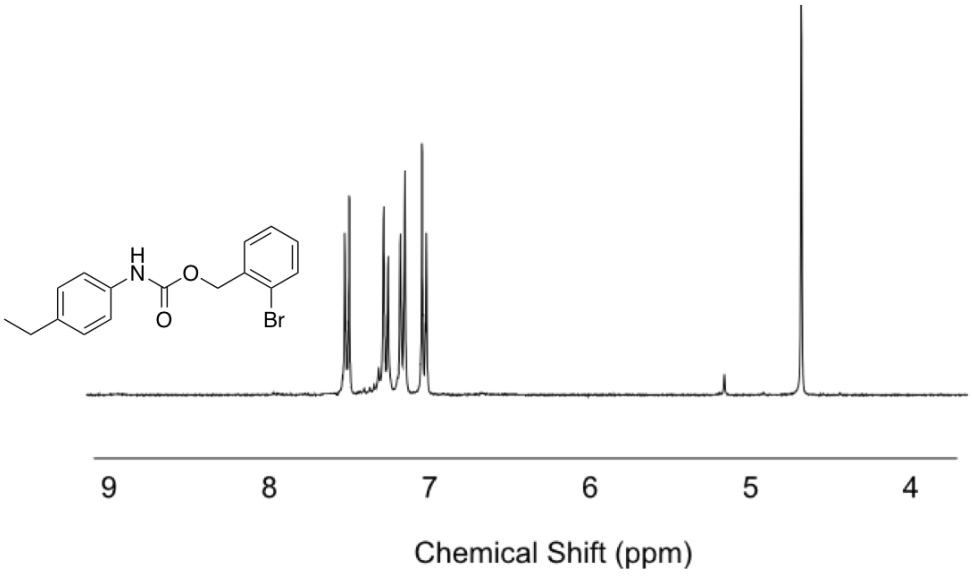

146f- Reaction of p-ethyl phenylisocyanate with o-bromo benzyl alcohol in the ball mill for 10 minutes. Partial crude NMR (CDCl3, 500 MHz)

8 References

1. C. E. C. Jr., *Carraher's Polymer Chemistry*, Taylor and Francis, Florida, 9th edn., 2013.
2. T. E. Patten and K. Matyjaszewski, *Advanced Materials*, 1998, 10, 901-915.
3. R. H. Grubbs and W. Tumas, *Science*, 1989, 243, 907-915.
4. C. J. Hawker, A. W. Bosman and E. Harth, *Chemical Reviews*, 2001, 101, 3661-3688.
5. W. H. Carothers, *Journal of the American Chemical Society*, 1929, 51, 2548-2559.
6. H.-W. Engels, H.-G. Pirkl, R. Albers, R. W. Albach, J. Krause, A. Hoffmann, H. Casselmann and J. Dormish, *Angewandte Chemie International Edition*, 2013, 52, 9422-9441.
7. O. Bayer, *Angewandte Chemie*, 1947, 59, 257-272.
8. O. Bayer, E. Müller and E. Muller, *Angewandte Chemie*, 1960, 72, 934-939.
9. M. A. Tasdelen, M. U. Kahveci and Y. Yagci, *Progress in Polymer Science*, 2011, 36, 455-567.
10. E. Delebecq, J.-P. Pascault, B. Boutevin and F. Ganachaud, *Chemical Reviews*, 2012, 113, 80-118.
11. K. Nakayama, T. Ino and I. Matsubara, *Journal of Macromolecular Science: Part A - Chemistry*, 1969, 3, 1005-1020.
12. T. A. Speckhard, K. K. S. Hwang, S. L. Cooper, V. S. C. Chang and J. P. Kennedy, *Polymer*, 1985, 26, 70-78.
13. J. W. C. Van Bogart, P. E. Gibson and S. L. Cooper, *Journal of Polymer Science: Polymer Physics Edition*, 1983, 21, 65-95.
14. S. Corneillie, P. N. Lan, E. Schacht, M. Davies, A. Shard, R. Green, S. Denyer, M. Wassall, H. Whitfield and S. Choong, *Polymer International*, 1998, 46, 251-259.
15. R. Bonart and E. H. Müller, *Journal of Polymer Science Part B: Polymer Physics*, 1974, 10, 177-189.
16. S. Burattini, B. W. Greenland, D. H. Merino, W. Weng, J. Seppala, H. M. Colquhoun, W. Hayes, M. E. Mackay, I. W. Hamley and S. J. Rowan, *Journal of the American Chemical Society*, 2010, 132, 12051-12058.
17. T. F. A. De Greef, M. M. J. Smulders, M. Wolffs, A. P. H. J. Schenning, R. P. Sijbesma and E. W. Meijer, *Chemical Reviews*, 2009, 109, 5687-5754.
18. T. Aida, E. W. Meijer and S. I. Stupp, *Science*, 2012, 335, 813-817.
19. L. Brunsveld, B. J. B. Folmer, E. W. Meijer and R. P. Sijbesma, *Chemical Reviews*, 2001, 101, 4071-4098.
20. J.-M. Lehn, *Polymer International*, 2002, 51, 825-839.
21. A. W. Bosman, R. P. Sijbesma and E. W. Meijer, *Materials Today*, 2004, 7, 34-39.
22. J. D. Fox and S. J. Rowan, *Macromolecules*, 2009, 42, 6823-6835.
23. R. J. Wojtecki, M. A. Meador and S. J. Rowan, *Nature Materials*, 2011, 10, 14-27.

24. P. Woodward, D. H. Merino, I. W. Hamley, A. T. Slark and W. Hayes, *Australian Journal of Chemistry*, 2009, 62, 790-793.
25. M. Burnworth, L. Tang, J. R. Kumpfer, A. J. Duncan, F. L. Beyer, G. L. Fiore, S. J. Rowan and C. Weder, *Nature*, 2011, 472, 334-337.
26. U. S. Schubert and C. Eschbaumer, *Angewandte Chemie International Edition*, 2002, 41, 2892-2926.
27. A. J. Wilson, *Soft Matter*, 2007, 3, 409-409.
28. J. D. Watson and F. H. C. Crick, *Nature*, 1953, 171, 737-738.
29. S. C. Zimmerman and P. S. Corbin, *Structure and Bonding (Berlin)*, 2000, 96, 63-94.
30. S. Sivakova and S. J. Rowan, *Chemical Society Reviews*, 2005, 34, 9-21.
31. M. Fathalla, C. M. Lawrence, N. Zhang, J. L. Sessler and J. Jayawickramarajah, *Chemical Society Reviews*, 2009, 38, 1608-1620.
32. P. K. Baruah and S. Khan, *RSC Advances*, 2013, 3, 21202-21202.
33. C. Fouquey, J.-M. Lehn and A.-M. Levelut, *Advanced Materials*, 1990, 2, 254-257.
34. T. Gulikkrzywicki, C. Fouquey and J. M. Lehn, *Proceedings of the National Academy of Sciences of the United States of America*, 1993, 90, 163-167.
35. Y. Yang and M. W. Urban, *Chemical Society Reviews*, 2013, 42, 7446-7467.
36. B. K. Kim, S. Y. Lee and M. Xu, *Polymer*, 1996, 37, 5781-5793.
37. S. Chen, J. Hu, C.-w. Yuen and L. Chan, *Polymer*, 2009, 50, 4424-4428.
38. M. L. Pellizzaro, A. M. McGhee, L. C. Renton, M. G. Nix, J. Fisher, W. B. Turnbull and A. J. Wilson, *Chemistry – A European Journal*, 2011, 17, 14508-14517.
39. W. L. Jorgensen and J. Pranata, *Journal of the American Chemical Society*, 1990, 112, 2008-2010.
40. B. A. Blight, A. Camara-Campos, S. Djurdjevic, M. Kaller, D. A. Leigh, F. M. McMillan, H. McNab and A. M. Z. Slawin, *Journal of the American Chemical Society*, 2009, 131, 14116-14122.
41. M. C. Etter, *Accounts of Chemical Research*, 1990, 23, 120-126.
42. A. M. McGhee, C. Kilner and A. J. Wilson, *Chemical Communications*, 2008, 344-346.
43. C. A. Hunter, *Angewandte Chemie International Edition*, 2004, 43, 5310-5324.
44. P. J. Flory, *Journal of the American Chemical Society*, 1936, 58, 1877-1885.
45. F. H. Beijer, R. P. Sijbesma, H. Kooijman, A. L. Spek and E. W. Meijer, *Journal of the American Chemical Society*, 1998, 120, 6761-6769.
46. R. P. Sijbesma, F. H. Beijer, L. Brunsveld, B. J. B. Folmer, J. H. K. K. Hirschberg, R. F. M. Lange, J. K. L. Lowe and E. W. Meijer, *Science*, 1997, 278, 1601-1604.
47. T. F. A. de Greef and E. W. Meijer, *Nature*, 2008, 453, 171-173.
48. V. G. H. Lafitte, A. E. Aliev, P. N. Horton, M. B. Hursthouse, K. Bala, P. Golding and H. C. Hailes, *Journal of the American Chemical Society*, 2006, 128, 6544-6545.
49. V. G. H. Lafitte, A. E. Aliev, E. Greco, K. Bala, P. Golding and H. C. Hailes, *New Journal of Chemistry*, 2011, 35, 1522-1527.
50. B. J. B. Folmer, R. P. Sijbesma, R. M. Versteegen, J. a. J. van der Rijt and E. W. Meijer, *Advanced Materials*, 2000, 12, 874-878.

51. J. Li, J. A. Viveros, M. H. Wrue and M. Anthamatten, *Advanced Materials*, 2007, 19, 2851-2855.
52. Y. Zhu, J. Hu and J. Liu, *The European Physical Journal E*, 2008, 3-10.
53. P. Amrhein, A. Shivanyuk, D. W. Johnson and J. Rebek, *Journal of the American Chemical Society*, 2002, 124, 10349-10358.
54. P. N. Taylor and H. L. Anderson, *Journal of the American Chemical Society*, 1999, 121, 11538-11545.
55. W. Jiang, H. D. F. Winkler and C. A. Schalley, *Journal of the American Chemical Society*, 2008, 130, 13852-13853.
56. G. G. Odian, ed., *Principles of Polymerisation*, Wiley-interscience, 2004.
57. T. Park and S. C. Zimmerman, *Journal of the American Chemical Society*, 2006, 128, 13986-13987.
58. D. W. Kuykendall, C. a. Anderson and S. C. Zimmerman, *Organic Letters*, 2009, 11, 61-64.
59. H. C. Ong and S. C. Zimmerman, *Organic Letters*, 2006, 8, 1589-1592.
60. E. M. Todd and S. C. Zimmerman, *Tetrahedron*, 2008, 64, 8558-8570.
61. G. B. W. L. Ligthart, H. Ohkawa, R. P. Sijbesma and E. W. Meijer, *Journal of the American Chemical Society*, 2004, 127, 810-811.
62. O. A. Scherman, G. B. W. L. Ligthart, H. Ohkawa, R. P. Sijbesma and E. W. Meijer, *Proceedings of the National Academy of Sciences*, 2006, 103, 11850-11855.
63. T. Park and S. C. Zimmerman, *Journal of the American Chemical Society*, 2006, 128, 11582-11590.
64. M. L. Pellizzaro, K. A. Houton and A. J. Wilson, *Chemical Science*, 2013, 4, 1825-1829.
65. W. H. Binder, S. Bernstorff, C. Kluger, L. Petraru and M. J. Kunz, *Advanced Materials*, 2005, 17, 2824-2828.
66. E. U. Okoroafor, J. P. Villemaire and J. F. Agassant, *Polymer*, 1992, 33, 5264-5271.
67. C. M. Roland and K. L. Ngai, *Macromolecules*, 1991, 24, 2261-2265.
68. K. P. Nair, V. Breedveld and M. Weck, *Macromolecules*, 2011, 44, 3346-3357.
69. O. Kreye, H. Mutlu and M. A. R. Meier, *Green Chemistry*, 2013, 15, 1431-1455.
70. Y. Ni, F. Becquart, J. Chen and M. Taha, *Macromolecules*, 2013, 46, 1066-1074.
71. M. J. O'Sickey, B. D. Lawrey and G. L. Wilkes, *Journal of Applied Polymer Science*, 2002, 84, 229-243.
72. H. Kautz, D. J. M. van Beek, R. P. Sijbesma and E. W. Meijer, *Macromolecules*, 2006, 39, 4265-4267.
73. L. Ning, W. De-Ning and Y. Sheng-Kang, *Polymer*, 1996, 37, 3577-3583.
74. B. Sharma, L. Ubaghs, H. Keul, H. HÃ¶cker, T. Loontjens and R. v. Benthem, *Polymer*, 2004, 45, 5427-5440.
75. P. Król, *Progress in Materials Science*, 2007, 52, 915-1015.
76. P. Woodward, A. Clarke, B. W. Greenland, D. Hermida Merino, L. Yates, A. T. Slark, J. F. Miravet and W. Hayes, *Soft Matter*, 2009, 5, 2000-2010.
77. P. J. Woodward, D. Hermida Merino, B. W. Greenland, I. W. Hamley, Z. Light, A. T. Slark and W. Hayes, *Macromolecules*, 2010, 43, 2512-2517.

78. D. H. Merino, A. T. Slark, H. M. Colquhoun, W. Hayes and I. W. Hamley, *Polymer Chemistry*, 2010, 1, 1263-1271.
79. A. Gooch, S. Barrett, J. Fisher, C. I. Lindsay and A. J. Wilson, *Organic & Biomolecular Chemistry*, 2011, 9, 5938-5940.
80. A. Gooch, C. Nedolisa, K. A. Houton, C. I. Lindsay, A. Saiani and A. J. Wilson, *Macromolecules*, 2012, 45, 4723-4729.
81. J. Ling, M. Z. Rong and M. Q. Zhang, *Journal of Materials Chemistry*, 2011, 21, 18373-18373.
82. X. Liu, P. Du, L. Liu, Z. Zheng, X. Wang, T. Joncheray and Y. Zhang, *Polymer Bulletin*, 2013, 70, 2319-2335.
83. P. Cordier, F. Tournilhac, C. Soulie-Ziakovic and L. Leibler, *Nature*, 2008, 451, 977-980.
84. F. Li, X. Zhang, J. Hou, M. Xu, X. Luo, D. Ma and B. K. Kim, *Journal of Applied Polymer Science*, 1997, 64, 1511-1516.
85. S. Chen, J. Hu, C.-w. Yuen and L. Chan, *Materials Letters*, 2009, 63, 1462-1464.
86. S. Chen, J. Hu, H. Zhuo, C. Yuen and L. Chan, *Polymer*, 2010, 51, 240-248.
87. P. Y. W. Dankers, M. C. Harmsen, L. A. Brouwer, M. J. A. Van Luyn and E. W. Meijer, *Nature Materials*, 2005, 4, 568-574.
88. P. Y. W. Dankers, T. M. Hermans, T. W. Baughman, Y. Kamikawa, R. E. Kieltyka, M. M. C. Bastings, H. M. Janssen, N. A. J. M. Sommerdijk, A. Larsen, M. J. A. van Luyn, A. W. Bosman, E. R. Popa, G. Fytas and E. W. Meijer, *Advanced Materials*, 2012, 24, 2703-2709.
89. M. Hutin, E. Burakowska-Meise, W. P. J. Appel, P. Y. W. Dankers and E. W. Meijer, *Macromolecules*, 2013.
90. P. Mukhopadhyay, P. Y. Zavalij and L. Isaacs, *Journal of the American Chemical Society*, 2006, 128, 14093-14102.
91. R. F. Ludlow and S. Otto, *Chemical Society Reviews*, 2008, 37, 101-108.
92. O. Chepelin, J. Ujma, P. E. Barran and P. J. Lusby, *Angewandte Chemie*, 2012, 124, 4270-4273.
93. K. A. Jolliffe, P. Timmerman and D. N. Reinhoudt, *Angewandte Chemie International Edition*, 1999, 38, 933-937.
94. R. Kramer, J. M. Lehn and A. Marquis-Rigault, *Proceedings of the National Academy of Sciences*, 1993, 90, 5394-5398.
95. C.-H. Wong and S. C. Zimmerman, *Chemical Communications*, 2013, 49, 1679-1695.
96. A. Wu and L. Isaacs, *Journal of the American Chemical Society*, 2003, 125, 4831-4835.
97. S. Y. Berezhna, J. P. Gill, R. Lamichhane and D. P. Millar, *Journal of the American Chemical Society*, 2012, 134, 11261-11268.
98. Y. Ma, S. V. Kolotuchin and S. C. Zimmerman, *Journal of the American Chemical Society*, 2002, 124, 13757-13769.
99. B. H. Northrop, Y.-R. Zheng, K.-W. Chi and P. J. Stang, *Accounts of Chemical Research*, 2009, 42, 1554-1563.
100. G. V. Oshovsky, D. N. Reinhoudt and W. Verboom, *Angewandte Chemie International Edition*, 2007, 46, 2366-2393.
101. M. M. Safont-Sempere, G. Fernández and F. Würthner, *Chemical Reviews*, 2011, 111, 5784-5814.

102. A. Shivanyuk and J. Rebek, *Journal of the American Chemical Society*, 2002, 124, 12074-12075.
103. I. A. Riddell, M. M. J. Smulders, J. K. Clegg, Y. R. Hristova, B. Breiner, J. D. Thoburn and J. R. Nitschke, *Nature Chemistry*, 2012, 4, 751-756.
104. X. Zhao, X.-Z. Wang, X.-K. Jiang, Y.-Q. Chen, Z.-T. Li and G.-J. Chen, *Journal of the American Chemical Society*, 2003, 125, 15128-15139.
105. T. F. A. de Greef, G. Ercolani, G. B. W. L. Ligthart, E. W. Meijer and R. P. Sijbesma, *Journal of the American Chemical Society*, 2008, 130, 13755-13764.
106. M. L. Pellizzaro, University of Leeds, 2012.
107. A. M. Piloto, S. P. G. Costa and M. S. T. Gonçalves, *Tetrahedron*, 2014, 70, 650-657.
108. P. Klán, T. Šolomek, C. G. Bochet, A. Blanc, R. Givens, M. Rubina, V. Popik, A. Kostikov and J. Wirz, *Chemical Reviews*, 2012, 113, 119-191.
109. D. Abate-Pella, N. A. Zeliadt, J. D. Ochocki, J. K. Warmka, T. M. Dore, D. A. Blank, E. V. Wattenberg and M. D. Distefano, *ChemBioChem*, 2012, 13, 1009-1016.
110. P. Bourbon, Q. Peng, G. Ferraudi, C. Stauffacher, O. Wiest and P. Helquist, *The Journal of Organic Chemistry*, 2012, 77, 2756-2762.
111. T. Furuta, S. S. H. Wang, J. L. Dantzker, T. M. Dore, W. J. Bybee, E. M. Callaway, W. Denk and R. Y. Tsien, *Proceedings of the National Academy of Sciences*, 1999, 96, 1193-1200.
112. V. Hagen, B. Dekowski, N. Kotzur, R. Lechler, B. Wiesner, B. Briand and M. Beyermann, *Chemistry – A European Journal*, 2008, 14, 1621-1627.
113. B. Schade, V. Hagen, R. Schmidt, R. Herbrich, E. Krause, T. Eckardt and J. Bendig, *The Journal of Organic Chemistry*, 1999, 64, 9109-9117.
114. M. Arun Kumar, C. N. Rohitha, S. J. Kulkarni and N. Narender, *Synthesis*, 2010, 2010, 1629-1632.
115. X.-Q. Li, X.-K. Jiang, X.-Z. Wang and Z.-T. Li, *Tetrahedron*, 2004, 60, 2063-2069.
116. T. W. Baughman, J. C. Sworen and K. B. Wagener, *Tetrahedron*, 2004, 60, 10943-10948.
117. F. G. Bordwell and W. T. Brannen, *Journal of the American Chemical Society*, 1964, 86, 4645-4650.
118. F. Rodríguez-Llansola and E. W. Meijer, *Journal of the American Chemical Society*, 2013, 135, 6549-6553.
119. T. Felder, T. F. A. de Greef, M. M. L. Nieuwenhuizen and R. P. Sijbesma, *Chemical Communications*, 2014, 50, 2455-2457.
120. A. Gooch, A. M. McGhee, M. L. Pellizzaro, C. I. Lindsay and A. J. Wilson, *Organic Letters*, 2010, 13, 240-243.
121. S. H. M. Söntjens, R. P. Sijbesma, M. H. P. van Genderen and E. W. Meijer, *Journal of the American Chemical Society*, 2000, 122, 7487-7493.
122. T. F. A. de Greef, G. B. W. L. Ligthart, M. Lutz, A. L. Spek, E. W. Meijer and R. P. Sijbesma, *Journal of the American Chemical Society*, 2008, 130, 5479-5486.
123. P. S. Corbin, L. J. Lawless, Z. Li, Y. Ma, M. J. Witmer and S. C. Zimmerman, *Proceedings of the National Academy of Sciences*, 2002, 99, 5099-5104.

124. P. Zhou, F. Tian, F. Lv and Z. Shang, *Proteins: Structure, Function, and Bioinformatics*, 2009, 76, 151-163.
125. B. M. Francuski, S. B. Novakovic and G. A. Bogdanovic, *CrystEngComm*, 2011, 13, 3580-3591.
126. H. M. Meshram, D. A. Kumar and B. R. Vara Prasad, *Synthetic Communications*, 2009, 39, 2317-2320.
127. G. Crank and H. R. Khan, *Australian Journal of Chemistry*, 1985, 38, 447-458.
128. A. Gooch, Thesis, University of Leeds, 2011.
129. R. M. Versteegen, R. Kleppinger, R. P. Sijbesma and E. W. Meijer, *Macromolecules*, 2005, 39, 772-783.
130. D. H. Napier and T. W. Wong, *British Polymer Journal*, 1972, 4, 45-52.
131. A. K. a. C. Sircar, R.P, *Measurement of the glass transition temperature of elastomer systems*, American society for testing and materials, Philidelphia, 1994.
132. R. Hagen, L. Salmén, H. Lavebratt and B. Stenberg, *Polymer Testing*, 1994, 13, 113-128.
133. D. J. Martin, G. F. Meijs, G. M. Renwick, S. J. McCarthy and P. A. Gunatillake, *Journal of Applied Polymer Science*, 1996, 62, 1377-1386.
134. C. Hilger and R. Stadler, *Macromolecules*, 1992, 25, 6670-6680.
135. S. A. Madbouly, J. U. Otaigbe, A. K. Nanda and D. A. Wicks, *Macromolecules*, 2005, 38, 4014-4023.
136. S. B. Clough and N. S. Schneider, *Journal of Macromolecular Science, Part B*, 1968, 2, 553-566.
137. E. A. Turi, *Thermal characterization of polymeric materials*, Academic Press, Brooklyn, New York, Second addition edn., 1997.
138. E. L. Rodriguez, *American Society for Testing and Materials*, 1994, 1249, 255-268.
139. R. Bonart, *Journal of Macromolecular Science, Part B*, 1968, 2, 115-138.
140. C. S. Paik Sung, C. B. Hu and C. S. Wu, *Macromolecules*, 1980, 13, 111-116.
141. C. R. Martinez and B. L. Iverson, *Chemical Science*, 2012, 3, 2191-2201.
142. J. T. Koberstein and T. P. Russell, *Macromolecules*, 1986, 19, 714-720.
143. L.-Z. Liu, F. Yeh and B. Chu, *Macromolecules*, 1996, 29, 5336-5345.
144. A. Saiani, A. Novak, L. Rodier, G. Eeckhaut, J. W. Leenslag and J. S. Higgins, *Macromolecules*, 2007, 40, 7252-7262.
145. A. Saiani, C. Rochas, G. Eeckhaut, W. A. Daunch, J. W. Leenslag and J. S. Higgins, *Macromolecules*, 2004, 37, 1411-1421.
146. Y. Bin, M. Fukuda, H. Kurosu and M. Matsuo, *Macromolecular Symposia*, 1999, 147, 1-14.
147. A. Pattanayak and S. C. Jana, *Polymer*, 2005, 46, 3394-3406.
148. R. D. Priestley, C. J. Ellison, L. J. Broadbelt and J. M. Torkelson, *Science*, 2005, 309, 456-459.
149. J. Rieger, *Polymer Testing*, 2001, 20, 199-204.
150. A. Saiani, W. A. Daunch, H. Verbeke, J. W. Leenslag and J. S. Higgins, *Macromolecules*, 2001, 34, 9059-9068.
151. B. Finnigan, D. Martin, P. Halley, R. Truss and K. Campbell, *Journal of Applied Polymer Science*, 2005, 97, 300-309.

152. S. Unal, C. Oguz, E. Yilgor, M. Gallivan, T. E. Long and I. Yilgor, *Polymer*, 2005, 46, 4533-4543.
153. L. T. J. Korley, B. D. Pate, E. L. Thomas and P. T. Hammond, *Polymer*, 2006, 47, 3073-3082.
154. Q. Cao, S. Chen, J. Hu and P. Liu, *Journal of Applied Polymer Science*, 2007, 106, 993-1000.
155. R. Hernandez, J. Weksler, A. Padsalgikar, T. Choi, E. Angelo, J. S. Lin, L.-C. Xu, C. A. Siedlecki and J. Runt, *Macromolecules*, 2008, 41, 9767-9776.
156. T. K. Kwei, *Journal of Applied Polymer Science*, 1982, 27, 2891-2899.
157. J. W. C. Van Bogart, D. A. Bluemke and S. L. Cooper, *Polymer*, 1981, 22, 1428-1438.
158. M. Yoshioka, B. C. Hancock and G. Zografi, *Journal of Pharmaceutical Sciences*, 1994, 83, 1700-1705.
159. Y. Yanagihara, N. Osaka, S. Murayama and H. Saito, *Polymer*, 2013, 54, 2183-2189.
160. M. E. Kazmierczak, R. E. Fornes, D. R. Buchanan and R. D. Gilbert, *Journal of Polymer Science Part B: Polymer Physics*, 1989, 27, 2189-2202.
161. J. C. Johnson, N. D. Wanasekara and L. T. J. Korley, *Biomacromolecules*, 2012, 13, 1279-1286.
162. S. Velankar and S. L. Cooper, *Macromolecules*, 1999, 33, 382-394.
163. S. L. Samuels and G. L. Wilkes, *Journal of Polymer Science: Polymer Physics Edition*, 1973, 11, 807-811.
164. J. A. Miller, S. B. Lin, K. K. S. Hwang, K. S. Wu, P. E. Gibson and S. L. Cooper, *Macromolecules*, 1985, 18, 32-44.
165. X. Wei, K. Bagdi, L. Ren, P. Shah, K. Seethamraju and R. Faust, *Polymer*, 2013, 54, 1647-1655.
166. J. T. Koberstein, A. F. Galambos and L. M. Leung, *Macromolecules*, 1992, 25, 6195-6204.
167. J. Blackwell and M. Ross, *Journal of Polymer Science: Polymer Letters Edition*, 1979, 17, 447-451.
168. O. A. Scherman, G. B. W. L. Ligthart, R. P. Sijbesma and E. W. Meijer, *Angewandte Chemie International Edition*, 2006, 45, 2072-2076.
169. G. Pruckmayr, P. Dreyfuss and M. P. Dreyfuss, in *Kirk-Othmer Encyclopedia of Chemical Technology*, John Wiley & Sons, Inc., 2000.
170. http://www.sigmaaldrich.com/catalog/product/aldrich/345326.
171. C. Drohmann and E. J. Beckman, *The Journal of Supercritical Fluids*, 2002, 22, 103-110.
172. J. Blackwell and M. R. Nagarajan, *Polymer*, 1981, 22, 202-208.
173. B. D. Kaushiva and G. L. Wilkes, *Journal of Applied Polymer Science*, 2000, 77, 202-216.
174. W. Li, A. J. Ryan and I. K. Meier, *Macromolecules*, 2002, 35, 5034-5042.
175. M. Furukawa, Y. Mitsui, T. Fukumaru and K. Kojio, *Polymer*, 2005, 46, 10817-10822.
176. Z. S. Petrović and I. Javni, *Journal of Polymer Science Part B: Polymer Physics*, 1989, 27, 545-560.
177. J. Blackwell, M. R. Nagarajan and T. B. Hoitink, *Polymer*, 1982, 23, 950-956.
178. K. K. Jena, D. K. Chattopadhyay and K. V. S. N. Raju, *European Polymer Journal*, 2007, 43, 1825-1837.

179. J. Scheirs, *Compositional and failure analysis of polymers. A practical approach*, John Wiley & sons, ExcelPlas, Australia, 2000.
180. P. M. Wood-Adams, J. M. Dealy, A. W. deGroot and O. D. Redwine, *Macromolecules*, 2000, 33, 7489-7499.
181. K. van Rijswijk and H. E. N. Bersee, *Composites Part A: Applied Science and Manufacturing*, 2007, 38, 666-681.
182. P. J. Flory, *Principles of Polymer Chemistry*, Cornell University Press, 1 edn., 1953.
183. M. Hutchby, C. E. Houlden, J. G. Ford, S. N. G. Tyler, M. R. Gagné, G. C. Lloyd-Jones and K. I. Booker-Milburn, *Angewandte Chemie International Edition*, 2009, 48, 8721-8724.
184. H. Kanno and R. J. K. Taylor, *Tetrahedron Letters*, 2002, 43, 7337-7340.
185. M. E. Bailey, V. Kirss, R. G. Spaunburgh, N. A. Division, A. Chemical and D. Corp, *Industrial & Engineering Chemistry*, 1956, 48, 794-797.
186. J. Alsarraf, Y. A. Ammar, F. Robert, E. Cloutet, H. Cramail and Y. Landais, *Macromolecules*, 2012, 45, 2249-2256.
187. M. Barrère and K. Landfester, *Macromolecules*, 2003, 36, 5119-5125.
188. H. Sardon, A. C. Engler, J. M. W. Chan, D. J. Coady, J. M. O'Brien, D. Mecerreyes, Y. Y. Yang and J. L. Hedrick, *Green Chemistry*, 2013, 15, 1121-1126.
189. X. Wei, P. N. Shah, K. Bagdi, K. Seethamraju and R. Faust, *Journal of Macromolecular Science Pure and Applied Chemistry*, 2013, 51, 6-15.
190. M. Hoch, *Applied Geochemistry*, 2001, 16, 719-743.
191. E. C. Steinle, F. E. Critchfield, J. M. Castro and C. W. Macosko, *Journal of Applied Polymer Science*, 1980, 25, 2317-2329.
192. J. Burkus, *The Journal of Organic Chemistry*, 1961, 26, 779-782.
193. J. Burkus and C. F. Eckert, *Journal of the American Chemical Society*, 1958, 80, 5948-5950.
194. W. J. Blank, Z. He and E. T. Hessell, *Progress in Organic Coatings*, 1999, 35, 19-29.
195. H. C. Brown and N. R. Eldred, *Journal of the American Chemical Society*, 1949, 71, 445-450.
196. A. Farkas and K. G. Flynn, *Journal of the American Chemical Society*, 1960, 82, 642-645.
197. S. Ephraim, A. E. Woodward and R. B. Mesrobian, *Journal of the American Chemical Society*, 1958, 80, 1326-1328.
198. K. Schwetlick, R. Noack and F. Stebner, *Journal of the Chemical Society-Perkin Transactions 2*, 1994, 599-608.
199. V. L. Furer, *Journal of Molecular Structure*, 1998, 449, 53-59.
200. M. Ouchi, T. Terashima and M. Sawamoto, *Chemical Reviews*, 2009, 109, 4963-5050.
201. I. Yilgor, B. D. Mather, S. Unal, E. Yilgor and T. E. Long, *Polymer*, 2004, 45, 5829-5836.
202. S. L. James and T. Friscic, *Chemical Society Reviews*, 2013, 42, 7494-7496.
203. S. L. James, C. J. Adams, C. Bolm, D. Braga, P. Collier, T. Friscic, F. Grepioni, K. D. M. Harris, G. Hyett, W. Jones, A. Krebs, J. Mack, L. Maini, A. G. Orpen, I. P. Parkin, W. C. Shearouse, J. W. Steed and D. C. Waddell, *Chemical Society Reviews*, 2012, 41, 413-447.

204. A. M. Belenguer, T. Friscic, G. M. Day, J. K. M. Sanders and T. Friščić, *Chemical Science*, 2011, 2, 696-700.
205. R. Trotzki, M. M. Hoffmann and B. Ondruschka, *Green Chemistry*, 2008, 10, 767-772.
206. B. Rodríguez, A. Bruckmann and C. Bolm, *Chemistry – A European Journal*, 2007, 13, 4710-4722.
207. Z. Zhang, Y.-W. Dong, G.-W. Wang and K. Komatsu, *Synlett*, 2004, 2004, 61-64.
208. S. E. Zhu, F. Li and G. W. Wang, *Chemical Society Reviews*, 2013, 42, 7535-7570.
209. W. Yuan, T. Friščić, D. Apperley and S. L. James, *Angewandte Chemie International Edition*, 2010, 49, 3916-3919.
210. A. L. Garay, A. Pichon and S. L. James, *Chemical Society Reviews*, 2007, 36, 846-855.
211. A. Delori, T. Friscic and W. Jones, *CrystEngComm*, 2012, 14, 2350-2362.
212. A. N. Swinburne and J. W. Steed, *CrystEngComm*, 2009, 11, 433-433.
213. L. Konnert, A. Gauliard, F. Lamaty, J. Martinez and E. Colacino, *ACS Sustainable Chemistry & Engineering*, 2013, 1, 1186-1191.
214. Z. Zhang, H.-H. Wu and Y.-J. Tan, *RSC Advances*, 2013, 3, 16940-16944.
215. J. W. Baker and D. N. Bailey, *Journal of the Chemical Society*, 1957, 4663-4668.
216. T. Friscic, *Journal of Materials Chemistry*, 2010, 20, 7599-7605.
217. Y. Zhao, F. Sakai, L. Su, Y. Liu, K. Wei, G. Chen and M. Jiang, *Advanced Materials*, 2013, 25, 5215-5256.
218. T. F. A. de Greef, M. M. L. Nieuwenhuizen, P. J. M. Stals, C. F. C. Fitie, A. R. A. Palmans, R. P. Sijbesma and E. W. Meijer, *Chemical Communications*, 2008, 4306-4308.
219. G. R. Newkome, S. J. Garbis, V. K. Majestic, F. R. Fronczek and G. Chiari, *The Journal of Organic Chemistry*, 1981, 46, 833-839.
220. X.-Z. Wang, X.-Q. Li, X.-B. Shao, X. Zhao, P. Deng, X.-K. Jiang, Z.-T. Li and Y.-Q. Chen, *Chemistry – A European Journal*, 2003, 9, 2904-2913.
221. J. W. Baker and J. Gaunt, *Journal of the Chemical Society*, 1949, 9-18.